



Report on Fuel Fragmentation, Relocation and Dispersal

Unclassified

NEA/CSNI/R(2016)16

Organisation de Coopération et de Développement Économiques
Organisation for Economic Co-operation and Development

10-Oct-2016

English text only

**NUCLEAR ENERGY AGENCY
COMMITTEE ON THE SAFETY OF NUCLEAR INSTALLATIONS**

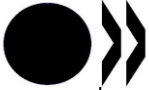
Cancels & replaces the same document of 05 October 2016

REPORT ON FUEL FRAGMENTATION, RELOCATION, DISPERSAL

JT03402445

Complete document available on OLIS in its original format

This document and any map included herein are without prejudice to the status of or sovereignty over any territory, to the delimitation of international frontiers and boundaries and to the name of any territory, city or area.



NEA/CSNI/R(2016)16
Unclassified

English text only

ORGANISATION FOR ECONOMIC CO-OPERATION AND DEVELOPMENT

The OECD is a unique forum where the governments of 35 democracies work together to address the economic, social and environmental challenges of globalisation. The OECD is also at the forefront of efforts to understand and to help governments respond to new developments and concerns, such as corporate governance, the information economy and the challenges of an ageing population. The Organisation provides a setting where governments can compare policy experiences, seek answers to common problems, identify good practice and work to co-ordinate domestic and international policies.

The OECD member countries are: Australia, Austria, Belgium, Canada, Chile, the Czech Republic, Denmark, Estonia, Finland, France, Germany, Greece, Hungary, Iceland, Ireland, Israel, Italy, Japan, Latvia, Luxembourg, Mexico, the Netherlands, New Zealand, Norway, Poland, Portugal, the Republic of Korea, the Slovak Republic, Slovenia, Spain, Sweden, Switzerland, Turkey, the United Kingdom and the United States. The European Commission takes part in the work of the OECD.

OECD Publishing disseminates widely the results of the Organisation's statistics gathering and research on economic, social and environmental issues, as well as the conventions, guidelines and standards agreed by its members.

NUCLEAR ENERGY AGENCY

The OECD Nuclear Energy Agency (NEA) was established on 1 February 1958. Current NEA membership consists of 31 countries: Australia, Austria, Belgium, Canada, the Czech Republic, Denmark, Finland, France, Germany, Greece, Hungary, Iceland, Ireland, Italy, Japan, Luxembourg, Mexico, the Netherlands, Norway, Poland, Portugal, the Republic of Korea, the Russian Federation, the Slovak Republic, Slovenia, Spain, Sweden, Switzerland, Turkey, the United Kingdom and the United States. The European Commission also takes part in the work of the Agency.

The mission of the NEA is:

- to assist its member countries in maintaining and further developing, through international co-operation, the scientific, technological and legal bases required for a safe, environmentally friendly and economical use of nuclear energy for peaceful purposes;
- to provide authoritative assessments and to forge common understandings on key issues, as input to government decisions on nuclear energy policy and to broader OECD policy analyses in areas such as energy and sustainable development.

Specific areas of competence of the NEA include the safety and regulation of nuclear activities, radioactive waste management, radiological protection, nuclear science, economic and technical analyses of the nuclear fuel cycle, nuclear law and liability, and public information.

The NEA Data Bank provides nuclear data and computer program services for participating countries. In these and related tasks, the NEA works in close collaboration with the International Atomic Energy Agency in Vienna, with which it has a Co-operation Agreement, as well as with other international organisations in the nuclear field.

This document and any map included herein are without prejudice to the status of or sovereignty over any territory, to the delimitation of international frontiers and boundaries and to the name of any territory, city or area.

Corrigenda to OECD publications may be found online at: www.oecd.org/publishing/corrigenda.

© OECD 2016

You can copy, download or print OECD content for your own use, and you can include excerpts from OECD publications, databases and multimedia products in your own documents, presentations, blogs, websites and teaching materials, provided that suitable acknowledgment of the OECD as source and copyright owner is given. All requests for public or commercial use and translation rights should be submitted to rights@oecd.org. Requests for permission to photocopy portions of this material for public or commercial use shall be addressed directly to the Copyright Clearance Center (CCC) at info@copyright.com or the Centre français d'exploitation du droit de copie (CFC) contact@cfcopies.com.

COMMITTEE ON THE SAFETY OF NUCLEAR INSTALLATIONS

The NEA Committee on the Safety of Nuclear Installations (CSNI) is an international committee made up of senior scientists and engineers with broad responsibilities for safety technology and research programmes, as well as representatives from regulatory authorities. It was created in 1973 to develop and co-ordinate the activities of the NEA concerning the technical aspects of the design, construction and operation of nuclear installations insofar as they affect the safety of such installations.

The committee's purpose is to foster international co-operation in nuclear safety among NEA member countries. The main tasks of the CSNI are to exchange technical information and to promote collaboration between research, development, engineering and regulatory organisations; to review operating experience and the state of knowledge on selected topics of nuclear safety technology and safety assessment; to initiate and conduct programmes to overcome discrepancies, develop improvements and reach consensus on technical issues; and to promote the co-ordination of work that serves to maintain competence in nuclear safety matters, including the establishment of joint undertakings.

The priority of the CSNI is on the safety of nuclear installations and the design and construction of new reactors and installations. For advanced reactor designs, the committee provides a forum for improving safety-related knowledge and a vehicle for joint research.

In implementing its programme, the CSNI establishes co-operative mechanisms with the NEA Committee on Nuclear Regulatory Activities (CNRA), which is responsible for issues concerning the regulation, licensing and inspection of nuclear installations with regard to safety. It also co-operates with other NEA Standing Technical Committees, as well as with key international organisations such as the International Atomic Energy Agency (IAEA), on matters of common interest.

FOREWORD

The NEA Working Group on Fuel Safety (WGFS) is promoting the understanding of fuel-safety issues by assessing the technical basis for current safety criteria and their applicability to high burnup and to new fuel designs and materials. The group aims at facilitating international convergence in this area, including the review of experimental approaches as well as the interpretation and use of experimental data relevant for safety.

In a previous activity of WGFS, this group evaluated the safety significance of the recently observed phenomena on fuel fragmentation, relocation and dispersal (FFRD) occurring in simulated LOCA transients. This evaluation was laid down in a CSNI report on “Safety significance of the Halden IFA-650 LOCA test results” (NEA/CSNI/R(2010)5 published in the year 2010). It provides recommendations on future tests, suggestions on code modelling and how to address regulatory needs.

Since the publication of this CSNI report, the experimental landscape developed further on. New findings on FFRD are available. This motivated the WGFS to establish a separate task group which will compile the status of present knowledge in this field.

Therefore, the present report aims to summarise and analyse the results from FFRD related studies and to revisit recommendations and conclusions given in the previous CSNI report.

ACKNOWLEDGEMENTS

This report is prepared by the fuel fragmentation, relocation and dispersal (FFRD) Task Group of the Working Group of Fuel Safety (WGFS).

The report was prepared on the base of the contributions from the following WGFS members and experts:

- Chapter 1: Heinz Sonnenburg (GRS, Germany)
- Chapter 2: Wolfgang Wiesenack (Halden, Norway), Joakim Karlsson (Studsvik, Sweden), Jean Noirot (CEA, France), Heinz Sonnenburg (GRS, Germany)
- Chapter 3: Veronique Garat (AREVA, France), Jean Noirot (CEA, France), Nicolas Waeckel (EDF, France)
- Chapter 4: Farida Khattout (EDF, France), Andrea Cabrera-Salcedo (EDF, France), Nicolas Waeckel (EDF, France), Wolfgang Wiesenack (Halden, Norway), Jinzhao Zhang (TRACTEBEL, Belgium)
- Chapter 5: Grigory Khvostov (PSI, Switzerland), Andreas Gorzel (ENSI, Switzerland), Vladimir Brankov (PSI, Switzerland), Fumihisa Nagase (JAEA, Japan)
- Chapter 6: Patrick Raynaud (NRC, United States), Michelle Bales (NRC, United States)
- Chapter 7: Tatiana Taurines (IRSN, France), Patrick Raynaud (NRC, United States), Jinzhao Zhang (TRACTEBEL, Belgium)
- Chapter 8: Heinz Sonnenburg (GRS, Germany), Tetsuo Nakajima (S/NRA, Japan), Anna Alvestav (SSM, Sweden)

The following WGFS members and experts participated in the review of the report and provided valuable comments:

- Anna Alvestav (SSM, Sweden)
- Masaki Amaya (JAEA, Japan)
- Michelle Bales (NRC, United States)
- Patrick Blanpain (AREVA, France)
- Winfried Beck (AREVA, Germany)
- Dietmar Deuble (AREVA, Germany)
- Lisa Gerken (AREVA, France)
- Luis Enrique Herranz (CIEMAT, Spain)
- Zoltán Hozer (MTA, Hungary)
- Katsuichiro Kamimura (S/NRA; Japan)
- Jan Klouzal (UJV, Czech)
- Fumihisa Nagase (JAEA, Japan)
- Nobuo Nakae (S/NRA, Japan)
- Marc Petit (IRSN, France)

- Patrick Raynaud, (NRC, United States)
- José M. Rey Gayo (CSN, Spain)
- Harold Scott (NRC, United States)
- Alexey Shestopalov (Bochvar, Russia)
- Nicolas Waeckel (EDF, France)
- Andreas Wensauer (E.ON, Germany)
- Wolfgang Wiesenack (Halden, Norway)
- Ken Yueh (EPRI, United States)
- Jinzhao Zhang (TRACTEBEL, Belgium)

TABLE OF CONTENTS

Executive summary	23
1. Introduction	27
2. Experimental findings	29
2.1 OECD halden reactor project test series IFA-650.....	29
2.2 Tests at STUDSVIK.....	37
2.3 CEA tests related to FFRD.....	43
2.4 VVER fuel bundle tests related to FFRD.....	50
3. Mechanism of fuel fragmentation	55
3.1 Analysis of the potential influence of the fuel rod initial state to the development of fuel fragmentation.....	57
3.2 Analysis of the potential influence of the fuel rod operational conditions on the development of fuel fragmentation	68
3.3 Analysis of the potential influence of the transient conditions to the development of fuel fragmentation.....	71
3.4 Conclusions about fuel fragmentation mechanism during a LOCA	77
4. Applicability of existing experimental data to the reactor conditions	79
4.1 Semi-integral test conditions versus in-reactor conditions	79
4.2 About separate effect tests	87
4.3 Discussion	87
5. Lack of experimental data	89
5.1 Fuel fragmentation thresholds.....	89
5.2 “Hot-spot” effect of fuel relocation on cladding temperature	92
5.3 LOCA-specific transient FGR.....	95
5.4 Characteristics and effects of the ejected fuel.....	96
5.5 Characteristics and effects of the fragmented/relocated fuel in the balloon around the rupture on secondary hydrogen uptake	98
5.6 Non-standard fuels	100
5.7 OECD/NEA SCIP-III research program on FFRD in LOCA transients.....	101
5.8 JAEA envisaged tests related to FFRD.....	103
5.9 Summary of phenomena of potential interest for ffrd evaluation	108
6. Thresholds for fragmentation, relocation and dispersal	111
6.1 Fuel fragmentation during LOCA.....	111

6.2	Fuel relocation during LOCA	116
6.3	Fuel dispersal during LOCA	121
6.4	Summary: preliminary thresholds for fuel fragmentation relocation and dispersal	126
7.	Necessity of code modelling	127
7.1	Introduction to necessity of code modelling	127
7.2	Key phenomena to model ffrd impact in codes.....	127
7.3	Scoping studies	145
7.4	Consideration of fuel cladding failures and ffrd in loca safety analyses in different countries	161
7.5	Conclusions.....	161
8.	Consequences of relocation and dispersal	163
8.1	Coolability.....	163
8.2	Re-criticality.....	173
8.3	Radiological consequences	178
9.	Appendices	187
9.1	Appendix: Development of high burnup structure during normal operation.....	187
9.2	Appendix: Consideration of fuel cladding failures and ffrd in loca safety analyses in different countries.....	192
	References	205

LIST OF ABBREVIATIONS AND ACRONYMS

ALCYONE	Computer code for fuel behaviour
ANL	Argonne National Laboratory
ATHLET	Analysis of thermal-hydraulics of leaks and transients
BART	Best-estimate Analysis of reflood transients' computer code
BOL	Beginning of life
BWR	Boiling-water reactor
CEA	Commissariat à l'Énergie Atomique et aux Energies Alternatives
CP-ECR	Cathcart&Pawel correlation for ECR prediction
DBA	Design basis accident
DRACCAR	Déformation et renoyage d'un assemblage de crayons combustibles pendant un accident de refroidissement computer code
ECR	Equivalent cladding reacted
EDGAR	Experimental facility for fuel-rod behaviour during LOCA
EHPG	Enlarged Halden programme group
ENSI	Swiss Federal Nuclear Safety Inspectorate
EOL	End of life
EPMA	Electron-probe micro-analyzer
EPRI	Electric Power Research Institute
EXAFS	Extended x-ray absorption fine structure
FALCON	PSI computer code for fuel behaviour
FEBA	Flooding experiments with blocked arrays
FFRD	Fuel fragmentation, relocation and dispersal
FGR	Fission gas release
FLASH	Experimental programme on fuel behaviour during LOCA
FRAPCON	Steady-state fuel-rod computer code
FRELAX	PSI Computer model for thermal behaviour and fuel relocation in the fuel rods
HBRP	High burn-up rim project
HBS	High burnup structure
HBU	High burnup fuel

HBWR	Halden boiling-water reactor
HM	Heavy metal
HPCI	High pressure coolant injection system
HRP	Halden reactor project
HVE	Hot vacuum extraction
INL	Idaho National Laboratory
IRSN	Institut de Radioprotection et de Sûreté Nucléaire
JAEA	Japan Atomic Energy Agency
KfK	Kernforschungszentrum Karlsruhe (today KIT)
LBLOCA	Large break LOCA
LHGR	Linear heat generation rate
LOCA	Loss-of-coolant accident
LPSI	Low-pressure safety injection system
MAPRAT	Maximum average power ratio
MATARE	Coupled computer code, MABEL-TALINK-RELAP5
MIMAS	Micronized masterblend, manufacturing technique
MIR	Modernised international reactor
MOL	Middle of life
MOX	Mixed oxide fuel
NRC	Nuclear Regulatory Commission
NSRR	Nuclear safety research reactor (located at JAEA in Japan)
NSSS	Nuclear steam supply system
PBF	Power burst facility (at the Idaho National Engineering Laboratory)
PCMI	Pellet-clad mechanical interaction
PCT	Peak cladding temperature
PIRT	Phenomena identification and ranking table
PSI	Paul Scherrer Institute
PWR	Pressurized-water reactor
RIA	Reactivity-initiated accident
RIP	Rod internal pressure
SAR	Safety assessment report
SBLOCA	Small-break loss-of-coolant accident
SCIP	Studsвик cladding integrity project
SEM	Scanning electron microscope
SILOE	French research reactor, now dismantled

SIMS	Secondary-ion mass spectrometry
S/NRA	Secretariat of Nuclear Regulation Authority
TEDE	Total effective dose equivalent
TRACE	System thermal-hydraulic code
TRIGA	Training, research, isotopes, General Atomics
U.S. NRC	Nuclear Regulatory Commission of the United States
V&V	Verification and validation
VVER	Water-cooled water-moderated energy reactor
VNIINM	A.A. Bochvar High-Technology scientific research Institute for Inorganic Materials

LIST OF FIGURES

Figure 2.1-1	Cross section of fuel pin, heater and pressure tube used in HRP IFA-650 LOCA studies	29
Figure 2.1-2	A typical IFA-650 transient (P = rod pressure; solid curve TCC 1, 2,3 = cladding temperature; dashed curves TCH 1, 2 = heater temperature; TIA=temperature at inlet; TOA=temperature at outlet)	30
Figure 2.1-3	Appearance of fuel fragmentation with different visualisation techniques	31
Figure 2.1-4	Details of fuel fragmentation at different burnups.....	31
Figure 2.1-5	Overview of all HRP IFA-650 LOCA tests (arranged in order of increasing burnup – here fuel rod segment averaged burnup)	33
Figure 2.1-6	Comparison of system pressure development in Halden tests IFA-650-3/4/5/9	34
Figure 2.1-7	Hydraulic diameter derived from pressure change in test IFA-650.9.....	35
Figure 2.1-8	Comparison of fragmentation in LOCA tested fuel with (upper part) and without (lower part) cladding tube burst	35
Figure 2.1-9	Axial fuel relocation at the upper end of the test segments in Halden tests a) 650.12, b) 650.13 and c) 650.14.....	36
Figure 2.2-1	The Studsvik LOCA test equipment.....	38
Figure 2.2-2	Temperature and pressure history of a LOCA test in cell [2.2-4].....	39
Figure 2.2-3	The fuel loss during each test (from [2.2-3])	39
Figure 2.2-4	The size distribution of the fuel fragments collected from the samples tested in the NRC LOCA test programme. The results show a characteristic difference in fragmentation size between 70 and 55 MWd/kgU rods (from [2.2-6])	41
Figure 2.2-5	The tube furnace used for separate effects heating tests at Studsvik [2.2-9].	41
Figure 2.2-6	Sample held by manipulator fingers before and after test. In the right figure ejected fuel debris is shown on the white paper in the background [2.2-9].....	42
Figure 2.3-1	FLASH-5, clad surface temperature history for the thermocouple on the side towards the core and for that on the opposite side.	44
Figure 2.3-2	FLASH-5, rod diameter and radial cuts, a) maximum power level, b) clad rupture level, and c) above rupture.	45
Figure 2.3-3	FLASH-5, details in the central area at maximum power level.....	45
Figure 2.3-4	FLASH-5, periphery details a) maximum power level, b) clad rupture level, c) above rupture.....	46
Figure 2.3-5	a) Furnace view and b) Principle.	46

Figure 2.3-6	Examples of temperature and fission gas release histories during heating tests a) within the Gaspard programme and b) within the NFIR programme.....	47
Figure 2.3-7	Examples showing the state of the fuel after 1 200°C heating tests a) and aa) UO ₂ fuel with a local burnup of 71.8 MWd/kgU after a ramp at 0.2°C/s, b) and bb) same fuel after a ramp at 20°C/s, c) MIMAS MOX fuel with a local burnup of 52.4 MWd/kgHM after a ramp at 20°C/s.....	48
Figure 2.3-8	Examples showing the fragmentation of an IFA-649 103 MWd/kgHM UO ₂ fuel disc after a 0.2°C/s, 1 200°C heating test.....	48
Figure 2.3-9	HBS fragment extracted in the rim of a 83 MWd/kgU UO ₂ fuel slice so that the estimated fragment burnup was 140 MWd/kgU, a) before annealing, b) after a 1 330°C annealing in an SEM chamber.....	49
Figure 2.3-10	83 MWd/kgU UO ₂ fuel fragments that moved out of a pre-cut cladding after a 1 200°C heating test.	49
Figure 2.4-1	Thermocouple located in the fuel rod bundle in test MIR/LOCA-50 [2.4-3].....	51
Figure 2.4-2	Temperature history in MIR/LOCA-50 test [2.4-3]	51
Figure 2.4-3	Cross-cut of test assembly of MIR/LOCA-50 test at elevation 830 mm from bottom [2.4-3].....	52
Figure 2.4-4	Scanning of test rod in MIR/LOCA-72 test (left) and cross-cuts (right) [2.4-3].....	53
Figure 3.1-1	Optical macrographs of a 64 MWd/kgU UO ₂ fuel, after chemical etching revealing the thin bubble areas (dark areas), [3.1-8]	58
Figure 3.1-2	SEM fractograph of trans-granular intentionally induced cracks in a 73 MWd/kgU fuel at a) 0.34R and b) 0.00R [3.1-9].....	59
Figure 3.1-3	SEM fractograph of an intentionally induced crack, inter-granular on the left side of the image, trans-granular on the right, in a 73 MWd/kgU fuel at 0.34R [3.1-9]	59
Figure 3.1-4	Increasing depletion in the EPMA Xe measurement in the central part of the pellets at a) 39 MWd/kgU, b) 61 MWd/kgU and c) 83 MWd/kgU, from [3.1-9], [3.1-10] and [3.1-11]	60
Figure 3.1-5	Increasing Xe content in large bubbles, measured with a SIMS at 61 MWd/kgU, 73 MWd/kgU and 83 MWd/kgU, from [3.1-9].....	61
Figure 3.1-6	Examples of macrographs on UO ₂ fuel, after chemical etching at high burnup, showing a complex distribution of bubble formation (dark areas).....	61
Figure 3.1-7	Radial cut of a MOX MIMAS pellet irradiated at 50 MWd/kgHM [3.1-13]	62
Figure 3.1-8	Examples of pellet-cladding bonding, a) first zirconia island before bonding, b) 68 GWj/tU section: interpenetration of rim area and internal corrosion layer [3.1-9]	63
Figure 3.1-9	Periphery of a UO ₂ fuel with an average section burnup of 83 MWd/kgU, zirconia inter-twinning with HBS and cracks in the HBS due to bonding and cooling periods, [3.1-9]	64
Figure 3.1-10	Local intergranular fission gas retention for IFA-650.4, 650.5, 650.10 and Studsvik test No.192, [3.1-23].....	66
Figure 3.1-11	Comparison of HBS fragmentation after normal operations (left, 83 MWd/kgU) [3.1-9] and after an out-of-pile heating test at 1 200°C (right, 72 MWd/kgU) [3.1-24]	67

Figure 3.2-1	Appearance of fuel and fuel rod after test MIR-LOCA/72 (segment averaged burnup of 76 MWd/kgU) [2.4-3].....	69
Figure 3.2-2	Post-test appearance, local burnup and 106 Ru activity for sibling rods tested by Studsvik for EPRI [3.2-1].....	70
Figure 3.3-1	Calculated temperature radial profile in IFA-650.4 and in Studsvik's test No.192, compared to base irradiation profile for test No.192 [3.1-23].....	71
Figure 3.3-2	Ceramography of test No.192 performed at Studsvik after LOCA and shaking [3.1-1] ...	74
Figure 3.3-3	Evolution of rod inner pressure during the heat treatment test calculated by TRANSURANUS code for the three tested rods	76
Figure 4.1-1	Axial temperature profile in Studsvik semi-integral LOCA tests derived from the oxidation axial profile.....	80
Figure 4.1-2	Axial power distribution in test specimen of HALDEN IFA650 test.....	81
Figure 4.1-3	Fuel rod cladding load in a double-ended cold leg break LOCA [4.1-3]	82
Figure 4.1-4	Blow-down and heat-up in an HBWR in-core LOCA test	83
Figure 5.1-1	Calculated temperature distribution across a pellet radius at the end of base irradiation and during a Halden LOCA test [5.1-8].....	91
Figure 5.1-2	Measured temperature for two thermocouples at the same axial level in Halden LOCA test IFA-650.13	92
Figure 5.2-1	Measured heater temperature at the level of balloon during IFA-650.4 test against calculation by the FRELAX-FALCON codes [5.2-1].....	93
Figure 5.5-1	Axial distribution of measured H-content and cladding diameter (top) against the relevant PIE images (bottom) after LOCA test IFA-650.7 [5.5-2].....	99
Figure 5.7-1	A schematic illustration of the threshold curve for fragmentation as a function of burnup and last cycle power.....	102
Figure 5.8-1	Key phenomena and parameters for FFRD	103
Figure 5.8-2	a) NSRR pulse irradiation in 80's with fresh fuel particles and pellets, b) Fragmentation of heated and quenched fuel particles, c) Cracking of heated and slowly-cooled fuel pellets.....	105
Figure 5.8-3	Radial cross-section of 47 MWd/kgU PWR fuel pellets heated to 2 500°C.....	106
Figure 5.8-4	Effect of oxidation (ECR-%) on the maximum circumferential strain.....	106
Figure 5.8-5	Effect of oxidation (ECR-%) on the size of rupture opening	107
Figure 6.1-1	Low-magnification images of the post-LOCA test ICL No.2 fuel samples a) at ≈ 12 mm above the rupture centre (15–35% strain), b) at ≈ 50 mm above the rupture centre (2–4% strain), c) at ≈ 130 mm below the rupture centre, and d) prior to LOCA testing (180 mm from the LOCA sample) [6.1-4]	111
Figure 6.1-2	Ceramography images and strain profiles from IFA-650.5 (83 MWd/kgU segment average burnup [6.1-1]	112
Figure 6.1-3	Ceramography images, sieving results and cladding strain profiles from Studsvik test 192 (segment average burnup of 78 MWd/kgU, father rod average burnup of 68 MWd/kgU),[6.1-5]	112

Figure 6.1-4	Spectrum of fuel fragments collected from integral LOCA test segments from 44 to 90 MWd/kgU. Results shown here are to their segment average burnup value. [6.1-3] [6.1-5] [6.1-7]	113
Figure 6.1-5	Size distribution of fuel fragments collected after Studsvik LOCA and shake testing, [6.1-6]	114
Figure 6.1-6	Photographs of test samples after heating test, a) sample taken above test 189, 72 MWd/kgU segment average burnup, 15 kW/m last cycle power, b) sample taken below test 189, 13.5 kW/m last cycle power, and c) sample taken from a different rod, 66 MWd/kgU segment average burnup, 5 kW/m last cycle power.....	115
Figure 6.2-1	Neutron radiograph of test LOC-6, rod 12, showing extensive axial fuel relocation [6.2- 7].....	118
Figure 6.2-2	Neutron radiography and cladding strain profiles from a) IFA-650.7 (44 MWd/kgU, BWR), [6.1-3], b) IFA-650.10 (60 MWd/kgU, PWR), [6.2-8], c) IFA-650.11 (56 MWd/kgU, VVER), [6.2-9], d) IFA-650.12 (72 MWd/kgU, BWR); for IFA-650.12, a transition between axially relocated fuel and non-relocated fuel is highlighted, [6.2-10], all burnup values are segment average.....	119
Figure 6.2-3	Circumferential strain profiles for all rods in tests MT-1, MT-2, MT-3, and MT-4, showing coplanar ballooning pinned by grid spacers [6.2-15].....	121
Figure 6.2-4	Pellet stack reduction as a function of cladding hoop strain for pre-irradiated fuel rods (based on the increase in volume in cladding balloon with no axial elongation) [6.2-16]	121
Figure 6.3-1	A wire probe is inserted into the fuel rod to measure the voided cladding length, [6.1-5]	123
Figure 6.3-2	Approximate percentage of fuel loss during each test, color coded by when fuel loss occurred. Note: Measured mass loss was compared to an estimated initial fuel mass of 150 g for the 300 mm segment.	124
Figure 6.3-3	Approximate percentage of fuel loss during each test, in comparison to the length of cladding strain >10%, as measured by wire probe.....	124
Figure 6.3-4	Summary table of Halden LOCA tests of the IFA-650 series, with regards to fuel dispersal [6.3-1].....	125
Figure 7.2-1	β -phase fraction at different heating rates derived from calorimetric measurements (M5 alloy) [7.2-3]	128
Figure 7.2-2	Strain versus time illustrating primary, secondary and tertiary creep.....	129
Figure 7.2-3	Maximum circumferential strain versus rupture temperature for Zircaloy cladding under steam environment internally heated below 10°C/s [7.2-11].....	131
Figure 7.2-4	Maximum circumferential strain versus rupture temperature for Zircaloy cladding under steam environment internally heated greater than or equal to 25°C/s [7.2-11]	131
Figure 7.2-5	Correlation of rupture temperature as a function of engineering hoop stress and temperature ramp rate from internally heated Zircaloy cladding in aqueous atmospheres [7.2-11].	132
Figure 7.2-6	Comparison between the burst criterion for as-received and hydrided at 600 ppm Zry-4 cladding tubes [7.2-8].....	133

Figure 7.2-7 Total elongation at burst versus test temperature for iso-thermal tests (a) and transient tests (1°C/s, 10°C/s and 100°C/s) (b) from [7.2-12]133

Figure 7.2-8 Rupture area as a function of a) rupture pressure and b) rupture temperature from several experimental programmes, for both unirradiated and irradiated fuel, as well as proposed models135

Figure 7.2-9 Fragment size distribution for (a) PBF and (b) FR-2 tests.....137

Figure 7.2-10 a) Fragment size distribution for the NRC-Studsvik LOCA tests and b) NRC model based on NRC-Studsvik LOCA test measurements.138

Figure 7.2-11 EPRI's proposed map of fuel fragmentation as a function of burnup and last cycle power [7.2-22].....139

Figure 7.2-12 NFIR proposed threshold for different levels of pellet volume-% powder formation as a function of pellet average burnup and transient temperature [7.2-23].....140

Figure 7.2-13 Schematic view of the algorithm for evaluating the amount of fuel that relocates. The first step evaluates the amount of fuel that is free to fall from upper locations, the second step then estimates the amount of fuel that actually relocates (cited from [7.2-26]).....143

Figure 7.2-14 Pellet stack reduction as a function of cladding hoop strain for pre-irradiated fuel rods (based on the increase in volume in cladding balloon with no axial elongation).....144

Figure 7.2-15 Fuel dispersal model presented by IBERDROLA at Top Fuel 2 012 - mass of fuel dispersed per ruptured fuel rod as a function of burnup144

Figure 7.3-1 Impact of axial fuel relocation on cladding temperature at the rupture node of hot rod versus time (LB LOCA with irradiated UO₂ fuel) [7.2-30]146

Figure 7.3-2 Impact of axial fuel relocation on cladding temperature at the rupture node of hot rod versus time with filling ratios from 50 to 70% (LB LOCA with irradiated UO₂ fuel) [7.2-30]146

Figure 7.3-3 Evolution of peak cladding temperature and of the temperature at node at upper thermocouple position during the transient for the IFA-650.4 case [7.2-26]147

Figure 7.3-4 Case sensitivity study on effect of cladding balloon area and fuel relocation on peak cladding temperature at the balloon position from [7.2-27].148

Figure 7.3-5 a) Balloon filling ratio by relocated fragments [7.3-8], b) Circumferential strain for low ramp tests excluding low azimuthal temperature gradient tests: Best Estimate Curve (BED) [7.3-7]150

Figure 7.3-6 a) Axial temperature profile and b) Outer oxidation axial profile comparisons for IFA-650.4, for the different modelling options chosen by IBERDROLA (blue diamond represent Halden data, the red line is the base case, the green line is the second case with the filling ratio model from Figure 7.3-5 a), and the purple line is the third case with a filling ratio of 41% based on Halden measurements) [7.3-7]151

Figure 7.3-7 Axial temperature profile and b) ECR axial profile comparisons for IFA-650.7, for the different modelling options chosen by IBERDROLA [7.3-7]152

Figure 7.3-8 PCT Penalisation factor as function of balloon and filling ratio [7.3-7].....153

Figure 7.3-9 Calculated cladding outer surface temperature vs. axial position for the IFA 650.4 test at time of cladding rupture (a) and at time t = 500 s (b).....154

Figure 7.3-10 Estimated filling ratio of crumbled fuel versus relative amount of small fragments from pulverized high burnup fuel.....	155
Figure 7.3-11 Dispersed fuel mass analyses for the Westinghouse-4-Loop (W4LP) Large-Break LOCA scenario as a function of time of cycle and chosen fine fragmentation burnup threshold [7.2-20].....	156
Figure 7.3-12 Limiting pellet node for fuel types a) 1 and b) 2 in the Spanish BWR/6 modelled by IBERDROLA, for each fuel rod, as a function of burnup, over the course of a whole cycle [7.2-34].....	157
Figure 7.3-13 Number of failed rods required to challenge coolability and criticality limits, as a function of burnup [7.2-34].....	158
Figure 7.3-14 PCT and number of burst rods in the hot assembly for different MAPLHGR Ratios [7.3-9].....	159
Figure 7.3-15 Bundle MAPRAT distributions for a typical cycle in a U.S.BWR [7.3-9].....	160
Figure 8.1-1 Relationship between dry-out heat flux and particle diameters, particle bed depth with porosity of 40% (Lipinski-Model) [8.1-4].....	165
Figure 8.1-2 Dry-out heat flux depending on particle diameters and porosity for constant particle bed depth of 53.2 cm (Lipinski model) [8.1-4].....	166
Figure 8.1-3 Relationship between pellet stack reduction and cladding hoop strain from inpile-tests, [2.2-2].....	168
Figure 8.1-4 Average porosity p in fuel debris under strained cladding condition.....	168
Figure 8.1-5 Porosity of relocated fuel within strained and none-burst fuel rod cladding.....	169
Figure 8.1-6 Fragment sizes as measured in Studsvik Integral-LOCA-Tests (191, 192, 193, 196, 198) [8.1-5].....	170
Figure 8.1-7 Appearance of fuel particles in Halden IFA 650 LOCA tests and Studsvik tests when manually shaken out from test rod [8.1-5].....	170
Figure 8.1-8 Debris bed cooling via heat conduction.....	172
Figure 8.2-1 Typical 17x17 PWR fuel assembly with an average enrichment of 4.8% U-235 containing 24 Gd fuel rods [8.2-5].....	174
Figure 8.2-2 k -infinity trend of 4.8 wt% enriched PWR assembly due to depletion of U-235 and build-up of fissile Pu under HFP core conditions, Boron concentration at 600 ppm.....	175
Figure 8.2-3 Infinite multiplication factor (k_{∞}) for homogeneous fuel-water mixture as a function of fuel concentration, Boron concentration at 0 ppm.....	176
Figure 8.2-4 Sphere geometry model of fuel-water mixture reflected by an effectively infinite thickness of water.....	176
Figure 8.2-5 Critical masses of fuel within spheres of homogeneous fuel-water mixture as a function of fuel concentration.....	177
Figure 8.2-6 Critical volumes of spheres of homogeneous fuel-water mixture as a function of fuel concentration.....	178
Figure 8.3-1 Relative gamma source strengths for noble gases where all data points are normalized to the reference case given at time 0.5 h.....	184

Figure 8.3-2 Relative gamma source strengths for halogens where all data points are normalized to the reference case given at time 0.5 h.....185

Figure 8.3-3 Relative gamma source strengths for other fission products where all data points are normalized to the reference case given at time 0.5 h185

Figure 9.1-1 Penetration depth of the high burnup structure in PWR fuel, from [9.1-16], [9.1-3] and [3.1-9]188

Figure 9.1-2 Restructuration threshold observed on the UO2 disks irradiated in the HBRP, Burnup and irradiation temperature of the 16 stacks of HBRP [9.1-2].189

Figure 9.1-3 EPMA local Xe-detection versus local burnup in UO2 fuel (4.5% 235U) [9.1-17].....190

Figure 9.1-4 Optical micrograph of Pu rich agglomerates on a MOX MIMAS AUC after 55 GWd/t [3.1-13], a) periphery, b) mid radius, c) centre190

Figure 9.1-5 Local HBS restructuration rate versus local burnup for UO2 and MOX) [9.1-17]191

Figure 9.2-1 Numbers of the failed fuel rods among the 1 000 rods simulated in each of the 59 global scenarios from [9.2-52].....194

Figure 9.2-2 Example of assumed pre-LOCA axial power distortion in the core196

Figure 9.2-3 Exemplary results of a failure rate analysis.197

LIST OF TABLES

Table 2.1-1	Fuel weight and normalized weight fraction depending on particle size.
Table 2.2-1	Summary of test data from the six NRC LOCA tests from [2.2-3], [2.2-4] and [2.2-7].
Table 3-1	Characterisation of fuel fragmentation before and after integral LOCA testing as a function of burnup.
Table 3.2-1	VVER fuel tests ordered with increasing burnup [2.4-3].
Table 5.3-1	Retention (in %) of total activity measured in post-test fuel rods.
Table 5.7-1	Summary of phenomena of potential importance for FFRD evaluation.
Table 5.7-2	Special features of non-standard fuels to be addressed.
Table 6.3-1	Summary of strain and rupture measurements from Studsvik LOCA tests [6.1-5].
Table 6.4-1	Preliminary list of thresholds for fragmentation, relocation and dispersal.
Table 8.2-1	Actinide and fission product nuclides taken in fuel compositions for criticality calculations.
Table 8.2-2	Minimum critical masses and critical volumes for fuel-water mixture within sphere geometry.
Table 8.3-1	Gap inventories for a high burnup fuel assembly according to Reference [8.3-2].
Table 8.3-2	Release fractions during gap and early in-vessel release phases [8.3-2].
Table 8.3-3	Timing of release phases [8.3 2].
Table 9.1-1	Fuel failure rate considered in radiological assessment and FFRD consideration in safety analyses.

EXECUTIVE SUMMARY

Since the time of the first loss-of-coolant accident (LOCA) experiments, which were largely conducted with fresh fuel, changes in the fuel design, the introduction of new cladding materials and in particular the move to high burnup have generated a need to re-examine the LOCA safety criteria and to verify their continued validity. As part of international efforts to this goal, the OECD Halden Reactor Project programme implemented a LOCA test series. The fourth test of the series, IFA-650.4, caused particular attention in the international nuclear community. The fuel in this experiment had a high burnup, 92 MWd/kgU. The rod ballooned as intended, but the burst caused substantial fuel relocation, and post-irradiation examination (PIE) revealed considerable fuel fragmentation.

Further tests in Halden and later in Studsvik followed, confirming the fuel fragmentation, relocation and dispersal (FFRD) phenomena observed in Halden test IFA-650.4. It became evident that for high burnup fuel (HBU), the LOCA transient has the potential to fragment fuel, to axially relocate fuel within the fuel rod as far as ballooning of the fuel provides space for this relocation and even has the potential that fuel gets expelled from the fuel rod burst opening into the coolant channel partially blocking a coolant channel. Because of the fact that certain quantities of the fuel fragments expelled are small enough in size to be transported with the emergency coolant throughout the primary circuit, there is a potential that fuel fragments may even reach compartments of the containment between the location of the large break and the containment sump contributing to radiological loads in the containment beyond those already considered in safety assessments.

The discussions of the recent test results between experts showed that there were different possible interpretations. Even the consistency between the various results was questioned. Additionally, questions were raised about the safety significance of these new technical elements. Therefore, it is the intention of this report to summarise and analyse the results from related experimental studies, to summarise experimental findings as well as modelling results, and to provide an outlook on implications for core coolability, reactivity control and radiological consequences.

Chapter 2 of this report provides an overview on experimental findings related to FFRD. Halden, Studsvik, specific Commissariat à l'Énergie Atomique (CEA) tests and MIR/LOCA tests provide a complex phenomenological picture on fuel fragmentation. While the first Halden tests of the series 650 indicate a certain burnup threshold for the occurrence of fine fragmentation, further Halden tests and later Studsvik tests, especially Studsvik tests designed by Electric Power Research Institute (EPRI), identified cladding distension, fuel transient temperature and last cycle power level as additional parameters for the occurrence of fine fragmentation. FFRD related CEA tests, especially Flash tests and tests in the frame of the "Gaspard" programme, allow the conclusion that at high burnup fine fragmentation is not restricted to the development of high burnup structure (HBS) along the pellet rim. Also interior parts of the pellet may be involved in fine fragmentation. In any case, these CEA tests support that transient fuel temperature must exceed 1 000°C in order to reach fine fragmentation of the fuel pellet which is in contrast to related Studsvik tests determining a temperature¹ of 750°C for this fine fragmentation. The MIR/LOCA tests on VVER fuel support the present phenomenological analyses that fragmentation and relocation are

1. The temperature distribution is rather flat in the pellet during LOCA transients so no distinction is made regarding average pellet temperature or pellet surface temperature.

depending on a burnup threshold. Therefore, it is the overall conclusion from Chapter 2 that experimental tests are still required to close gaps in the phenomenological picture.

Seeking for mechanisms driving the fuel fragmentation, Chapter 3 provides a comprehensive description of all relevant processes taking place in fuel under irradiation. Microscopic analyses illustrate how fission gases are retained in fuel. While the development of HBS is illustrated in detail, it is not the only driver for fragmentation. The summary of this survey ceases with open questions on the driving mechanisms, but at least provides a list of potential drivers which should be investigated in further experiments. These are: gas precipitation at intra-grain locations and grain boundary, temperature (gradient, magnitude and kinetic), hydrostatic pressures surrounding the fuel, pellet/cladding bonding and the presents of particular fission products either within the fuel matrix or at grain boundaries which may weaken the adhesive strength.

Representativeness of available experimental investigations has been discussed in Chapter 4 in relation to the reactor case. This investigation draws an overall conclusion that, in general, test results cannot always be directly applied to reactor cases. The representativeness for each kind of testing (rod bundle test versus single rod test versus separate effect test) is always limited and therefore it requires qualified codes to ensure the applicability of the test results to the in-reactor conditions and to evaluate their real safety significance.

The lack of experimental data has been discussed in Chapter 5 along known FFRD phenomena like onset of fine fragmentation, 'hot spot effect', fission gas release (FGR), fuel ejection, secondary hydriding and cladding oxidation near burst opening, effect of expelled fuel on neighbouring fuel rods, etc. While this chapter does not provide a phenomena identification and ranking table (PIRT), it summarises these phenomena relative to their parameters of importance. It also gives hints on which mechanisms need to be investigated in greater detail in order to achieve the basis for a conclusive code modelling.

Chapter 6 compiles the present (2015) state of the art regarding parameter thresholds triggering fuel fragmentation, fuel relocation and fuel dispersal:

- The dominating parameter for occurrence of fuel fragmentation is determined to be burnup. This burnup threshold ranges from 60 MWd/kgU to 75 MWd/kgU (segment average burnup). Less dominant parameters are proximity of fuel to burst location, cladding strain above 5% to 10%, fuel temperature increase above 750°C and elevated linear heat generation before LOCA. These less dominant parameters can be regarded as contributors to a mechanical non-equilibrium of the fuel matrix.
- Axial fuel relocation is observed in each LOCA test which shows a cladding hoop strain exceeding 8%. Fine fragmentation is not a prerequisite for this axial relocation. But, in case the burnup level may provoke fine fragmentation, the cladding hoop strain threshold may even be reduced to 2%. Thus, axial fuel relocation threshold presumably depends also on fuel fragment size.
- LOCA tests suggest a dependence of the quantity of dispersed fuel on the axial length of the cladding which experienced a hoop strain above 10%. Additionally to that, some other conditions need to be met. These are: a) occurrence of fuel rod rupture, b) burst opening width which allows passing of fuel particles, c) cladding strain above 2% to 10% in order to mobilize fuel particles inside the fuel rod and d) burnup level provoking fine fragmentation.

Chapter 7 compiles available modelling approaches for a more realistic evaluation of the impact of FFRD on the design basis LOCA safety analyses. In addition, the results of some recent scoping studies are presented in this chapter. These studies reveal that code predictions strongly depend on the assumptions taken to model FFRD phenomena. The importance of consideration of FFRD in the current licensing is a secondary consideration in most of the OECD countries, except for France where the relocation will be considered in coolability analyses in the new regulation. In a few countries, a limit on the number of failed

rods is imposed for radiological assessment, which may also limit the impact of FFRD. Due to that the motivation to foster FFRD modelling will be different among the OECD countries.

Chapter 8 investigates the consequences of FFRD, namely consequences on core coolability, core re-criticality and radiological impact. The situation is very complex if one needs to take into account the fact that HBU rods in a core would burst and, due to that, fuel disperses among coolant channels. Here the safety demonstration would widen to various non-trivial considerations on particle bed cooling. The investigations on re-criticality of a core containing spherical agglomerates of dispersed fuel comprise various neutron-kinetic analyses for different burnup levels. These analyses allow concluding, there is no concern for re-criticality if the burnup level exceeds 50 MWd/kgU. Finally, a case study on the FFRD regarding the radiological impact reveals that, for the cases studied and the methods used, conservative assumptions cover the additional contribution from FFRD.

Overall we conclude that:

- The dominant parameter for fuel fragmentation is burn-up with a threshold between 60 and 75 MWd/kgU.
- Fuel fragmentation typically requires a cladding hoop strain exceeding 8% to manifest itself.
- The quantity of axially relocatable and potentially dispersible fuel depends on the axial length of the cladding that was subjected to a hoop strain above 10%.
- The coolability of dispersed fuel depends on a number of characteristic parameters, but the assessment of the safety significance does not, at present, lead to strong concern.
- Experiments are still required to complete the phenomenological picture given some divergence on the temperature/burn-up criteria for FFRD and the evaluation of the coolability of dispersed fuel.

1. INTRODUCTION

Since the time of the first LOCA experiments, which were largely conducted with fresh fuel, changes in the fuel design, the introduction of new cladding materials and in particular the move to high burnup have generated a need to re-examine the LOCA safety criteria and to verify their continued validity.

As part of international efforts to this end, the OECD Halden Reactor Project programme implemented a LOCA test series. The fourth test of the series, IFA-650.4, caused particular attention in the international nuclear community. The fuel in this experiment had a high burnup, 92 MWd/kgU. The rod ballooned as intended, but the burst caused substantial fuel relocation, and PIE revealed considerable fuel fragmentation. A similar result was obtained with a later test, IFA-650.9, likewise using HBU.

After these Halden tests, the Nuclear Regulatory Commission of the United States (U.S.NRC) initiated the Studsvik LOCA test series focussing on the new fuel fragmentation and dispersal (FFRD) phenomena. These Studsvik LOCA tests confirm the findings of the Halden LOCA test series although heating of the Studsvik specimens were indirect while in Halden tests it were both nuclear and indirect.

Objectives of this report are to summarise experimental findings on FFRD (Chapter 2), to mechanistically interpret these findings on FFRD as far as available experimental data allow such interpretations (Chapter 3), to discuss the applicability of such findings to reactor condition (Chapter 4), to identify lacking experimental investigations (Chapter 5), to identify thresholds for occurrence of FFRD phenomena (Chapter 6), to discuss the necessity for modelling efforts (Chapter 7) as well as to finally discuss potential consequences of FFRD for LOCA safety analyses (Chapter 8).

2. EXPERIMENTAL FINDINGS

2.1 OECD Halden Reactor Project Test Series IFA-650

The Halden Reactor Project LOCA testing in IFA-650 started in 2003 with the commissioning of the experimental system (IFA-650.1/2 using fresh fuel) and continued with IFA-650.3 using HBU in 2004. Since then, eleven tests with pre-irradiated fuel segments from commercial reactors have been carried out. FFRD has been the main focus of the test series after the execution of IFA-650.4 which showed considerable fuel fragmentation and dispersal.

The eleven tests with pre-irradiated fuels can be grouped as follows:

- PWR fuel IFA-650.3/4/5/9/10
- BWR fuel IFA-650.7/12/13/14
- VVER fuel IFA-650.6/11.

They experienced various degrees of FFRD and showed effects presumed to influence FFRD, e.g. a range of cladding distensions and burst openings, and restricted axial gas communication in some cases.

2.1.1 Test design and execution

A single fuel rod is inserted into a pressure flask connected to a water loop (Figure 2.1-1). A low level of nuclear power generation in the fuel rod is used to simulate decay heat, whereas the electrical heater surrounding the rod simulates the heat from surrounding rods. The heat flow and temperature distribution is thus similar to the situation during a real LOCA in contrast to hot laboratory set-ups where the pellets are a heat sink and the temperature distribution is reversed.

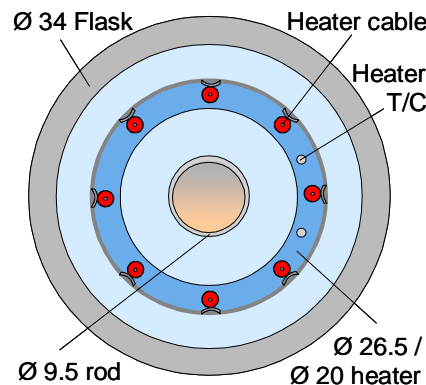


Figure 2.1-1: Cross section of fuel pin, heater and pressure tube used in HRP IFA—650 LOCA studies

The rod instrumentation consists of two cladding thermocouples at the upper part of the rod, one cladding thermocouple at the lower part, two heater thermocouples at different axial elevations, a cladding extensometer and a rod pressure sensor. The rig contains coolant thermocouples and three axially distributed vanadium neutron detectors to measure the axial power distribution.

Before test execution, the reactor is operated for some hours at about 15 MW (fuel average linear heat rate about 85 W/cm). After power calibration, the LOCA test is performed at a reactor power of 4.0 MW and a low rod power (10-30 W/cm depending on target peak clad temperature). The axial power profile is nearly symmetric with an axial peak to average power factor of ≈ 1.04 – 1.08 .

Loss of coolant is initiated by opening the blow-down line at the bottom of the rig. Then, changes like heat-up, ballooning and burst go their course according to the dynamic behaviour of the system without interference by experimenters.

A typical transient is shown in Figure 2.1-2. The example is from an experiment without significant fuel relocation.

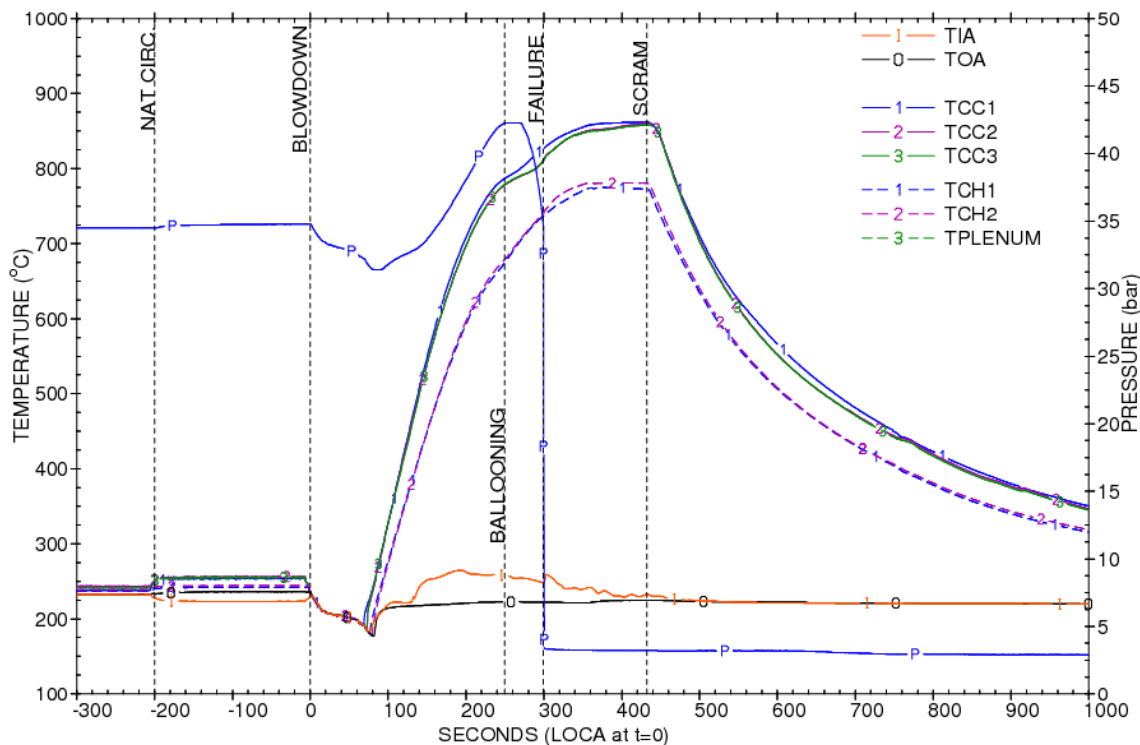


Figure 2.1-2: A typical IFA-650 transient (P = rod pressure; solid curve TCC 1, 2, 3 = cladding temperature; dashed curves TCH 1, 2 = heater temperature; TIA=temperature at inlet; TOA=temperature at outlet)

The experiments are terminated by switching off the electrical heating and scrambling the reactor, causing the fission heat generation in the fuel rod to cease as well. The test rods are allowed to cool down relatively slowly with the reactor.

2.1.2 Detection of FFRD

Gamma scanning is carried out a few days after test execution. The test rig is slowly moved to the scanning compartment, keeping the fuel segment vertical in order to not change the fuel distribution in the cladding tube.

The ragged appearance of the fuel column in the left gamma scan, Figure 2.1-3 indicates coarse fragments which have moved laterally where ballooning has created some extra space. A small axial gap at the upper end indicates a little downward movement of the fuel column.

The scan to the right shows no discernible structure and is an example of fine fragmentation and no lateral movement due to little ballooning.

The gamma signal from the bottom of the pressure flask (line on left side of the scan) is an indication of fuel driven out of the rod.

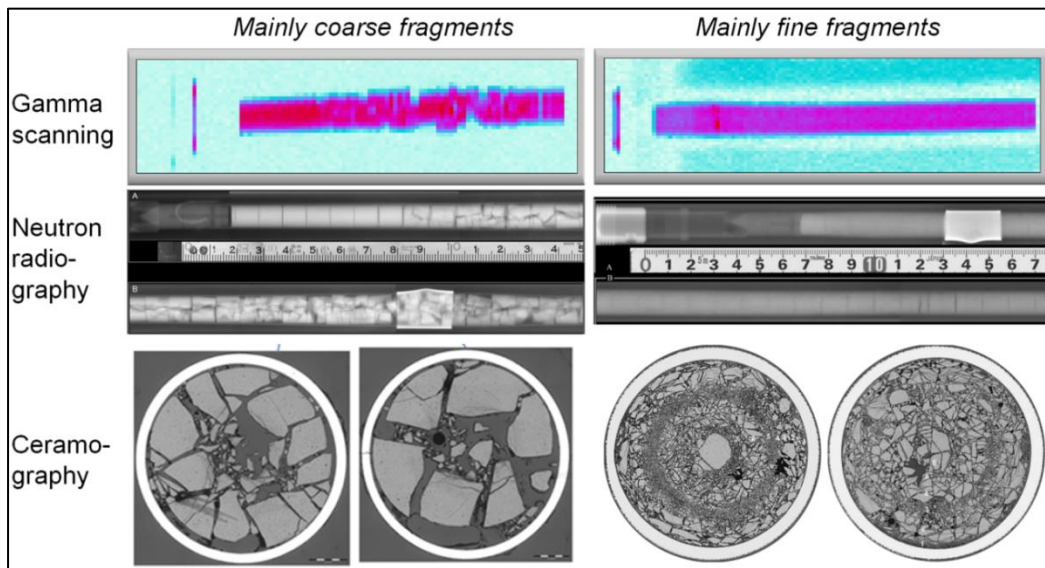


Figure 2.1-3: Appearance of fuel fragmentation with different visualisation techniques

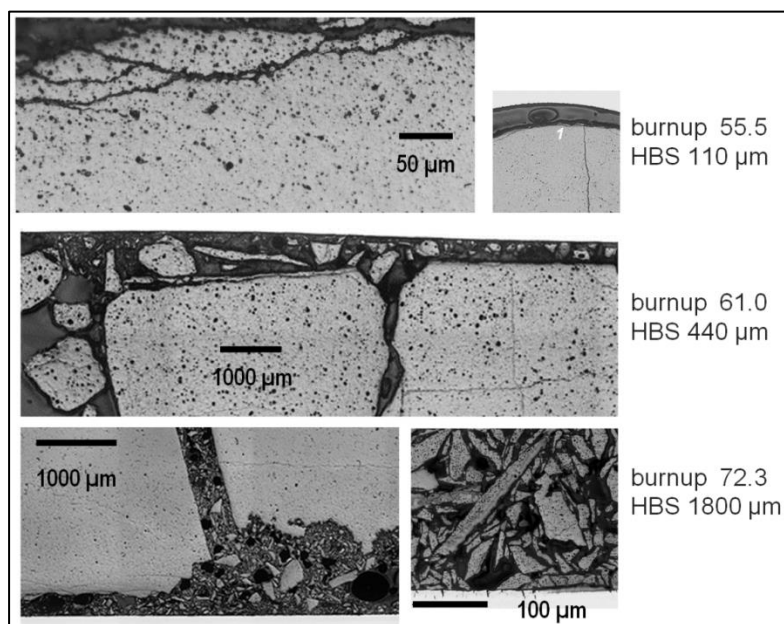


Figure 2.1-4: Details of fuel fragmentation at different burnups

Neutron radiography is done a few months after test execution when the fuel has cooled sufficiently. The pictures show the same fuel as the gamma scan. Neutron radiography reveals more details. The left sub-picture shows intact pellets and coarse fragments. The right sub-picture shows that the lower part of the segment must be strongly fragmented since pellet-pellet interfaces and dishings are not visible while they are discernible in the upper part.

Ceramo-graphy is the final examination. The ceramo-graphs confirm the fragmentation deduced from gamma scanning and neutron radiography, but with much more detail at selected locations.

Figure 2.1-4 shows details of fragmented fuel at different burnups and thicknesses of the HBS. The HBS fuel in the periphery of the pellets disintegrates more strongly with increasing burnup.

2.1.3 Overview of results related to FFRD

Figure 2.1-5 gives an overview of FFRD, arranged in increasing order of burnup. Qualitatively, an increasing propensity for fragmentation and dispersal can be seen. The burnups of two extreme cases (IFA-650.4 and 650.9) with considerable fuel dispersal apparent as empty cladding tube in the upper half of the tested segments go far beyond current discharge burnups of the fuels for commercial light water reactors.

The results from these tests are discussed in detail and analysed in Chapter 4.

A prominent feature shown by radiography and ceramography is the similarity of the fragmentation experienced by the fuel in the range 44 – 74 MWd/kg. Coarse, clearly visible fuel pieces are dominant. It can also be seen that VVER fuel (tests 6 and 11) retains the mainly wedge-shaped fragments already formed during normal operation. This more regular pattern is probably caused by the centre hole since test fuel with a centre hole for a thermocouple shows a similar behaviour.

Most of the burst openings produced in the Halden LOCA tests were too small to allow the coarse (>1 mm) fragments to be ejected.

test #	burnup, MWd/kg	balloon strain, %	radio-graphy	ceramo-graphy	fragment size	gamma scan	flask bottom ↑	HBS width	dispersal (qualitative)
2	0	54			coarse				none
7	44.3	23			coarse				none
6	55.5	49			coarse				none
11	56	25			coarse				none
10	60	15			coarse & some fine				some
12	72.3	40			coarse & fine				some more
13	74.1	45		fragment size distribution only	coarse (& fine?)				nearly none
14	71.1	55		fragment size distribution only	coarse (& fine?)				did not fail
3	81.9	8			medium & fine				n/a
5	83	15			medium & fine				much
9	90	61			medium & fine				much more
4	92	62			medium & fine				much more

Figure 2.1-5: Overview of all HRP IFA-650 LOCA tests (arranged in order of increasing burnup – here fuel rod segment averaged burnup)

2.1.4 Slow pressure drop

The in-pile rod pressure measurements most often showed an instantaneous pressure drop after rod burst, which is the expected behaviour. In some cases, however, the rod pressure decreased slowly and took minutes to equilibrate with the system pressure. In these cases, the fuel maintained tight contact with the cladding along a certain length. The slow pressure drop after burst of IFA-650.3/5/9 in comparison to the fast development in IFA-650.4 is shown in Figure 2.1-6.

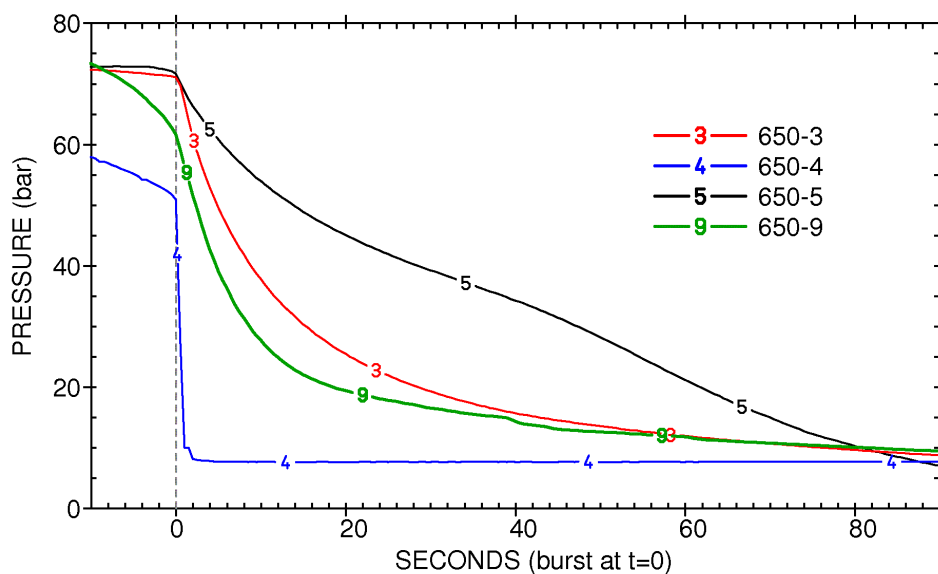


Figure 2.1-6: Comparison of system pressure development in Halden tests IFA-650-3/4/5/9

The gas permeability of HBU can be assessed with the technique of “hydraulic diameter measurement”. The technique employs a reservoir that is emptied through the fuel rod, at the same time measuring the pressure in the reservoir. This setup resembles the situation in the LOCA tests where the rod plenum assumes the role of the reservoir that is emptied through the fuel stack.

The formalism to derive the hydraulic diameter is described in [2.1-1] based on work in [2.1-2], [2.1-3] where gas flow in zero and low burnup fuel rods was investigated. The conclusion at that time (1 976, 1 977) was that there is sufficient gas supply to drive the ballooning. However, the situation may be different at high burnup since the general experience from HBWR gas flow measurements is that HBU is rather tight. It is virtually impossible to impose gas flow at power.

The hydraulic diameter evaluation of the IFA-650.9 pressure drop data is shown in Figure 2.1-7. In this case, three pellets remained intact in tight contact with the cladding at the upper end of the segment between the plenum and the burst opening as shown by the gamma scan insert in Figure 2.1-5 (column labelled 9). Assuming the stack length restricting gas flow to be 3 cm, the derived hydraulic diameter, about 25 μm , is typical of HBU.

Transferring the observation of severely restricted gas flow to HBU LOCA behaviour means that (parts of) the fuel stack will hinder gas flow as long as general cladding distension has not opened the fuel-clad gap. In this situation, ballooning will be driven by the locally available gas and gas pressure.

Khvostov [2.1-4] evaluated the impact with a model add-on to the Falcon code and concluded that there is in fact an impact in certain situations. He found that cladding burst can be delayed by up to about 1 min due to axial non-uniformity of gas pressure in a full-length PWR fuel rod where the peak power and balloon position is sufficiently away from the plenum.

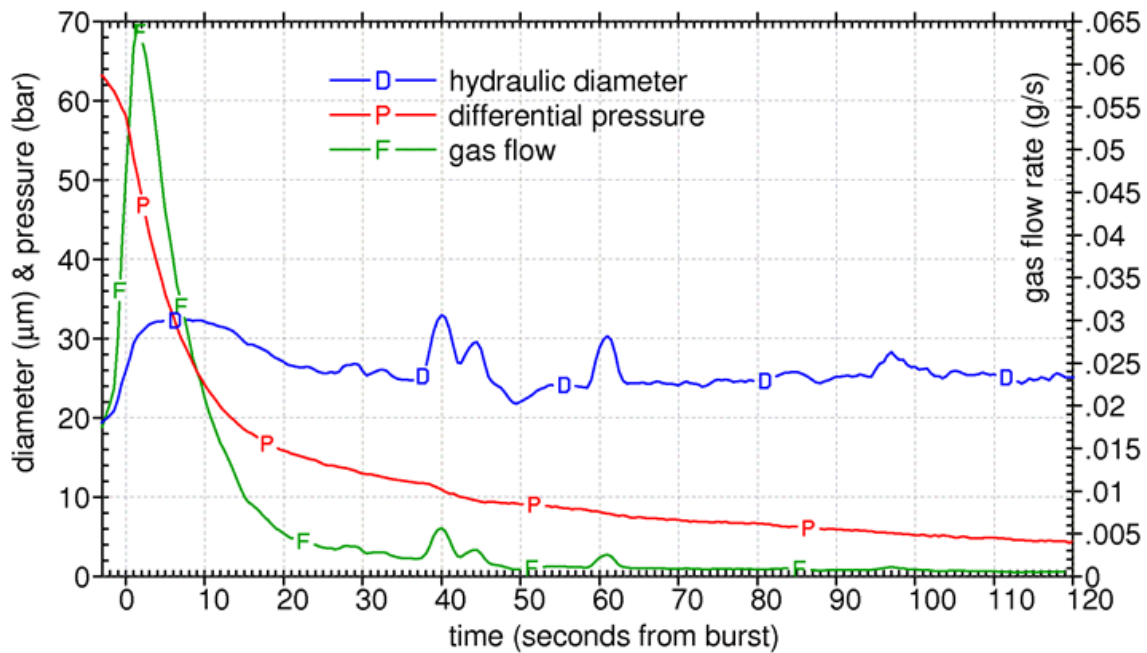


Figure 2.1-7: Hydraulic diameter derived from pressure change in test IFA-650.9

2.1.5 When does fragmentation occur?

The mechanisms driving fuel fragmentation are complex and not entirely clear. Effects with a possible influence on fragmentation are discussed in Chapter 3. The question whether fuel fragmentation requires burst of the cladding tube, or at least is influenced by the sudden loss of counter-pressure on burst, was addressed in one of the IFA-650 LOCA tests in the Halden reactor.

The comparison with sibling fuel tested in the same way except that the cladding was allowed to burst, did not show a qualitative difference on the neutron radiography level of resolution, Figure 2.1-8.

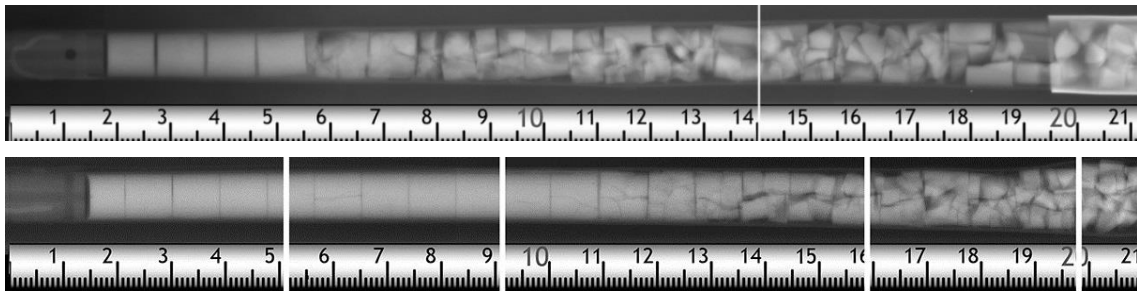


Figure 2.1-8: Comparison of fragmentation in LOCA tested fuel with (upper part) and without (lower part) cladding tube burst

Sifting of the fragments confirmed the similarity, but a slight tendency to somewhat more fine fragmentation in conjunction with burst cannot be excluded. However, the data are too limited to allow drawing a firm conclusion. Particles greater than 4 mm yield by far the largest amount by weight. Particles < 0.125 mm have as much weight as all the fragments with size 0.125–1 mm together for 650.13 and 650.14. The data are shown in Table 2.1-1.

Particle size mm	Fuel weight (g)			Normalised weight fraction (%)		
	650.12	650.13	650.14	650.12	650.13	650.14
>4	139.26	172.405	133.246	97.78	99.18	98.03
4 – 2	2.68	0.017	1.486	1.88	0.01	1.09
2 – 1	0.19	0.028	0.047	0.13	0.02	0.03
1 – 0.5	0.16	0.233	0.164	0.11	0.13	0.12
0.5 – 0.24	0.08	0.239	0.199	0.06	0.14	0.15
0.25 – 0.125	0.04	0.211	0.160	0.03	0.12	0.12
<0.125	0.01	0.695	0.628	0.01	0.40	0.46
total sieved	142.42	173.828	135.930	100.00	100.00	100.00
blocked fuel	n/a	18.972	45.570			
total weight	n/a	192.800	181.500			

Table 2.1-1: Fuel weight and normalised weight fraction depending on particle size

2.1.6 Axial fuel relocation

Axial fuel relocation requires a certain distension of the cladding such that the pellets and pellet fragments become detached from the cladding and moveable. The neutron radiographies show axial gaps in the upper part of IFA-650.12, 650.13 and 650.14 of 10 – 15 mm length for the three high burnup Boiling water reactor (BWR) segments (Figure 2.1-9). The size of the major fragments (≥ 4 mm) and the burst openings (≤ 2 mm) exclude the possibility that the missing fuel was ejected. The shrinking fuel column must therefore have expanded laterally into some of the increased space created by cladding distension.

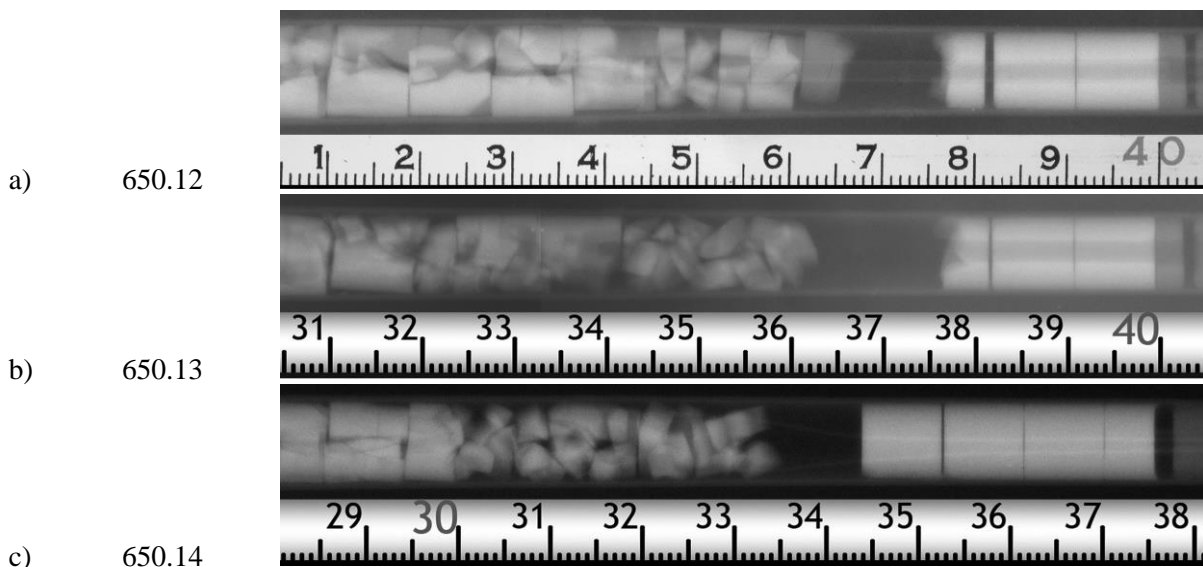


Figure 2.1-9: Axial fuel relocation at the upper end of the test segments in Halden tests
a) 650.12, b) 650.13 and c) 650.14

The analysis of the neutron radiographs showed that the fuel moved laterally where the cladding distension exceeded about 20%. The resulting filling ratios were 60%, 61% and 55%, and the average mass increase 12%, 12% and 8% for IFAs-650.12, 13 and 14, respectively.

2.1.7 Summary of IFA 650 LOCA test results

Fuel fragmentation is not an obvious function of a single parameter. The qualitative impression from eleven HRP LOCA tests with burnup from 44 to 92 MWd/kgHM is that up to about 60 MWd/kg, fragmentation is more or less caused by the cracking during normal operation.

The test segments with burnup of 72 MWd/kg and higher showed additional fragmentation which progressively affects more and more of the pellet as burnup increases. The formation of HBS fuel plays an important role in this context (see also Chapter 3.1.2).

Another important influence on fuel fragmentation seems to be cladding distension. Where the pellets stay in contact with the cladding, they can remain quite unaffected by the LOCA transient and even form a plug that hinders gas flow and limits the amount of fuel available for relocation and dispersal. It can be surmised that such plugs will form underneath the spacers of a long fuel rod. At the same time, the driving force (gas flow) for fuel expulsion on cladding burst is diminished.

Axial fuel relocation was limited in most cases except two with extreme burnup (90 – 92 MWd/kg). For cases with lower burnup and coarse fragments, a maximal local mass increase of about 10% in the balloon area could be deduced. However, this result is probably affected by handling and transport which cause fuel relocation in addition to the situation that developed in-core during the test.

2.2 Tests at STUDSVIK

2.2.1 The NRC LOCA tests on high burnup fuel

The NRC LOCA test programme at Studsvik had the objective of investigating the strength and ductility of HBU rods after ballooning, rupture, oxidation and quench. The results of the test programme focusing on these original objectives are reported in [2.2-1]. The fine fragmentation and dispersal observed in the first four Studsvik tests was unexpected. In response to the findings NRC carried out an extensive review of past experimental programmes [2.2-2]. Furthermore, a detailed report of the results of the Studsvik LOCA tests with focus on fuel fragmentation and dispersal was also published [2.2-3].

For the NRC LOCA programme Studsvik designed and built an integral LOCA test apparatus for in-cell testing of irradiated fuel rods [2.2-4]. The design of the apparatus is originally from Argonne National Laboratory (ANL). The LOCA apparatus is designed to heat up a 30 cm long refabricated fuel test segment up to 1 200°C using an infra-red radiation furnace. The test segment temperature is measured by a thermocouple attached to the rod 50 mm above the axial mid plane. The test segment is pressurised by helium and the pressure is measured outside the furnace both above and below the fuel stack. The test rod is placed in a quartz glass chamber in a flowing steam environment with controlled steam flow.

The LOCA apparatus is shown in Figure 2.2-1 during commissioning tests before it was placed in the hot cell. The test apparatus was thoroughly benchmarked and qualified through an extensive series of oxidation tests performed on un-irradiated Zry-4 cladding tubes [2.2-5].

In the integral LOCA tests performed in the NRC programme the fuel segment was pressurised to 80-110 bars and heated with a 5°C/s heat-up ramp. At 650-750°C the rod ballooned at the axial mid plane and ruptured. The heating ramp was then continued to 1 100 – 1 200°C and held there for a predetermined time to obtain the desired level of oxidation. After the high temperature oxidation the temperature was decreased by 3°C/s to 800°C and then quenched by room temperature water which fills the chamber from the bottom up.

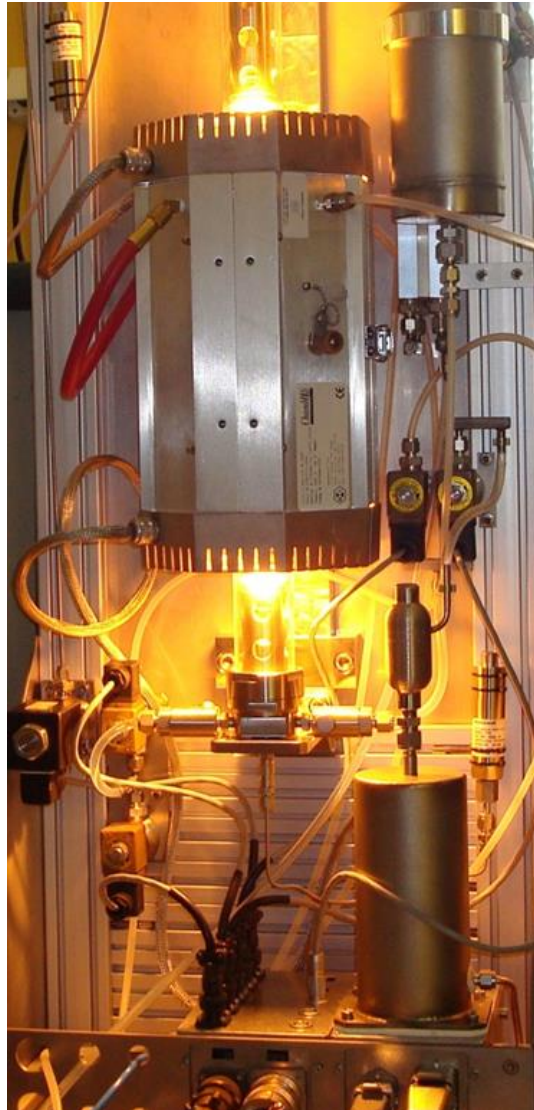


Figure 2.2-1: The Studsvik LOCA test equipment

A plot of the temperature and pressure history from one of the in-cell tests is shown in Figure 2.2-2. The post-test examinations included visual inspection, profilometry, 4-point-bend testing of the ruptured segment, evaluation of the equivalent cladding reacted (ECR) by metallographic examinations and determination of the hydrogen content by hot vacuum extraction (HVE).

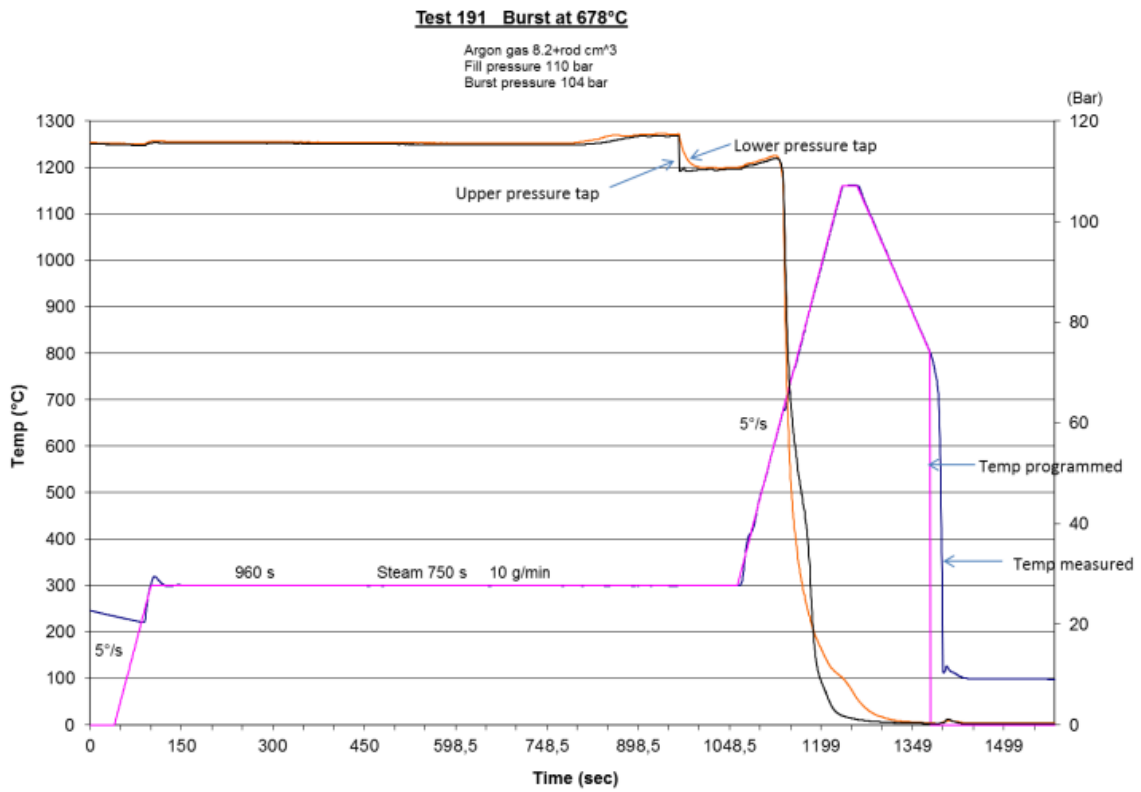


Figure 2.2-2: Temperature and pressure history of a LOCA test in cell [2.2-4]

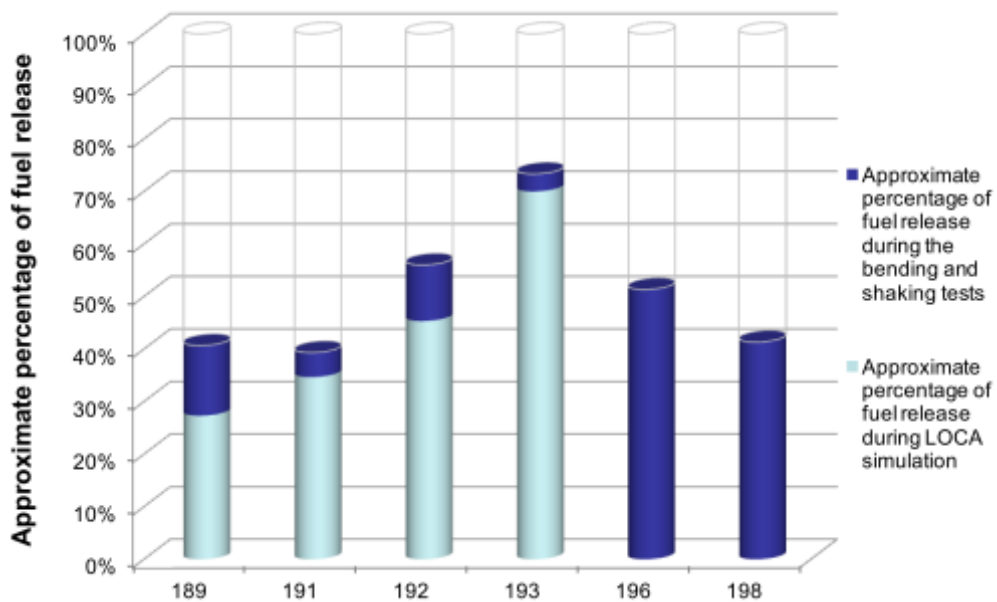


Figure 2.2-3: The fuel loss during each test (from [2.2-3])

Four integral LOCA tests were performed on irradiated high burnup PWR fuel segments. The rod average burnups of the father rods were ~70 MWd/kgU. Each of the tests resulted in a large ballooning strain, large rupture opening and significant fuel dispersal into the quartz glass tube. The fuel was weighed

before and after the LOCA test, after the 4-point bend test and after shaking the broken rod halves. The voided length of the fuel segment was measured after the LOCA test and after the bend test and shaking of the broken halves.

The total fuel loss after LOCA test and after the bend test and shaking is illustrated in Figure 2.2-3, [2.2-2]. A large fraction of the total fuel loss dispersed already at the time of rupture in the LOCA test. The fuel loss was in the form of powder and fine fragments much smaller than the typical size of fragments encountered after normal operation. The conclusion was that the LOCA test caused the observed fine fragmentation/powderisation.

A second campaign of LOCA tests were performed on two PWR fuel rod segments. The rod average burnup of the father rod was ~55 MWd/kgU. In each of the two LOCA tests the cladding ballooning strain was small, the rupture opening was small and there was no dispersal of fuel.

After the bend test, break of the fuel rod and shaking of the rod halves, the total fuel loss was measured and the pieces collected. Almost all of the fuel consisted of large fuel fragments greater than 4 mm diameter consistent with the fuel cracking observed in normal operation. A summary of the test data for all six tests performed in NRC programme are given in Table 2.2-1.

Test	Father rod average burnup [MWd/kgU] (Segment average burnup)	Rod internal pressure [bar]	Rupture temp [°C]	Max strain [%]	Rupture dimensions (width/length) [mm]	CP-ECR [%]	Fuel mass loss (during test / after bend test and shake) [g]
189	68.2 (72)	110	700	48	10.5 / 23.9	0	41 / 61
191	69.3 (75)	110	680	50	17.5 / 21.6	13	52 / 59
192	68.2 (78)	82	700	56	9 / 22.7	11	68 / 84
193	69.3 (76)	82	728	50	13.8 / 17.8	17	105 / 146
196	55.2 (61)	82	686	25	0.2 / 1.5	0	0 / 79
198	55.2 (60)	82	693	25	1.6 / 11	15	0 / 66

Table 2.2-1: Summary of test data from the six NRC LOCA tests from [2.2-3], [2.2-4] and [2.2-7]

Sieving of the collected fuel fragments was performed to determine the size distribution of fuel fragments. The size distribution of the total fuel mass loss is shown in Figure 2.2-4. The size distribution clearly shows a characteristic difference between the 70 and 55 MWd/kgU (father rod average) rods.

The 70 MWd/kgU fuel shows a significant fraction of very small fragments less than 0.125 mm diameter. These fine fuel fragments, essentially powder, were analysed by SEM and LA-ICP-MS to determine the radial origin of the fragments [2.2-8]. The analysis showed that the small fraction of powder from the ~55 MWd/kgU sample predominately originates from the HBS at the fuel periphery. For the sample with high burnup ~70 MWd/kgU, the fine fragments appear to originate from almost any radius, not only from the fuel periphery.

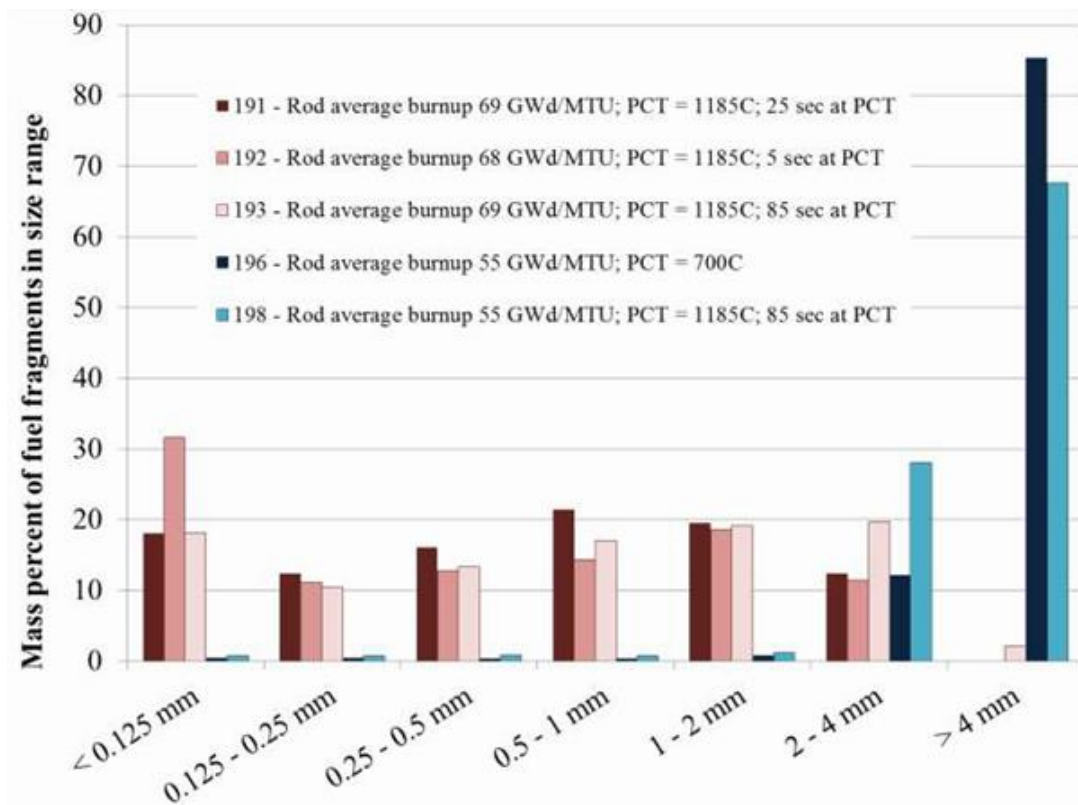


Figure 2.2-4: The size distribution of the fuel fragments collected from the samples tested in the NRC LOCA test programme. The results show a characteristic difference in fragmentation size between 70 and 55 MWd/kgU rods (from [2.2-6])

2.2.2 The EPRI heating tests

The test data generated by Halden and Studsvik NRC tests indicated the existence of a fuel fragmentation threshold below which there would be negligible fine fragmentation. To generate additional data to characterise the threshold a simplified separate-effects test was developed by EPRI. The test involves heating of a short section of fuel with an axial slit in cladding [2.2-9].

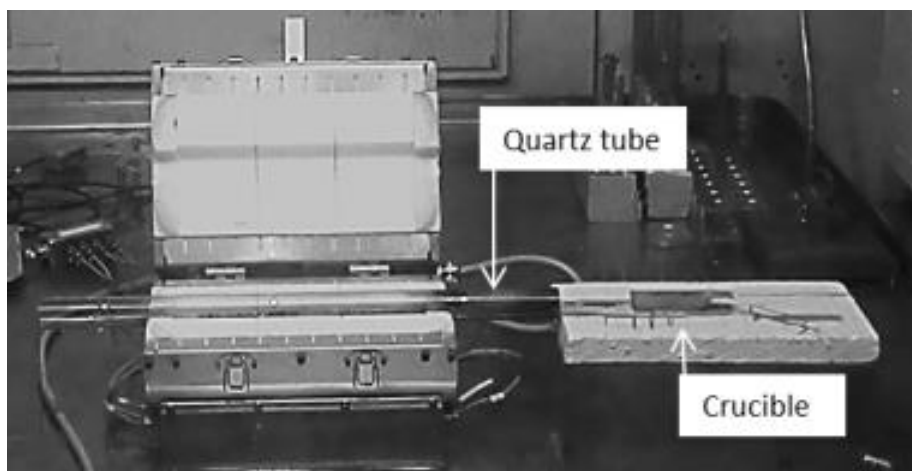


Figure 2.2-5: The tube furnace used for separate effects heating tests at Studsvik [2.2-9]

A standard tube furnace, as shown in Figure 2.2-5, equipped with a quartz tube and pre-heated to 1 000°C was used for the tests. Apart from a few of the early scoping tests, the samples have been tested with a thermocouple attached to the sample by an Inconel clamp.

Three types of tests were performed:

- Test samples were inserted from room temperature into the furnace preheated to 1 000°C in air and withdrawn after reaching 1 000°C.
- Test sample from neighbouring position of parent rod was inserted into furnace preheated to 1 000°C in an inert cover gas and withdrawn after reaching 1 000°C.
- Test samples were inserted into the furnace preheated to 1 000°C and withdrawn at different test sample temperatures. The heat-up rate decreases with increasing sample temperature, but up to around 800°C the average heat-up rate is $\sim 20^{\circ}\text{C}/\text{s}$.

Samples from the same parent rods as used in the high burnup LOCA tests in the NRC programme were tested with and without an axial slit of the cladding. The samples were visually observed during the heating test. The sample with the slit started to show gas release and fuel fragmentation at 550°C and it was complete at around 850°C. There was no evidence of gas release from 850°C to 1 000°C.

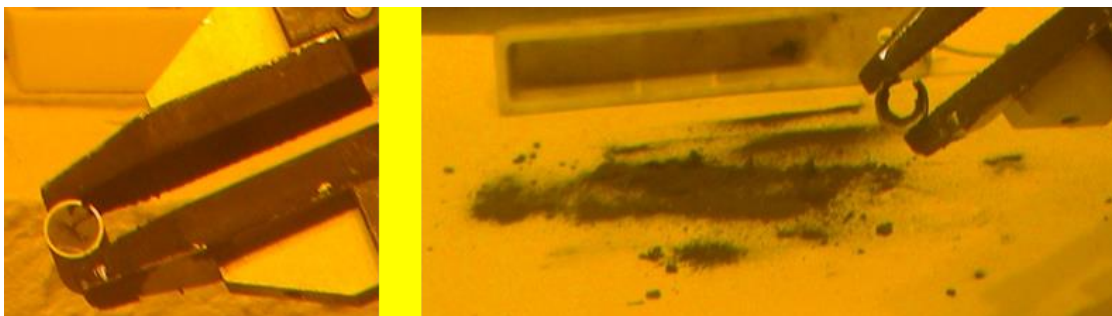


Figure 2.2-6: Sample held by manipulator fingers before and after test. In the right figure ejected fuel debris is shown on the white paper in the background [2.2-9]

Samples with intact cladding, i.e. without the axial slit, survived the heating test with only minor fuel loss at the sample ends. Metallography was performed on samples without slit. The heating test caused many fine cracks to occur in the inner restructured “dark” zone. The HBS at the periphery, however, did not fragment in the heating test, most probably because of the compressive stress induced by the cladding restraint.

The results indicate that the fine fragmentation is not only associated with the high burnup rim structure. Fine fragmentation may occur at the rim, but it may also occur further inside the pellet.

In order to rule out that oxidation of the fuel had an effect on fragmentation in the heating tests, a heating test was performed in an Argon inert atmosphere. The high burnup sample showed similar fragmentation and mass loss as the samples heat treated in air. This shows that oxidation of the fuel during a few minutes of heat-up has no or very little effect on the degree of fuel fragmentation for HBU.

A sample taken from the rod in the NRC test programme with a rod average burnup of ~ 55 MWd/kgU showed very little fragmentation in the heating test. It could be concluded that the fragmentation behaviour observed in the heating tests agreed with behaviour observed in the NRC LOCA tests. This showed that the straightforward heating tests could be used to determine the fragmentation threshold as a function of sample properties, such as local burnup and power history.

Heating tests to different target temperatures of 650, 750, 800 and 850 °C were performed in the EPRI programme [2.2-9]. This provided data on the temperature threshold for fragmentation. The fuel loss

increased with increasing temperature. The tests indicated that the temperature threshold for fragmentation of the samples was 750°C. Below this temperature no significant fuel fragmentation occurred.

Another observation in [2.2-9] was that samples taken at different axial positions on the same fuel rod, and therefore having somewhat different burnup and power history, showed a notable difference in their degree of fragmentation. This indicated that the local power may also be an important parameter for fragmentation.

2.3 CEA tests related to FFRD

2.3.1 *Integral tests, the FLASH programme*

Within EDF, IRSN and CEA collaboration, between 1977 and 1985, five LOCA transient tests have been conducted in the SILOE test reactor. The main purpose of those tests was to study the release of the fission products from the rods, during such an event. Details on these tests and on their main outcomes can be found in [2.3-1] and [2.3-2].

The first four tests, FLASH 1 to FLASH 4, were performed, starting from a stack of 30 cm of un-irradiated fuels, but pre-irradiating them in SILOE, in a specific pressurised loop at 13 MPa and a linear heat rate around 35 kW.m⁻¹. These pre-irradiations led to burn ups between 1.6 and 3.3 MWd/kgU.

The last test, FLASH 5, used a 50.3 MWd/kgU rodlet, refabricated from a commercially PWR rod irradiated four cycles with an average rod burnup of 47 MWd/kgU. Prior to the test itself, this rod was irradiated for three weeks in SILOE in a rig at 13 MPa and a linear heat rate around 18 kW.m⁻¹ so that short-lived fission products were present during the LOCA test itself. With the additional SILOE irradiation, this fuel burnup was 51.7 MWd/kgU.

Those tests themselves were started by adjusting the linear power to ~7 kW/m. Then the coolant was expelled while the loop pressure was reduced. The cooling procedure was not the same for all tests, depending on the procedures for collecting the released fission products or for scanning the deposits on the loop component, in test FLASH-4, for example, the power was kept for 10 min after reflooding to maximise fission product transfer into water. In tests FLASH-1 and FLASH-2 the maximum temperature reached in the cladding was 1 100 and 1 120°C respectively. In tests FLASH-3 and FLASH-4, it was 1 270°C. For all these very low burnup fuels, no fragmentation was detected that could be attributed to the LOCA test itself. In addition no noticeable axial relocation of the pre-existing fragments was detected.

The 51.7 MWd/kgU fuel used for FLASH-5 was a 3.1% 235U enriched UO₂ fuel irradiated for four cycles in the Fessenheim 2 reactor. The average irradiation power, for the segment used for this test, was in the range of 17 kW/m, except during the second cycle (22 kW/m). The entire rod puncturing showed that the average FGR was 0.41% of the total production. Examination on a sibling rod showed no sub-micrometric bubble formation in the central area. However, HBS was observed at the periphery.

The tested fuel length was 30.1 cm, the plenum length was 13.85 cm, corresponding to a volume of 6.7 cm³. This large plenum volume was decided aiming to obtain a large balloon strain. It was filled with 3.2 MPa He. The cladding was Zircaloy-4.

The accidental sequence was:

- adjustment of the linear power to 7.2 kW/m
- depressurisation of the loop from 12.4 MPa to 0.5 MPa
- removal of the water. This took 4 s
- as a consequence, the fuel and cladding temperatures raised. The linear power also increased to reach 8.8 kW/m

- The clad temperature rise was measured around 42°C/s during the first 16 s of the rise, then of about 26°C/s during the following 19 s, before the reflooding. During this period, the rod burst occurred when the clad thermocouples average measurement was 995°C .
- The reflooding started when the warmer measurement reached $1\,150^{\circ}\text{C}$. However, before the thermocouple level was reached by the water, the maximum clad temperature measurement reached $1\,345^{\circ}\text{C}$ while the average value was $1\,270^{\circ}\text{C}$.
- After reflooding and before reactor scram, the irradiation power was kept constant for 12 minutes at 7.2 kW/m with pressure below 1.2 MPa .

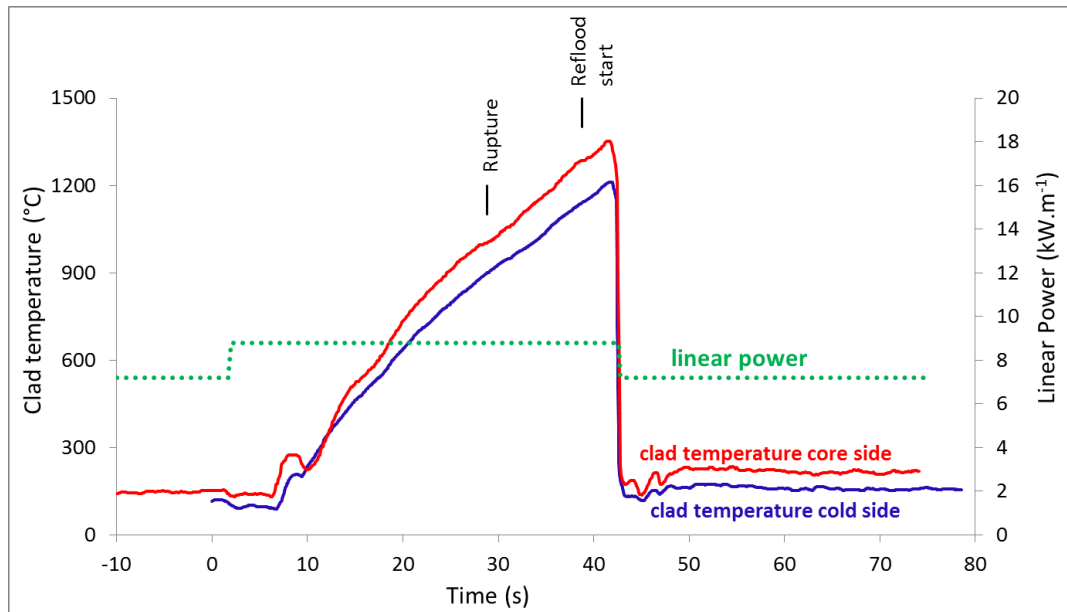


Figure 2.3-1: FLASH-5, clad surface temperature history for the thermocouple on the side towards the core and for that on the opposite side.

Figure 2.3-1 shows the temperature measured at the surface of the cladding with the thermocouple on the side towards the core and with that on the opposite side.

Considering the power generated in the pellets and the poor knowledge of the history of the gap width during the test, the centreline temperature evaluation is likely to have a high uncertainty. The evaluation performed after the test was that the central temperature had reached $1\,600^{\circ}\text{C}$ to $1\,650^{\circ}\text{C}$ with a temperature rise between 30°C/s and 35°C/s .

The rod failure occurred 93 mm above the maximum power plane, on the warmest side of the cladding, i.e. on the side turned towards the core of the reactor. It was a ductile failure. The local mean strain was of 16%. In the maximum power area, the strain was around 7%.

A radial cut, performed at the maximum power plane showed that fragmentation had occurred in the central part of the pellet (Figure 2.3-2 a) and Figure 2.3-3). It was measured that the grain size, in this central part had significantly grown, from $\sim 7.5\ \mu\text{m}$ to $\sim 14\ \mu\text{m}$. The fuel fragmentation and the grain growth were understood as to have occurred mainly during the period when the rod was opened, the loop reflooded, but the irradiation power was still at 7.2 kW/m , before the scram. The mechanisms considered implied oxidation of the UO_2 by water steam at temperatures above 800°C . No major axial movement was found in that area.

Fragmentation had also affected the rim of the pellet, at the maximum power plane, forming small HBS fragments, below $20\ \mu\text{m}$, but also large ones, above $100\ \mu\text{m}$ (Figure 2.3-4 a).

At the cladding rupture level, more fragment relocation was found, but no central fragmentation was observed. At the periphery, HBS fragments can be found bound to the cladding through internal zirconia, in a few places (Figure 2.3-4 b), but most of it appeared to be missing (Figure 2.3-2 b). It does not seem to have been still present at the surface of the peripheral fragments, so that HBS fragmentation must have also occurred at this level.

Above the rupture level (Figure 2.3-2 c) where the rod strain was very small, no fragmentation was observed, not even at the rim of the pellet (Figure 2.3-4 c).

The opening of the cladding was only a thin slit (3 mm long, 0.3 mm wide). 103 Ru and 140 Ba gamma-scanning measurements on the rig and water storage vessels after fuel rod removal showed that less than 90 mg of fuel had left the rod, less than 0.05% of the fuel. Part of this departure was certainly due to the reflooding period.

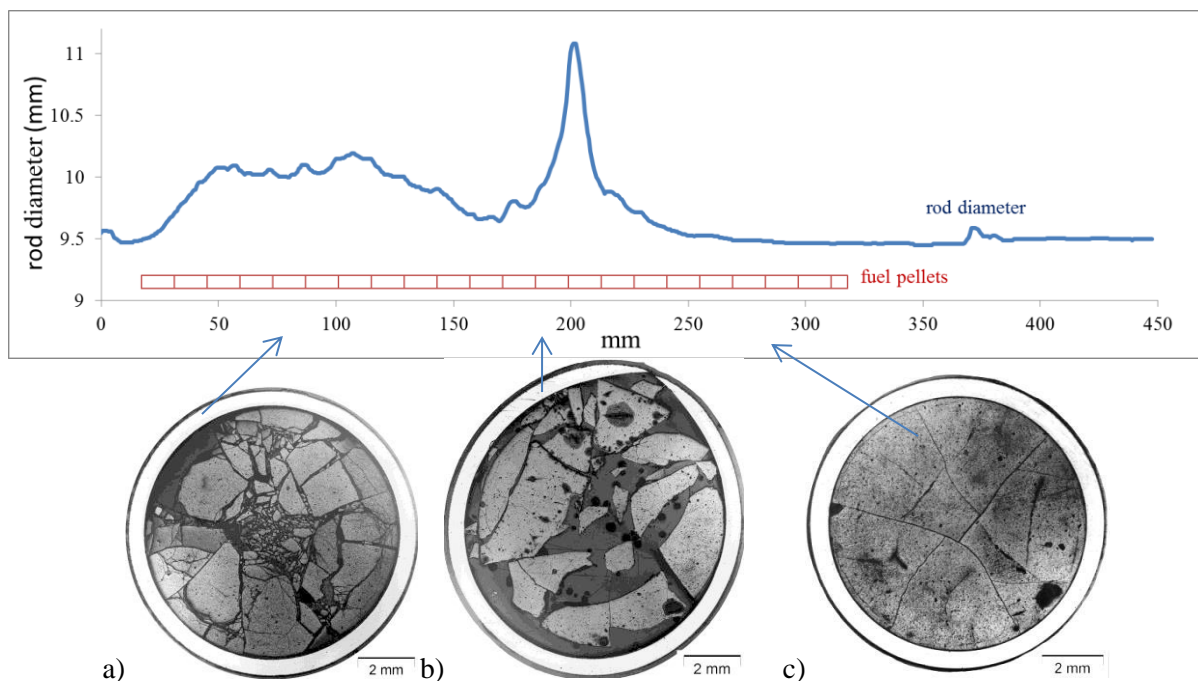


Figure 2.3-2: FLASH-5, rod diameter and radial cuts, a) maximum power level, b) clad rupture level, and c) above rupture.

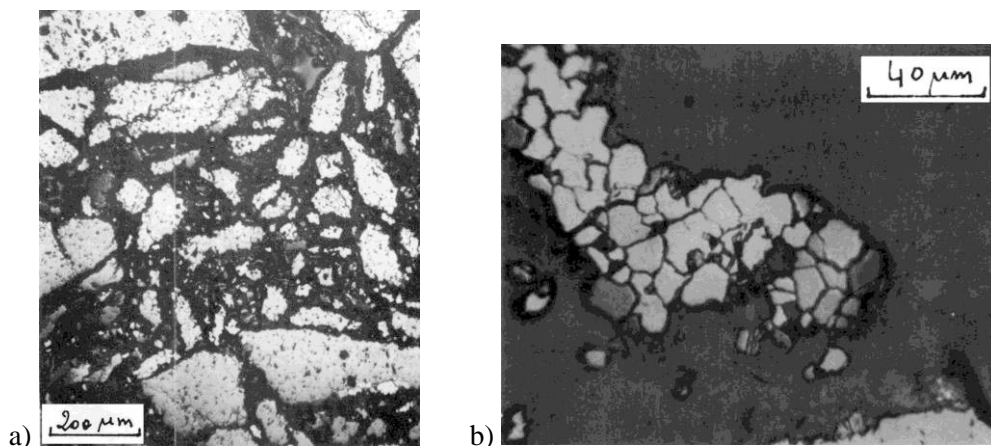


Figure 2.3-3: FLASH-5, details in the central area at maximum power level.

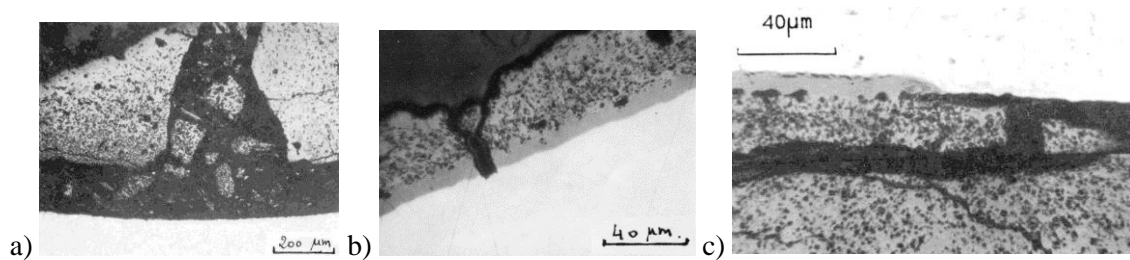


Figure 2.3-4: FLASH-5, periphery details a) maximum power level, b) clad rupture level, c) above rupture.

2.3.2 Out-Of-Pile heating tests

After the FLASH programme, the study of the release of fission products during LOCA type accidents went on but using out-of-pile heating tests on irradiated fuels. The "Gaspard" programme, involving EDF and the CEA, was partly reported in [2.3-3] and [2.3-4]. It was followed by a series of similar out-of-pile heating of irradiated fuels within EDF-AREVA-CEA collaboration. Some of these test results have been published in [2.3-5] and [2.3-6].

All these tests have been performed in circulation furnaces (Figure 2.3-5). These high frequency (50 kHz) induction furnaces were located in hot cells and were coupled with an on-line gas release measurement. The gas used in the circulation furnace, and therefore surrounding the sample, was argon with a pressure close to 0.1 MPa. The main measurement was an online gamma spectrometry of the released gas.

The furnace consists in a metallic crucible (on the centreline of the coil) in which the fuel sample is located.

Most of these tests have been performed on an open segment of fuel corresponding to the length of one pellet, with its cladding. Immediately prior to some of the tests, short low linear power re-irradiations induced the build-up of short-lived fission products such as ¹³³Xe in intra-granular position.

Within the NFIR programme, other tests have been conducted on fuel discs, without cladding, irradiated in the Halden reactor [2.3-7], [2.3-8].

The tests started by rising the sample temperature to 300°C. That temperature was maintained while checking that all instrumentation was operating. The sample was then heated again until its temperature reached 1 200°C. The most typical ramp rates used were 20°C/s and 0.2°C/s (Figure 2.3-6). The purpose of the low ramp rates was to allow establishing a link between the temperature histories and the release histories. The maximum temperatures was typically held for 10 min to 15 min, but for a few tests the cooling period started immediately when 1 200°C was reached.

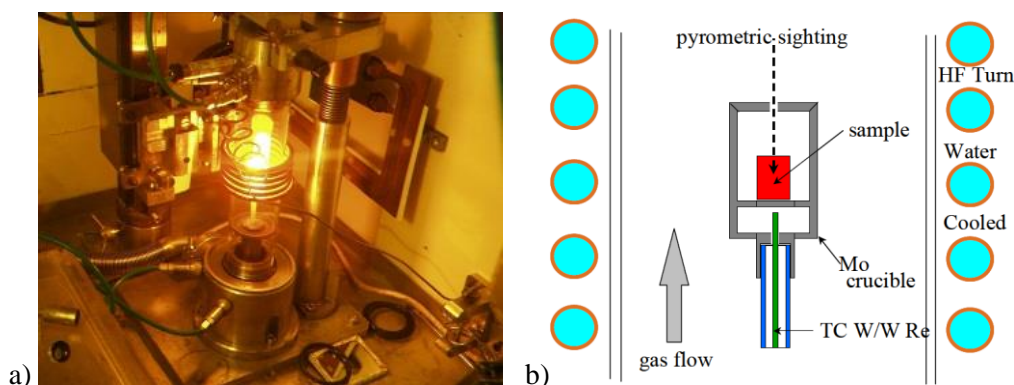


Figure 2.3-5: a) Furnace view and b) Principle.

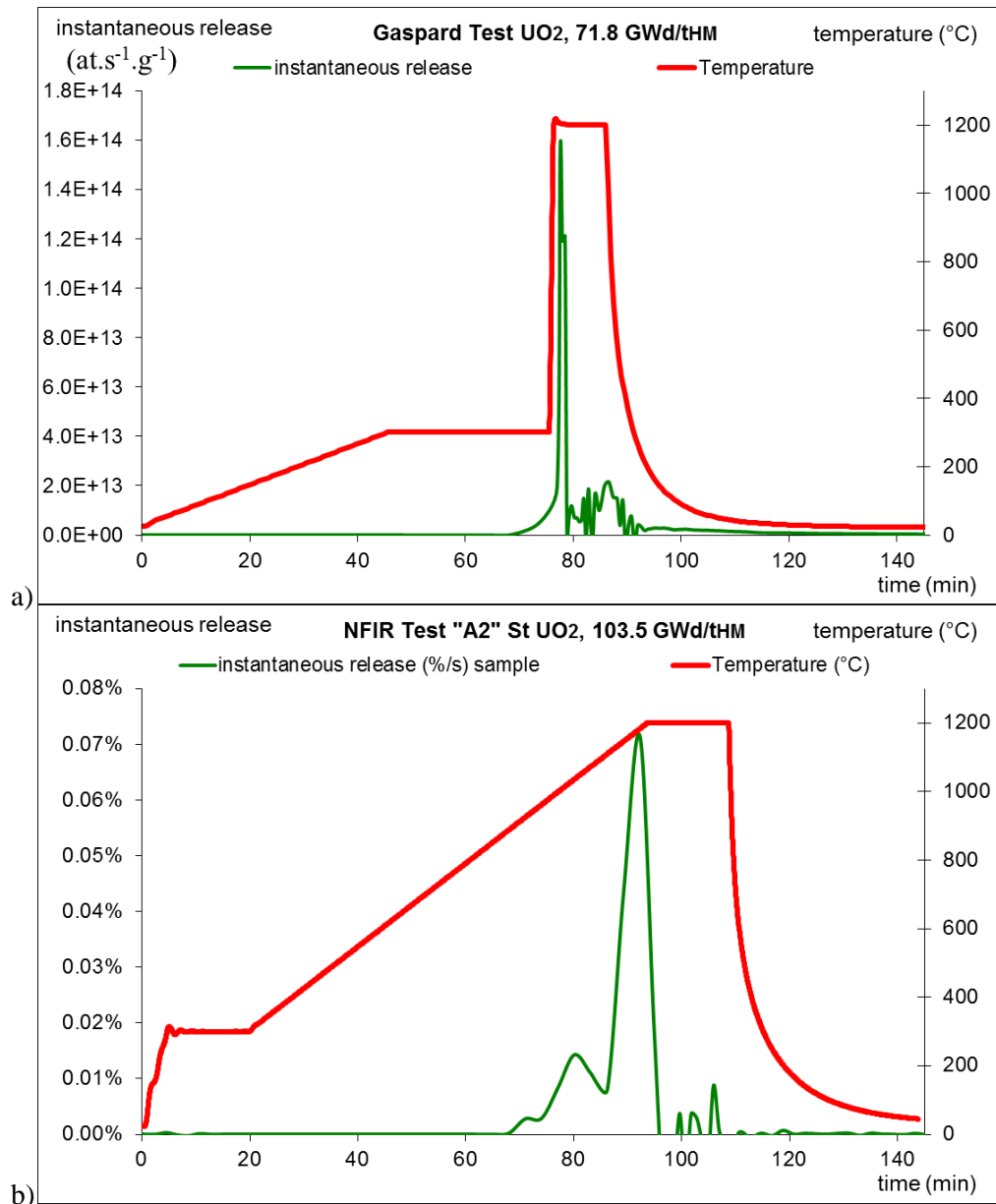


Figure 2.3-6: Examples of temperature and FGR histories during heating tests a) within the Gaspard programme and b) within the NFIR programme

Figure 2.3-7 gathers post-test examinations of some of those fuels. In Figure 2.3-7 a) and Figure 2.3-7 aa), 71.8 MWd/kgU after a 1 200°C ramp at 0.2°C/s shows the formation of a thin network of cracks in the central part of the pellet, in an area where high irradiation temperatures and high burnup led to the formation of inter-granular and intra-granular sub-micrometric to micrometric bubbles.

In Figure 2.3-7 b) and bb), a neighbour sample, submitted to the 20°C/s test with the Figure 2.3-6 a) history, exhibited less cracking in the central part. In both cases, cracks due to the test were found in the HBS at the rim of the pellet.

In Figure 2.3-7 c), a thin crack network can be seen in MIMAS MOX fuel sample with a local burnup of 52.4 MWd/kgHM after a ramp at 20°C/s.

These samples being open at both ends, there is no ballooning effect. In spite of the cracking and of the high temperatures (1 200°C), no major fuel departure was observed.

Figure 2.3-8 shows fragments formed during the Figure 2.3-6 b) history using a 103.5 MWd/kgU UO₂ disc fully transformed in HBS. As it can be seen in Figure 2.3-6 b), the main release peak was when the temperature of the sample was between 1 110 C and 1 200 C.

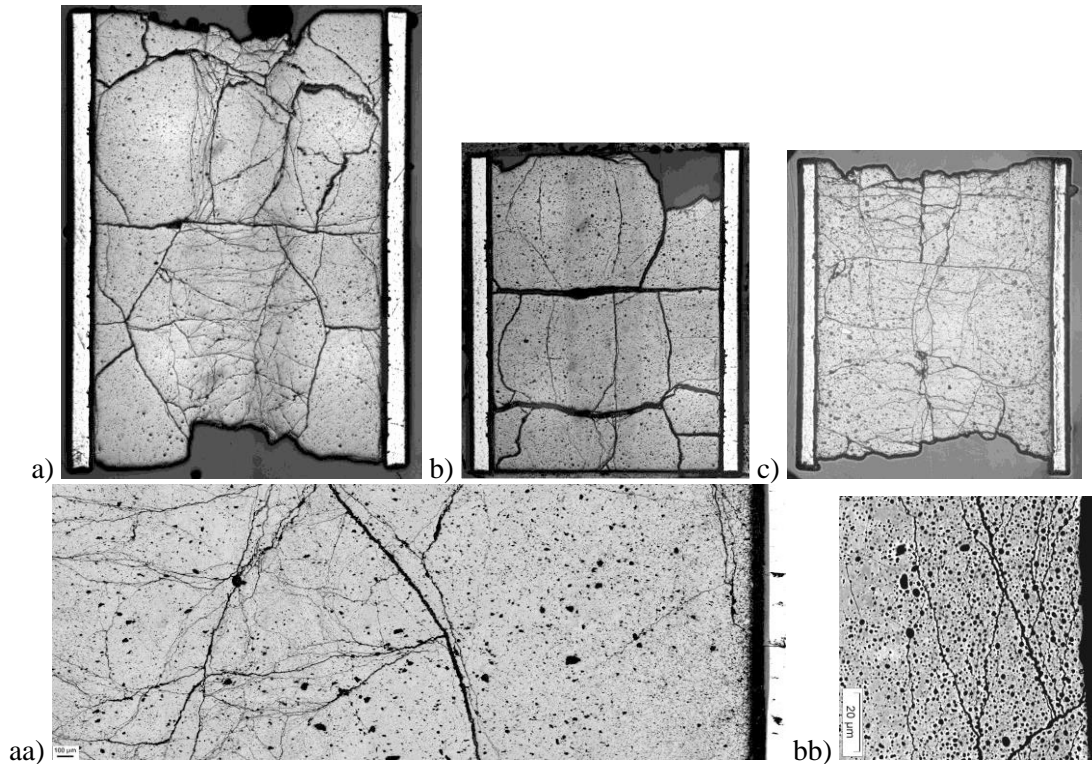


Figure 2.3-7: Examples showing the state of the fuel after 1 200°C heating tests a) and aa) UO₂ fuel with a local burnup of 71.8 MWd/kgU after a ramp at 0.2°C/s, b) and bb) same fuel after a ramp at 20°C/s, c) MIMAS MOX fuel with a local burnup of 52.4 MWd/kgHM after a ramp at 20°C/s

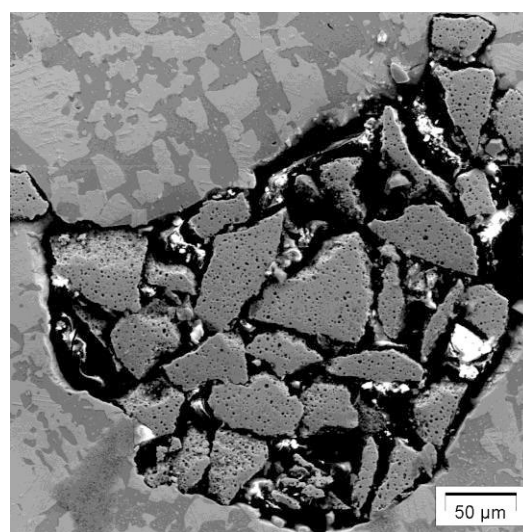


Figure 2.3-8: Examples showing the fragmentation of an IFA 649 103 MWd/kgHM UO₂ fuel disc after a 0.2°C/s, 1 200°C heating test

In addition to those heating tests performed on pellet size samples, a particular test was performed in a completely different way, using the heating stage of a SEM to bring a very small sample of HBS to 1 330°C under vacuum [2.3-9]. This HBS fragment had been mechanically extracted from the rim of 83 MWd/kgU UO₂ fuel, so that the burnup of this fragment was estimated to be 140 MWd/kgU. No extra fragmentation, due to this heating, was detected (Figure 2.3-9).

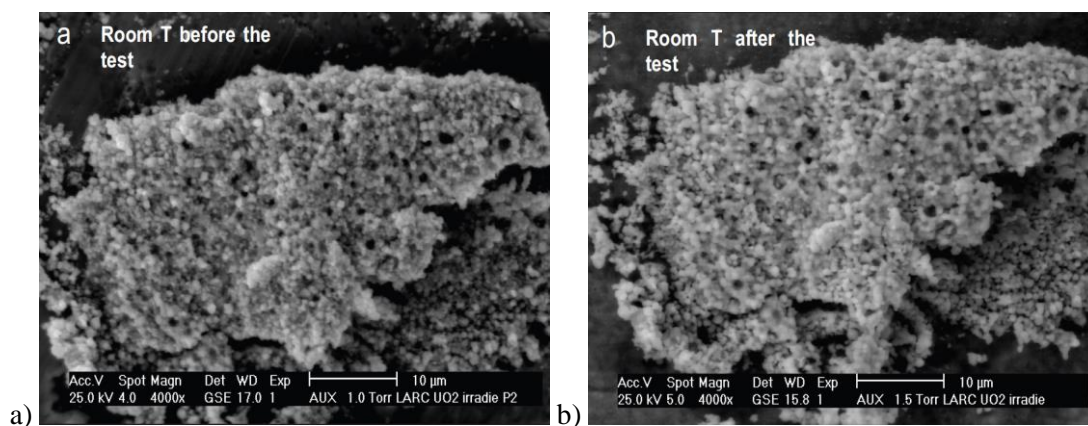


Figure 2.3-9: HBS fragment extracted in the rim of a 83 MWd/kgU UO₂ fuel slice so that the estimated fragment burnup was 140 MWd/kgU, a) before annealing, b) after a 1 330°C annealing in an SEM chamber

A segment from the same 83 MWd/kgU UO₂ fuel was also submitted to a temperature history similar to that of Figure 2.3-6 b), but before the test, the whole thickness of the cladding had been cut longitudinally. In that case, the fuel fragmentation led to a departure of the fragments out of the cladding section.

Also, the cladding was deformed and after cooling the cladding diameter had increased of about 15% as it can be seen in Figure 2.3-10, [2.3-10]. Before the test, it had been shown that this fuel had undergone a high fission gases precipitation into bubbles almost everywhere in the pellets, leaving only relatively small rings of fuel with low gas precipitation [2.3-11].

A similar test but without the initial cladding cutting has not led to such a fuel departure from the cladding section.

However, another sample from the same fuel, submitted to a similar 1 200°C heating test, but with a ramp rate of 20°C/s did exhibit fuel fragmentation, the fragments being found outside the cladding section inside the crucible, after the test. A detailed characterisation of fragments formed during this test showed that there were large fragments and small fragments and that all the large fragments came from the two rings in this fuel that had no, or only very little, gas precipitation before the test [2.3-12].



Figure 2.3-10: 83 MWd/kgU UO₂ fuel fragments that moved out of a pre-cut cladding after a 1 200°C heating test.

2.3.3 *Summary of CEA tests*

Setting apart the fragmentation observed in the central part of FLASH-5 and attributed to an interaction with water steam at high temperatures, all fragmentation, observed in these CEA tests, occurred in areas where fission gas bubbles visible with optical microscopy had formed. HBS at the periphery of the UO₂ fuels is clearly one of those areas, but not the only one.

The test temperatures, reaching 1 200°C and more, the fragmentation events can only be monitored through the release histories. The main release being found at temperatures above 1 000°C, for these tests where the samples are surrounded by ~1 bar Argon, it was deduced that the main fragmentation events occurred at these high temperatures. This observation is one of the reasons supporting the need to evaluate a possible effect of the fast pressure drop in the balloon in the integral tests where fragmentation occurred at lower temperatures.

2.4 **VVER fuel bundle tests related to FFRD**

Since 2001 A.A. Bochvar High-Technology scientific research Institute for Inorganic Materials (VNIINM) performed fuel rod bundle tests in the MIR research reactor to investigate the behaviour of HBU rods under LOCA condition. The experimental set-up consists of a hexagonal fuel rod bundle of 19 VVER-1 000 fuel rods surrounded by hexagonal shroud.

2.4.1 *MIR/LOCA test bundle*

The pellet stack inside the test rod is of 1 m height. The test bundle assembles irradiated and non-irradiated fuel rods. Test bundle of test MIR/LOCA-50 consists of 16 rods with fresh fuel plus 3 rods which have been refabricated from commercial fuel rod. The rod average burnups of these 3 rods are 47.2, 49.0 and 45.8 MWd/kgU. Irradiated rods in test MIR/LOCA-60 have burnups between 58.1 MWd/kgU and 58.6 MWd/kgU. The test bundle of test MIR/LOCA-72 contains among 18 non-irradiated rods one single rod with burnup of 76 MWd/kgU.

Cladding material is E110. During normal operation, this type of cladding experiences a low level of corrosion only. The refabricated fuel rod for test MIR/LOCA-72 stems from Kalinin NPP after 6 cycles of irradiation. This highly burned fuel rod developed an oxide thickness on cladding's surface of less than 10 µm and received hydrogen uptake into the cladding of less than 100 ppm. This refabricated fuel rod is of 9.08 mm outer cladding diameter, the total free volume is 8.5 cm³ and the filling gas is helium at 3.4 bars.

The VVER fuel pellet design with central hole allows placing thermocouples in the centre of the fuel rod, see Figure 2.4-1. The temperature history of test MIR/LOCA-50 is shown Figure 2.4-2. Maximum temperature of 930°C is reached at 2 500 seconds after start of heat-up with a heating rate of 0.3 K/s. In contrast to that MIR/LOCA-72 test approaches the maximum temperature with heat-up rate of about 4 K/s.

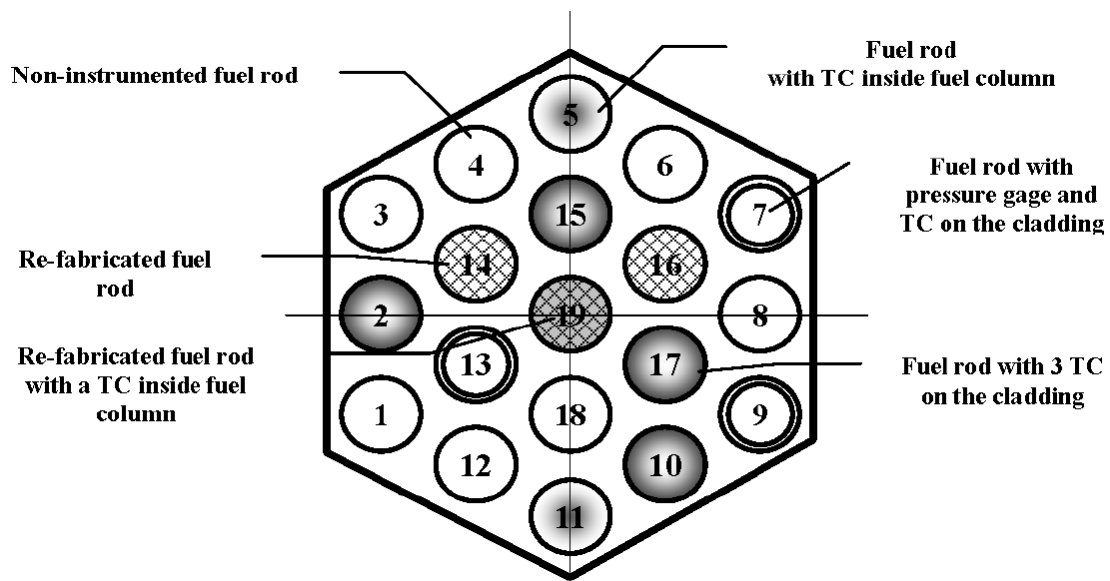


Figure 2.4-1: Thermocouple located in the fuel rod bundle in test MIR/LOCA-50 [2.4-3]

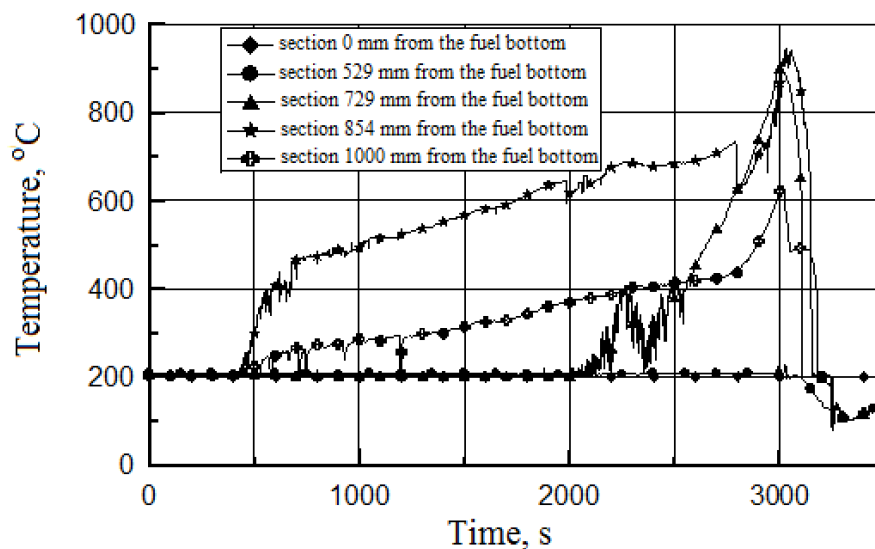


Figure 2.4-2: Temperature history in MIR/LOCA-50 test [2.4-3]

2.4.2 MIR/LOCA test results

In test MIR/LOCA-50 the cladding of refabricated rods did not burst although the hoop strain reached 25%. Whereas some fresh fuel rods showed 18% to 20% hoop strains at burst location.

Fuel pellets in test MIR/LOCA-50 (irradiated and non-irradiated) show radial cracks which are to be expected for radial temperature gradients. When comparing the microstructure appearance of fresh fuel against irradiated fuel, no significant difference can be observed, see also Figure 2.4-3.



Figure 2.4-3: Cross-cut of test assembly of MIR/LOCA-50 test at elevation 830 mm from bottom [2.4-3]

In test MIR/LOCA-60 the refabricated fuel rods reached hoop strains of less than 2% only. Fragmentation or even relocation was not observed in this test. Maximum cladding temperature was in the range of 700 to 800°C which allows a limited phase transition from α -to β -phase for E110 cladding only. Consequently, significant cladding hoop strain was not observed.

In test MIR/LOCA-72 maximum cladding temperature is of 1 070°C. This maximum temperature is reached at a heat-up rate of 3 to 5 K/s. When cladding temperature reached 741°C the refabricated fuel rod burst at two locations around the spacer grid at midlevel position, see Figure 2.4-4. Both burst openings are separated by the spacer grid. The maximum hoop strain is 36% at lower burst location.

Fuel with 76 MWd/kgU (segment averaged burnup) shows fine fragmentation mainly in the pellet periphery which allows significant axial relocation into the ballooned fuel rod region and furthermore it allows dispersal of fuel into coolant channel, please see fuel depletion at lower burst opening in Figure 2.4-4.

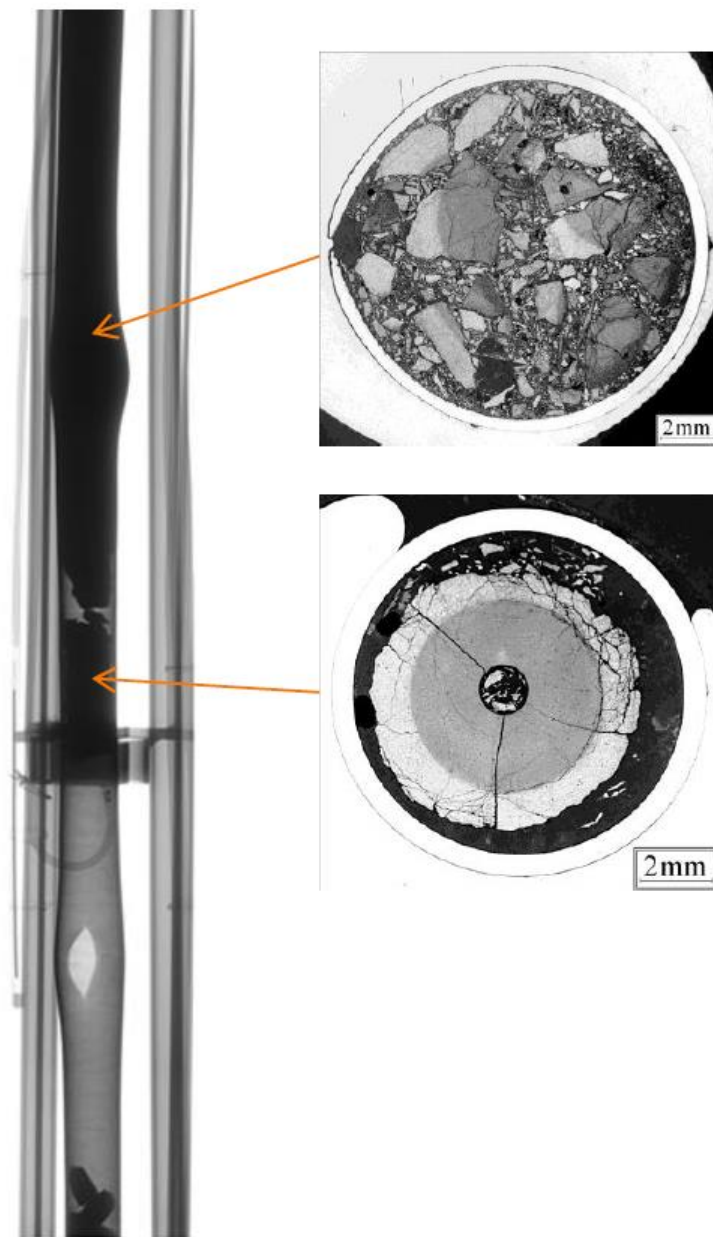


Figure 2.4-4: Scanning of test rod in MIR/LOCA-72 test (left) and cross-cuts (right) [2.4-3]

2.4.3 Conclusion from MIR/LOCA tests

VVER fuel with central hole reveals similar behaviour as fuel without central hole, that is, significant fuel fragmentation and consequently fuel relocation occurs if the pellet average burnup exceeds 70 MWd/kgU. These phenomena vanish for both burnup levels below 60 MWd/kgU and for hoop strain below 2%.

3. MECHANISM OF FUEL FRAGMENTATION

As discussed above, fuel fragmentation is a term that can refer to any separation of the fuel pellet into more than one piece, regardless of when or why it occurred. During normal operation, oxide fuel pellets develop cracks to relieve thermal stresses. Experiments that subject fuel rods to transient conditions have revealed that additional fuel fragmentation into smaller pieces can take place during the transient. For the purposes of this report, the following definitions were established:

- Pellet cracking: coarse usual cracking due to (macro scale) thermal stresses appearing in the fuel pellet during normal operation or during power transients. Fragments sizes range from $\sim 500 \mu\text{m}$ to several millimetres, with large fragments concerning virtually all of the pellet mass.
- Pellet fragmentation: additional fragmentation specific to accidental conditions. This fragmentation is a result of specific micro- and macro- scales stresses induced by the transient within the fuel pellet. Fragments sizes range from $\sim 100 \mu\text{m}$ to $500 \mu\text{m}$. It is worth noticing that fragmentation can occur with or without subsequent axial or radial fuel fragments relocation. Figure 3-1 shows an example of fragmentation without axial fuel relocation despite significant fragmentation of the central part due to the LOCA transient.
- Pellet pulverising, powdering, or fine fragmentation: specific to high burnup pellet, the fragments sizes range from several μm to $100 \mu\text{m}$. In Table 3-1, fuel pulverising or powdering can be seen at the pellet periphery and at some locations in the pellet centre, without fuel axial relocation.

Thus, in the following, a difference will be made between fine fragmentation or powdering and fragmentation.

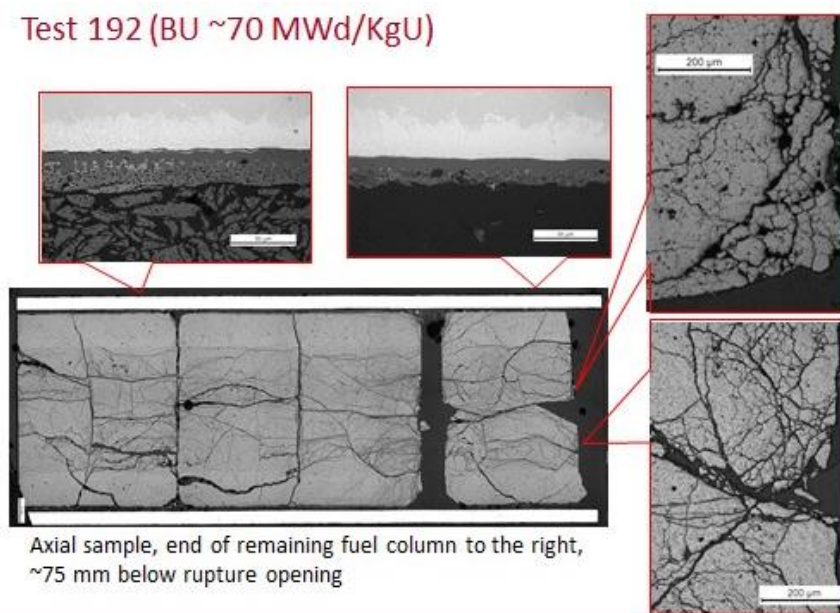


Figure 3-1: Ceramography of the 70 MWd/kgU (father rod average burnup) rod tested at Studsvik, after LOCA transient and shaking [3.1-1]

The table below includes micrographs of test segments before and after LOCA tests. The “pre-test” images are examples of the extent and nature of pellet cracking that takes place during normal operation and the “post-test” images are examples of the extent and nature of transient fuel fragmentation. From these images, it can be seen that there is variability to the extent and nature of transient fuel fragmentation.

Pellet fragmentation can occur during a transient because of the thermal-mechanical response to the transient. An example can be seen in the second row in the Table 3-1, the post-test micrograph for IFA-650.7.

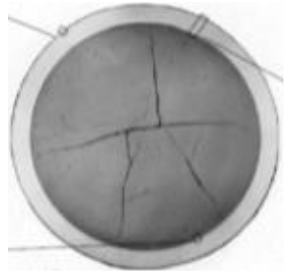
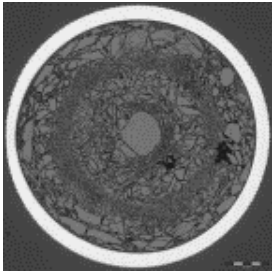
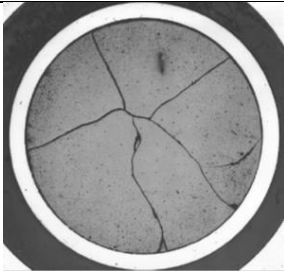
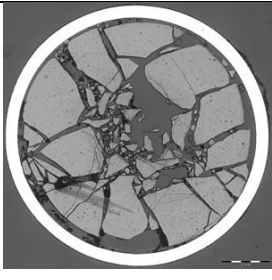
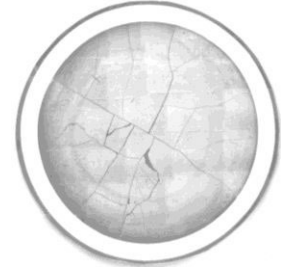
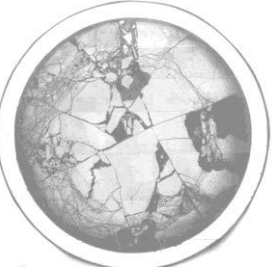
Test /laboratory	Segment	Pre-test	Post-test: near rupture + high strain
IFA-650.5, Halden	83 MWd/kgU PWR rod		
Reference		[3.1-2]	[3.1-2]
IFA-650.7, Halden	44 MWd/kgU BWR rod		
Reference		[3.1-3]	[3.1-4]
ICL No.2, ANL	56 MWd/kgU BWR rod		
Reference		[3.1-5]	[3.1-5]

Table 3-1: Characterisation of fuel fragmentation before and after integral LOCA testing as a function of burnup.

Pellet powdering or fine fragmentation likely occurs as a result of separate mechanisms that are likely associated with the fuel pellet evolution with burnup. An example can be seen in the first row in Table 3-1, the post-test micrograph for IFA-650.5.

The aim of section 3 is to report the current understanding of pellet fragmentation mechanisms and to identify the parameters which play a role. This section also tries to identify the remaining open questions

and the lack of understanding regarding fragmentation/powdering of the fuel pellet during a LOCA transient.

The first sub-section recalls the key points regarding the fuel microstructural evolutions during normal operation in order to analyse their potential impact on fragmentation and powdering during a LOCA. In the second sub-section, the effects of rod design and rod power history are discussed. In the third sub-section, the influence of the transient parameters is discussed.

3.1 Analysis of the potential influence of the fuel rod initial state to the development of fuel fragmentation

From the analysis of the tests described in Section 2, several consensuses arose during the HRP LOCA Workshop in Aix-en-Provence (20-21 May 2015):

- There is a burnup threshold below which the LOCA transient leads to coarse fragments. Post LOCA tests sieving at Studsvik showed that most of the fragments of the high burnup rods were less than 2 mm whereas most of the fragments of the lower burnup rods were above 2 mm (nevertheless some micrometre size fragments were also measured), [3.1-6], [3.1-7]. In Sections 3.1.1 to 3.1.3, the pellet microstructural evolution has been described as a function of burnup. It is important to remind that burnup is only a macroscopic parameter which covers all these changes.
- The bubbles in the pellet (and probably the high pressure reached by the fission gas located within those bubbles), mainly in the HBS but also in other regions of the pellet, are the key parameters favouring fuel fragmentation and powdering.

Various mechanisms can facilitate fuel fragmentation:

1. local stress increase (micro- and macro-scales)
2. local fuel material strength properties decrease
3. fuel pellet elasto-viscoplastic behaviour change.

These mechanisms are analysed in the following sections.

3.1.1 Fuel pellet microstructural evolution with burnup

In pile and out of pile LOCA tests on irradiated fuel rods have shown that HBU are more susceptible to fragment in small size particles. In this paragraph we will describe how burnup modifies the fuel pellet microstructure. In certain conditions, a specific HBS appears in the fuel pellets periphery. The main features of this HBS, which could be a source for small size particles, will be described in Appendix 9.1.

The fuel pellet is a ceramic resulting from the pressing and sintering of UO_2 or $(\text{U}, \text{Pu}) \text{O}_2$ powder, possibly using some additives. Its density is about 95% of theoretical density. Before irradiation, the grain size is generally around 10 μm but can reach 50 to 100 μm for specially designed large grain fuels. Initial grain size and pore distribution in the pellet are globally homogeneous across the pellet radius.

The first power ramp to nominal power in the reactor induces thermal stresses within the fuel pellets which then exhibit multiple radial macro-cracks. Radial and axial temperatures gradients depend on the fuel rod design itself, (geometry of the fuel pellet, initial gap), on its burnup (through the degradation of the thermal conductivity of the pellet, the pellet-cladding gap evolution, the thickness of the inner and outer cladding oxide layer) but mainly on the fuel rod linear powers. Indeed, as the pellet peripheral temperature is usually around 350-600°C in a PWR, the fuel central temperature varies between less than 500°C (for linear power below 10 kW/m) to above 1 800°C (for linear powers around 40 - 45 kW/m).

During the first stages of irradiation, densification phenomenon (due to small (a few microns) pores annealing), and swelling phenomenon (due to fission products generation) are competing. Depending on the pellet type and initial porosity distribution, macroscopic densification is usually observed during the first reactor cycle. It is followed by a macroscopic pellet swelling. The pellet swelling and the concomitant creep-down of the cladding lead to pellet-cladding gap closure, which occurs around 30 MWd/kgHM. This burnup threshold depends on the cladding creep rate at low stress level, on the fuel rod design (initial rod internal pressure for instance) and on the fuel core management. When the contact between the pellet and the inner side of the cladding is well established, an internal zirconia layer forms at the interface (see Section 3.1.3).

Since fission rate, fuel temperature and stresses radial distribution are not homogeneous within the fuel pellet, various distinctive zones can be identified in the pellet. The most visible differences between these zones are linked to the gas location in the fuel, with bubble formation, and to metallic fission product formation.

The gas precipitation process is rather complex as the gaseous fission products, generated within the fuel matrix can be under the form of nanometre-bubbles only visible with a transmission electron microscope (TEM) but can also diffuse and form larger inter-granular or intra-granular bubbles visible by optical microscopy or scanning electron microscopy. The amount of gas in the large bubbles (thus, depending on the bubble size and on the bubble pressure level), the bubble size distribution and the extent of each precipitation region, mainly depend on the pellet burnup and on the local temperature history.

Nevertheless a prototypical microstructural evolution can be described as follows:

- At low burnup, very few gas or metallic fission products are observed.
- With the increasing burnup and fission product build-up, a central precipitation area forms.
- For high linear heat generation rates (LHGR), this central precipitation occurs at lower burnups than for moderate LHGR. It is usually clearly established after 30 MWd/kgU and is generally associated with an increase of the FGR rate.
- Nonetheless, the rate of gases which precipitate into bubbles increases with the increasing burnup.

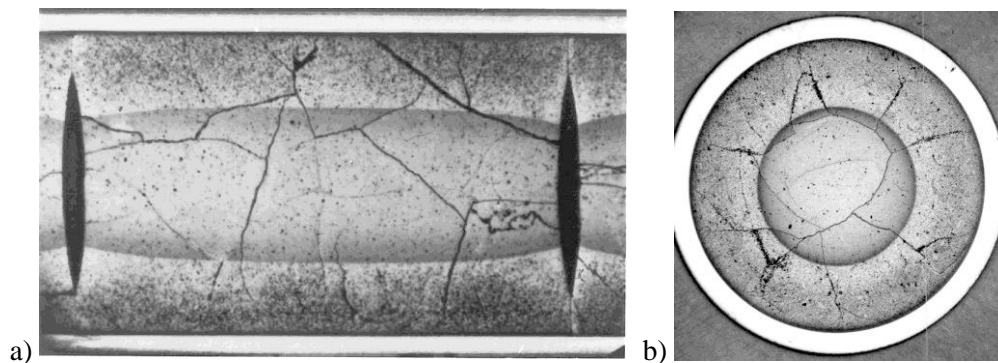


Figure 3.1-1: Optical macrographs of a 64 MWd/kgU UO_2 fuel, after chemical etching revealing the thin bubble areas (dark areas), [3.1-8]

In Figure 3.1-1, at 64 MWd/kgU, the central precipitation area is delimited by a dark ring. On the longitudinal cut, the isothermal nature of this limit is evidenced by its lower extension near the dishes, where the local temperature gradient is modified. This ring is darker than the very centre because of a high density of small bubbles. When approaching the centre, larger bubbles are observed, but with a lower density.

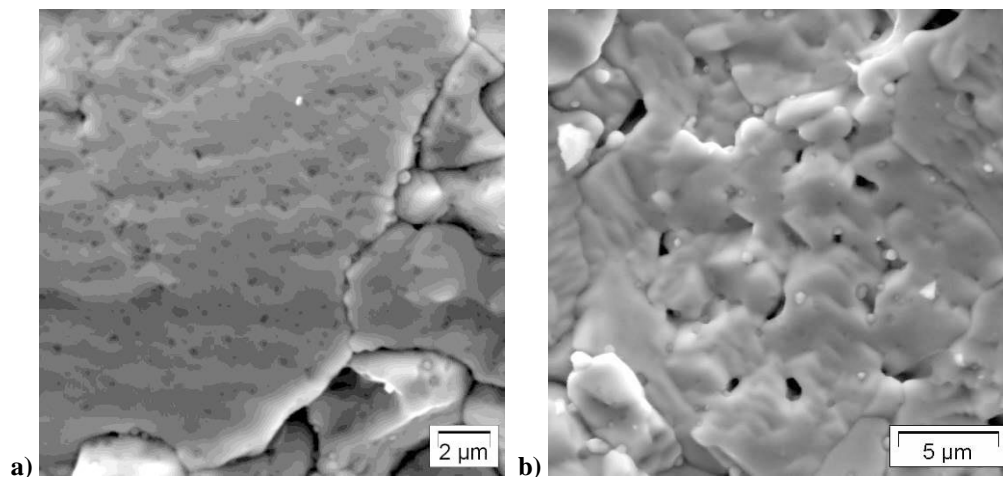


Figure 3.1-2: SEM fractograph of trans-granular intentionally induced cracks in a 73 MWd/kgU fuel at a) 0.34R and b) 0.00R [3.1-9]

A detailed view of such radial change can be seen in Figure 3.1-2 and Figure 3.1-Figure 3.1-3. In these figures, metallic precipitates are visible, in inter-granular position, but also in intra-granular position in the very centre.

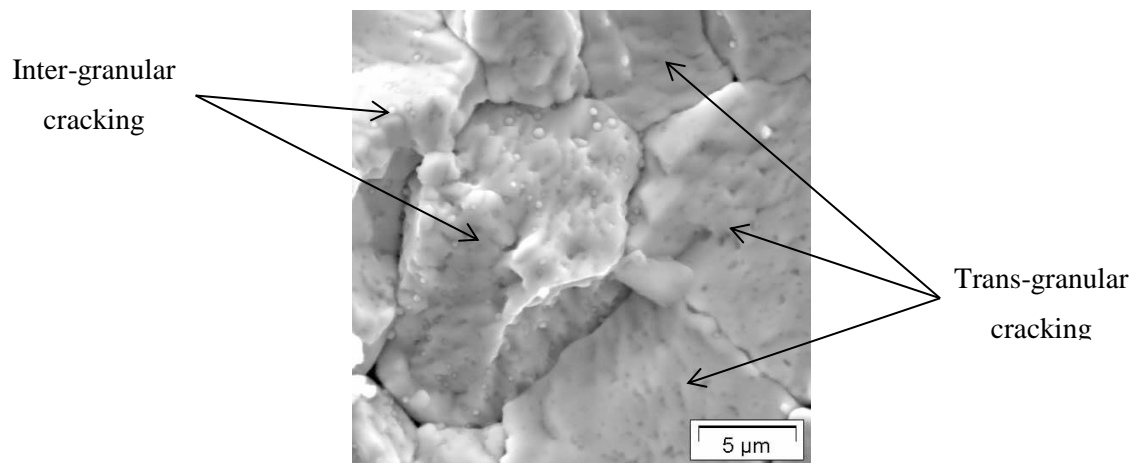


Figure 3.1-3: SEM fractograph of an intentionally induced crack, inter-granular on the left side of the image, trans-granular on the right, in a 73 MWd/kgU fuel at 0.34R [3.1-9]

The central gas precipitation is also monitored through electron probe micro-analyzer (EPMA) measurements of Xe, the formation of large bubbles leading to a drop in the Xe measurements, in addition to the real Xe release. Examples in Figure 3.1-4 show the gradual decrease of the Xe still measured in the bulk or in nanometre-bubbles in the central part of the pellets. Figure 3.1-5 shows the corresponding gradual increase of the amount of Xe found in bubbles with a SIMS.

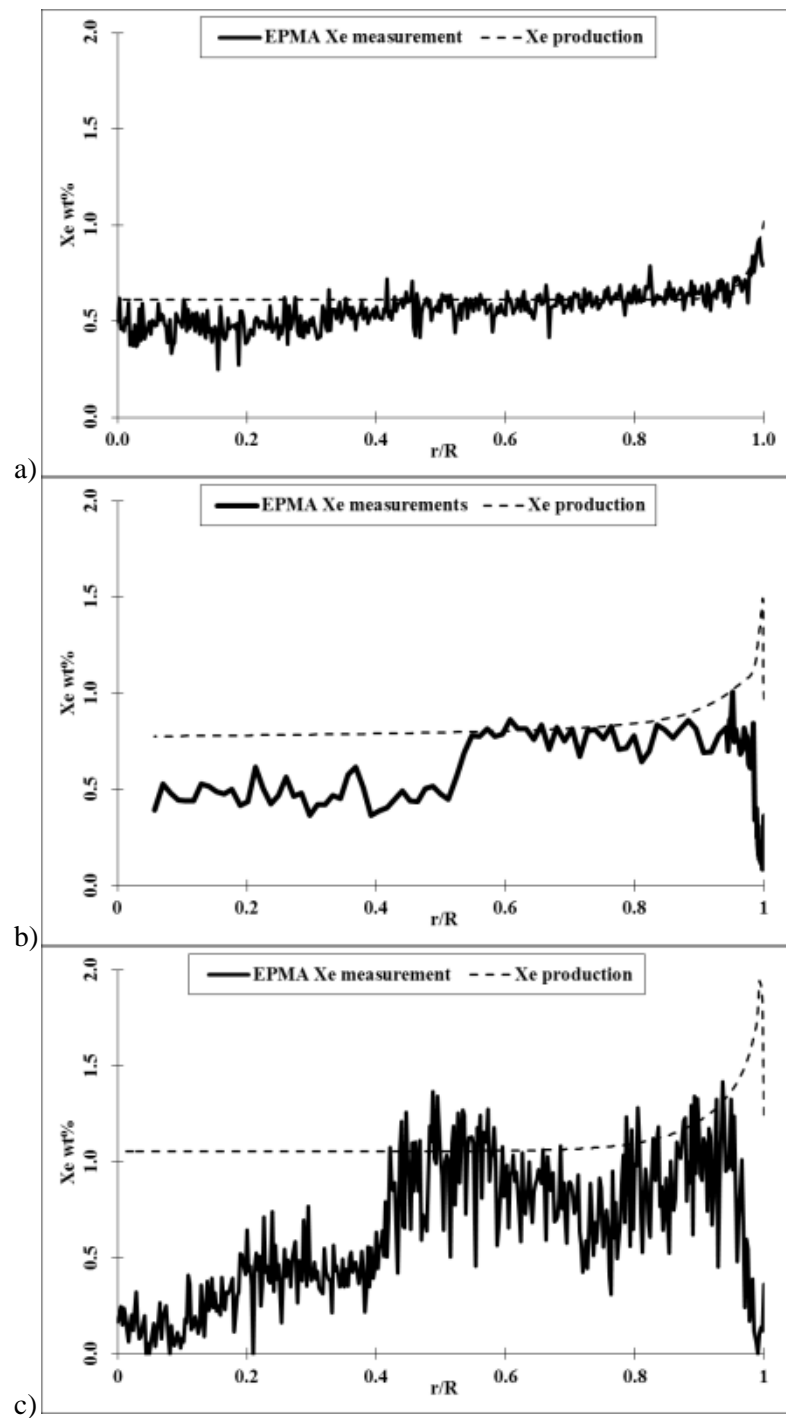


Figure 3.1-4: Increasing depletion in the EPMA Xe measurement in the central part of the pellets at a) 39 MWd/kgU, b) 61 MWd/kgU and c) 83 MWd/kgU, from [3.1-9], [3.1-10] and [3.1-11].

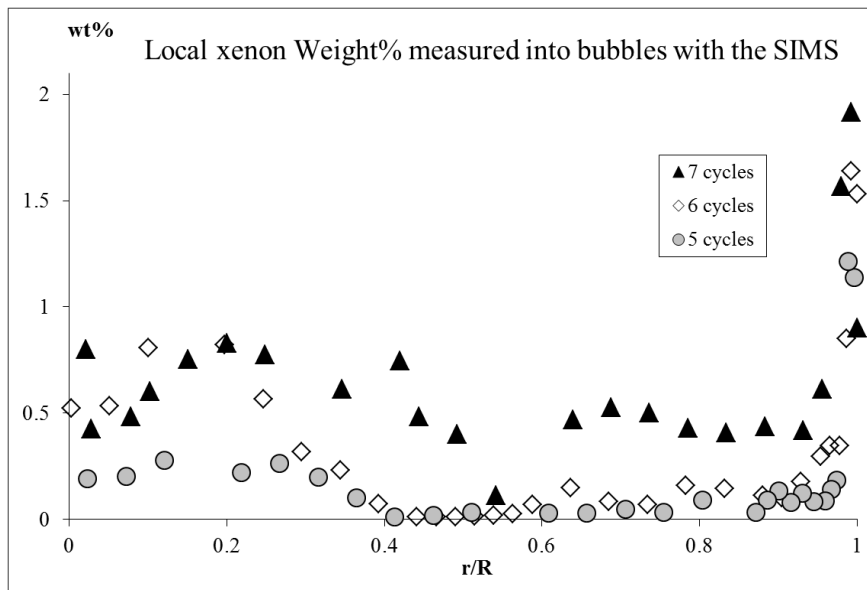


Figure 3.1-5: Increasing Xe content in large bubbles, measured with a SIMS at 61 MWd/kgU, 73 MWd/kgU and 83 MWd/kgU, from [3.1-9]

It must be noted that transitions between various concentric precipitation zones can be smooth within the central precipitation area, but can also be sharp with a more complex radial evolution, as it can be seen in [3.1-12] or [3.1-11], see Figure 3.1-5. Outside the central precipitation area, a zone is usually found in which no major precipitation is observed.

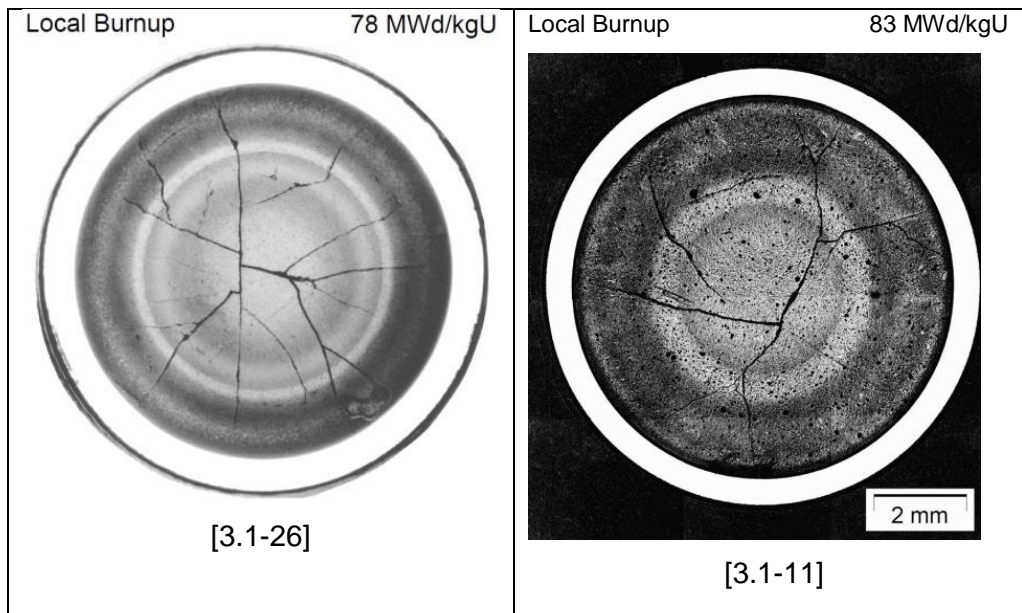


Figure 3.1-6: Examples of macrographs on UO₂ fuel, after chemical etching at high burnup, showing a complex distribution of bubble formation (dark areas)

The other major evolution in the fuel pellet microstructure is the HBS which appears in the fuel pellet periphery (rim). Fission gas precipitation associated with this dramatic transformation of the fuel can also be seen in Figure 3.1-4 close to $r/R=1$.

The main characteristics and evolution of HBS are described in the following section (3.1.2).

For MOX fuels, the microstructural evolution with burnup depends on the initial microstructure [3.1-13], [3.1-14]. The MOX microstructure depends on the fabrication process and can be fully homogeneous or can be heterogeneous with several phases containing different Pu concentrations.

The amount of Pu in the potential Pu-rich agglomerates depends on the Pu concentration of the master blend. The main features for MOX compared to what has been previously described for UO₂ can be summarised as follows:

- Helium is produced in larger quantities in MOX fuel (it is also depending on the initial amount of Americium in the PuO₂ fuel).
- Plutonium content in the Pu-rich agglomerates decreases with burnup: starting with a value of about 25-30 wt%Pu, the Pu content of the agglomerates after 3 cycles is about 10 wt%.
- Intermetallic precipitates appear in the agglomerates after only one cycle. At high burnup, these precipitates reach up to 10 µm in the central area.
- Thermal conductivity is slightly degraded due to the presence of Pu, about 4% for 10% Pu [3.1-14].

In the standard MOX fuels, presenting some Pu heterogeneities, the microstructural changes are highly linked to the HBS transformation of the high Pu content areas and of their close surrounding. The HBS is thus localised because of the high local burnup induced by the high local Pu content of the clusters. The characteristics will be described in the following section on HBS (Section 3.1.2). Nonetheless, like in the UO₂ fuels, some distinction will have to be made between the hot central part of the pellets and its periphery as it can be seen in Figure 3.1-7.

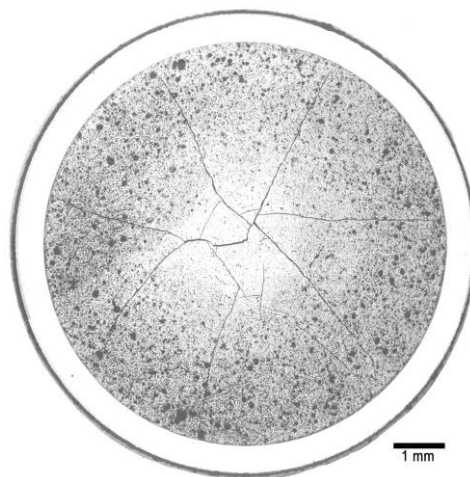


Figure 3.1-7: Radial cut of a MOX MIMAS pellet irradiated at 50 MWd/kgHM [3.1-13]

The use of additives in UO₂ fuels modifies several of the above mentioned features but the influence of additives will depend on the nature of these additives (Alumino-silicates, Chromia, etc.) and their amount. Their usual impact on microstructure evolution can be summarised as follows:

- During fabrication additives usually increase the grain size of the pellet (as large as 60 µm in commercial fuels).
- Larger grains help reducing FGR in normal and transient operations.

- Larger grains lead also to a lower number of small pores after fabrication. This leads to a reduction of the densification.
- The large grains modify the distribution of the fission gas (in solution, intra- or inter-granular).
- The pellet creep properties are usually higher.

3.1.2 Pellet-Cladding bonding during normal operation

At high burnup, the pellet-clad gap is usually tightly closed. As a consequence, the HBS rim described in the above will interact with the cladding, both mechanically and chemically. This interaction, and its potential impact on the FFRD, will be analysed here.

When the pellet-cladding gap starts closing at power conditions, an internal zirconia layer forms on the cladding inner surface. The formation of this zirconia layer starts with the formation of small local islands and grows as burnup increases.

The minimum thickness of the internal zirconia layer is about 5 μm , suggesting a rapid growth up to this value [3.1-15]. The thickness usually saturates, for the observed burnups (up to 70–80 MWd/kgU) around 10–15 μm .

Figure 3.1-8 illustrates the initiation of the internal zirconia layer and its morphology at high burn up. At intermediate burn up, when internal zirconia formation is still recent, after cooling down and due to thermal dilatation differences, the fuel to clad gap re-opens. With the increasing burnup, a strong bonding between the fuel and the internal zirconia prevails.

At high burnup, the bonding layer takes a wavy shape, strongly interconnected with the HBS formed on the pellet periphery. The bonding between the pellet and the cladding is very strong, enough for the initial gap not to re-open during fuel rod cooling down, despite the thermal dilatation difference between pellet and cladding (Figure 3.1-9).

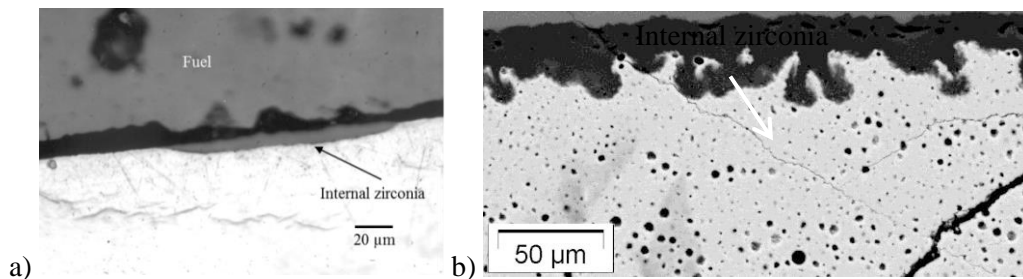


Figure 3.1-8: Examples of pellet-cladding bonding, a) first zirconia island before bonding, b) 68 GWj/tU section: interpenetration of rim area and internal corrosion layer [3.1-9]

Circumferential cracks usually form within the HBS [3.1-15], [3.1-16]. This strong bonding at high burnup is also observed in post-irradiation examinations after lift-off experiments [3.1-17].

Due to fission product recoil, the internal zirconia contains all kind of fission products, [3.1-15], [3.1-18], [3.1-19]. Their implantation may play a role in the internal zirconia formation.

X-ray diffraction at room temperature showed that the crystal structure is not the usual stable monoclinic one, but is either a tetragonal structure, [3.1-27], or a cubic one, [3.1-28]. Nevertheless, the same material may have been interpreted differently in the two teams, knowing that the two microstructures exhibit similar X-ray diffractograms.

Some authors distinguish two layers: zirconia and a uranium-rich layer also called “bonding layer”. Both layers form simultaneously. The U-rich layer is not always observed.

In heterogeneous MOX fuels, the HBS formation in the peripheral Pu-rich agglomerates leads to a local swelling which induces an early local gap closure. These spots lead to the first internal zirconia islands, [3.1-15]. As burnup increases, these local spots exhibit larger waves than in front of the surrounding matrix but eventually, the zirconia layer observed at high burnup appears to be very similar in MOX fuels and in UO₂, both in terms of thickness and kinetics, [3.1-18].

The inner liner used on BWR Zry-2 cladding does not modify the growth kinetics of the layer [3.1-18].

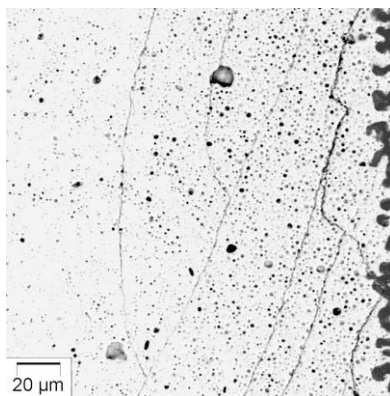


Figure 3.1-9: Periphery of a UO₂ fuel with an average section burnup of 83 MWd/kgU, zirconia inter-twining with HBS and cracks in the HBS due to bonding and cooling periods, [3.1-9]

The start of the zirconia layer formation depends mainly on the gap closure kinetic, thus on initial fuel rod gap and on linear heat rate. Consequently, the bonding layer formation is not axially homogeneous.

The effect of the zirconia layer on fuel fragmentation during a LOCA transient might be twofold:

- The chemical evolution of the fuel pellets–cladding interface, inducing the formation of one or two additional layers of mixed materials, associated with oxygen diffusion doesn't seem to play a direct role of fuel fragmentation but has not been studied thoroughly.
- The fuel-cladding mechanical bonding can be mentioned among the possible reasons for fuel fragmentation when ballooning occurs. Indeed, with the cladding strain, radial tensions could be applied to the pellets. However, during normal operation cooling down periods, this bonding induces the formation of circumferential cracks within the HBS rim area. With the presence of these circumferential cracks, during a LOCA event, no tensile stress can be applied to the fuel beyond these cracks. This is confirmed by lift-off experiments on high burnup rods, [3.1-17], where circumferential macro-cracks appear in the pellet periphery have been observed after the tests, without any fine fragmentation of the HBS regions.

Nevertheless, the analysis of Figure 3.1-9 above shows that some part of the HBS imbedded in the pellet-cladding interface layers did not fragment whereas the underneath HBS layer was highly fragmented. This phenomenon has not been systematically observed but as matter of fact, small fragments often remain attached to the cladding.

3.1.3 *Effect of fission gas in the bubbles*

The analysis of the results presented in Chapter 2 shows that:

- Several Halden Tests show a mix coarse and fine fragmentation. When fine fragmentation occurs, the post-test ceramographics show that fine fragmentation can be located at the pellet periphery and at intermediate radius (see for instance IFA-650.5 on Table 3-1). Fragments

coming from the rim are oblong. This needle shape may come from circumferential cracks due to the loss of the mechanical balance between base-irradiation conditions and LOCA conditions (thermal radial temperature gradient evolutions and cladding straining), [3.1-20].

- Studsvik tests on the high burnup rod No.192, [3.1-1], show that, at locations where the pellet did not move outside the cladding, the pellet rim is fragmented into pieces sizing from about several microns to 50 μm , needle-shape. Each fragment shows several of the HBS-typical round-bubbles and contains several of the sub-micronic grains of the HBS structure. A significant part of the pellet rim is still bounded to the cladding. On the same pellet, the central part is also fragmented into small pieces which can be less than 50 μm (entering in the definition of “powder”, as defined earlier). In the central zone of the pellet, the fragments do not have this needle-shape. This difference between central fine fragmentation and peripheral fine fragmentation underlines that the mechanism could be different between the different locations in the pellet and that grain boundaries may play a role in the fragmentation of pellet centre.
- Studsvik tests on the intermediate burnup rod No.198, [3.1-1], showed also some small fragments but less numerous (fragments < 125 μm represent less than 1% of the weighted fragments after test and shaking).
- Post-test SEM and WDS examination on Studsvik LOCA test, [3.1-7], showed that at intermediate burnup, fine fragmentation comes only from the rim whereas at high burnup, fine fragmentation may come from other parts of the fuel pellet.
- Post-test EPMA examination on CEA out-of-pile annealing test performed on an 83 MWd/kgU UO_2 pellet, in which various areas had been identified prior to the test, showing high differences in bubble precipitations, large fragments only came from areas where bubble density was low. Small fragments came from the whole pellet, [3.1-21].
- In the out-of-pile heating tests performed at CEA and Studsvik on high burnup segments (see Chapter 2) with an axial slit in the cladding and no end plugs, most of the central part of the pellet was dispersed outside the crucible, leaving a remaining annulus shape pellet within the cladding tube. This shows that the usual precipitation rings observed in a pellet after irradiation play a role in the fragmentation. It should be noted that the heating tests where the open ends samples are inserted in a pre-heated furnace, lead to a specific, un-prototypical axial and radial thermal gradients within the pellets. It is not clear whether the axial slit(s) in the cladding and the associated lack of cladding restrain have an impact on fuel fragmentation or on fuel repositioning and dispersal only.

These results allow concluding that the local bubbles density and the amount of gas (i.e. gas pressure) in the bubbles are key parameters for fuel powdering. This was a significant conclusion of the HRP LOCA workshop in Aix-en-Provence, May 2015, [3.1-21], [3.1-7], [3.1-22].

Calculations performed by CEA with ALCYONE code and MARGARET advanced gas model show that for IFA-650.4, 650.5, 650.10 and Studsvik test No.192, the gas pressure in the inter-granular bubbles is rather low in the pellet centre (local temperature is decreasing during a LOCA) while it can be significantly higher in the pellet HBS peripheral zone (where the local temperature is increasing during a LOCA transient). This is illustrated in Figure 3.1-10. This plot suggests that gas generation and gas pressure increase more in the HBS bubbles, during a LOCA transient, than in the central zone of the pellet.

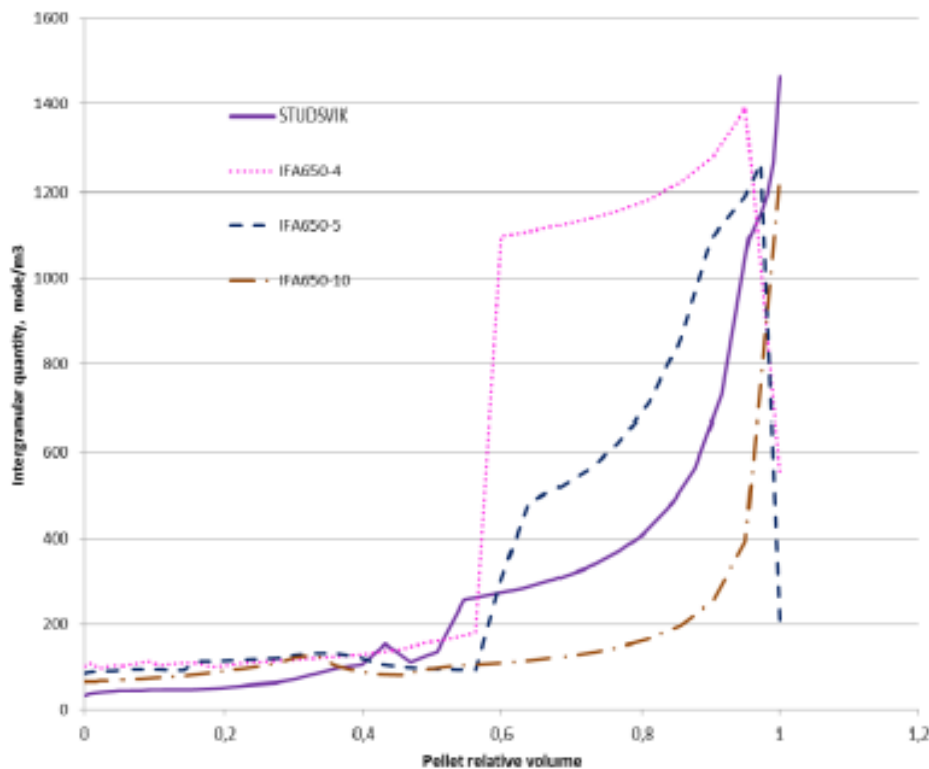


Figure 3.1-10: Local intergranular fission gas retention for IFA-650.4, 650.5, 650.10 and Studsvik test No.192, [3.1-23]

The temperature gradient evolutions (and their kinetics) have an impact on the transient behaviour of the various zones of the pellet. Before the transient, the gas pressure is higher in the central bubbles than in the HBS bubbles but this difference is counterbalanced by the LOCA thermal transient. Fragmentation cannot be linked only to initial bubble pressurisation.

Depending on the precipitation pattern, and base irradiation local FGR, it is possible to observe a lower fragmentation at the pellet very centre (see Figure 3-1). This will be discussed in Section 3.3.1.2.

At this stage, the fuel fragmentation mechanisms involving the size of the bubbles, their location within the pellet, the local bubbles density, the amount of fission gas generated before the transient and the gas pressure within the bubbles still need to be investigated with proper separate effect tests. The bubbles may play two roles:

1. increasing the local stress in the matrix due to bubble pressure increase when temperature increases
2. reducing the macroscopic strength of the matrix whose porosity increases with burnup. It is not known whether the local strength of the matrix may be further reduced by other burnup dependant parameter (fission products inventory, fission defects, etc.).

Comparing ceramographies at equivalent magnification after base irradiation followed by cool-down and after a heat treatment at 1 200°C (see Figure 3.1-11), it is worth noticing that the cracking patterns are similar: mainly circumferential cracks, going through the matrix from a bubble to another. The difference between the two pictures left and right may be the larger number of cracks after the heat treatment. In this case, the thermal gradient during cooling down after normal operation was high enough to promote the

HBS cracking in oblong or needle-shape fragments. The size of the fragments is however larger than after a LOCA.

As already described in Section 3.1.2, the bubbles in the HBS are not interconnected. This means that if one bubble breaks out the surrounding matrix, the remaining other bubbles continue imposing some stress in the matrix. If a range of bubble pressure in the HBS is expected, maybe linked to the different sizes of bubbles, if bubble pressurisation was the main parameter for fragmentation, all the large/high pressurised bubble should break first and the shape of the fragments would be more random, not like needles as it is observed in the rim. There may be an additional stress relaxation mechanism occurring as soon as a fragment is formed.

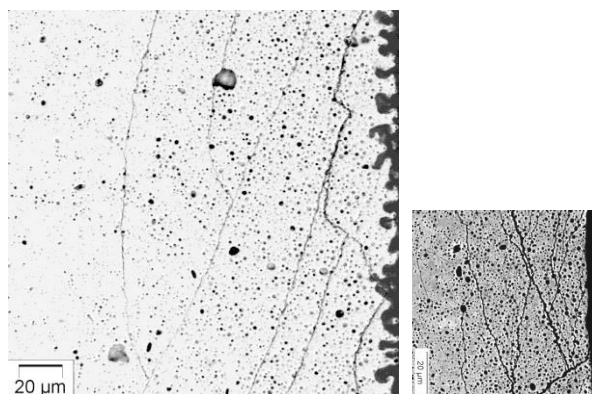


Figure 3.1-11: Comparison of HBS fragmentation after normal operations (left, 83 MWd/kgU) [3.1-9] and after an out-of-pile heating test at 1 200°C (right, 72 MWd/kgU) [3.1-24]

A heat treatment performed by CEA at 1 300°C on a ~40 µm HBS fragment mechanically extracted from the rim (estimated burnup: 140 MWd/kgU) showed no additional fragmentation. This underlines that there is a limit in the fragmentation of the HBS and that bubble pressurisation alone cannot be responsible for the whole fragmentation behaviour.

3.1.4 *Effect of fission products (Cs) on pellet fragmentation*

To explain the results regarding gas release during the heat treatments (see Section 2.3), it has been suggested that a phase transformation involving Cs compounds could be responsible for the fragmentation (or part of it). For the time being, no data are available to assess such a mechanism.

This effect could be through either a reduction of the matrix or grain boundaries strength or by sublimation or phase transformation of volatile fission products or their compounds, in addition to the effect of the fission gases.

Indeed, heat treatments under vacuum performed on very HBU samples (around 200 MWd/kgHM sample average) show that the volatile fission products start to be significantly released at 1 000 K, excepted Sr (above 1 800 K) and Ba (above 1 500 K) and that their release roughly follow the FGR [3.1-25].

3.1.5 *Lowered failure stress in fuel matrix*

During irradiation, the failure strength of the matrix decreases as it is modified by the irradiation defects, the fission products (including the gas) in solid solution or the precipitation of metallic compounds. However, the failure strength in the HBS is not well known and it is not clear whether it is higher or lower than the UO₂ matrix.

During a LOCA, the pellet rim undergoes a rapid temperature increase at the beginning of LOCA transient (see Section 3.3.1.1). In the temperature range below $\sim 800^{\circ}\text{C}$, the UO_2 matrix is fragile and its mechanical strength does not vary significantly with increasing temperature. Above this temperature range, the behaviour of the matrix turns to visco-plastic. The effect of temperature is thus expected to be limited below 800°C .

3.2 Analysis of the potential influence of the fuel rod operational conditions on the development of fuel fragmentation

3.2.1 Effect of VVER design (central hole in the pellet) on pellet fragmentation

Hollow fuel pellets are usually used in VVER power plants. The central hole modifies slightly the cracking pattern after base irradiation, with more radial regular cracking. This allows also, even at high burnup, a rod inner pressure equilibrium during a LOCA transient. Subsequent description compares results of LOCA tests on VVER fuel with LOCA tests on PWR and BWR fuels.

For example, the appearance of a single VVER fuel rod (segment averaged burnup of 76 MWd/kgU) after simulated LOCA transient is shown in Figure 3.2-1; illustration taken from [2.4-3]. This test performed by VNIINM in the MIR reactor (MIR/LOCA-72) with fuel rod test assembly comprising of 19 fuel rods (18 fresh fuel rods, 1 refabricated fuel rod from 6 cycle irradiation in Kalinin NPP) reached a maximum cladding temperature of $1\,070^{\circ}\text{C}$ during LOCA test. The tested fuel rod bursts when cladding temperature reached 741°C .

The post-test investigation shows two burst openings along the fuel rod length, see Figure 3.2-1. These burst openings are separated by a spacer grid. It is obvious from the X-ray in Figure 3.2-1, that the spacer grid affects the axial fuel relocation. The maximum hoop strain reached 36% before burst of cladding and a quantity of about 5 cm of fuel column height had been expelled from the burst opening.

The tested fuel with 76 MWd/kgU (segment averaged burnup) shows fragmentation into small particles which allows significant axial relocation of these fuel particles into the ballooned fuel rod region and furthermore it allows dispersal of fuel into coolant channel.

The analysis of VVER fuel tests performed at Halden (see Section 2 about IFA-650.6 and IFA-650.11) combined with MIR-LOCA tests (MIR-LOCA/50, MIR-LOCA/60 and MIR-LOCA/72) show unique fragmentation behaviour; see Table 3.2-1 summarising results of these tests.

The test results of VVER tests compare with test results from Halden and Studsvik indicating a threshold for transition to fine fragmentation for pellet averaged burnups between 60 MWd/kgU and 70 MWd/kgU .

It could be concluded that micro-scale mechanisms occurring at the bubbles size level are more important than those activated at the pellet macro-scale level, thus the centre hole of the VVER pellet has no or at least a negligible effect on fragmentation, relocation and dispersal. Furthermore, the burnup threshold for FFRD seems to be equivalent to PWR or BWR fuels.

No	Experiment	Reactor	Fuel rods	Burnup, MW·d/kgU	PCT, °C	Cladding	Fuel
1	MIR-LOCA/50	MIR (RIAR)	3 ref. rods VVER-1000 in EFA with 19 fuel rods	47,2; 49,0; 45,8	930	Cladding ballooning and depressurization, ECR \approx 5 %	Coarse fragments, small relocation, no dispersal
2	IFA-650.6	Halden	Single ref. fuel rod VVER-440	56	830	Cladding ballooning and depressurization, ECR < 1 %	Coarse fragments, small relocation, no dispersal
3	IFA-650.11	Halden	Single ref. fuel rod VVER-440	56	935	Cladding ballooning and depressurization, ECR \leq 3 %	Coarse fragments, small relocation, no dispersal
4	MIR-LOCA/60	MIR (RIAR)	3 ref. rods VVER-1000 in EFA with 19 fuel rods	58,1; 58,1; 58,6	\leq 800	Impact claddings, deformation \leq 2%, ECR < 1 %	No fragmentation and relocation
5	MIR-LOCA/72	MIR (RIAR)	Single ref. fuel rod VVER-1000	76	1070	Cladding ballooning and depressurization in two regions, ECR \approx 5 %	Fragmentation into small particles, axial relocation, fuel dispersal through cladding burst

Table 3.2-1: VVER fuel tests ordered with increasing burnup [2.4-3]

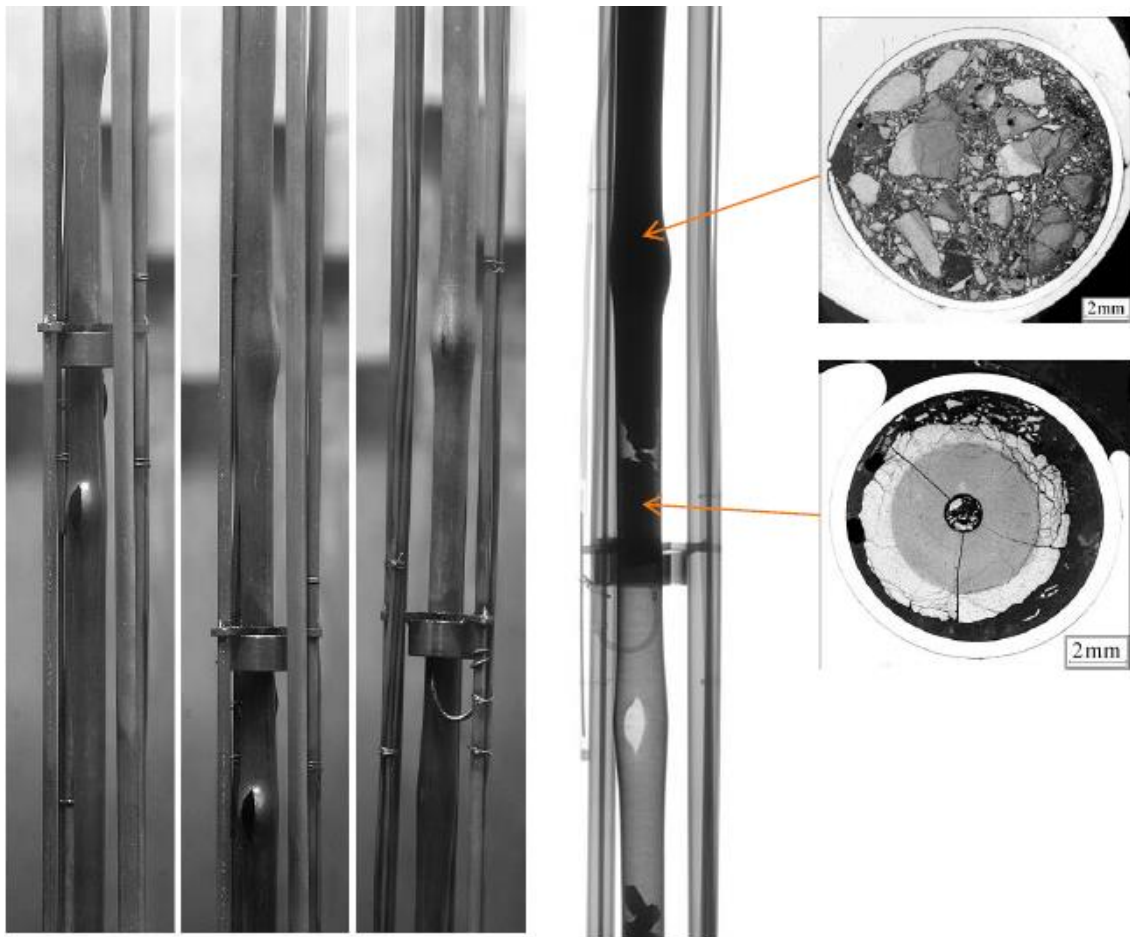


Figure 3.2-1: Appearance of fuel and fuel rod after test MIR-LOCA/72 (segment averaged burnup of 76 MWd/kgU) [2.4-3]

3.2.2 Rod power history

Out-of pile tests were conducted at Studsvik for EPRI using fuel materials taken from the same rods and in adjacent locations to the NRC Studsvik LOCA tests 189 (segment average burnup of 72 MWd/kgU) and 192 (segment average burnup of 78 MWd/kgU). Post-test images are presented in Figure 3.2-2. The separate effect test sample cut from the parent rod above test 189 showed a high level of fragmentation when heated to 1 000°C in both air and inert atmosphere while a test sample section taken from the same rod at a location below that of test 189 only partially fragmented, [3.2-1], [3.1-1].

The conclusion of these two tests is that a higher last cycle LHGR appears to enhance fuel fragmentation [3.1-1]. Nevertheless, quantitative information regarding fragment sizes and their origins are not available.

Explaining this effect without a deeper characterisation of the pellet microstructure before the transient and of the fragment size repartition, ideally with a characterisation of the fragment location as performed by Puranen [3.1-7] or Noirod [3.1-21] for other cases, is difficult.

As discussed by Yueh et al. [3.2-1], different in-reactor LHGR levels modify the local distribution of the fission gases within the pellet, which cannot be anticipated without dedicated calculations using a validated thermal-mechanical code or by post irradiation examinations. A higher LHGR level during base irradiation would increase the stresses during the LOCA in the pellet due to the temperature evolution across the pellet.

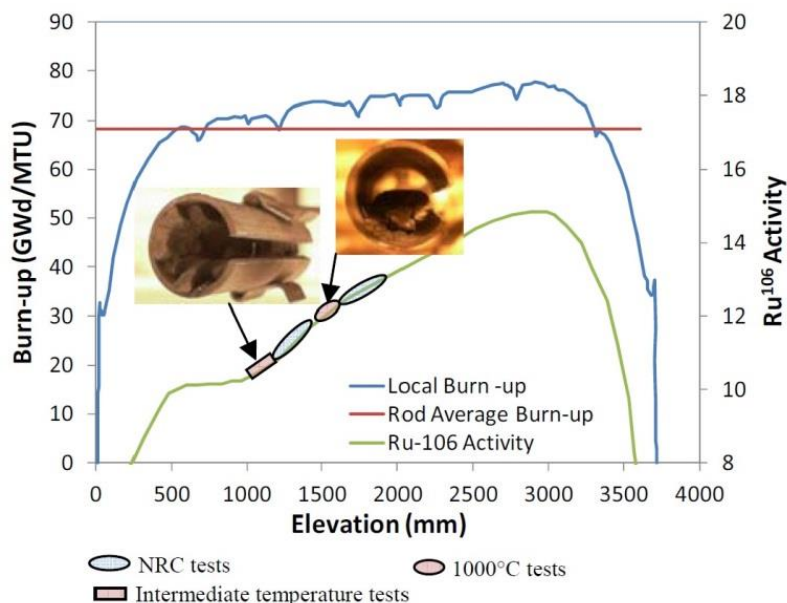


Figure 3.2-2: Post-test appearance, local burnup and ¹⁰⁶Ru activity for sibling rods tested by Studsvik for EPRI [3.2-1]

Nevertheless, the effect of the rod power is not straightforward:

- A low in-reactor LHGR is expected to increase the HBS extent, by reducing the fuel temperature. This could increase fuel fragmentation at pellet periphery.
- A high in-reactor LHGR can increase the central precipitation area, hence increasing fragmentation in the central part.

- At very high in-reactor LHGR, FGR from the very centre can be high enough to locally inhibit fuel fragmentation (cf Table 3-1, IFA-650.5).

3.3 Analysis of the potential influence of the transient conditions to the development of fuel fragmentation

3.3.1 Effects of temperature evolution in the pellet during the transient and impact on fuel fragmentation

The analysis of the temperature impact should consider four points:

1. the temperature gradients across the pellet in the radial direction
2. the absolute maximum temperature value reached in each location of the pellet during the transient
3. the heating rate
4. the axial temperature profile, which is in fact linked to the point No.2 above.

These four points are detailed in the following subsection and a focus on the pressure in the bubbles is made in the second subsection.

3.3.1.1 Transient temperature and stresses in the pellet

The temperature gradients across the pellet in the radial direction are responsible for stress evolution across the pellet. During in-reactor irradiation, the temperature profile across the pellet is quasi-parabolic, with a higher temperature in the pellet interior and much lower near the periphery.

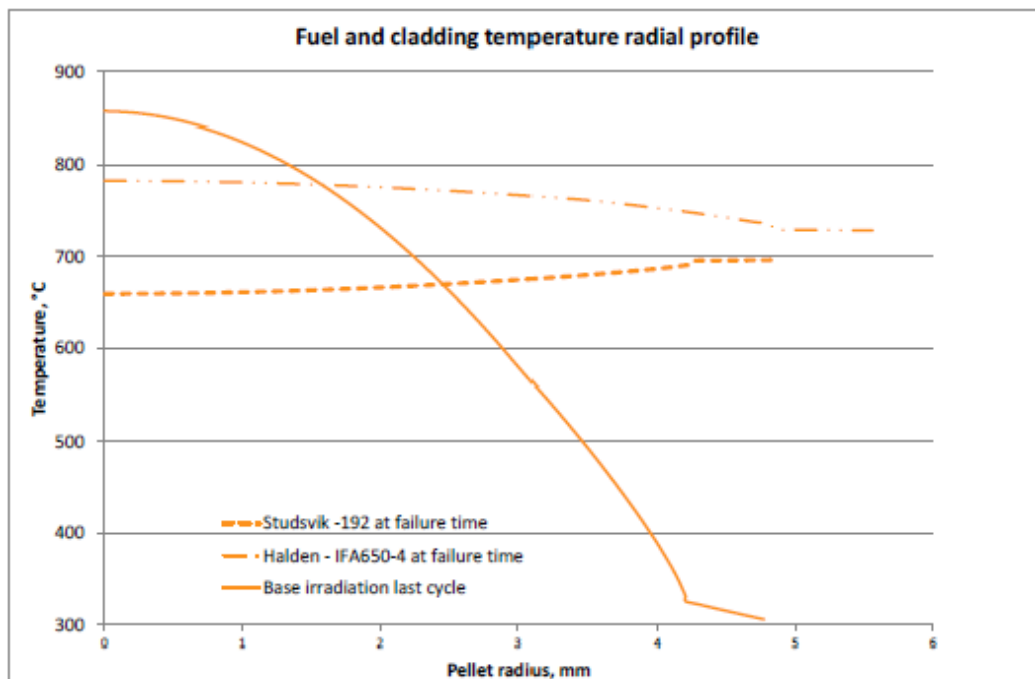


Figure 3.3-1: Calculated temperature radial profile in IFA-650.4 and in Studsvik's test No.192, compared to base irradiation profile for test No.192 [3.1-23]

In a LOCA transient, the temperature in the outer portion of the pellet significantly increases above the steady-state rim temperature value to reach an almost flat profile across the pellet. This evolution of local temperature in the simulated LOCA transient is presented in Figure 3.3-1.

The thermal mechanical stresses in the centre part of the pellet due to the temperature transient are low and do not seem to be high enough to promote fragmentation. Moreover, the temperature in the pellet centre during the transient is lower than the temperature reached during base irradiation, leading to lower stresses in this region [3.1-23].

The maximum temperature value reached at pellet periphery during the transient is higher than during normal operation. Out-of pile furnace heating tests performed at Studsvik under atmospheric pressure show that fragmentation for high burnup samples (father rod was ~70 MWd/kgU) starts at 550°C and is completed at 850°C, with no additional FGR between 850°C and 1 000°C [3.2-1].

Out-of pile furnace heating tests performed at CEA under atmospheric pressure show that the main FGR starts above 1 000°C for high burnups. The NFIR data based on out of pile heating tests performed in various test conditions under atmospheric pressure gives a fragmentation temperature threshold around 640°C for burnups above 60 MWd/kgU, [3.3-1].

Heating tests on high burnup HBS sample in a Knudsen cell (local average burnup about 200 MWd/kgHM) shows that FGR starts at ~330-530°C (1% of the inventory), with a second step around 630-730°C (20% of the inventory) and a third step around 1130-1 230°C (70% of the inventory). Helium release was also similar to Xe and Kr release [3.1-25]. The sample is fragmented (big pieces of 200×300 µm) after heating at 650°C and pulverised (about 10-20 µm size) after heating at 1 230°C.

At 1 230°C, HBS grains are restructured, interconnection between pores and start of re-sintering is also observed [3.1-25]. The gas release observed at 630°C is associated to the periphery region where HBS is fully restructured ($0.96 < r/r_0 < 1$) and the release at 1 230°C is mainly associated to the internal part of the sample ($0.91 < r/r_0 < 0.96$). As the peripheral region shows larger pores than the internal part, it is suggested that it is more fragile [3.1-25]. The authors estimate that the pressure levels inside the large and the small pores are similar.

According to Figure 3.3-1, the fuel temperature at burst location is about 670°C, which is above the fragmentation threshold determined by out-of pile tests [3.2-1]. It is also about 350°C above base-irradiation temperature in the rim. This will generate significant bubble pressurisation in the rim and a possible evolution of the matrix strength. The question of whether this over-pressurisation is enough to promote fine fragmentation and to explain the needle-like shape of the fragments needs further code calculations.

Nevertheless, as presented in Figure 3.3-1, the absolute maximum temperature value reached at the pellet centre and at about mid-radius of the pellet during the transient is necessarily below operating condition. Thus, the absolute value of temperature cannot explain on its own the refined fragmentation observed in the pellet centre.

Regarding the heating rate, out of pile heating tests performed by EPRI on a 71 MWd/kgU sample (local burnup) show that FGR and fuel disintegration are higher at a heating rate of 9 350°C/s than at 6 050°C/s [3.1-22]. On out of pile heating tests on 83 MWd/kgU UO₂ pellet long open samples, after a test at 0.20°C/s, most of the fuel remained in the cladding whereas after a test at 20°C/s almost all fuel was found outside the cladding [3.1-21].

The axial temperature profile can help to determine the temperature limit above which fragmentation occurs. This point has been discussed by W. Wiesenack [3.1-20] by comparing the axial temperature profile to the fragmentation threshold observed by neutronographic analysis. In this analysis, the fragmentation is defined when cracks are open enough to be visible in the post-test examinations (see the comment above related to Table 3-1). The analysis leads to a temperature threshold for visible fragmentation of about 900°C in areas with little cladding strain [3.1-20].

Using rod inner pressure measurement, the estimation of FGR onset is lower, around 500°C on cladding temperature [3.1-20], estimated around 650°C on fuel temperature. The threshold value depends somehow on how visible the cracks are. Since the cracks are more detectable when the cladding strains out (a value of 5% clad strain is necessary to allow opening of the fuel cracks and repositioning of the fuel fragments), the fact that no cracks are visible where the cladding didn't strain out enough doesn't mean the fuel pellet didn't crack.

The conclusion regarding the temperature evolution during the transient is that it may play a role on the fuel fine fragmentation in the peripheral zone of the pellet, where the level of temperature is higher than the one reached during base irradiation. Matrix strength and bubble pressurisation would be then part of the mechanism. It can also explain a refined fragmentation at pellet mid-radius, if the gas precipitation can lead to bubble pressurisation. It cannot explain alone a fine fragmentation in the pellet centre.

3.3.1.2 *Fission gas pressure in pores during the transient*

As mentioned earlier, to assess the local stress increase due to the pressure increase in the bubbles under local temperature rise is not straightforward and needs to know, among other parameters, the initial gas content (or gas pressure) in the bubbles. Direct measurement of gas pressure in the bubbles of the HBS is very complex. In addition, the measured value depends highly on the local temperature at which the measurement is performed. This temperature is usually different from the local temperature during the accident.

Very seldom data are available and estimations depend also on calculation hypothesis. Measurements by EXAFS spectrum analysis on synchrotron measurement gives a value ranging between 2 and 4 GPa (temperature, bubble location and burnup are not given) [3.3-2]. Nogita and Thomas estimate from TEM bubble characterisation that the nano-bubbles in HBU ranges between 1.6-15 GPa at 427°C, above the equilibrium pressure, [3.3-3], [3.3-4].

As previously mentioned, the pressure in the bubbles in the HBS area has been estimated between 65 and 80 MPa at 377 °C for UO₂ at 62 and 78 MWd/kgU pellet average burnup [3.1-16] (with an appropriate equation of state). Another estimation based on gas released measured and porosity estimation gives a pressure of 30 MPa at room temperature and 90 MPa at 650°C, 150 MPa at 1 230°C [3.1-25]. Calculations with the MARGARET model at CEA on a ~70 MWd/kgU UO₂ rod estimate at 700°C the bubble pressure in the HBS about 71 MPa, while the pressure in intra-granular bubbles at pellet centre is about 7.28 GPa and in the inter-granular bubbles about 227 MPa [3.3-5]. It is mentioned that the bubble pressure alone cannot discriminate the different rods, some with significant fragmentation (IFA-650.4 and Studsvik No.192) and other with coarser fragmentation only (IFA-650.10).

The gas release process during heat-treatment of high burnup samples is explosive [3.1-25] showing that the bubbles suddenly explode when their internal pressure reaches the matrix strength.

As described in Chapter 2, CEA performed a heat treatment at 1 300°C on a HBS fragment mechanically extracted from the rim (that is to say that the gas was not removed from the HBS bubbles) at an estimated burnup of 140 MWd/kgU. The test shows no additional fragmentation. This shows that the bubble pressurisation on its own was not enough to promote the fragmentation of the pellet fragment.

Bubble pressure in the pores could be also increased by non-gaseous fission products sublimation during the transient. This would rather be in pellet periphery, where temperature rises above base irradiation temperature. There is no data on the topic to conclude on the potential effect on bubble pressurisation.

To conclude on the subject, a more precise analysis of the gas location in the pellet (size and density of bubbles), of the pressure in the bubbles and a better characterisation of the matrix and grain boundaries strength should be done. Modelling of the thermal transient would then allow calculating the local stresses

in the pellet. A good characterisation of the pellet fragmentation as a function of pellet radius is also necessary to validate the fragmentation modelling.

3.3.2 Effect of loss of confinement due to strained cladding

As already mentioned at the beginning of Chapter 3, it is important to distinguish fragmentation and relocation/fuel repositioning. Semi-integral tests performed at Halden and Studsvik described in Chapter 2 show that the contact between the pellet and the cladding reduces the effect of the LOCA burst on fuel relocation. As shown on Figure 3.3-2, with a low cladding deformation (about 1.5% at room temperature), the HBS area can be fully powdered and the pellet centre can be fragmented for a high burnup rod (local burnup > 70 MWd/kgU). In this case, there has been no major axial fuel movement and cladding restraint does not seem to suppress fragmentation. Does it limit fragmentation / powdering to certain areas only?

The out of pile tests performed on high burnup samples (~70 MWd/kgU) at Studsvik with and without an axial slit show that the compressive stresses imposed by the cladding inhibits cracking in the external HBS zone but not in the inner precipitation parts of the pellet (see Section 2.2.2).

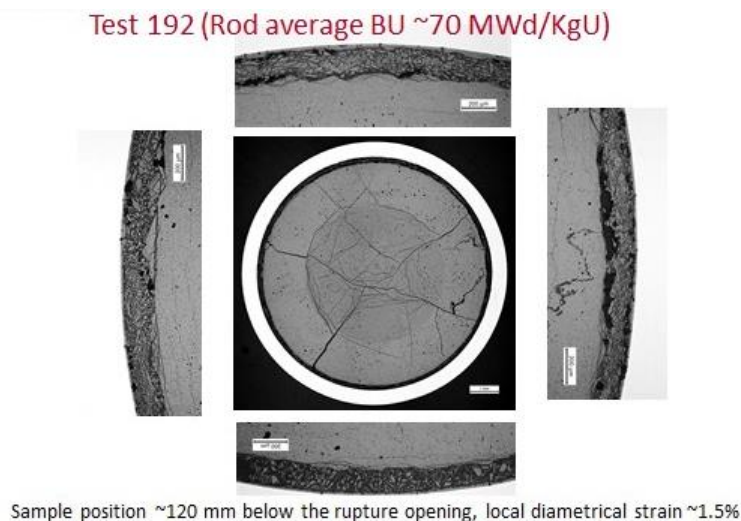


Figure 3.3-2: Ceramiography of test No.192 performed at Studsvik after LOCA and shaking [3.1-1]

In CEA test on an 83 MWd/kgU UO₂ sample with the cladding shows already some fragmentation due to the thermal transient, with no fuel movement. The same test with an axial slit shows some fuel movement outside the sample.

According to the published information, if the effect of the axial slit seems clear on fuel movement outside the sample, it is not clear it has an impact of fuel fragmentation/powdering occurrence.

Is there any impact on fragment size and repartition in the out-of pile tests? Is there a difference between 0% of cladding deformation and ~1.5% of cladding deformation? Those questions are still open and need further investigations.

As described in Section 2, a heat treatment performed by CEA at 1 300°C on a HBS fragment mechanically extracted from the rim (estimated burnup: 140 MWd/kgU) shows no additional fragmentation. There was no constraining on this fragment. This fragment was tested outside of the usual macroscopic environment (the pellet inside a rod) of such a fragment when subjected to a LOCA transient. Such separate effect test is also interesting when trying to de-convolute individual phenomena.

The cladding restraint depends also on the cladding temperature as the cladding mechanical properties will significantly decrease with increasing temperature. As a result, the level of restraint brought by the cladding is temperature dependent and evolves during the transient.

Finally, it is worth noticing that cutting a slit in a cladding of an irradiated rod, at room temperature, does not induce by itself fuel fragmentation.

3.3.3 *Effect of burst / no burst*

In Halden and Studsvik semi-integral LOCA tests, fuel characterisation is always performed after the burst. Questions can be raised about the potential influence of the burst (sudden pressure loss at rupture location, gas from the plenum flowing across the pellets) on pellet fragmentation (relocation/dispersal issues are not addressed in this section).

Is there a mechanical effect of the gas flow?

The comparison of two sibling rods in Halden with and without burst shows that fragmentation measured by post-test sieving is similar in both cases [3.1-20]. This result confirms that rod almost instantaneous depressurisation during the burst may not play an additional role on the mechanisms leading to fuel fragmentation (at the test burnup level).

Moreover, out of pile heating tests used to study fragmentation and fragmentation thresholds are generally performed under atmospheric pressure (or under vacuum) and do not simulate the depressurisation associated to the cladding burst. Nevertheless, they provided similar outcomes as the semi-integral tests including the burst phase.

Does the axial fuel fragments relocation observed in the semi-integral tests induce additional fragmentation of the pellets?

In high burnup rods, at axial location where the fuel did not relocate, for instance in the Studsvik test No.192 presented on Figure 3.3-2, HBS is powdered and the fuel central part is fragmented. These fragmentations cannot be induced by the movement of neighbouring fuel. Nevertheless, it is possible that axial relocation induces a refining of the fragments but it is not the main driver for fuel fragmentation in a LOCA transient.

3.3.4 *Effect of rod ballooning (hydrostatic pressure / rod internal gas pressure reduction)*

During the ballooning and the burst, there is a pressure drop in the rod due to the inner rod volume increase and later to the cladding burst. Does this pressure drop play a role in the pellet fragmentation?

During the test mentioned above performed on two sibling rods in Halden with and without burst, the rod ballooning led to a rod inner pressure decrease of about 20 bars from maximum pressure to the scram and about 30 bars from maximum pressure to the moment where cladding temperature reached 500°C.

Out of pile furnace heating tests performed by NFIR on 71 MWd/kgU (local burnup) samples under various levels of hydrostatic pressure show that at 1500°C terminal temperature, FGR (thus pellet fragmentation) is inhibited when the hydrostatic pressure is above ~40-60 MPa [3.3-1] [3.1-22]. This shows that a pellet constraint, in this case by hydrostatic pressure, inhibits fuel powdering.

What would be the minimum hydrostatic pressure for FGR and fragmentation inhibition at 600-800°C (fuel average temperature in the semi-integral Halden and Studsvik tests)?

It is also worth noticing that during rod puncturing at room temperature of an irradiated fuel rod, the induced pressure drop does not lead to fragmentation.

An out-of pile heating test at ~900°C performed on three 52 MWd/kgU segments with different rod inner pressures showed that, [3.3-6]:

1. With balloon without burst, no fuel fragmentation could be observed but some fuel powdering has been detected. In this test, significant cladding strain along the entire fissile column has been measured, showing that mechanical constrain from the cladding was lost.
2. With balloon and burst, fuel fragmentation and relocation was observed on three pellets. A localised balloon around burst was achieved.
3. Without ballooning/burst showed no evidence of fuel fragmentation.

Above observations were based on neutronography, with a 40 μm resolution which does not allow to visualise fragmentation without fuel relocation (axial or radial).

TRANSURANUS calculations give the evolution of rod inner pressure for each case (see Figure 3.3-3):

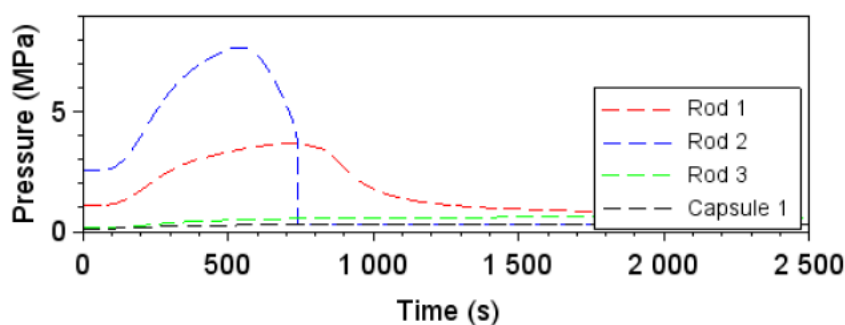


Figure 3.3-3: Evolution of rod inner pressure during the heat treatment test calculated by TRANSURANUS code for the three tested rods

Post-test fuel fragments sieving exhibited similar trends regarding fragments size for rods 1 and 2, with slightly larger number of small fragments in rod No.1. In both cases, there is only a small fraction of fine particles (< 5% below 5 mm diameter particles). FGR is similar in rods 1 and 2 (slightly above for rod No.2) but is roughly 50% lower for rod N°3.

Cladding stress (Yield stress of Zircaloy-4) is evaluated to vary from 700 MPa at 300°C to 5 MPa at 900°C [3.3-6].

This shows that cladding restraint, even at a low level, limits FGR and that burst does not significantly promote FGR. Authors conclude that both ballooning and burst increase pellet fragmentation [3.3-6] but those conclusions are based mainly on neutronography which reveals clearly fuel relocation but may not be able to reveal the actual fuel cracking/fragmentation as defined in this report when there is no relocation.

As a result, the above conclusion should be rephrased as follows: cladding ballooning increases fuel relocation but its direct impact on fuel fragmentation still needs to be investigated/confirmed.

3.3.5 Effect of thermal stresses during quench

In Studsvik tests on the high burnup rod No.192 (70 MWd/kgU father rod average burnup), the camera used to film the test clearly shows that fragmentation occurred before or during the burst. Quench occurs after burst and does not play a role on the observed fragmentation.

This statement is confirmed by the fact that the experimental results of the in-pile semi-integral LOCA tests in Halden (without any quench phase) and those performed in Studsvik hot cell (with a quench phase) are quite similar (as far as FFRD is concerned).

3.3.6 *UO₂ oxidation in steam*

In CEA's test FLASH 5, some fuel fragmentation and grain growth was observed on a 51.7 MWd/kgU rodlet in the central part at the peak power location. It was attributed to UO₂ oxidation with water during the long time (12 minutes) at power (7.2 kW/m) after the burst, leading to fuel temperatures close to 1 600°C and not to the LOCA transient itself.

Halden test duration at high temperature is rather short. With the oxidation kinetics of UO₂ in steam, the level of oxidation is expected to be negligible.

In Studsvik tests on the high burnup rods (70 MWd/kgU father rod average burnup), the movie of the test shows that fragmentation occurs before or during the burst. Oxidation cannot have taken place before/during fragmentation.

In Studsvik tests at low burnup (55 MWd/kgU father rod average burnup), fragmentation is not significantly higher than usual base irradiation cracking. The test duration at high temperature (above 1 000°C) is rather long (up to 15% Cathcart-Pawel-ECR cladding oxidation) with an open burst and vapour ingress into the rod (see Chapter 2). In this test, the vapour/pellet interaction after burst did not play a significant role in additional fragmentation.

Moreover, the dedicated out of pile test for EPRI performed at Studsvik (see Section 2.2.2) in an inert atmosphere showed similar fragmentation as the sibling test performed in air. This test demonstrates that pellet oxidation does not play a role on fragmentation.

The conclusion is that pellet fragmentation cannot be related to UO₂ oxidation in steam nor in air.

3.4 **Conclusions about fuel fragmentation mechanism during a LOCA**

Halden and Studsvik semi-integral LOCA experiments and other separate effect tests (see Chapter 2) show that there is a burnup below which there is no significant additional fragmentation compared to base irradiation normal cracking. Above this threshold, there is an additional fragmentation leading to smaller fragment sizes. The threshold value is discussed in Chapter 6 but it is about 60 MWd/kgU for Halden tests (segment average burnup) and between 55 MWd/kgU (corresponds to segment average burnup of 60 MWd/kgU) and 69 MWd/kgU (corresponds to segment average burnup of 72 MWd/kgU) for Studsvik tests. The same burnup threshold has been obtained by NFIR by compiling hundreds of heating tests, performed in various test conditions.

The main conclusion from these test results is that the fragmentation mechanism during a LOCA and its associated key parameters are not completely understood. Nevertheless, some partial conclusion can be derived from the large number of tests results already available.

Experiments and detailed fragments analysis suggest that powdering starts at pellet periphery, in the HBS structure as burnup increases, but fine fragmentation may also concern other areas in the pellet, where gas precipitation is high. This allows concluding that there is a link between gas precipitation during base irradiation and fragmentation, confirming HBS is not the only area that may result in potential fine fragmentation.

In this section, the main parameters susceptible to have an effect on fuel fragmentation have been analysed individually. From this individual analysis, the main conclusions are summarised below.

The analysis shows that temperature (gradient, magnitude and kinetics) is a key parameter but it is not the only one. Hydrostatic pressure could also be another key parameter but advanced modelling is needed to quantify the actual effort of hydrostatic pressure on the fuel behaviour during a LOCA transient.

Fuel rod is a complex system in equilibrium during base irradiation and cooling down phases. The loss of this equilibrium, due to the modification of one or several parameters, will favour fuel

fragmentation. Further analysis and dedicated fuel rod modelling are required to propose a complete mechanistic scenario and to quantify the impact of each parameter on the stress distribution in the pellet.

Comparing the cracking pattern and the fragments sizes distribution in the centre and in the periphery of the pellet suggests that various temperature dependant mechanisms are involved in each zone where the influence of the main parameters may play in different ways.

Bubbles (pressurised and not pressurised) and irradiation (defects, fission products) also modify the matrix or the grain boundaries strength and can play a role in fuel fragmentation.

Separate effect tests suggest that hydrostatic pressure above ~40-60 MPa inhibits transient FGR and therefore the pellet fine fragmentation.

Pellet to cladding bonding seems to reduce HBS powdering at the very interface (and perhaps not in a generic way) but does not inhibit HBS powdering in the remaining HBS layer.

Parameters which do not seem to play a role, according to the available results:

Experiments confirm oxidation at high temperature and quench phases do not impact the level of fine fragmentation.

Parameters which role is still unclear:

Rod burst, apart from the rod internal depressurisation and the associated reduction of the hydrostatic pressure, does not seem to play a key role in fuel fragmentation. This statement should be nevertheless documented further, in particular for high burnup rod.

The role of fission products, either in the matrix mechanical properties evolution or on bubble pressurisation/grain boundaries resistance hasn't been fully addressed today.

Rod power history seems to have an impact on fragmentation but the underlying mechanism is not understood.

Cladding strain plays a key role in fuel relocation but it does not seem to play a direct role on fuel fragmentation itself. At the most, it only reduces the fragmentation extent or impacts the fragment size and fuel fragments relocation.

One possible mechanism is that under the temperature rise in pellet periphery, the gas pressure increases in the HBS bubbles leading, for some of these bubbles, to violent grain boundaries separation. As a result, crack propagates along weakened or highly stressed areas. Does this mechanism apply also when needle-shape fragments are observed, still need to be confirmed. It is likely that at lower burnup, the local stresses due to thermal gradients or stress balance evolution from base irradiation should play a larger role than at higher burnup.

Regarding fine fragmentation occurring at high burnup in the centre of the fuel pellet, other mechanisms have to be identified (pressure levels in the pellet centre bubbles are quite high at the beginning of the LOCA transient but shouldn't increase during the transient as the temperature in the pellet centre decreases). At pellet centre, the weakening of the matrix, for instance by intra-granular or inter-granular bubbles inherited from base irradiation cannot explain on its own the observed fine fragmentation. Additional modelling would be necessary to identify the driving force which promotes fragmentation.

4. APPLICABILITY OF EXISTING EXPERIMENTAL DATA TO THE REACTOR CONDITIONS

4.1 Semi-integral test conditions versus in-reactor conditions

4.1.1 Heating methods

Experimental heating method used in the LOCA semi-integral tests may play a role on fuel fragmentation phenomena. Two heating techniques are available:

- infrared heat transfer
- partial nuclear heating.

This section presents both techniques and a tentative analysis of their potential effect on FFRD.

4.1.1.1 Infrared heat transfer

Heaters radiating energy, for example tungsten-halogen lamps, are installed in a furnace around a quartz tube. The radiated energy is maximal at the furnace focus point, where the specimen is located. However, the specimen is gradually out of focus when the cladding balloons or if the rod bows, making its temperature evolution measurement more uncertain.

The efficiency of the radiant energy transfer, i.e. the absorption on the surface of the specimen, depends on the emissivity of the surface. For non-shiny surfaces such as oxidised Zircaloy cladding, the emissivity is high and contributes to an efficient heat-up. The impinging energy is transferred by conduction through the cladding into the fuel pellets which act as a heat sink.

Since the heat flux comes from outside of the fuel rod, the pellet's temperature radial gradient and its evolution are reversed as compared to in-reactor LOCA conditions. At the beginning of the experimental transient, the cladding is hotter than the pellets. The temperature difference may increase when the cladding strains out and balloons but this trend is likely compensated by the fact the cladding is more and more out of focus (and thus less heated).

Infrared heating technique is used in Studsvik LOCA semi-integral tests. An example of calculated pellet's temperature radial gradient is presented in Figure 3.3-1 for test No.192 at failure time.

4.1.1.2 Nuclear heating

The energy driving the development in a LOCA is mainly the decay heat from radioactive fission products and fissions induced by delayed neutrons, the latter playing a minor role. This rod-internal power generation can be simulated by a low level of nuclear heating on the order of the decay power which is about 6-7% of the power at which the LOCA started after a longer period of steady state operation. For a linear power of 200 W/cm at the start of the transient, the initial decay power would thus be 12-14 W/cm.

Since nuclear heating produces heat flux going from inside to outside the fuel rod, the temperature gradient in the pellet resembles the one developing in a reactor LOCA, and the pellets are at a higher temperature than the cladding. The temperature difference increases when cladding distension and ballooning separate the cladding from the pellets.

The implementation of nuclear heating is demanding and less often used than external heating. Nuclear heating technique has been used in 5x5 PWR bundle tests in the Phebus reactor [4.1-1] and, more recently, in the single rod IFA-650 series in the Halden reactor [4.1-2]. Nevertheless, in Halden's IFA

650 test series, the insufficient nuclear heating of the single rodlet has been combined with an external electrical heating (which could simulate the radiation effect of neighbour rods in a bundle).

In Figure 3.3-1 calculated pellet's temperature radial gradient in test IFA-650.4 at failure time and in Studsvik's test No.192 at failure time are compared. We can notice a slight inversion of the radial temperature distribution between the two experimental rigs, due to the fact that there is no nuclear heating in the case of Studsvik experiment, but only an external heating. It has been checked that this radial gradient difference does not induce any major difference in term of stress distribution within the pellet [4.1-9]. It can be concluded at this stage that the heating technique has likely very limited impact on the fuel fragmentation of the pellet.

No information is available about azimuthal temperature gradient for IFA-650 and Studsvik's devices.

4.1.2 Axial power and temperature distribution

In out-of-pile LOCA tests the axial power distribution in the specimen depends on the furnace geometry, i.e. the distance between the specimen and the heaters and the additional length of the heater relative to the specimen length in order to minimise the end effects.

In Studsvik test device, the approximate oxidation temperatures is calculated on the basis of measured oxide thicknesses by using Cathcart-Pawel equation and considering the programmed heat up ramp, a 200 second hold time and the observed cool down. The measurements give an image of the axial temperature profile, see Figure 4.1-1. This profile is not much different from the one observed in the in-pile LOCA tests (see Figure 4.1-2 below)

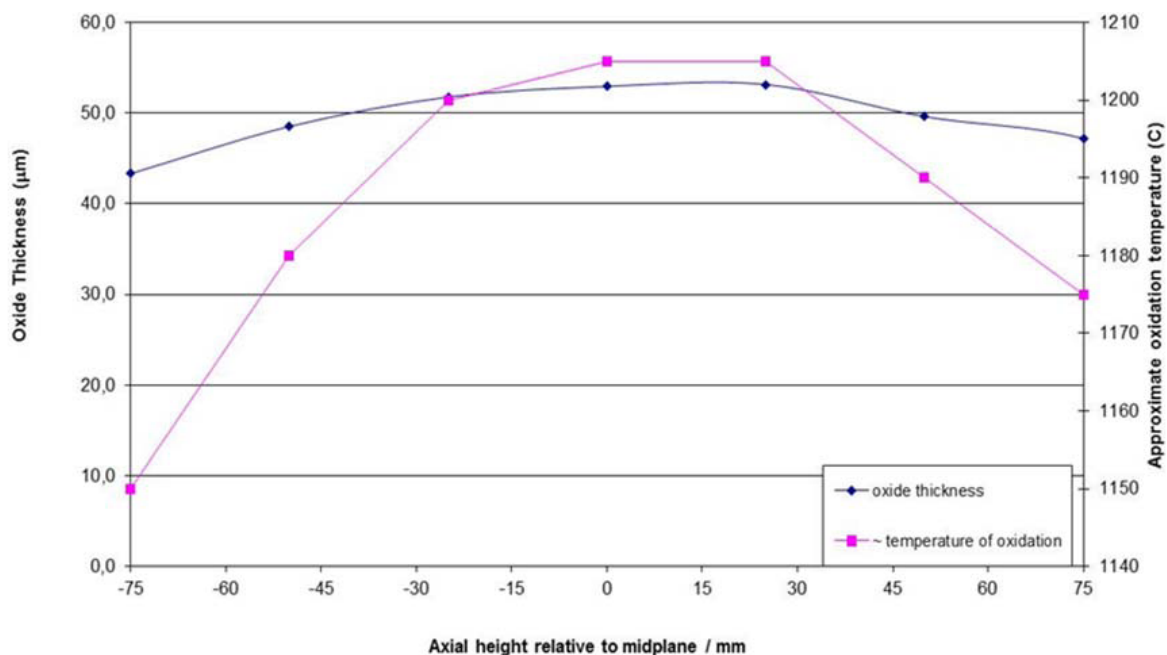


Figure 4.1-1: Axial temperature profile in Studsvik semi-integral LOCA tests derived from the oxidation axial profile

In In-pile LOCA tests, the axial temperature distribution is linked to the core axial power distribution and to some extent to the insulation conditions along the test rig. This insulation is designed to minimise the axial temperature gradient, but minor end effects are difficult to avoid.

The axial power distribution depends also on the in-reactor irradiation conditions of the specimen. To facilitate further analysis, test specimens are usually taken from locations in the father fuel rods where the

burnup distribution is uniform (middle spans). Given a uniform distribution of the fissile content, the axial power distribution follows the neutron flux distribution which is determined by the geometry of the test reactor core. For a given length of the specimen, the power distribution will be more peaked for shorter than for longer cores. An example is shown in Figure 4.1-2 for a segment tested in the Halden reactor.

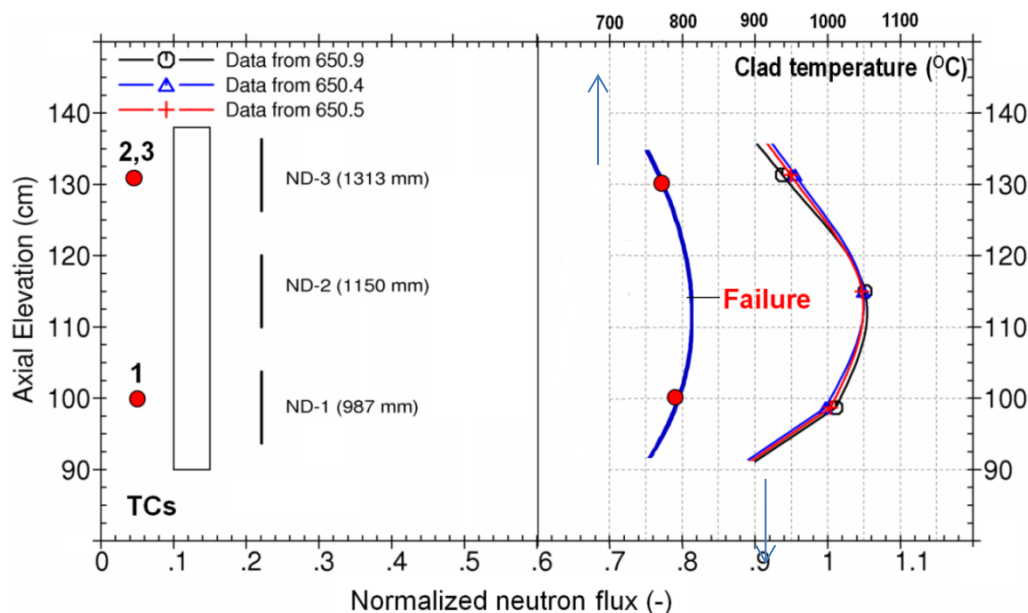


Figure 4.1-2: Axial power distribution in test specimen of HALDEN IFA650 test

The cladding temperature is measured at two axial elevations as indicated in Figure 4.1-2. At the time of failure, the temperature close to the upper end was lower than at the corresponding position at the lower end in agreement with the neutron flux measured at the same elevations.

The active height of the Halden reactor core is 80 cm, and the peak-to-average neutron flux or power is 1.05 over the length of the specimen (48 cm). Experimentally, the slight power peak is an advantage because it makes the position of maximal ballooning and burst more predictable.

As in-reactor axial temperature profiles (and their evolution during a LOCA transient), are highly dependent on the LOCA case to be considered, it is then difficult to assess how prototypical are the semi-integral tests conditions.

Nevertheless, the differences between in-reactor and out-of-reactor tests conditions are mainly related to:

- the rod length and the possible distance between the plenum and the burst location
- the ratio between the plenum volume and the rod length
- the presence of at least one spacer grid between the plenum and the area susceptible to balloon and burst (the axial gas communication between the plenum and the burst location might be impaired by the over-cooled grid)
- the presence of neighbour fuel rods and guide tubes which can create azimuthal temperature gradients in the fuel rod (and reduce consequently the balloon sizes)
- the temperature evolution which can promote axially extended balloons.

All these parameters might have an impact (to be quantified) on FFRD.

4.1.3 Evolution of the thermal transient

The evolution of a large break LOCA (LBLOCA) is known through code calculations validated on dedicated thermal hydraulic loops. The accident takes a different course in different reactor types, and even for the same type (e.g. PWR), design differences will lead to different developments.

Figure 4.1-3 illustrates the pressure difference across the cladding and the temperature transients for fuel rods at normal and high rating predicted by a conservative evaluation model applied to a PWR [4.1-3].

Although LOCA transients might be quite different from one plant design to another, conservative scenarios can be defined and used to quantify the LOCA limits and assess the available margins.

After the coolant blowdown, we usually define the 4 specific phases in each rod:

1. fuel heating
2. cladding ballooning and burst (if conditions are met)
3. high temperature steam oxidation
4. quenching.

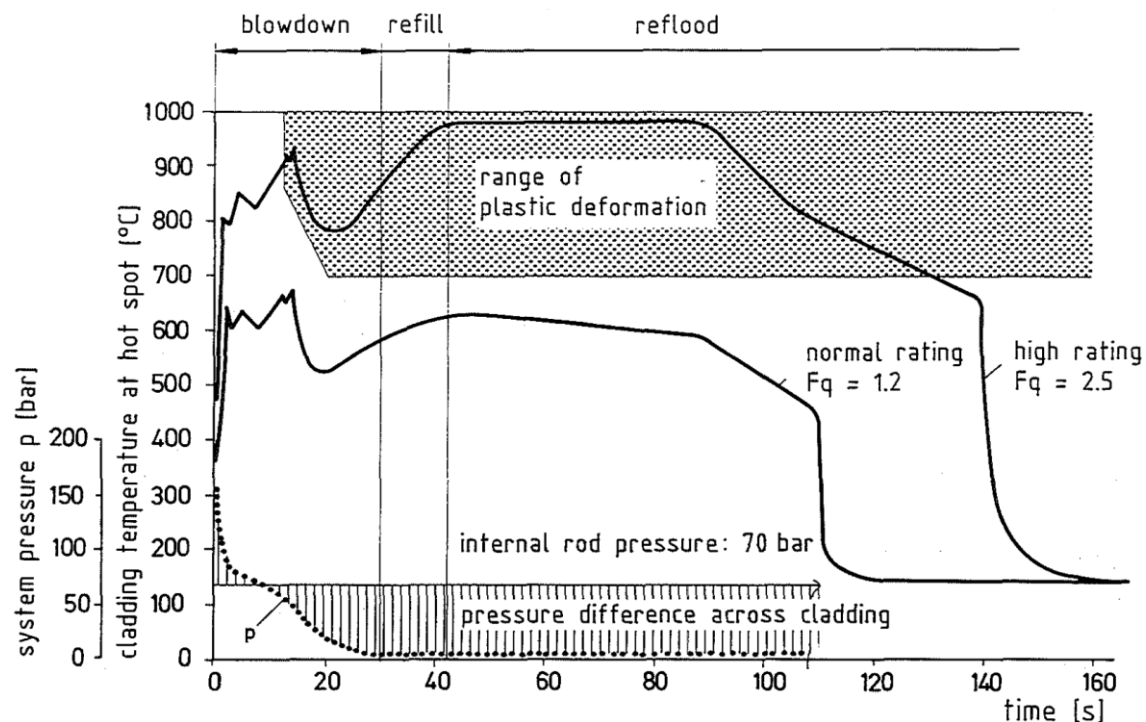


Figure 4.1-3: Fuel rod cladding load in a double-ended cold leg break LOCA [4.1-3]

While not intended to reproduce the dynamics of a reactor blow-down, semi integral tests, and in particular in-pile tests, can reproduce the general features of a LOCA as shown in Figure 4.1-4 from the HBWR IFA-650.2 commissioning test which was used in LOCA code benchmarking [4.1-4].

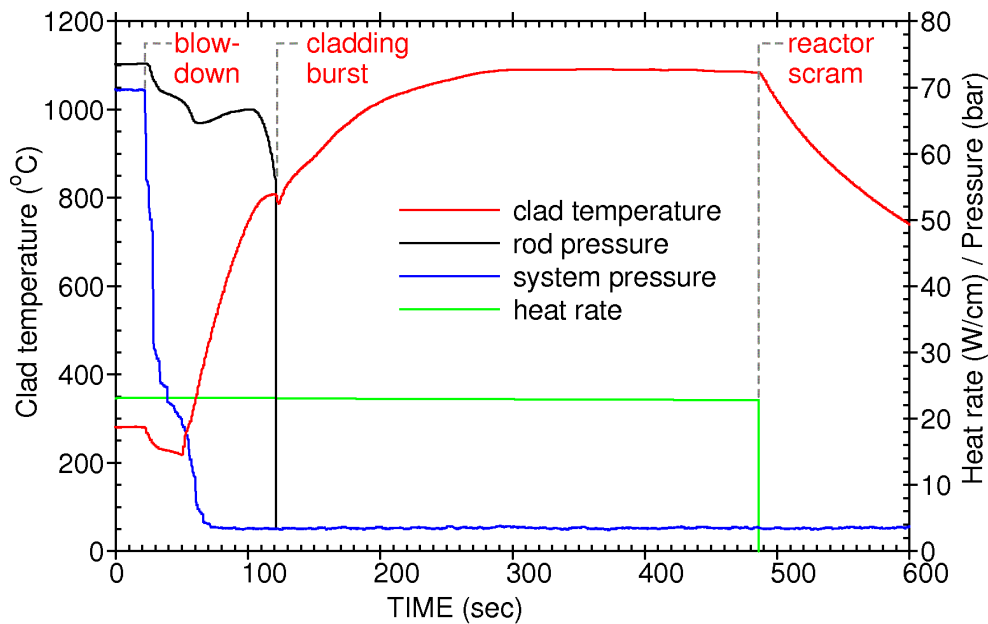


Figure 4.1-4: Blow-down and heat-up in an HBWR in-core LOCA test

Nevertheless, some in-reactor LOCA transient conditions cannot be reproduced with the available techniques or have not been reproduced intentionally:

- Temperature oscillations due to primary coolant flowing phenomena are expected during the in-reactor fuel heating phase have not been simulated in the semi-integral LOCA tests. These temperature peaks may modify the cladding's mechanical properties and by that affecting the strain at burst of the fuel rod and, possibly, the level of FFRD (which is known to be highly related to clad deformation).
- The quench temperature and kinetics have an impact on the cladding mechanical properties and the way the fuel rod is loaded. In-pile semi-integral tests such as Halden LOCA test cannot simulate the quench phase. This limitation may have an impact on the final amount of fuel particles dispersed in the coolant (additional dispersal could occur during the quench phase). Out-of-pile semi-integral LOCA tests, which can simulate prototypical quench phases, could provide relevant information regarding this issue. Unfortunately, the times the fuel particles are ejected out of the burst opening are not precisely measured in those tests. It is expected that most of FFRD occur at the burst time.

4.1.4 Steam environment during reflood stage

For some LOCA transients, in particular when the breach is small, the depressurisation of the primary circuit is incomplete and the coolant pressure remains at a level much higher than during a LBLOCA.

It has been shown that oxidation under pressure may introduce a slight oxidation kinetics' enhancement of the cladding for specific alloys [4.1-10]. Since the high temperature oxidation occurs after ballooning and burst of the cladding (when FFRD phenomena has already been activated), this enhanced oxidation kinetics is not expected to have a specific impact on FFRD. As a consequence, the fact experimental semi-integral LOCA tests devices cannot simulate high steam pressure conditions; it is not a concern as far as the FFRD issue is concerned.

In a few IFA-650 tests, a spray has been used during the high temperature oxidation phase to regulate the fuel rod temperature and to provide enough steam flow. Nevertheless, the actual steam flow is not controlled and non-prototypical steam starvation may occur locally. In these specific conditions, inner and outer oxidation of the ballooned zone after burst may be insufficiently representative of in-reactor-cases. This may have an impact on how the balloon area, its temperature and its additional oxidation, is affected by fuel relocation.

4.1.5 Test geometry versus in-reactor geometry

Experimental conditions of in-pile semi-integral LOCA tests performed in test reactors like PBF, Phebus, MIR or Halden are usually recognised as more prototypical than those of out-of-pile semi-integral LOCA tests. In-pile LOCA tests exhibit the following features:

- a depressurisation phase can be simulated
- heat can be generated within the fuel pellet
- impact of fuel fragments relocation on axial power and temperature distributions or on other temperature dependant phenomena (cladding oxidation, secondary hydriding, etc.) can be investigated.

Nevertheless, as mentioned earlier, test conditions cannot reproduce the wide variety of in-reactor LOCA conditions and not all the tests outcomes can be used directly: in fact, in-pile (or out-of-pile) LOCA tests aim at validating models and calculation tools which are used to simulate in-reactor LOCA transients.

4.1.5.1 Single rod versus bundle

A fuel assembly consists of an $n \times n$ array of fuel rods in contrast to many of the in-pile LOCA experiments which are single rod tests (excepting Phebus or MIR LOCA tests).

The “bundle effect” during a LOCA transient is mainly related to the azimuthal temperature distribution generated by the guide tube or the neighbour rods. Experimental data show that uniform azimuthal temperature in the cladding promotes larger ballooning [4.1-5]. As a consequence, single rod tests, where azimuthal temperature gradients are minimised by construction, tend to provide bigger balloon sizes than in multi-rods tests. In the opposite, multi-rods tests allowing for rod-to-rod contact during and after ballooning should exhibit inhomogeneous temperature distributions, early burst and limited balloon sizes.

However, according to the review of many single and multi-rods LOCA tests in [4.1-3], the deformation behaviour of zirconium cladding tubes in bundle geometry follows the same phenomena as those observed in single-rod tests. The burst temperatures and burst pressures determined in the bundle tests as well as the burst strains as a function of the azimuthal cladding temperature difference agree with the burst data measured on single rods. Unfortunately no information is available about azimuthal temperature gradient for IFA-650 and Studsvik’s devices.

Even if balloon strain seems to have a first order effect, other parameters play a role on FFRD. This conclusion does not allow concluding about the relation between azimuthal temperature gradient and fuel fragmentation and dispersal. It is then difficult to extrapolate single rod tests results to bundle in-reactor geometry FFRD studies.

Even if the quench/re-flood phase is included in a single rod test, flow blockage due to ballooning and/or ejected fuel is difficult to address in a realistic manner in single rod geometry.

4.1.5.2 *Test rodlet (versus actual rod) length, plenum volume and internal pressure*

Rod length is one of the unavoidable differences between a test rod and a full length commercial fuel rod. A typical segment length in the Halden IFA-650 tests is 40-50 cm and 30 cm in the Studsvik/U.S.NRC tests [4.1-6].

The design of an experiment must carefully consider the free volume in the test segment. Should the fuel-to-volume ratio be about the same as for a commercial fuel rod (meaning that the absolute free volume would be quite small due to the shorter length of the test rod) or should the absolute volume be about the same?

The answer depends on the test objectives, but in many cases it is more important to keep the absolute volume (and the number of gas moles and the pressure) comparable to the values of commercial fuel rods, which enhances balloon size and consequently, fuel fragmentation. In the alternative, the pressure in the rod would drop very quickly due to the volume increase by ballooning which in turn would unrealistically influence the ballooning process and limit the size of the balloon.

The total free gas volume (including the gas line, pellet cracks, gaps volumes...) is not always well known. The actual gas communication during the transient between the plenum and the balloon area isn't well known either and may play a key role.

The potential contribution of the above (initial free volume and axial gas communication) on ballooning and burst is hard to quantify because plenum and pressure line volumes, temperature and flow conditions are not always well known either in semi-integral tests.

Restricted axial gas flow was observed in several Halden and Studsvik tests where the pressure dropped slowly after burst (see e.g. Figure 2.1-6 in Chapter 2). The existence of this phenomenon influences the analysis/interpretation of the experiment. It can be assumed that the flow of gas from the plenum to the ballooning area is more impeded in a long rod than in a short rod. For the latter, the plenum is closer to the balloon, and gas availability can impact the ballooning and burst process more directly than in a typical high burnup commercial fuel rod where the plenum is at a greater distance from the peak cladding temperature (PCT) location. Combined with reduced gas transport caused by reduction of the pellet-cladding gap or even bonding as commonly observed at high burnup, this will reduce or delay the ballooning and burst process in a long rod, [4.1-7].

Plenum and pressure line conditions effect on sample's free volume conditions have been investigated in Studsvik's semi-integral tests [4.1-11]. It has been concluded that sample's hot gas may expand into the instrumentation line during test which causes a global delayed pressure increase. As plenum conditions are not fully known, these phenomena are not taken into account in most of the test modelling. As a consequence, FGR contribution to swelling, burst, or FFRD phenomena, are uneasy to quantify. To overcome this difficulty and to improve the analysis of the LOCA, it has been suggested to continuously measure the gas temperature within the instrumentation line.

IFA-650 tests have also been simulated (fuel device and connecting pipes, valves, break) with thermal-hydraulic specific code [4.1-12]. It was concluded that some unavailable experimental data (initial liquid mass/steam velocity...) are necessary to correctly simulate tested transient. Transient thermal-hydraulic parameters that may have an effect on FFRD phenomena are not fully known and their effect is difficult to investigate. To overcome this difficulty, it has been recommended to improve device's instrumentation.

In both cases making the link between FFRD test results and in-reactor cases has to be done with care, and it is observed that supplementary experimental data are still needed to succeed in full-scale analysis.

4.1.5.3 *Spacer grid impact on clad ballooning, burst opening and fuel relocation*

If a spacer grid is located between the fuel rod upper plenum and the PCT location, it will constitute an additional obstacle to the axial gas communication (at the spacer grid elevation, the burnup depletion will lower the local decay heat and thus will prevent the cladding to strain out). If the gas moles of the upper plenum cannot participate to the clad straining below the spacer grid, the localised balloon size will be smaller and fuel fragmentation and relocation will be reduced accordingly. Burst opening (and thereby fuel fragment dispersal) might be reduced for the same reasons.

Also it is assumed that a spacer grid, and the related localised strain restriction, could influence the fuel fragments relocation (the spacer grid could serve as a chokepoint to limit the extent of fuel relocation when fuel is fragmented above and below the grid location).

To confirm the potential impacts of a spacer grid on clad ballooning and fuel relocation, dedicated semi-integral LOCA tests have to be performed.

4.1.5.4 *Initial thermo-mechanical conditions of the test rods*

In an in-reactor LOCA transient the fuel rods are thermo-mechanically conditioned at linear heat rate (LHR) levels usually ranging from 15 to 25 kW/m, meaning that, at the beginning of the in-reactor LOCA transient, the pellet-to-clad gap is closed and the stresses in the cladding fully relaxed in most of the HBU rods (i.e. at burnups corresponding more or less to the FFRD burnup threshold).

In the semi-integral LOCA tests in Halden, the initial LHR is limited to 1 to 3 kW/m (see Chapter 2.1.1), preventing the test rod to be fully conditioned at the beginning of the LOCA transient. In other words, the experimental initial test conditions, by maintaining the pellet-to-clad gap opened, facilitate the initial axial gas communication between the upper plenum and the PCT location (thus enhancing clad straining) and reduce the amount of restraint provided by the cladding to the pellets (thus favouring fuel fragmentation). These two combined mechanisms will enhance most of the FFRD phenomena.

This is also true for the tests performed out-of-pile (Studsvik or JAEA semi-integral LOCA tests) with no initial LHR.

As a consequence, we could consider that the in-pile and out-of-pile initial test conditions are penalising as far as FFRD phenomena are concerned.

4.1.6 *Fuel relocation and dispersal*

Fuel relocation and dispersal are caused and influenced by a number of phenomena. Fuel relocation requires a volume increase. It was pointed out previously that distension and ballooning of the cladding tube depend on factors such as non-uniformity of the temperature distribution, gas flow or locally available gas, and physical restrictions due to the presence of neighbour rods. If the ballooning is small due to these reasons, there is less fuel relocation into the ballooned area. Accordingly, the local power increase caused by this relocation and its consequences would be less significant.²

After ballooning and burst, fuel dispersal may occur. Major factors influencing the phenomenon are the size of the burst opening and the gas pressure driving force. Both can be biased by a test set-up. As pointed out in Sections 5.3.2 and 5.3.3, rod length, plenum volume, rod pressure and gas flow are design

2. It must be noted that the impact of the relocated fuel on the local power enhancement and related cladding temperature rises in the ballooned area have not been measured : the enhanced local power assessment results from a calculation based on a filling ratio measured after the LOCA test (and further handling phases).

parameters or phenomena with an influence on the driving force for fuel expulsion and thus on the outcome of a test compared to the real case.

4.2 About separate effect tests

As they are performed on small fuel samples, separate effect tests are well suited to identify and study the main physical parameters that may have an influence on the FFRD mechanisms and phenomena (level of constraint, heating and cooling rates, temperature distribution, local burnups, type of environment, etc.). They can be conveniently used to confirm semi-integral test outcomes (e.g. fuel fragmentation burnup threshold) but generally separate effect tests need to be carefully analysed with appropriate tools, before drawing conclusions applicable to in-reactor conditions.

4.3 Discussion

Semi-integral LOCA tests on single fuel rods are obviously less prototypical than LOCA bundle tests but they are well suited to study various parameters by running a large number of tests in slightly different conditions. If the single rod test device is well instrumented, it will provide valuable data to validate the calculation tools that will be used in turn to qualify the test conditions, to evaluate the actual safety significance of the test results and to transpose the test conditions to the in-reactor conditions [4.3-1].

Test instrumentation improvements are still requested to improve test analysis. In particular, plenum and connecting pipes supplementary instrumentation are needed.

It has been also identified that reliable experimental measurements of the localised power enhancement and cladding temperature excursion due to fuel fragments relocation in the balloon area are still missing.

5. LACK OF EXPERIMENTAL DATA

In previous sections, numerous tests have been presented aiming at identifying the different mechanisms for FFRD and the potential consequences for reactor safety. Nevertheless, previous sections also show that these phenomena are not fully understood and additional data is still lacking to draw a self-standing conclusion. Many questions are also pending regarding the representativeness of the out-of-pile tests. This section identifies the current needs in complementary tests.

Enhanced fuel fragmentation seems to be the main prerequisite for all the detrimental consequences of relocation and dispersal. Therefore, the subsequent chapter begins with a discussion of potentially interesting data on the conditions for fuel fragmentation.

5.1 Fuel fragmentation thresholds

5.1.1 *Examination and validation of the threshold for fuel fragmentation*

Fuel fragmentation during LOCA transient is a phenomenon that has only become a concern since recently. Earlier LOCA tests were executed with fresh fuel and the fuel fragmented to sizes that were too large to be considered a concern, [5.1-1]. Such large fragments did not have relocation and ejection potential and, consequently, fuel dispersal and impact on PCT were not considered a safety significant issue.

The phenomenology of fuel fragmentation under the conditions of LOCA is discussed in Section 3 of this report. One of the important observations is that in the case of high-burnup fuel, large portion of the fuel fragments can be less than 1 mm [5.1-3]. Once fuel fragments with sizes less than 1 mm make up large fraction of all fuel fragments, they may have the increasing potential to easily relocate to different parts of the rod.

The fuel in high-porosity pellet rim of the high-burnup pellets, referred to as high-burnup structure (HBS), can have higher susceptibility for fragmentation to finer fragment sizes, and also for axial fuel relocation. That would have potential effect on a hot-spot formation in the ballooned region, due to higher decay heat generation in the pellet rim, and result in LOCA specific FGR from the high-pressure HBS specific pores.

At present, there is still a lack of the systematised data on the above hypothesised phenomena, and such data on well characterised fuel of PWR and BWR types with different conditions of last cycle power, fuel and cladding temperature, pore-pressure, particle size distribution, bonding, filling ratio, transient FGR, internal rod pressure and balloon sizes (see Table 5.7-1), is of great interest. Noting that, in burst rods, characteristics of fuel state of interest can be essentially modified by the axial gas flow, experiments with single rods that are ballooned, but not burst would be appropriate to this study, e.g. using a design similar to that of the recent ‘non-burst’ tests with BWR HBU fuel in Halden [5.1-6].

Upon fuel rod failure, the fragments could be entrained by the gas outflow and expelled through the cladding rupture into the core. An example of a LOCA test with severe fuel dispersal was Halden’s IFA-650.4 experiment. Online measurement signals, such as cladding and heater temperature, indicated onset of fuel relocation either during the clad ballooning, or immediately after the cladding rupture. The gamma scanning following the Halden LOCA tests revealed large region voided of fuel at the top. The level of burnup was about 90 MWd/kgU and the fuel fragmented to very small sizes. On the other hand,

LOCA tests IFA-650.12-14, that were manufactured from the same, or similar father rods of approximately 72 MWd/kgU burnup, showed medium to large fuel fragment sizes.

Similar observation was made in Studsvik's LOCA tests. The LOCA test 191 was prepared from a rod of average burnup close to 70 MWd/kgU and the test rod in LOCA test 196 was prepared from a rod at average burnup of about 55 MWd/kgU. Both of the rods are classified as "high-burnup" but only in test 191 large fraction of fuel fragments below 1 mm were observed. The experimental evidence from LOCA testing suggests, that there exists a fuel fragmentation threshold, which appears strongly correlated with the level of burnup but it may not be the only factor.

Halden's LOCA tests are executed 'in-pile', whereas Studsvik conducts 'out-of-pile' tests and this implies different LOCA testing conditions that may be influential. A paper by K. Yueh et al. [5.1-7], presented at WRFPM2014 conference, suggested a burnup threshold of 70-75 MWd/kgU (segment average burnup) that was derived from the evidence of the tests that they did on HBU fuel. They observed that all test samples that experienced severe fuel fragmentation came from fuel rods that were inserted in fresh fuel assemblies during their last cycle, and therefore experienced higher end-of-life power. They hypothesise, that the burnup threshold for fine fuel fragmentation also depends on the last-cycle power.

Besides the last cycle power and the level of burnup, there could be other factors that impact the fuel fragmentation threshold which are yet unknown. A limiting factor for fuel fragmentation is the cladding, because if there is no cladding deformation then there can only be limited fragmentation. Yueh et al. [5.1-7] observed, that the test samples, which had no cladding restraint (via pre-manufactured axial slit) fragmented considerably more than those with intact cladding.

Fuel fragmentation became of interest only recently, and as such there are still limited experiments studying this phenomenon, let alone appropriate models to be used in large system codes. For model development and Verification and Validation (V&V), further experimental study is needed to explore feasibility and quantify major dependency for the potential mechanisms of fuel fragmentation, shedding light on:

- the role of outward cladding deformation due to radial displacement of fragments stuck to the cladding by bonding
- the role of gas pressure in the HBS pores
- the role of the stress condition of the central pellet region by the pellet periphery, which has essentially higher temperature during the LOCA than during the base irradiation, as shown in Figure 5.1-1
- the potential impact of axial gas flow after the cladding rupture, and the potential role of fuel entrainment through the rupture on additional fragmentation.

While other phenomena, such as fuel dispersal, could be studied with mock-up tests, there is, most likely, no substitute for a high-burnup fuel in tests with the internal heat source to explore the fragmentation during the cladding heat-up and ballooning.

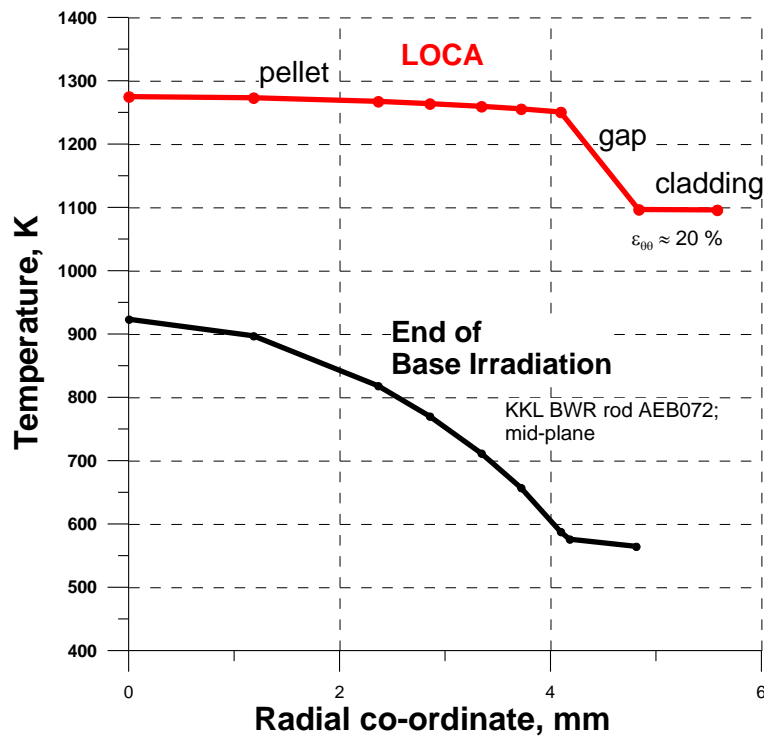


Figure 5.1-1: Calculated temperature distribution across a pellet radius at the end of base irradiation and during a Halden LOCA test [5.1-8]

5.1.2 Accounting for specific test conditions

As discussed in Section 4.1.5.1, the rod bundle may be characterised by essentially higher azimuthal temperature non-uniformity, than that in single-rod experiments. Therefore, the latter may show significantly higher cladding strain at burst, than in the conditions of a power reactor. Thus, e.g. in Halden LOCA test IFA-650.13, the very high uniformity of circumferential temperature distribution was shown through measurement, using two thermocouples set on the two sides of the cladding at the same axial level. The signals from the thermocouples were virtually the same, as shown in Figure 5.1-2.

In other LOCA tests, such as those using external heating, the azimuthal non-uniformity of cladding temperature may be more significant. Since the cladding strain has crucial impact on fuel fragmentation, proper quantification of the specific test conditions, such as azimuthal cladding temperature non-uniformity must be paid particular attention.

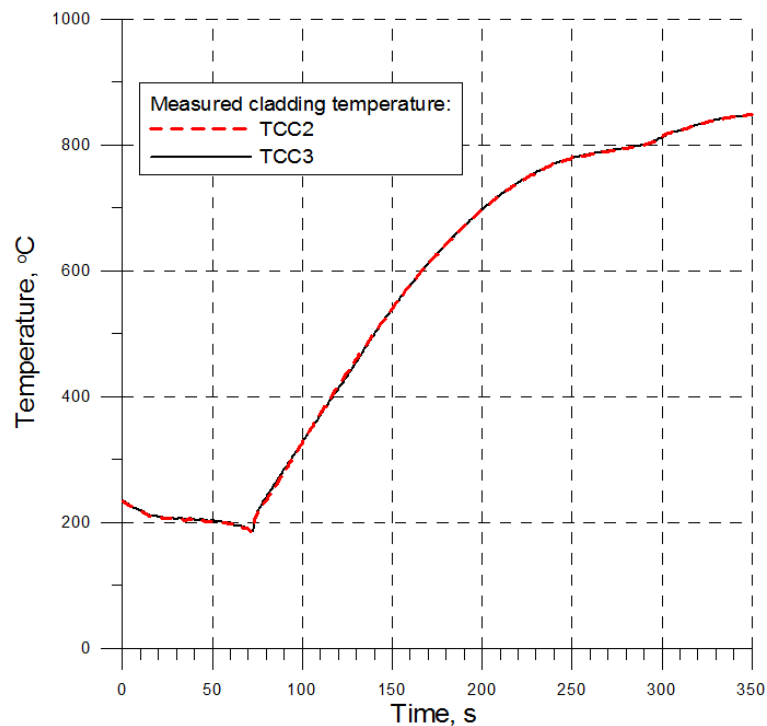


Figure 5.1-2: Measured temperature for two thermocouples at the same axial level in Halden LOCA test IFA-650.13

5.2 “Hot-spot” Effect of fuel relocation on cladding temperature

5.2.1 Combined effect of axial relocation and ballooning on the PCT of the ballooned rod and surrounding ones

Halden LOCA tests IFA-650.4 and IFA-650.9 are examples of significant fuel relocation. In case of IFA-650.4 fuel relocated from virtually the entire upper half of the rod and this event was captured by the heater and cladding thermocouples. Specifically, the upper cladding temperature dropped and the heater temperature at the mid-height or near the bottom of the rod increased. Clearly, the fuel that relocated was contributing to the cladding and heater temperatures. It is logical to assume, that fuel relocation into the balloon will contribute to the PCT. The extent of contribution will be dependent on the amount of relocated fuel (filling ratio), which ultimately depends on the fuel fragment size.

Ballooning and relocation will effectively move heat source closer to the neighbouring rod(s) (within the fuel bundle), which may impact the temperature of the neighbour rod(s). This conclusion is also supported by the thermocouple readings of the heater in IFA-650.4 LOCA test against the results of modelling [5.2-1], as shown in Figure 5.2-1, where the relocated fuel could impact the heater temperature.

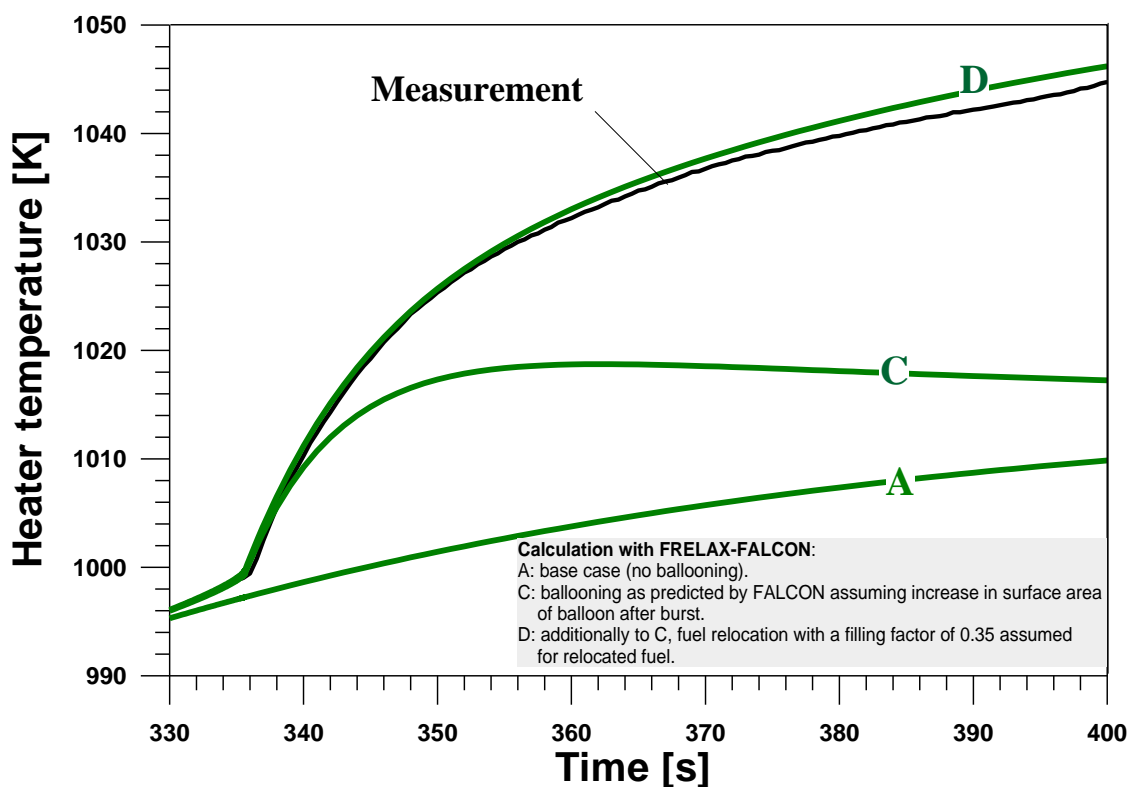


Figure 5.2-1: Measured heater temperature at the level of balloon during IFA-650.4 test against calculation by the FRELAX-FALCON codes [5.2-1]

As presented in Figure 7.3-4, the estimated temperature of the fuel at the level of the balloon can exceed PCT by $\sim 100^{\circ}\text{C}$ due to ballooning with a filling ratio of 70% (curve D3 vs curve C): a very important preliminary result of modelling, which is to be verified experimentally. In order to confirm experimentally this theoretically assumed behaviour, it is necessary to have well instrumented tests which will be able to measure the fuel and cladding temperature at the balloon or at least near the balloon area and with a good characterisation of the filling ratio and fragments size.

Attention is to be paid to experimental studies on the direct (immediate) effects of the ballooned rod and/or ejected fuel on the neighbouring rods, aiming to address the question whether these effects are able to increase PCT, or even cause a ‘burst chain’.

Perhaps mock-up experiments can be designed with real cladding tubes and pre-manufactured balloons. To simulate the heating from inside the rod, a specially-shaped heater can be introduced which will supply more heat at the balloon level.

Precise positioning of the balloon will allow for precise positioning of the cladding thermocouples. Such experiments would thus address the thermal effects of ballooning without the use of radioactive nuclear fuel as the heat source.

Experiments without fuel can be done, which will significantly reduce the difficulties associated with handling and post-irradiation examinations.

Nevertheless, all the above separate effect tests are relevant only if the actual heat transfer between the relocated fragments within the ballooned area and the cladding is well quantified. This is not the case today: the equivalent conductivity of the debris bed is well known but the conductance of the gap between the fragments and the inner side of the cladding is still undetermined. It would be valuable to set up specific experiments to quantify this gap conductance as a function of fragment sizes and filling ratio. The

nature of the gas mixture present in the gap might be an important parameter as well. Once the complete thermal chain is well known, separate effect tests with no real fuel fragments in the ballooned area, could be adequately designed to study the impact of superheated balloons and blocked channels on the overall thermal- hydraulic behaviour of a bundle.

5.2.2 Whether or not any “hot-spot” effect due to relocation on ECR is feasible

The combined effect of fuel relocation and ballooning on cladding temperature during the LOCA is not straightforward, due to the competing effects on the local LHGR and heat-exchange conditions, as discussed in Section 7.3.1 relating to the FALCON (PSI) code analysis for the test IFA-650.4 (see Figure 7.3-4).

If the hot-spot effect increases the cladding temperature locally, this will lead to an enhancement of the local oxidation and may eventually result in a loss of ductility. According to the embrittlement related safety criterion [5.1-4], the calculated local ECR is not to exceed a certain critical value. The above mentioned competing effects of relocation and ballooning on cladding ductility should be evaluated experimentally, which may result in a necessity to correct the modelling of ECR for the appropriate safety calculations.

The time to rod rupture is relatively short and therefore the hot-spot effect may have limited time to impact ductility. On the other hand, if the cladding temperature, which increases due to the hot-spot effect, approaches the oxidation runaway regime, then there may be significant impact on the ductility and threshold-ECR. The effect of a hot-spot on both local embrittlement and PCT is thus an important question and there is a lack of relevant experimental data, because temperature distribution is not known at all axial locations of the fuel rod and therefore the temperature increase due to the hot-spot effect cannot be measured.

Experiments to quantify the hot-spot effect on the ductility are necessary. As mentioned in the previous section, the heat source could be substituted by an appropriate design of the heater, the steam environment can be easily simulated and the cladding test tubes can be pre-oxidised. Until now, it remains uncertain, whether the impact of the ‘hot-spot’ on the ductility will be significant given the short time to cladding rupture and lack of evidence for a significant build-up of the relocated fuel in the balloon.

A detailed experimental setup has to be discussed with the experts from the experimental facilities.

5.2.3 Whether or not a “hot-spot” due to the relocation into the balloon is able to affect the burst of the rod in question

Precise experimental evaluation of the hot-spot effect does not exist. However, if fuel axially relocates in the balloon before burst, it is logical to assume, that increased local heat generation will increase the temperature of the cladding which means that a lower internal pressure already causes rod rupture.

Under the hypothesised effects of the hot-spot, the time to rod rupture will decrease. The driving force behind rod burst is temperature and pressure/stress. The heat source does not necessarily need to be supplied by fragmented fuel inside the rod. Hypothetically, special tests can be designed to investigate, whether and under which conditions a hot-spot in one of the two cladding tubes with the same parameters will result in significant difference in the burst time.

5.3 LOCA-specific transient FGR

5.3.1 Further experimental confirmation of the phenomenon and dependencies

LOCA-specific FGR, as high as ca. 20% of the total generated gas quantity, was directly measured after the Halden's IFA-650.14 test [5.3-1], which was a non-burst test [5.1-6] that experienced significant rod deformation and fuel relocation/fragmentation. This is just one test of particular level of burnup.

On the other hand, a study performed by Halden and presented at the EHPG in March 2013, showed that the actual releases of I-131 and Cs137 during the LOCA tests IFA-650.9, IFA-650.10, IFA-650.11 and IFA-650.13 [5.3-1] are much lower than the amount taken into account in the Safety Case Analysis (i.e. 30 to 40% releases of I-131 and Cs-137).

Halden Test	IFA-650.9	IFA-650.10	IFA-650.11	IFA-650.13
Nuclide I-131	98 and 86	96	99	99
Nuclide Cs-137	93	95	98	97
Reactor Type	PWR	PWR	VVER	BWR
Burnup (MWd/kg U)	90	60	55	72
PCT (°C)	1 100	850	950	850

Table 5.3-1: Retention (in %) of total activity measured in post-test fuel rods

To confirm IFA-650.14 test result other non-burst LOCA tests with both BWR and PWR HBU fuel should be planned, where the burnup level is varying in order to capture FGR for different conditions. In the experiments described by K. Yueh et al. [5.1-7] it was observed, that test samples with axial slit in the cladding (this measure was used to simulate the loss of cladding constraint due to ballooning) showed FGR starting at a temperature of 550°C until 850°C.

In the other samples, those with intact cladding, there was no indication of FGR up to 1 000°C. The striking difference between the two sets of samples was the degree of fuel fragmentation. The samples with the axial slit fragmented considerably more. It can be inferred, that some fuel fragmentation is necessary in order to observe transient FGR. Since fuel fragmentation is dependent on the cladding deformation, it can also be hypothesised, that if the LOCA transient is interrupted 'early enough' there may not be any transient FGR.

While some phenomena can be investigated without using nuclear fuel, insight into the LOCA-specific transient FGR cannot be obtained without the use of HBU nuclear fuel inside the rods. At least some tests must be conducted "in pile", using the fuel as an internal heat source.

5.3.2 Experimental clarification on whether transient FGR may affect the burst of the ballooned rod

The increase in temperature due to the LOCA transient will increase the pressure of the gas bubbles inside the fuel matrix. Until the cladding begins to deform radially outward, there can only be limited fragmentation, because the cladding exerts back pressure on the fuel and will counteract the increased pressure in the gaseous pores and bubbles.

In the high-burnup structure region of the fuel, where the fuel grain is very small, the fission gas is primarily contained at the grain boundaries. The fuel will fragment along the weakest region – which are, likely, the grain boundaries – and all the gas which is trapped there will be released. This is one mechanism of LOCA-specific FGR.

Experimental evidence of intact pellet-cladding bonding layer in high-burnup BWR fuel exists and the reason for this is hypothesised to be azimuthal non-uniformity of the burnup distribution in BWR fuel pellets (due to non-uniform exposure to thermal neutron flux) which is characterised by “high-burnup and low-burnup side”.

During normal operation, fission gas will strive for redistribution to establish pressure uniformity in the rod free volume. In hot conditions, the pellet-cladding gap is closed and the fission gas can be locally trapped until the power is reduced and pellet-cladding gap is reopened (for example, at refuelling) in which case the fission gas will be vented axially to the plenum.

In case of BWR fuel, the high-burnup side will develop stronger bonding layer than the low-burnup side and the low-burnup side will be able to accommodate gap opening at power reductions. This creates the condition for permanent bond-layer on the high-burnup side.

However, during LOCA, at high enough cladding deformation, this bonding can be broken and the trapped fission gas can be released. The difference with the first mechanism is that this gas is trapped in “pockets” within the bonding layer and not at the grain boundary pores, or in the fuel matrix.

It is without a doubt that transient FGR will contribute to the rod-internal pressure, which may in turn shorten the time to fuel rod rupture. Also, the rod is more likely to develop larger balloon, if the pressurisation is gradual (plastic deformation will be allowed to happen) as opposed to if the pressurisation is sudden. Therefore, the transient FGR may not only impact the time to rupture, but also balloon size, fuel relocation and ultimately the amount of ejected fuel.

So far, it is not quite clear which of the two mechanisms, just mentioned (i.e. gaseous pore/bubble opening, or trapped FGR due to pellet-cladding de-bonding), is the driving force for LOCA specific FGR, or both are in play. To shed light on these questions, special experiments should be designed and conducted.

5.4 Characteristics and effects of the ejected fuel

5.4.1 Quantified effects of initial gas quantity/pressure in the plenum and transient FGR on fuel dispersal

The thermocouples on the cladding and heater of IFA-650.4 LOCA test suggest that significant fuel relocation started either during clad ballooning or immediately after the cladding ruptured. Therefore in that particular test the significant portion of fuel relocation could be driven by the rod-depressurisation.

There was considerable fuel dispersal, which means that the gas had high entraining potential. Large gas plenum at the same pressure as small gas plenum implies that more gas needs to pass through the fuel stack and the rupture. It is logical to assume, that there will be greater solid-gas interaction for fuel rods with large plenums.

Transient FGR will increase the rod internal pressure (RIP) and will add extra gas to the gas plenum, which may increase the fuel dispersal. The discussed phenomena could be simulated by mock-up experiments that do not require irradiated fuel material, which might be used for V&V of the appropriate analytical models.

5.4.2 Any correlations for rupture size and shape with cladding pressure/temperature at burst

The rupture size will impose a limit on the fuel fragment sizes that can pass through. Also, the situation cannot be ruled out, that a larger piece will get stuck at the rupture opening and prevent smaller fragments from escaping.

In the case of Halden's IFA-650.11 LOCA test, the rupture opening was 5 mm long with 1 mm at its widest point. Very small amount of fuel was dispersed as it is evident from the gamma scanning after the LOCA test. Clearly, only fuel fragments smaller than 1 mm could get out.

Shape of the rupture opening will be an influencing factor on fuel dispersal. A long narrow crack will have the same surface area as a short but wider opening, while the difference in terms of quantity of ejected fuel can be dramatic. Mode of cladding rupture will be influenced by the cladding's ability to deform plastically and the pressure increase within the rod.

The general belief [5.4-1] is that high temperature ruptures are characterised by pin-hole rupture sizes, whereas low-temperature cladding burst – by wider openings. The HBU may show deviation from the empiric rules, that are established based on testing of the un-irradiated, or low-burnup fuel, in terms of rupture shape/size against rod pressure and PCT.

Abrupt pressure increase, for example due to transient FGR, may have severe impact on the pressure and rod burst. If the pressure quickly increases then the potential for achieving large balloon sizes is low. The rod burst will be abrupt and the balloon volume would likely be smaller. That could have happened in the Halden LOCA tests IFA-650.12/13, where a significant FGR during the LOCA transient, most likely, took place [5.4-2]. As a result, the cladding burst at low temperature (~850°C) led to a relatively small rupture opening (5 mm long and only 0.5 mm wide).

Non-nuclear fuel tests could be designed, in order to study fuel ejection (especially for gathering data for code V&V). RIP, balloon volume, rupture opening shape and fragment size can be precisely controlled in a mock-up experimental setup. Such experiments will be inexpensive, compared to those with real irradiated fuel samples.

5.4.3 *Temperature/enthalpy and heat-exchange surface area of the dispersed fuel*

The smaller the fuel fragments, the faster the heat transfer, because the surface area to volume ratio increases with the decrease in fragment size. In case of core re-flood, the interaction of dispersed fuel with the coolant may be as dramatic as small steam explosions (if the fuel is finely fragmented).³ Also it should be considered whether a possible ingress of water by a failed rod may cause further cladding damage by local steam explosions.

In the LOCA tests conducted at Halden and Studsvik, there was no simulation of core re-flood and hence this possibility has not been studied. Also, dispersed fuel interaction with neighbour fuel rods may be very different depending on the fragment size.

LOCA experiments with full length rods have not been done. If the fuel dispersal from IFA-650.4 and IFA-650.9 is transferred to NPP condition, then there could be half-meter fuel stack that will be expelled through the rupture. Of course, in reality NPPs do not operate fuel up to a segment average burnup of 90 MWd/kgU, therefore such tests can be treated as bounding cases for conservative estimates.

Provided that this stream of ejected fuel is targeted at a particular spot of neighbour cladding it may create problems. Thus, the effect of ejected fuel on neighbouring rods should also be addressed. This and other important questions might be addressed by specially designed bundle experiments, e.g. multi-rod, out-of-pile and in-pile experiments, using both mock-up and irradiated fuel, as recently proposed by NRA-Japan and U.S.NRC [5.3-3].

3. NB: It is expected that the fuel fragments dispersed in the coolant are sufficiently cold at the time of the reflooding phase not to generate any localized 'steam explosions'

5.4.4 Thermal ‘interaction’ of the ejected fuel with the surrounding rod(s)

The coolant flow blockage by the ejected fuel has been conventionally considered as a concern, in the context of potential consequences of FFRD. This effect, if any, would need certain time to manifest itself, and should be ascribed to long-term effects.

On the other hand, if the ejected fuel somehow gets stuck to the neighbouring rods it will virtually immediately raise the temperature of the cladding locally. In Halden’s test IFA-650.4 some of the ejected fuel was in fact stuck between the cladding and the heater.

In the LOCA test rig geometry at Halden, the heater wall is about 5 mm from the cladding surface. The typical fuel rod pitch in BWR/PWR assemblies is about 15 mm. This means, that the shortest distance between neighbouring rods is about 5 mm. Considering, that fuel was stuck between the cladding and heater in IFA-650.4 test such possibility appears to be feasible in a fuel bundle.

Without a doubt, during dispersal, the ejected fuel will be projected towards the neighbouring rods and it has the potential to get stuck, and to have impact on the local cladding temperature.⁴ However, it is not clear whether ejected fuel of a burst rod may cause the rupture of neighbour rod. The implications of such scenario are far-reaching and this question must be investigated experimentally, and through modelling.

5.5 Characteristics and effects of the fragmented/relocated fuel in the balloon around the rupture on secondary hydrogen uptake

After cladding cracking, or rupture, the steam from the core will ingress into the rod interior, and further penetrate axially. Axial propagation of the steam along with oxygen starvation due to cladding inner oxidation depends on the effective hydraulic diameter of the fuel stack and the specific open surface area of the fuel, which are closely linked to the characteristics of fuel fragmentation and relocation.

4. NB: Opposite to Halden LOCA tests, there are strong axial steam flows in LWR LOCAs. What has been observed in IFA650.4 in stagnant steam is unlikely to occur in reactor conditions

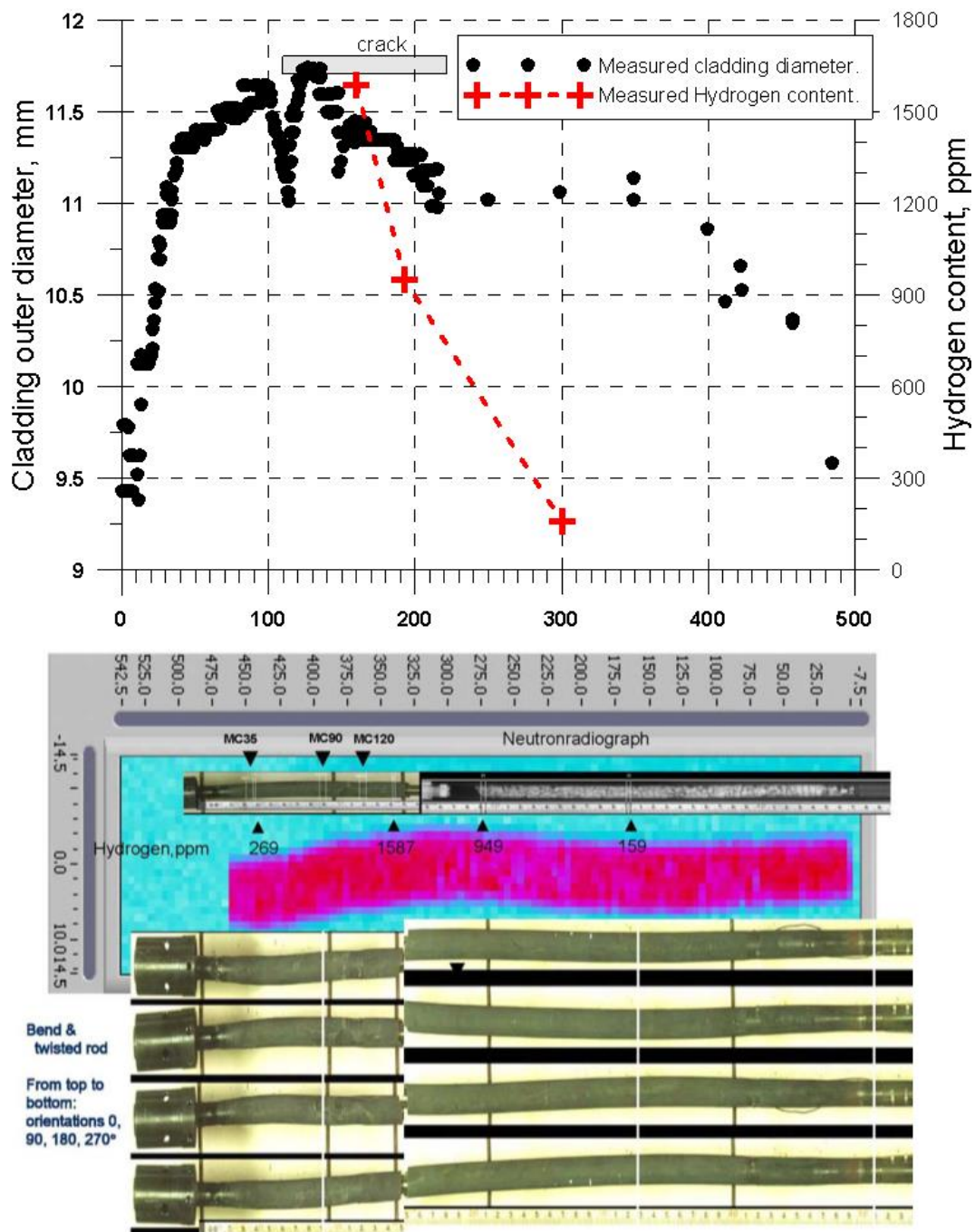


Figure 5.5-1: Axial distribution of measured H-content and cladding diameter (top) against the relevant PIE images (bottom) after LOCA test IFA-650.7 [5.5-2]

The combination of the processes just mentioned, will form the boundary conditions for H-uptake by the inner surface of the cladding. For example, hydrogen profiles often show peaks (<3 000 ppm for <30% ECR) at positions about 30–50 mm away from the rupture position [5.5-1].

Cladding embrittlement is particularly enhanced at those regions. This effect may become important during core re-flood because of the thermal shock on the embrittled cladding.

Halden IFA-650.7 LOCA test [5.5-2] was investigated for hydrogen content and showed “exponential” decrease of hydrogen content with the distance from the rupture, as shown in Figure 5.5-1. Similar observation is done in NUREG-2 160 [5.1-3] with respect to Studsvik's test 198 where the peak was shifted a little from the rupture, whereas test 196 showed flat hydrogen profile. This would be explicable if there were pellet fragments that are stuck to the cladding wall by bonding: then, there would be little to no hydrogen uptake.

Obviously, extension and systematisation of the experimental database for the phenomena in question is necessary, with a view to further development and V&V of the appropriate predictive models.

5.6 Non-standard fuels

The phenomena of FFRD were discovered and examined in the IFA-650 test series in the OECD Halden Reactor project. The test series has been continued. The main outcomes are described in the Halden report [5.6-1] and in Chapter 2 of this report. The integral tests covered standard fuel, i.e. with a UO_2 matrix, originating from PWRs, BWRs and VVERs.

In many reactors worldwide, different kinds of non-standard fuel are in operation. This section aims at assessing a possible lack of experimental data concerning the most widely used non-standard fuels: fuels with burnable absorbers, doped and additive fuel, as well as MOX fuel.

5.6.1 Fuel with burnable absorbers

Fuel with burnable absorbers is widely used in PWRs, BWRs and VVERs to ensure a flat power profile as well as the required shut-down margin even for Uranium-235 enrichments of up to 5 wt.%. By far, the most common absorber currently in use in LWRs is Gadolinium Oxide (Gd_2O_3).

Fuel rods containing Gd_2O_3 produce less energy at the beginning of life until the absorber is burned. In a fuel assembly, this mechanism results, in general, in a lower burnup of the Gd fuel rods compared to fuel rods without absorber. On the other hand, Gd-containing fuel differs from pure uranium-dioxide due to the lower thermal conductivity and the non-uniform radial power distribution starting from the beginning of irradiation.

Since the threshold for fragmentation, relocation and dispersal is strongly correlated with burnup, the Gd rods are not expected to show a more sensitive behaviour during a LOCA compared to rods with standard UO_2 fuel and the same operation time, even if the difference in burnup might decrease in the high burnup range. The microstructure and mechanical properties of Gd_2O_3 fuel do not provide any evidence for other mechanisms that could aggravate the LOCA behaviour significantly.

Thus, according to the current level of knowledge, additional tests concerning the behaviour of Gd_2O_3 fuel during a LOCA are of minor significance.

5.6.2 Doped and additive fuels

The objective of reaching higher discharge burnups led to new developments that should improve the fuel behaviour. For reducing the FGR and fuel swelling, which are enhanced at higher burnups, the optimisation of the fuel microstructure was in the focus of the main fuel developers.

Different kinds of doped fuel were developed with the aim to enlarge the grain size and thus the diffusion paths for the fission gases. Cr and Al/Cr are the major dopants in commercially used fuel [5.6-3] [5.6-4] and significantly larger grain sizes of up to 70 μm could be reached compared to standard fuel, which has a grain size of around 10 μm .

Other major differences compared to standard UO₂ fuel are a lower creep resistance and a higher fuel density. In these fuels, the dopants are predominantly in solid solution. A comprehensive overview of the chemical and physical properties of doped fuel is given in a report [5.6-5] by the Swedish nuclear regulator SSM.

Doped fuels are used in LWRs and examinations have shown that their FGR is lower, in particular during transients. In addition, the shape and distribution of the gaseous pores and bubbles differ from standard uranium-dioxide fuel.

As another alternative for enhancing fuel behaviour, fuels with additives have been developed. This was done for improving the creep properties, i.e. for a “softer” pellet. One of the main developments is a fuel with alumino-silicate additives that are insoluble in UO₂ and are present as inter-granular glassy phase [5.6-6]. The grain size is in the range 28–40 µm. The fuel showed positive ramp behaviour and as a secondary effect, FGR was reduced [5.6-6]. The reduced FGR of doped fuel and fuel with additives could result in a higher resistance to fragmentation, relocation and dispersal during a LOCA.

Since there is no corresponding experimental verification, an integral test comparable to the Halden LOCA tests would be appropriate. This should be done for widely used doped fuel types as well as for a fuel with additives, since the microstructure of both types of modified fuel differs significantly.

5.6.3 Mixed-oxide fuel

Mixed-oxide (MOX) fuel is used in some countries. Major differences among different kinds of MOX fuel originate from different fabrication processes that determine, amongst others, the degree of homogeneity of the Pu distribution. One of the most used processes is the MIMAS process. It produces a slightly heterogeneous final product with mixed oxide agglomerates, embedded in the UO₂ matrix [5.6-7].

In general, performance of MOX fuel is similar to standard UO₂ fuel. On the other hand, the development of areas with high porosity in Pu-rich zones at rather low average burnup and differences in the isotope inventory might influence the characteristics of FGR [5.6-2] and thus could have an impact on LOCA behaviour, as explained in Chapter 3.

Because of the neutronic properties of the plutonium isotopes in MOX fuel, reactivity decreases less rapidly with burnup than in uranium fuel and thus MOX fuel dissipates more power later in its life, releasing more fission gas [5.6-8].

In addition, the thermal conductivity of MOX is known to be lower than that of uranium by a few percent, which may give rise to higher fuel temperatures and thus higher FGR [5.6-8]. It was also shown that at similar burnup, the grain boundary gas content is much higher in MOX fuel than in UO₂ fuel [5.6-9].

The difference in microstructure could also have some relevance for LOCA behaviour. The Pu-rich agglomerates lead to locally enhanced porosity that varies along the pellet radius. This is shown for example in Reference [5.6-8]. Even in the low and mid burnup range, small parts of the fuel may contain a HBS. However, it should be noticed that the difference in FGR between MOX fuel and uranium fuel decreases when the homogeneity of the plutonium distribution is improved [5.6-8].

Since FGR and microstructure are two of the major factors influencing fuel behaviour during a LOCA, an integral test comparable to the Halden LOCA tests would be appropriate. This should be done for a widely used MOX fuel at high burnup.

5.7 OECD/NEA SCIP-III research programme on FFRD in LOCA transients

In response to the observation of fine fragmentation in NRC LOCA tests and in the Halden LOCA tests it was clear that more research was needed to investigate this phenomenon in more detail. The Studsvik

Cladding Integrity Project (SCIP) phase III was launched with its main objective to investigate and quantify empirical thresholds for the observed fuel fragmentation behaviour. This programme also includes studies of the degree of fragmentation and the size distribution of the fragments since these are important parameters for determining the amount of fuel that might be released through a rupture in the ballooned zone of a fuel rod exposed to a LOCA.

The analysis work in SCIP-III will support the development of a theoretical understanding of mechanisms behind fuel fragmentation and dispersal in LOCA transients. Modelling is an integrated part of the programme and will support the assessment and interpretation of the experimental results. The collected data will support estimates of fuel dispersal in LOCA safety assessments carried out by utilities and regulators. The data will also support development of fuel fragmentation models to be incorporated in fuel performance and transient codes.

SCIP III includes investigations into the following parameters to determine the impact on fuel fragmentation and dispersal:

- Burnup. The burnup threshold will be determined more accurately by performing tests in the range of 55 to 70 MWd/kgU rod average burnup.
- Power history. Results obtained recently suggest last cycle power is an important parameter for fragmentation. The power threshold will be investigated by separate effects tests.
- Cladding strain. With increasing cladding strain the fuel is less constrained. This increases the extent of fragmentation. Data will be obtained to determine the strain threshold for fine fragmentation.
- Temperature. Pressure in the fission gas bubbles increases with temperature. If there is no constraint the pressure causes fragmentation of the fuel. Separate effects tests (Heating tests) will be performed to examine the dependence of fragmentation on temperature.
- Gas pressure, plenum volume and depressurisation on rupture. The rapid depressurisation on rupture may impact both fuel fragmentation and dispersal (ejection of fragments). Tests are planned to determine quantity and size distribution of fuel fragments as a function of pressure.
- Microstructural effects. The connection between the pre-transient fuel structure and the degree of fragmentation and the characteristics of the fuel fragments will be investigated in order to improve understanding of the fragmentation mechanism.

The SCIP-III programme started in June 2014 and will continue for five years until June 2019. During the first year more than 10 heating tests have been performed to quantify the burnup and power thresholds. The results support a threshold map of the kind shown in Figure 5.7-1.

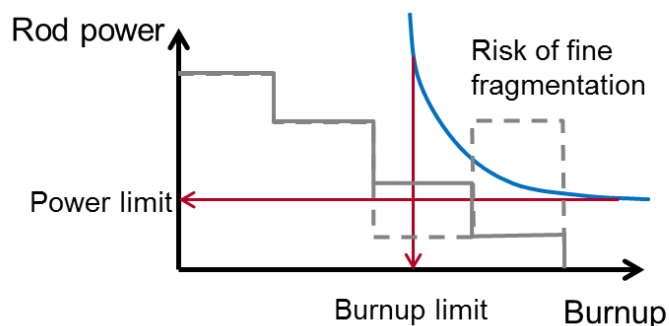


Figure 5.7-1: A schematic illustration of the threshold curve for fragmentation as a function of burnup and last cycle power

The figure shows a schematic illustration of the threshold curve for fragmentation as a function of burnup and last cycle power. The power histories for two different samples are illustrated by grey solid and dashed lines. One of the samples (dashed line) would give rise to fine fragmentation in a LOCA transient and the other (solid line) would not.

The data is so far unpublished and only available to the SCIP-III membership. The current plan is to perform two LOCA integral tests in Studsvik this spring (2015) to confirm the observed threshold limit. A counter-part LOCA test in both Halden and Studsvik on fuel rod material from the same rod will also be carried out to benchmark the in-pile and out-of-pile LOCA test techniques. In total about 20 LOCA tests at Studsvik are planned during the full five year programme.

5.8 JAEA envisaged tests related to FFRD

Although some pieces of information on transient behaviour of fuel pellets were obtained by previous RIA/LOCA experiments, JAEA has just started the experimental programme related to FFRD. They consider it is necessary to clarify the mechanism and evaluate conditions (criteria) of the occurrence of FFRD for the regulatory judgment.

As summarised in Figure 5.8-1, the existing data from the Halden IFA-650 test series, the NRC/Studsvik tests and the EPRI's separate effects tests suggest that fuel pellet fragmentation is mainly affected by fuel burnup, power history, restraint by the cladding (ballooning) and peak temperature. Axial relocation of fragmented pellets possibly depends on the balloon size of the cladding and fragmented size of pellets, and the filling ratio of the fragmented and relocated pellets finally determines the influence on PCT.

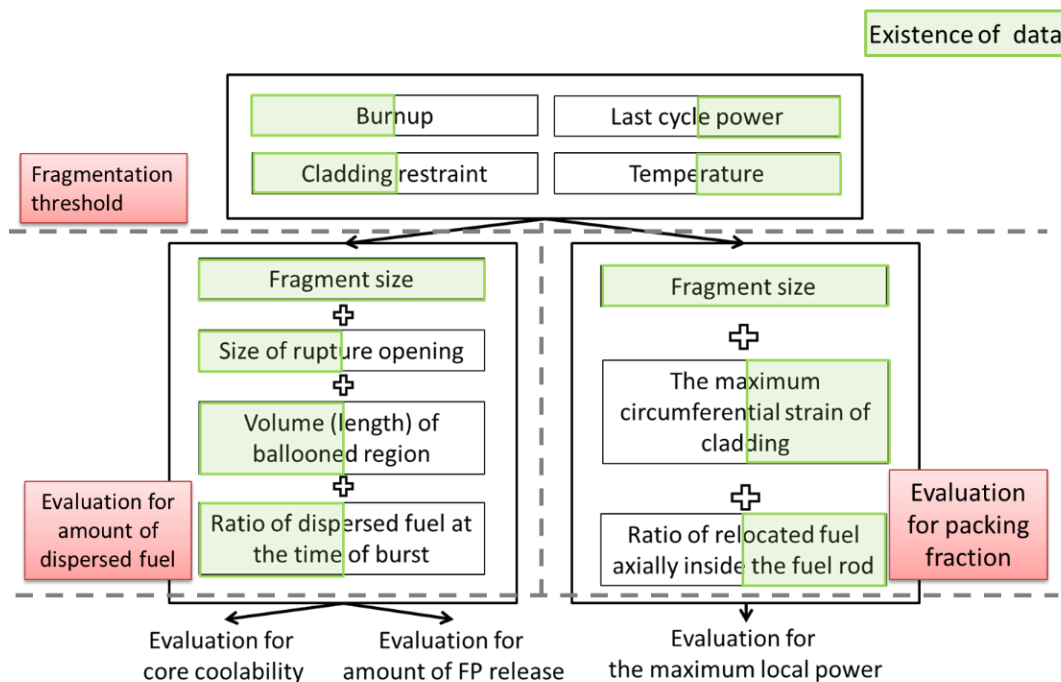


Figure 5.8-1: Key phenomena and parameters for FFRD

Considering the existing information, JAEA is conducting the experimental programme to clarify the mechanism and evaluate the influence of possible parameters for the occurrence of FFRD.

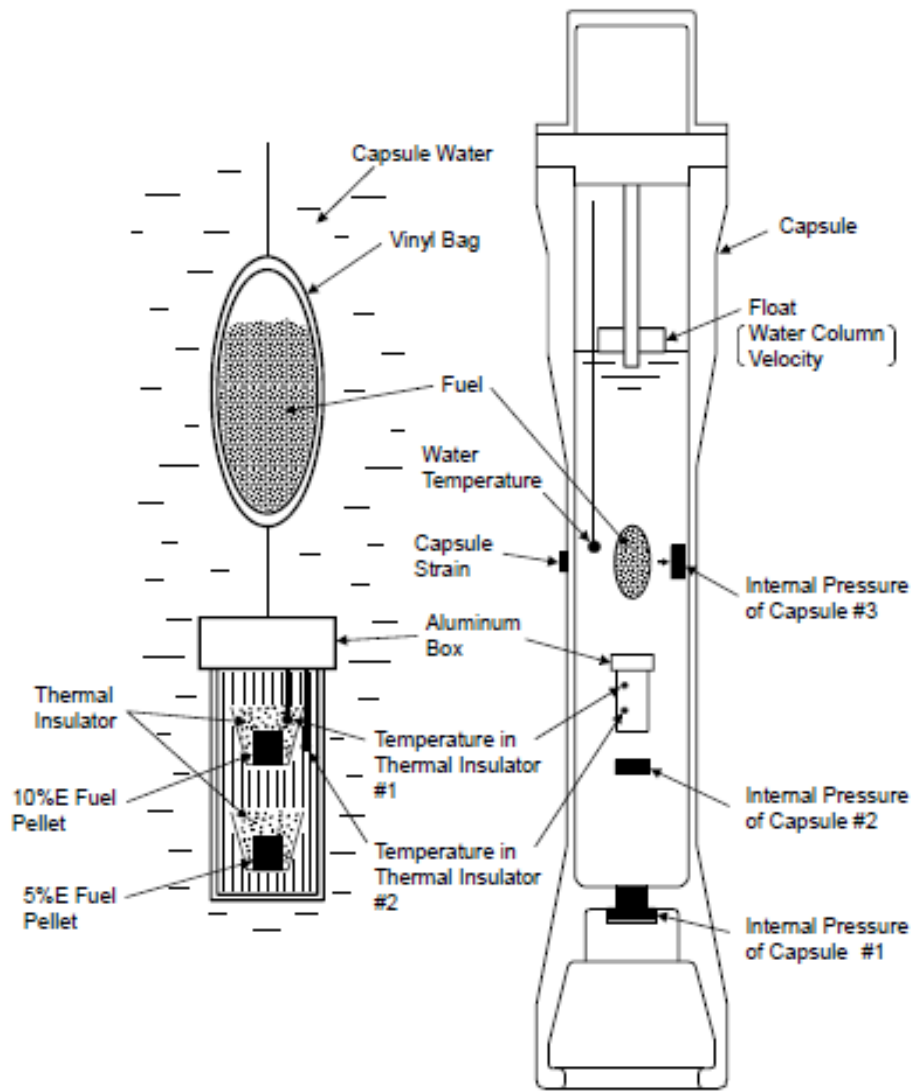
5.8.1 Previous experiences

The Nuclear Safety Research Reactor (NSRR) is a TRIGA reactor, and fuel behaviour under reactivity-initiated accident (RIA) conditions has been investigated by pulse irradiations in the NSRR.

As shown in Figure 5.8-2, fresh unclad UO_2 fuels in the shape of particles and pellets with or without container were pulse-irradiated in the water-filled capsules to examine mechanical energy generation due to the interaction between hot fuel and coolant (water). The fuel generally cracked or fragmented possibly by temperature gradient (thermal stress) in it and the thermal shock due to rapid temperature increase and quenching by contact with water.

Irradiated fuel segments are also used in the RIA experiments. Dispersal of fuel pellets has been observed in the experiments with the HBU. In these cases, some cracking and fragmentation might occur during transient and fuel pellet pieces dispersed through the opening of cladding generated by the PCMI failure.

Therefore, the dispersal of pellets during the RIA transient should be separated from that during the LOCA-type transient though the mechanism of fuel pellet cracking may have common causes.



a)



b)



c)

Figure 5.8-2: a) NSRR pulse irradiation in 80's with fresh fuel particles and pellets, b) Fragmentation of heated and quenched fuel particles, c) Cracking of heated and slowly-cooled fuel pellets

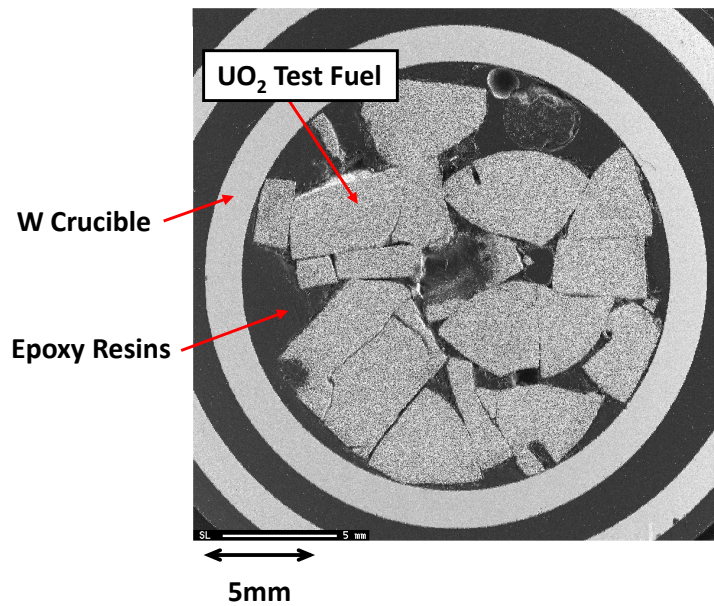


Figure 5.8-3: Radial cross-section of 47 MWd/kgU PWR fuel pellets heated to 2 500°C

Figure 5.8-3 shows post-test cross sections of UO₂ fuel pellets after fission-product-release tests (VEGA-2). Two to three PWR fuel pellets (47 MWd/kgU) were heated in the tungsten crucible to 2 500°C in helium atmosphere of 1 MPa. The heat-up rate was 40 K/min (<1 350°C) and 60 K/min (>1 350°C). The fuel pellets cracked but not fragmented. Therefore, it is not considered that fragmentation is caused only by the temperature increase in such a mid-burnup pellet.

5.8.2 Experimental programme on FFRD

5.8.2.1 Separate effects tests on cladding deformation and rupture

Experiments are needed to obtain data concerning the extent of cladding deformation (ballooning) and the size and shape of rupture opening. Laboratory-scale experiments on non-irradiated Zircaloy-4 (Zry-4) cladding tubes are being conducted.

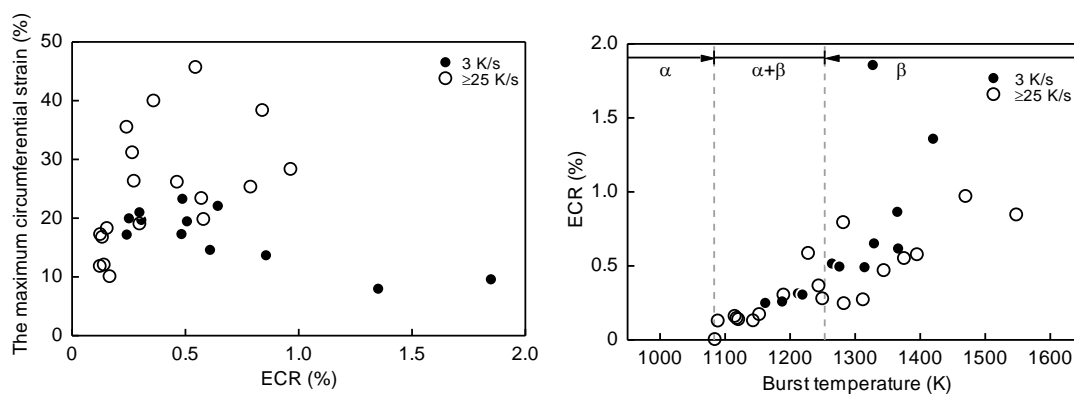


Figure 5.8-4: Effect of oxidation (ECR-%) on the maximum circumferential strain

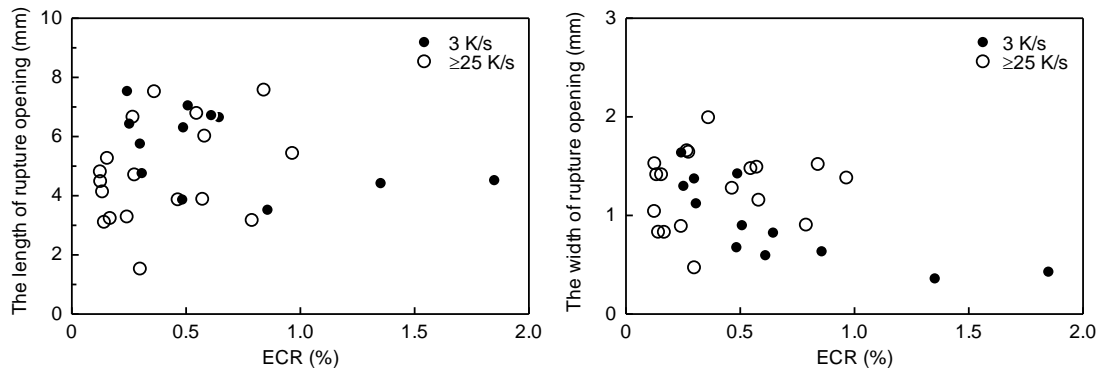


Figure 5.8-5: Effect of oxidation (ECR-%) on the size of rupture opening

Figure 5.8-4 and Figure 5.8-5 show recent results from burst tests with non-irradiated Zry-4 cladding tubes under simulated LOCA conditions for reducing uncertainty in ballooning and rupture behaviour to improve prediction of FFRD, [5.8-1].

The results indicate that the reduction in cladding ductility due to the high temperature oxidation has an impact on the ballooning behaviour greater than the reduction of cladding strength due to the burst temperature increase. In addition it is considered that reduction in cladding ductility due to the oxidation decreases the width of rupture opening.

5.8.2.2 *Separate effects tests on mechanism of pellet fragmentation*

To investigate the mechanism of pellet fragmentation, out-of-pile annealing tests on irradiated fuel pellets are planned. The effects and changes of the following parameters will be examined:

- restraint by cladding
- heating rate
- macro- and micro-structure changes in the pellets during out-of-pile heating
- the size of pellet fragment
- threshold of fragmentation phenomenon, etc.

5.8.2.3 *Integral tests with irradiated fuel segment*

As for the cladding deformation behaviour, data concerning the amount of deformation of the irradiated fuel (cladding) containing fuel pellets will be obtained. The effect of pellet on the cladding deformation will be also investigated by comparison with the experiments with non-irradiated cladding.

As for the FFRD, the acquisition of the following data is expected

- effects of bonding and restraint by cladding tube on FFRD
- the size distribution of pellet fragment in the rod
- filling ratio of fragmented pellet in the rod
- the amount and size distribution of pellet dispersed from the opening
- macro- and microstructure changes in the pellets, Threshold of FFRD phenomenon, etc.

An apparatus for this purpose will be developed or the current apparatus for semi-integral LOCA tests [5.6-1] will be modified.

5.9 Summary of phenomena of potential interest for FFRD evaluation

The above-discussed lack of experimental data for safety evaluation of the FFRD during the LOCA is summarised in Table 5.7-1, including:

- single-effect experiments of potential importance
- physical mechanisms and parameters that should be addressed
- safety related outcomes of the phenomena in question, as also
- generic types of tests that are deemed to be appropriate for the corresponding investigation.

Effect	Parameters of importance	Mechanisms	Outcome	Tests
Fragmentation	Frag. threshold (BU), last cycle power, temperature, pore-pressure, particle size distribution, bonding, filling ratio, trans. FGR	Ballooning, de-bonding, depressurisation, pellet stresses	Susceptibility to relocation and dispersal	Single rod, nuclear
Relocation	Degree of PCT increase, filling ratio in ballooned cladding, cladding strain, fuel fragment sizes	Ballooning, additional heating	PCT increase, enhanced oxidation, local embrittlement, burst time, PCT of neighbour rods	Single rod, Bundle, Two rods, non-nuclear
Gap conductance between the relocated fragments and the cladding	Fragments sizes, filling ratio, gap environment	Ballooning, decay heat, steam ingress, additional heating	PCT increase quantification for a given filling ratio, debris size distribution and decay heat	Separate effect tests with proper boundary conditions
Grid spacer impact on relocation	Location of the grid spacer	Spacer grid acts as a chokepoint for axial fuel relocation	Balloon size and burst opening, degree of fuel fragments relocation, PCT increase	In-pile single rod test with a prototypical spacer grid between the upper plenum and the ballooned area
Dispersal	Before burst: Gas amount, fuel structure, transient FGR, fragment size, hydraulic diameter	Fragmentation	Burst chain, steam explosions, flow blockage	Two-rod and bundle, non-nuclear
	Ejected fuel: Amount, stored heat, size distribution, burst-opening size	Burst, gas-solid friction, particle entrainment		
Transient FGR	BU, structure, temperature, pore-pressure, burst	Fragmentation, pulverisation	Additional FGR, burst time, balloon size, relocation,	Single rod, nuclear
	BU, bonding	Ballooning, de-bonding, gas flow, pellet stresses	amount of ejected fuel	Single BWR rod, nuclear, non-nuclear
Interaction with coolant	Fuel amount, size distribution, stored heat	Steam explosions	Additional fuel damage	Bundle experiments with prototypical axial steam flow, nuclear, non-nuclear
Accumulation on spacer grids		Flow blockage	Cladding heat up	Bundle experiments with prototypical axial steam flow, non-nuclear
Secondary embrittlement	Burst opening size, hydraulic diameter, bonding	H-Uptake	Damage by thermal shock (re-flooding)	Single rod, non-nuclear

Table 5.7-1: Summary of phenomena of potential importance for FFRD evaluation

The summary of the specific data of potential importance for the non-standard fuels, as discussed in Section 5.6, is presented in Table 5.7-2.

Non-standard fuel	Main impacts concerning HBU LOCA behaviour	Probability for less conservative behaviour⁵
Fuel with burnable absorber	Less BU than standard fuel	Low
Doped fuel	Less transient FGR	Low
Additive fuel	Less transient FGR Different microstructure	Middle
MOX	Higher EOL power Lower thermal conductivity Heterogeneous microstructure	High

Table 5.7-2: Special features of non-standard fuels to be addressed

5. Compared to standard fuel

6. THRESHOLDS FOR FRAGMENTATION, RELOCATION AND DISPERSAL

6.1 Fuel fragmentation during LOCA

In Chapter 6.1, the threshold for the onset of pellet powdering or fine fragmentation will be discussed.

6.1.1 Experimental results and proposed thresholds

Over the last 40 years, many LOCA experimental programmes have been conducted that provide valuable observations of fuel behaviour under LOCA conditions. In most cases, the experimental programmes did not explicitly investigate fuel fragmentation and many of the programmes tested fresh or low burnup fuel where fine fragmentation or pulverisation would not be expected. However, a few observations related to fragmentation were noted in historical LOCA programmes and will be reiterated here.

Loss-of-Coolant Accident tests at ANL revealed variability in fragmentation behaviour at various axial locations of ICL No.2 (segment average burnup of 57 MWd/kgU). Figure 6.1-1 shows low-magnification images of the fuel structure of the ICL No.2 sample at axial locations: (a) about 12 mm above the rupture centre, (b) about 50 mm above the rupture, and (c) about 130 mm below the rupture centre (45 mm above the bottom end-cap). Also shown in (d) is the fuel structure of the as-received fuel. Comparison between the images of the fuel structure and the local cladding strain value suggests that fragmentation is enhanced by increased local strain.

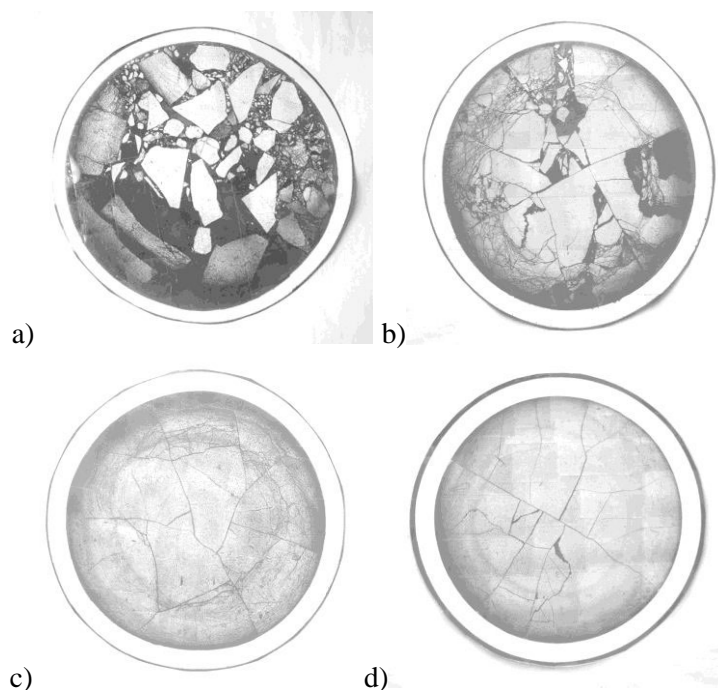


Figure 6.1-1: Low-magnification images of the post-LOCA test ICL No.2 fuel samples a) at ≈ 12 mm above the rupture centre (15–35% strain), b) at ≈ 50 mm above the rupture centre (2–4% strain), c) at ≈ 130 mm below the rupture centre, and d) prior to LOCA testing (180 mm from the LOCA sample) [6.1-4]

Experimental results at Halden and Studsvik also suggest a trend in fragmentation behaviour that is correlated to local strain and proximity to the rupture location for fuel susceptible or above the fragmentation threshold. Ceramographic investigations of IFA-650.5 shown in Figure 6.1-2, [6.1-1], reveal extensively fragmented fuel near the rupture and where strain is large, and comparatively less fragmentation in regions where the strain is small. Many of these images reveal extensive fragmentation across the entire radius.

Ceramographic investigations of Studsvik test segments provide additional information on fuel fragmentation behaviour. Figure 6.1-3 combines the cladding strain profile, the size distribution of fuel fragments collected after LOCA and shake testing, and ceramography results of fuel remaining in end region of the test segment of Studsvik test 192 [6.1-5]. The fuel fragments collected from the mid-section were finely fragmented, while fuel in end section is characterised by hairline cracks.

The observations in Figure 6.1-2 and Figure 6.1-3 suggest that fragmentation is more extensive in regions of high cladding strain near the rupture than in regions of low cladding strain far from the rupture.

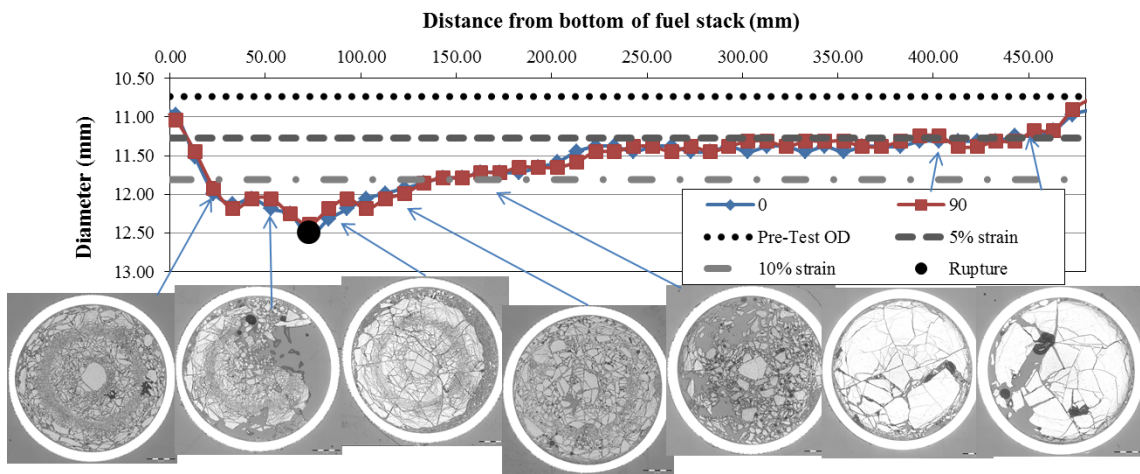


Figure 6.1-2: Ceramography images and strain profiles from IFA 650.5 (83 MWd/kgU segment average burnup [6.1-1])

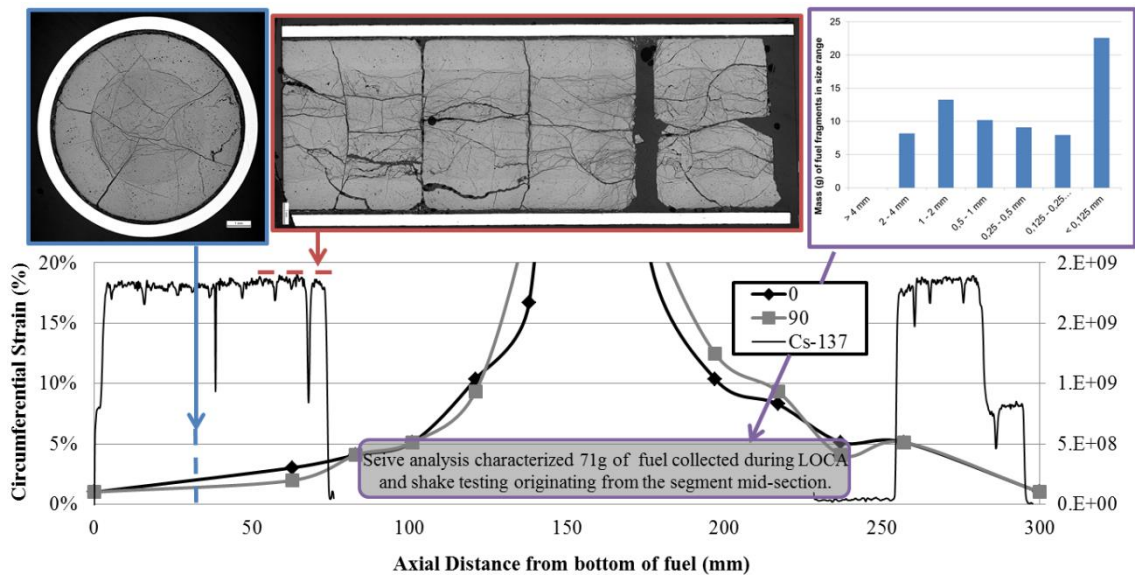


Figure 6.1-3: Ceramography images, sieving results and cladding strain profiles from Studsvik test 192 (segment average burnup of 78 MWd/kgU, father rod average burnup of 68 MWd/kgU), [6.1-5]

The observations from neutron radiography, ceramography and profilometry, in combination, from LOCA tests at ANL, Halden, and Studsvik suggest that a strain threshold for transient fragmentation or pulverisation may exist between 5 and 10% cladding strain. However, it should be noted that not all fuel is susceptible to fine fragmentation (pulverisation).

In fact, fuel that is below the burnup threshold for fine fragmentation (rod average burnup <68 MWd/kgU) predominantly fragments into large pieces, while fuel that is above the fine fuel fragmentation threshold mostly turns into powder (see IFA-650.7 and IFA-650.5 in Table 3.1-1, respectively). Nonetheless, Table 3.1-1 and [6.1-6] show that even for fuel that is not susceptible to pulverisation, some degree of fragmentation becomes visible where sufficient strain is present in the cladding.

Experimental results at Halden and Studsvik reveal a trend in fragmentation behaviour that is correlated to burnup. Halden and Studsvik conducted integral LOCA tests on rods with a range of burnup values and in some cases, the fuel fragments were collected from the rods after the LOCA transient and particle size distribution was quantified. The images of fuel fragments from IFA-650.9 and Studsvik test 191 are shown in Figure 6.1-4 and reveal very similar fuel fragmentation for these two tests. Images of fuel fragments from IFA-650.7 and Studsvik test 196 are shown in Figure 6.1-4. The fuel fragments in these two tests were similar to each other, but had noticeably higher burnup than IFA-650.9 and 191. The fragmentation size of fuel from IFA-650.7 and Studsvik test 196 seems to roughly correspond to the coarse fragmentation expected from normal operation to this burnup, but a few fine particles can be seen in the image of IFA-650.7.

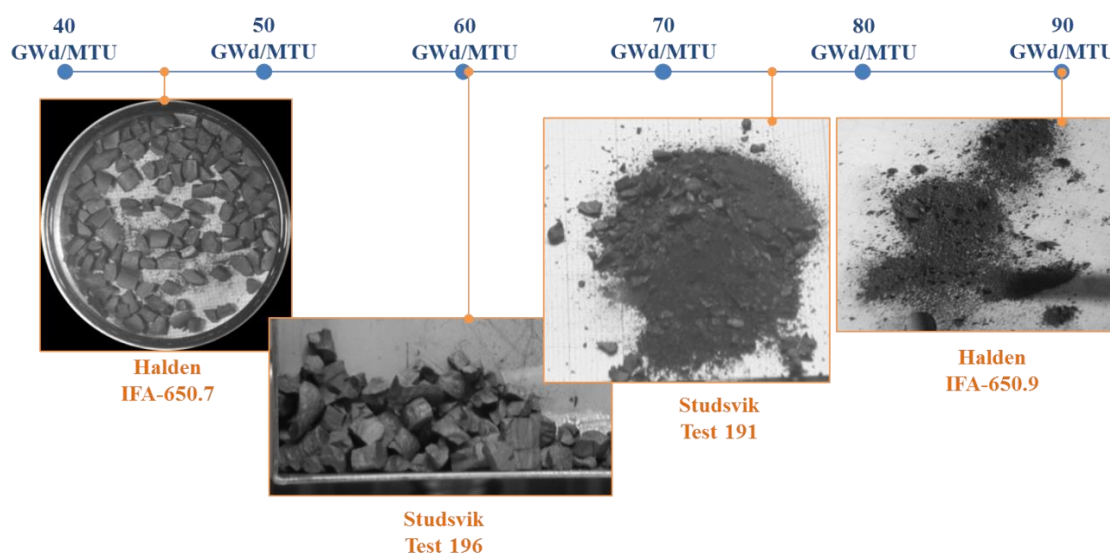


Figure 6.1-4: Spectrum of fuel fragments collected from integral LOCA test segments from 44 to 90 MWd/kgU. Results shown here are to their segment average burnup value. [6.1-3] [6.1-5] [6.1-7]

The fragment size distribution of the fuel collected after LOCA and shake testing of the six integral LOCA tests at Studsvik is quantified in Figure 6.1-5, [6.1-6]. A difference in fragmentation size distribution between test segments with ≈ 60 and ≈ 75 MWd/kgU burnup is apparent. Tests 191, 192, 193 are characterised by a large percentage of fragments less than 2 mm in size. Tests 196 and 198 are characterised almost exclusively by fragments larger than 2 mm, although a few micrometre sized fragments were measured.

Both Figure 6.1-4 and Figure 6.1-5 suggest a significant change in fragmentation behaviour for fuel with a local (segment average) burnup between ~ 60 and ~ 75 MWd/kgU.

A rapid change in fragmentation size is believed to be related to local changes in fuel microstructure that occur with high burnup. The microstructural characteristics of HBU make this fuel more vulnerable to fine fragmentation when subject to LOCA conditions. If the local cladding strain is large enough to result in fuel fragmentation, the observations of fuel fragmentation size distribution from LOCA tests at Halden and Studsvik suggest that the transition to fine fragmentation will begin at a pellet average burnup of 60 MWd/kgU and be complete at a pellet average burnup of 80 MWd/kgU.

However, other parametric pellet heating tests suggest the fuel fragmentation threshold is not simply a function of burnup. Separate effects tests were conducted using fuel materials taken from the same rods and in adjacent locations to the NRC Studsvik LOCA tests 189 (segment average burnup of 72 MWd/kgU) and 192 (segment average burnup of 78 MWd/kgU). The separate effect test sample sectioned from the parent rod above test 189 totally disintegrated when heated to 1 000°C in both air and an inert atmosphere while a test sample section taken from the same rod at a location below that of test 189 only partially fragmented.

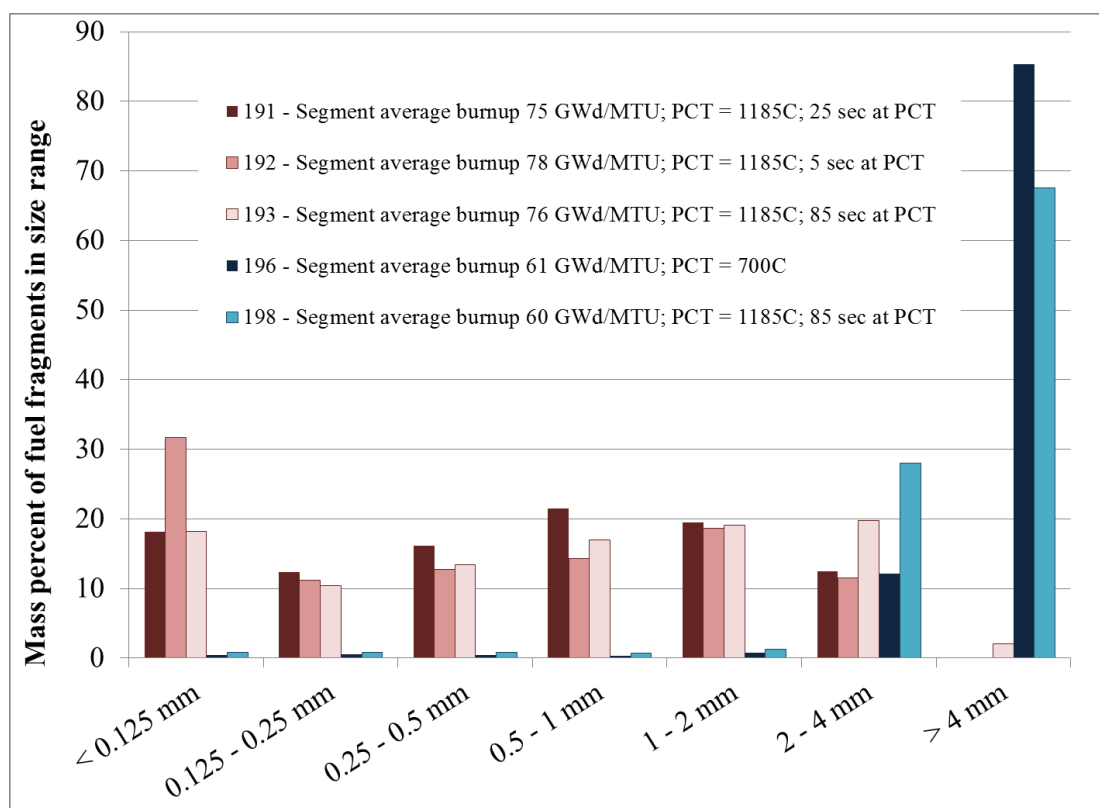


Figure 6.1-5: Size distribution of fuel fragments collected after Studsvik LOCA and shake testing, [6.1-6]

An examination of the hot-cell¹⁰⁶ Ru activity scan showed the rod had a power tilt in the last cycle of operation, such that the last cycle power of the lower separate effect test sample is approximately 10% lower compared to test 189, with a corresponding burnup decrease of 3%. A subsequent pellet heating test of a 66 MWd/kgU test sample irradiated at 40% power level of Studsvik test 189 in the last cycle had minimal fragmentation upon heating to 1 000°C, furthering supporting the effect of prior thermal history. Photographs of test samples after the three separate effect tests are shown in Figure 6.1-6.

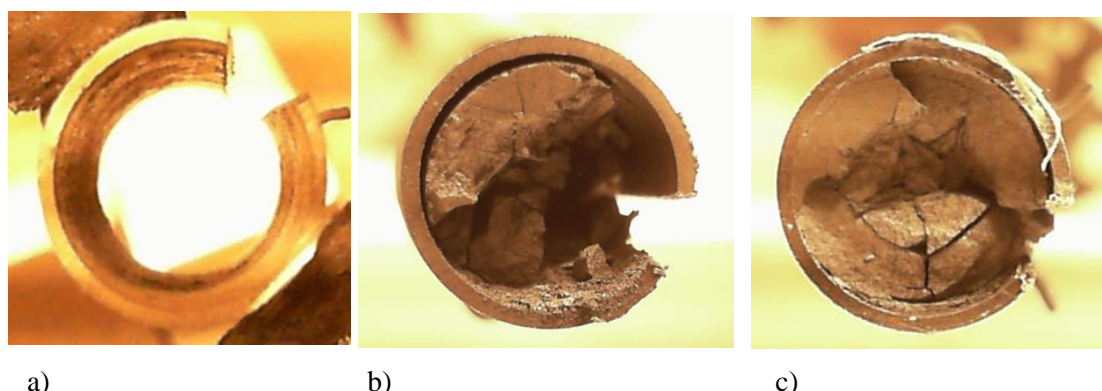


Figure 6.1-6: Photographs of test samples after heating test, a) sample taken above test 189, 72 MWd/kgU segment average burnup, 15 kW/m last cycle power, b) sample taken below test 189, 13.5 kW/m last cycle power, and c) sample taken from a different rod, 66 MWd/kgU segment average burnup, 5 kW/m last cycle power

6.1.2 Main parameters of potential influence: general trends

Potential fuel fragmentation mechanisms are discussed in detail in Chapter 3. In sum, data generated to date suggests fuel fragmentation is influenced by several variables. Amongst the most pronounced are burnup, loss of cladding constraints, fuel pellet temperature reached during a LOCA transient and power history. While the fragmentation is primarily driven by conditions created from fuel fission or burnup, the fragmentation threshold is noticeably influenced by the aforementioned variables which need to be captured to properly characterise susceptibility of irradiated fuel to the fragmentation phenomenon.

6.1.2.1 Power history

The effect of power history on fuel fragmentation during LOCA has been described in Chapter 3.2.2. Experimental results indicate the burnup threshold is inversely proportional to the pre-transient power level at high burnup. There is insufficient data to determine the burnup level above which this mechanism becomes active. It should be noted that even fresh fuel pellets crack at high power levels and thus a distinction should be made between normal cracking and fragmentation.

In fact, the HBU that has often been used in LOCA experiments was usually obtained by reinserting fuel rods in a power reactor after their normal end of life, often in relatively high power regions, so as to rapidly increase their burnup. Such practice often resulted in higher last-cycle powers than would normally be observed in a power reactor, where last-cycle fuel is often placed in low-power core locations. However, this practice could potentially create a bias in the experimental results.

Contributions to the power history effect most likely come from differences in the fission gas distribution and internal stress which are strongly influenced by the operating temperature profile. The temperature increase in the outer portions of the fuel pellets is a departure from the operational equilibrium and likely provides the driving force for fuel fragmentation.

The last cycle power has been correlated with the fragmentation threshold, but its use is an artefact of the experiment since discharged fuels were used in the experiments. Since a LOCA could occur at any time during an operational cycle, last cycle power would not apply, instead the pre-transient equilibrium state should be used. In cases where the fuel only operated under a new condition for short period of time and new equilibrium has not been established, prior power history need be considered.

Fuel rodlets used in semi-integral LOCA tests have been taken from full length fuel rods irradiated in commercial plants. Therefore their power histories are prototypical of commercial reactors normal

operation conditions, as well as their cladding's hydrogen pick-up and corrosion. Nevertheless, for a large part of the LOCA tests, the rodlet burnups were well beyond usual commercial discharge burnups.

It must be noted that, prior to the fuel rod shipment, fuel rodlet fabrication and in-pile LOCA tests, the fuel rods stayed a long period of time in the spent fuel pool for them to cool down until they can be shipped. These various stages may affect the initial conditions of the tested fuel rods (stress fields in the pellet and in the cladding, microstructure) as compared to those expected at the beginning of in-reactor transients. The potential impact of those inevitable changes may be a source of uncertainties when analysing and transposing FFRD phenomena.

6.1.2.2 *Fuel pellet temperature*

The dominant driving force for fuel fragmentation likely comes from temperature changes in the fuel pellet that upsets the equilibrium condition reached during steady-state operation. During operation the temperature is higher in the pellet interior and much lower near the periphery. In a LOCA transient the temperature in the outer portion of the pellet significantly increases above the steady-state equilibrium. The margin to fuel fragmentation therefore decreases as the temperature in the outer region of the pellet is increased, leading to onset of fragmentation.

Heating tests of fuel slightly above the fuel fragmentation burnup threshold show that the onset of fuel fragmentation occurs around 750°C. Test data for fuel significantly above the fragmentation burnup threshold is currently not available.

6.1.2.3 *Fuel-cladding geometry*

Experimental data indicate that a gap between the fuel and cladding is necessary for visible fragmentation to occur, even if the fuel is significantly above the fragmentation burnup threshold. This is a very interesting observation as the fuel cladding would only be able to exert minimal radial restraint above 1 000°C. Examples of such observations are evident in the Halden and Studsvik LOCA tests.

Figure 6.1-2 and Figure 6.1-3 in particular show that in portions of the test segment where cladding strain is low, there is little evidence of fine fragmentation even though these segments are well above the burnup range where fine fragmentation is expected and even though there is evidence of fine fragmentation in the portions of the test segment where cladding strain is high. This suggests that high burnup and high strain, in combination, are the main parameters of potential influence for fine fragmentation.

Because in LOCA tests such as Halden tests the axial cladding strain observed after LOCA transient correlates with maximal cladding/fuel temperatures distributed along fuel rod axis (the higher the temperature, the more the cladding strains), this correlation would alternatively allow interpreting the occurrence of fragmentation in LOCA tests in a different way. According to that visible fragmentation could be depending on axial temperature distribution (the higher the temperature, the more the pellet gets visibly fragmented). Such kind of interpretation cannot completely be ruled out.

The experimental results suggest that if the local strain is greater than 5-10% and the pellet average burnup is above 60 MWd/kgU, some degree of fine fragmentation would be expected. If the local strain is greater than 5-10% and the pellet average burnup is above 70 MWd/kgU, a larger degree of fine fragmentation would be expected and if the pellet average burnup is above 80 MWd/kgU, an extensive amount of fine fragmentation would be expected.

6.2 **Fuel relocation during LOCA**

If fuel pellets are fragmented and separated from each other, they could be free to move relative to their neighbours. Simply stated, fuel relocation can be described as any physical movement of fuel pellets or

fuel fragments within the cladding. Generally, radial fuel relocation is described as distinct from axial fuel relocation.

Radial fuel relocation is the movement of the fuel outward toward the fuel cladding. Measurements in instrumented test rods consistently showed lower fuel centreline temperatures than those predicted based only on fuel swelling and densification, and thermal expansion of cladding and fuel.

Microscopic examination of post irradiation fuel cross-sections has led to the conclusion that fuel pellet cracking promotes an outward relocation of the pellet fragments that causes additional gap closure. This process is widely recognised in fuel performance analysis. It starts at beginning of life and quickly reaches equilibrium by 5 MWd/kgU, according to the FRAPCON-3.4 computer code [6.2-17].

Axial fuel relocation is the vertical movement of fuel fragments or particles within the cladding. Under normal operation, this process is usually limited by the fuel pellet immediately above or below the pellet in question.

For the purpose of this report, axial fuel relocation is said to have occurred if post irradiation examination (PIE) reveals that fuel fragments have moved axially relative to their original location. Evidence that would support this determination includes voided regions of the fuel rod or the observation of additional fuel material in the enlarged volume of the balloon region, or both.

6.2.1 Experimental results and proposed cladding strain thresholds

Over the last 40 years, many LOCA experimental programmes have been conducted that provide valuable observations of fuel behavior under LOCA conditions. In most cases, the experimental programmes did not explicitly investigate fuel relocation. However, a few observations related to fuel relocation were noted in historical LOCA programmes and will be reiterated here.

A series of LOCA tests was conducted at the Karlsruhe Institute of Technology (KfK) in Germany in the FR-2 programme [6.2-1] [6.2-2]. Based on the data from these reports, NUREG-2121 noted that fuel relocation was evident in many tests and noted that no relocation was observed until the cladding hoop strain exceeded a value of 8%.

The results of the FLASH tests (see Section 2.3.1), carried out at the SILOE reactor at Commissariat à l'Énergie Atomique (CEA)/Grenoble, also indicate that fuel relocation occurred in the condition of cladding strain. The results of the FLASH tests suggest that axial and radial fuel relocation can occur for diametral strains as low as 16% [6.2-3] [6.2-4].

Fuel relocation was also observed in the Power Burst Facility tests conducted in Idaho National Engineering Laboratory, [6.2-5], [6.2-6], [6.2-7]. Figure 6.2-1 includes neutron radiographs of LOC-6, rod 12 (10.8 MWd/kgU). It can be seen the test resulted in fuel relocation, particularly in regions of large cladding strain.

Experimental results at Halden and Studsvik also reveal a trend in axial and radial fuel relocation behaviour that is correlated to local cladding strain. When neutron radiography results from Halden test segments are overlaid onto the strain profile for each test segment, as shown in Figure 6.2-2, a correspondence is apparent.

Where the local cladding strain is large, axial and radial fuel relocation is more extensive than in areas where the local cladding strain is small. In segments where the cladding strain is large (>10%) along the entire axial length, axial and radial fuel relocation is evident along the entire axial length, for example PIE of IFA-650.7 in Figure 6.2-2a).

In segments where the cladding strain is large in only a short axial length, axial and radial fuel relocation is only evident in a short axial length, for example PIE of IFA-650.10 in Figure 6.2-2b).

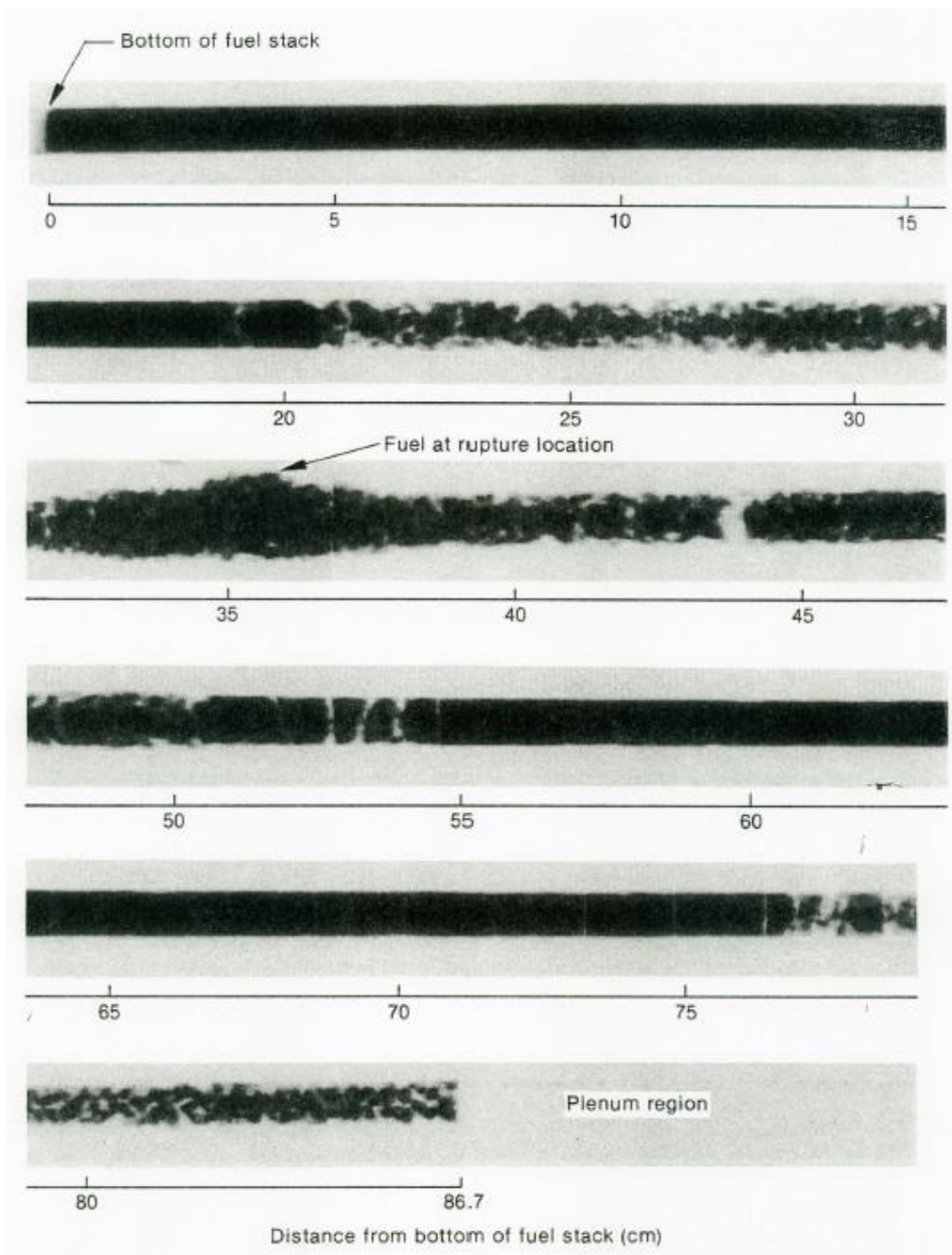


Figure 6.2-1: Neutron radiograph of test LOC-6, rod 12, showing extensive axial fuel relocation [6.2-7]

Further, in segments where the cladding strain profile is asymmetric, the extent of axial and radial fuel relocation is correspondingly asymmetric, for example PIE of IFA-650.11, Figure 6.2-2c), and IFA-650.12, Figure 6.2-2d). These observations suggest that the extent of axial and radial fuel relocation is related to local cladding strain.

Experimental results at Halden suggest a cladding strain threshold for axial fuel relocation. In Figure 6.2-2d), neutron radiography reveals a region of the fuel rod where fuel has relocated axially to leave an empty region adjacent to a region of fuel that has not relocated axially. The boundary between relocated and non-relocated fuel is around 2% strain in the test shown in Figure 6.2-2d).

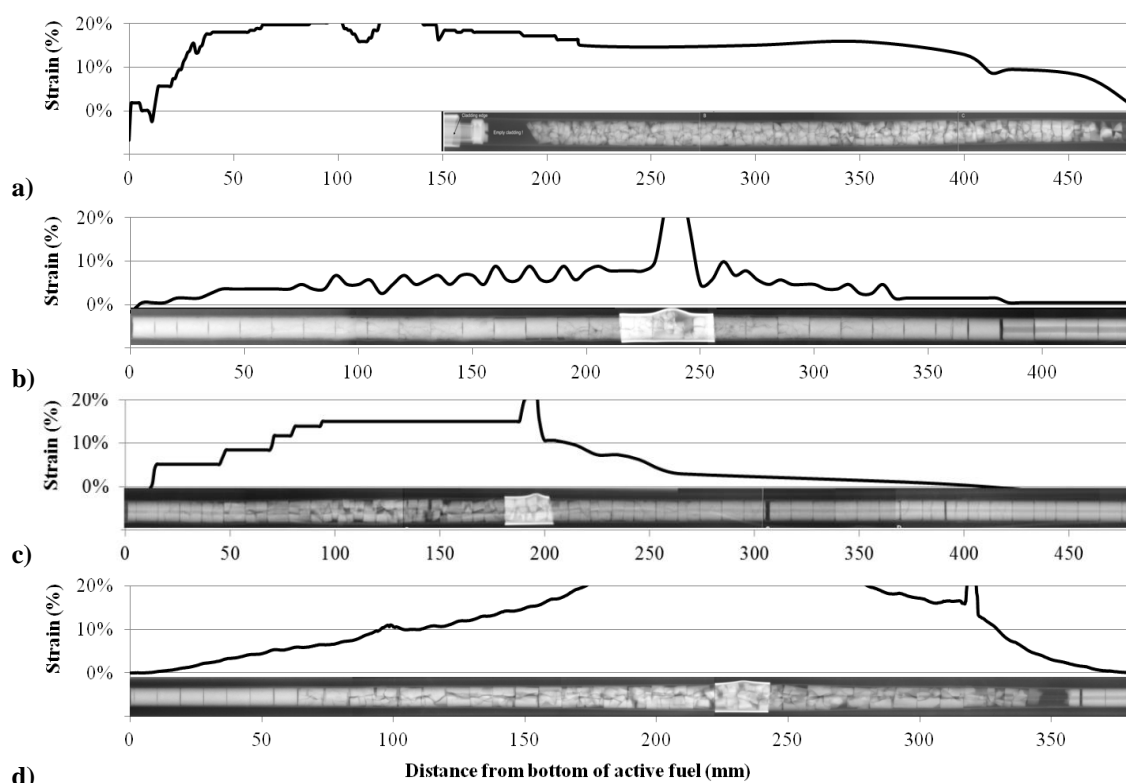


Figure 6.2-2: Neutron radiography and cladding strain profiles from a) IFA-650.7 (44 MWd/kgU, BWR), [6.1-3], b) IFA-650.10 (60 MWd/kgU, PWR), [6.2-8], c) IFA-650.11 (56 MWd/kgU, VVER), [6.2-9], d) IFA-650.12 (72 MWd/kgU, BWR); for IFA-650.12, a transition between axially relocated fuel and non-relocated fuel is highlighted, [6.2-10], all burnup values are segment average.

Experimental results at Studsvik also suggest a cladding strain threshold for axial fuel relocation. Integral LOCA testing at Studsvik was followed by a “shake” test, which exacerbated axial fuel relocation. Figure 6.1-3, shown earlier, combines gamma scan measurements of the test segment after the shake test, and ceramography results at the “boundary” of axial fuel relocation of the test segment of Studsvik test 192. Figure 6.1-3 indicates fuel in the end sections did not relocate even after the agitation of the shake test. Here the boundary between relocated and non-relocated fuel is around 3-4% cladding strain.

The observations from PBF, FR-2, Studsvik and Halden tests all suggest that fuel relocation is related to local cladding strain. The observations also suggest a threshold for axial fuel relocation related to local cladding strain. The minimum strain value reported for each programme ranges from 8%, in the case of FR-2 tests, 3-4%, in the case of Studsvik tests, to as low as 2% strain in the case of Halden tests. Most likely, the minimum strain required for fuel relocation varies with fragmentation size and other factors and ranges from 2-10% cladding strain.

6.2.2 Other considerations regarding LOCA fuel relocation

When considering the influences and implications of fuel relocation, a number of factors should be discussed.

First, there is a recurrent question regarding the timing of fuel relocation: does it occur during the ballooning and burst phase or does it occur later during post-test handling phase, prior to the PIEs? It seems that both causes might be involved in present findings. It is clear that fuel rod depressurisation at the time of burst acts as a driving force for axial fuel relocation. This transitory fuel relocation is confirmed by

the raise of temperature measured on the lower thermocouples. On the other hand, based on the LOCA test IFA-650.14 without burst, post-test examinations revealed some axial fuel relocation but during the test itself no change in the lower temperature measurements has been noticed (opposite to the tests with burst and actual transient fuel relocation) suggesting that fuel relocation in IFA-650.14 occurred mostly after the test, during the handling phase. This suggests that part of the fuel relocation which is observed on the LOCA tests PIEs might be due to the post-test handling of the fuel rods.

Second, considering the influence of cladding strain it is important to examine the potential for grid spacers to limit cladding strain and thereby limit fuel relocation.

Third, the implications of fuel relocation will depend greatly on the filling ratio of the relocated fuel in ballooned regions of the fuel rod.

A few observations from the many LOCA experimental programmes conducted over the last 40 years are available on the influence of grid spacers and the value of filling ratio. These observations will be summarised below. In addition, there are planned investigations in the Halden Reactor Project and the SCIP on these two factors.

The research programme conducted by PNL at the NRU reactor in Canada was the first series of tests performed on a bundle of rods instead of a single rod [6.2-11] [6.2-12] [6.2-13] [6.2-14] [6.2-15]. The thermo-mechanical tests were labelled the Material Test (MT)-1 through MT-4.

Two important findings of the MT series were that (1) the ballooning observed in the bundles of rods occurred in the same axial regions of the bundle for all rods in the bundle, thus resulting in flow blockage ratios up to about 70%, and that (2) grid spacers act to mostly prevent ballooning in the short section of the fuel rod that traverses them, thus “pinning” the balloons and potentially acting as choke points for fuel relocation. Same observation is already described in Chapter 2.4 of this report for VVER fuel bundle tests.

Figure 6.2-3 shows this phenomenon with a double balloon observed in all four tests, with the ballooned regions being pinned by the grid spacers. Grid spacers appear to “pin” rod ballooning, potentially acting as choke points for fuel relocation.

Axial relocation of fuel in ballooning or disrupted fuel rods shifts the position of heat generation and changes the temperature distribution. INEL developed the empirical model shown in Figure 6.2-4 to calculate the axial relocation based on PBF (length of tested fuel rod segment is of 1 m) and FR-2 data (length of fuel rod segment is of 50 cm).

Although the INEL model is dimensionless, the application of it requires scaling considerations when it is applied to fuel rods of standard length. A reasonable scaling consideration would be to restrict the INEL model evaluation to that quantity of fuel which is under axial relocation. As shown in Section 8.1.1, the INEL model can be re-casted into an expression for the average porosity of relocated fuel. It therefore restricts the application of the INEL model to this part of the fuel only.

Fourth, fuel fragmentation and related fuel relocation depend on the fragment size distribution, the smaller the fragments the higher degree of fuel relocation. NFIR investigations [7.2-23] have shown that the degree of pulverisation and resulting fragment size distribution depend on the temperature ramp rate. In addition it has been shown that pulverisation of the fuel can be precluded by increasing the hydrostatic pressure on the fuel pellet during the heating phase. This is consistent with the cladding strain thresholds proposed earlier. The scoping analysis in [7.2-23] allows identifying local burnups and temperature thresholds for various degrees of fuel pulverisation during a loss-of coolant accident (LOCA) which has been well confirmed by the post-test examinations in Halden and in Studsvik.

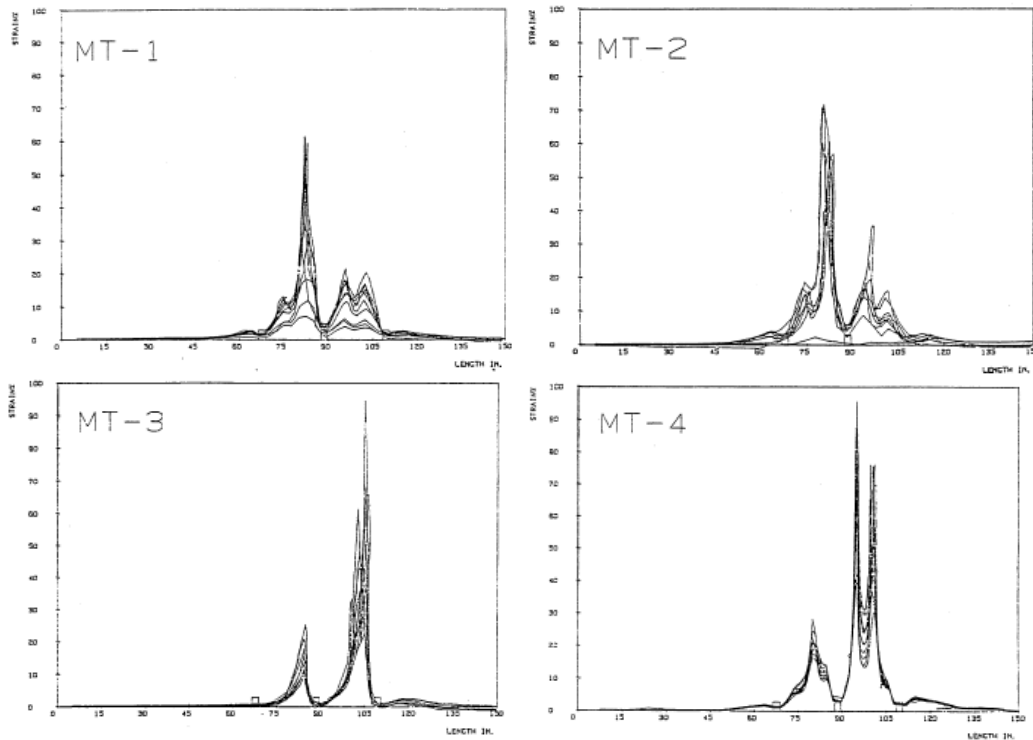


Figure 6.2-3: Circumferential strain profiles for all rods in tests MT-1, MT-2, MT-3, and MT-4, showing coplanar ballooning pinned by grid spacers [6.2-15]

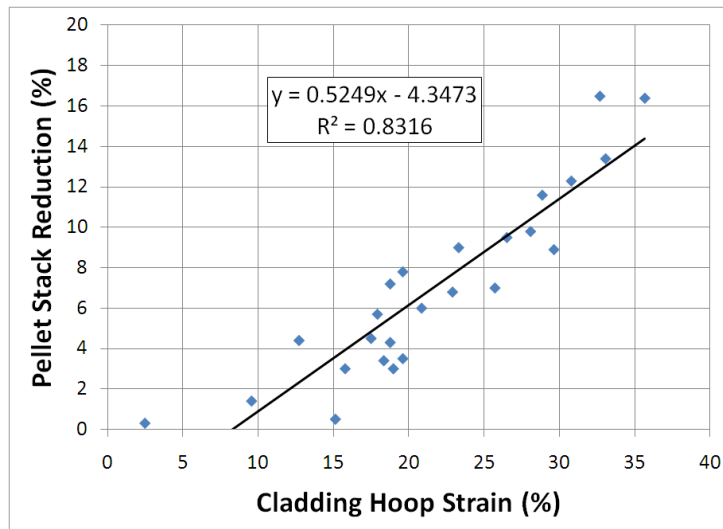


Figure 6.2-4: Pellet stack reduction as a function of cladding hoop strain for pre-irradiated fuel rods (based on the increase in volume in cladding balloon with no axial elongation) [6.2-16]

6.3 Fuel dispersal during LOCA

6.3.1 Necessary conditions for dispersal

Certain physical conditions are necessary for fuel dispersal to occur. For example, fuel can only be dispersed from rods that burst. Related to this, the fuel fragments that disperse must be smaller than the

rupture opening. Finally, fuel must be in the rupture region or move to the rupture region in order to be dispersed.

Considering that fuel fragments that disperse must be smaller than the rupture opening, fuel dispersal will be strongly correlated with fuel fragmentation behaviour, particularly the conditions for fine fuel fragmentation behaviour and burst opening size.

Considering that fuel must be in the rupture region or move to the rupture region in order to be dispersed, fuel dispersal will be strongly correlated with fuel relocation behaviour.

6.3.2 Experimental observations

There have been a number of observations of fuel dispersal in LOCA experimental programmes conducted over the last 40 years. The observations are predominantly available from relatively recent LOCA tests at Halden and Studsvik, however two other experimental programmes included observations of fuel dispersal.

In the report on ANL LOCA tests, it was reported that a fine dust of fuel particles was expelled from a high-burnup BWR rod with a local burnup of 64 MWd/kgU upon rupture during the ramp to 1 200°C [6.1-4]. The amount of fuel dispersal was not measured, but the report states that it was estimated to be about the quantity of one fuel pellet. The reports on PBF experiments also noted the observation of fuel dispersal; however it was also not quantified, [6.2-6], [6.2-7]. The results from Studsvik's LOCA tests provide a few notable observations related to fuel dispersal.

Table 6.3-1 provides the value of maximum circumferential cladding strain, the length of the fuel rod segment with a local cladding strain above 10% and rupture dimensions for each test. The values in Table 6.3-1 are in some way correlated with the capacity for fuel dispersal; where the maximum local cladding strain and the segment length with a cladding strain greater than 10% are expected to be correlated with fuel mobility and the rupture dimensions are expected to be correlated with the minimum dispersible fragmentation size.

This information suggests that tests 189 and 191-193 would be expected to have large fuel dispersal due to the high burnup, large balloon strain and rupture dimensions, while tests 196 and 198 would be expected to have small fuel dispersal due to the burnup value, small balloon strain and rupture dimensions. As will be shown below, the observations of fuel dispersal in the Studsvik tests were consistent with these expectations.

A wire probe was used to measure the length of voided cladding after all experimental steps (LOCA transient, bending, and shaking). The technique to measure the voided cladding is illustrated in Figure 6.3-1.

Test	Segment burnup (MWd/kgU)	Max Strain (%)	Length >10% Strain (mm)	Rupture Dimensions (mm) (Width/Length)
189	72	48	105	10.5 / 23.9
191	75	50	70	17.5 / 21.6
192	78	56	85	9 / 22.7
193	76	50	100	13.8 / 17.8
196	61	25	95	0.2 / 1.5
198	60	25	115	1.6 / 11

Table 6.3-1: Summary of strain and rupture measurements from Studsvik LOCA tests [6.1-5]

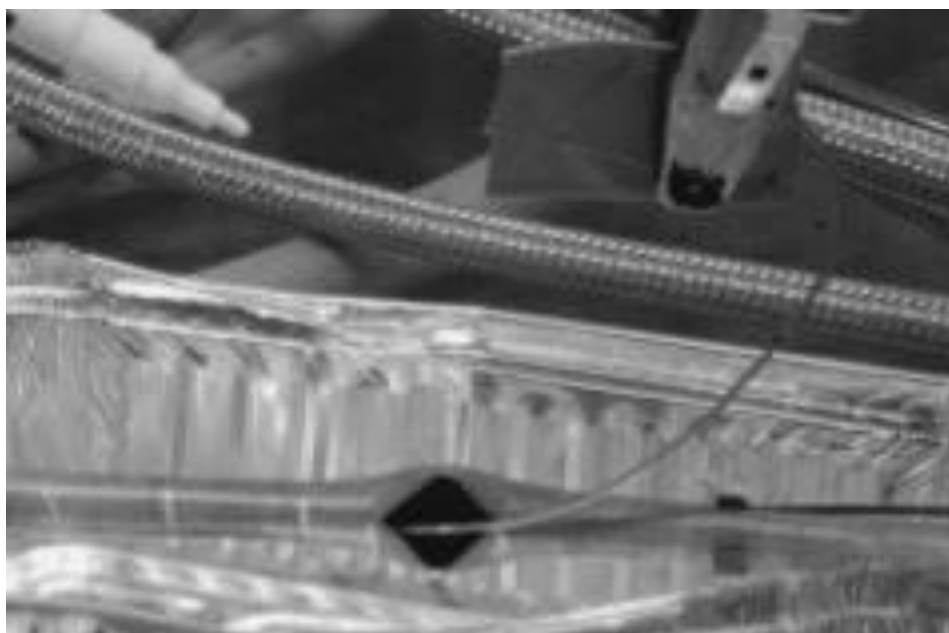


Figure 6.3-1: A wire probe is inserted into the fuel rod to measure the voided cladding length, [6.1-5]

Figure 6.3-2 and Figure 6.3-3 provide an indication of the approximate percentage of fuel loss during each test. It provides an estimate of the percentage of fuel loss during each test as determined by the mass of fuel fragments collected after the LOCA simulation and after the bending and shaking tests, where the initial mass was assumed to be 150 g for the 300 mm segment.

In Figure 6.3-2, the PCT and RIP are indicated. Total fuel release was similar in each test; however a distinct difference is apparent between tests 189-192 and tests 196 and 198.

It is also interesting to note that there does not appear to be an obvious trend between either PCT or RIP and fuel dispersal for this data set, possibly because fuel fragmentation was already complete by the time of fuel rod burst, which occurred below 850°C.

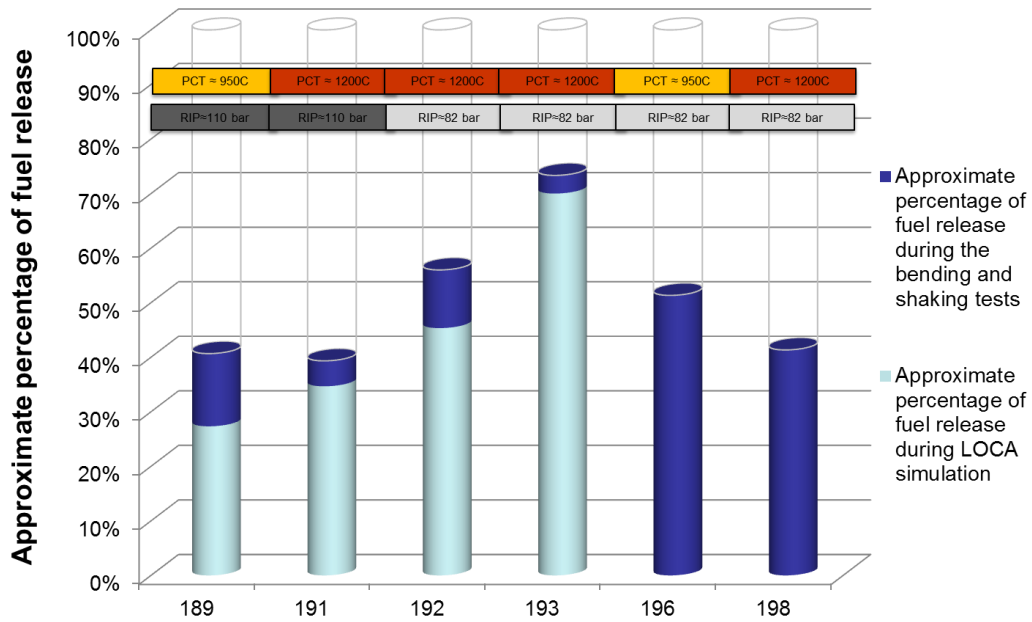


Figure 6.3-2: Approximate percentage of fuel loss during each test, color coded by when fuel loss occurred. Note: Measured mass loss was compared to an estimated initial fuel mass of 150 g for the 300 mm segment.

Figure 6.3-3 provides an estimate of the percentage of fuel loss during each test as determined by the wire probe measurements completed after the LOCA simulation and after the bending and shaking steps. In Figure 6.3-3, the percentage of the segment length with a cladding strain greater than 10% is also indicated.

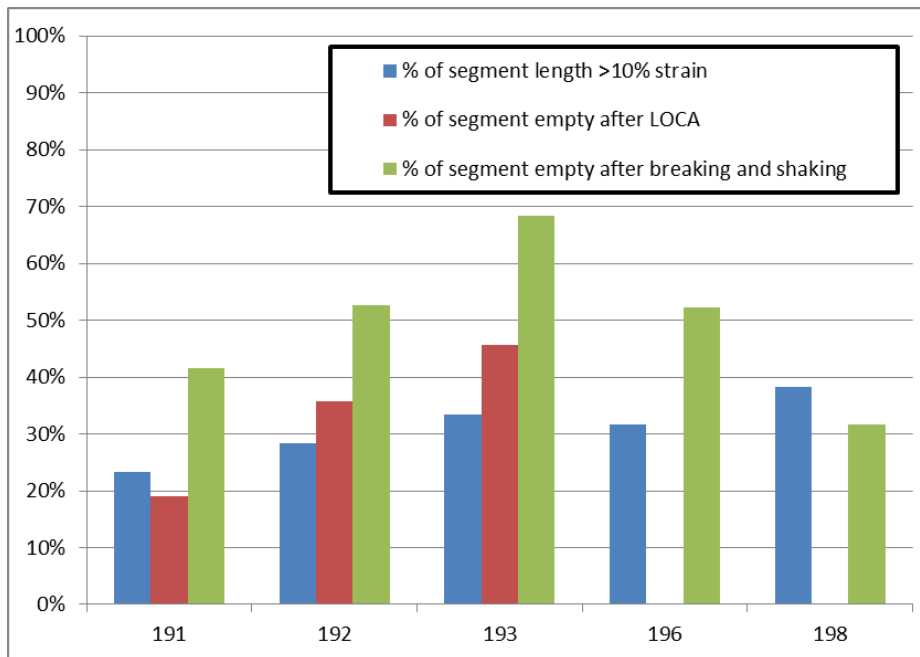


Figure 6.3-3: Approximate percentage of fuel loss during each test, in comparison to the length of cladding strain >10%, as measured by wire probe.

Fuel dispersal was also observed in the Halden LOCA tests, as summarised in previous chapters, and synthesised in Figure 6.3-4 [6.3-1]. The general observation from the Halden tests was that some degree of fuel dispersal could occur for rod burnups above ~60 MWd/kg, but the quantities were small below burnups around 80 MWd/kg. Furthermore, most of the dispersed fuel mass consisted of coarse fragments below a burnup around 80 MWd/kg.

test #	2	7	6	11	10	12	13	3	5	9	4
burnup, MWd/kg	0	44.3	55.5	56	60	72.3	74.1	81.9	83	90	92
balloon strain, %	54	23	49	25	15	40	45	8	15	61	62
balloon area, mm ²	270	8	?	1,5	38	1	10		7	224	434
fragment size	coarse	coarse	coarse	coarse	coarse & some fine	coarse & fine	coarse (& fine?)	medium & fine	medium & fine	medium & fine	medium & fine
gamma scan											
flask bottom →											
HBS width											
dispersal (qualitative)	none	none	none	none	some	some more	nearly none		much	much more	much more

Figure 6.3-4: Summary table of Halden LOCA tests of the IFA-650 series, with regards to fuel dispersal [6.3-1]

6.3.3 Proposed analytical thresholds

Fuel dispersal will be dependent on burst opening, cladding strain and fragment sizes distribution. Fine fuel fragmentation may more readily allow for fuel dispersal. The conditions required for fuel dispersal derived from physical restrictions and experimental observations can be summarised as follows:

- Fuel rod rupture must have occurred.
- Fuel fragments must be smaller than the burst opening. Cladding burst opening will be wider if the available amount of moles of gas within the fuel rod is large. In other words, a good axial gas communication between the upper plenum and the ballooned area will enhance the burst opening. Unfortunately, insufficient information is available to predict fuel rod rupture opening size reliably. Therefore it is difficult to define a fragment size threshold for fuel dispersal. However, it is considered that fine fragments will more readily allow for fuel dispersal. The conditions and thresholds for fine fragmentation have been discussed above and it is reasonable or at least conservative, to assume that inventory of fine fragments in the region of the fuel rod segment with cladding strain above the fuel relocation threshold could disperse. One possible (and likely conservative) approach would be to establish a “dispersible” fuel fragment size and postulate that all fuel particles and below the “dispersible” fuel fragment size are dispersed. Studies completed by the NRC have used a “dispersible” fuel fragment size of 1 mm.
- Experimental observations have established that there is a correlation between local pellet burnup and fragmentation size and that the transition to fine fragmentation can begin at a pellet average burnup as low as 60 MWd/kgU or as high as 70 MWd/kgU (depending on the irradiation history

of the fuel rod), and be complete at a pellet average burnup around 80 MWd/kgU. For analysis purposes, it is practical to assume that the fraction of fine fragments increases rapidly at a burnup somewhere in between 60 and 80 MWd/kgU. One possible approach to model the increase in the fraction of fine fragments is to use a multi-linear interpolation between known fragment size distributions at different burnups, with the fine fragmentation generally increasing as a function of burnup, as described in Chapter 7. Another possible approach is to model the increase in the fraction of fine fragments as a function of burnup based on the volume of the pellet radius to exceed a certain burnup threshold that is determined from available experimental observations.

- A given amount of cladding strain is required for fuel particles to be axially mobile within the cladding. This axial mobility strain threshold is believed to be between 2 and 10% permanent cladding strain.

6.4 Summary: Preliminary thresholds for fuel fragmentation relocation and dispersal

	Fine fragmentation	Relocation	Dispersal
Pellet average burn-up	> 65 - 70 MWd/kg	-	65 - 70 MWd/kg
Cladding strain	> 5 - 10%	>2% (fine fragmented) >7% (coarse fragmented)	> 7%
Pellet temperature	> 750 °C	-	> 750 °C
Burst opening	-	To be investigated in case of no burst	> 1 mm
Power history	To be investigated	To be investigated	To be investigated
Fragment size	-	-	< 1 mm

Table 6.4-1: Preliminary list of thresholds for fragmentation, relocation and dispersal

Table 6.4-1 provides preliminary FFRD thresholds. Consequently, some of these parameter values still need to be confirmed through appropriate experiments.

7. NECESSITY OF CODE MODELLING

7.1 Introduction to necessity of code modelling

In order to adequately predict the response of a nuclear reactor system as a result of a LOCA where some fuel rods are expected to fail, it is important to be able to model key phenomena that could influence fuel rod thermal mechanical behaviour.

The modelling requirements for the following key phenomena are detailed in Section 7.2:

- Fuel cladding ballooning and rupture, as well as the geometry of the resulting rupture opening, which are believed to have a direct impact on whether fuel fragmentation, relocation, and dispersal are possible for a given LOCA transient.
- Fuel fragmentation: the timing of fuel fragmentation and the particle size distribution could have an impact on both the filling ratio often used in relocation models, as well as the quantity of fuel that can be dispersed from a rupture rod.
- Fuel relocation: this phenomenon should be modelled to correctly predict temperatures in the balloon in calculations for safety analyses, because of the strong impact of temperature underestimation on ECR, balloon strain, and rupture predictions.
- Fuel dispersal: this phenomenon has possibly significant impacts on coolability, long-term cooling, and radiological consequences.

Although it is not yet known with a high degree of confidence if fuel fragmentation, relocation, and dispersal constitute a safety concern in all countries, codes should be developed and validated to take these phenomena into account so as to help performing thermal-hydraulic, thermal-mechanical, and radiological assessments of the safety significance of FFRD. Some scoping studies of those phenomena are presented in Section 7.3 as examples.

Finally, the last Section 7.4 focusses on the cladding failure prediction during a LOCA. The current practices of different countries for estimating cladding failure in safety analyses (best-estimate and/or conservative approach, burst criteria allowed cladding failure ratio, calculated cladding failure ratio, etc.) are described.

7.2 Key phenomena to model FFRD impact in codes

Modelling FFRD impact can be done with different levels of accuracy and at different scales with empirical, semi-empirical, and mechanistic approaches. Various key phenomena need to be modelled in order to describe FFRD during a LOCA.

The behaviour of fuel during a LOCA is strongly dependent on the behaviour of the cladding. Indeed, clad creep and rupture are of first importance since it impacts the balloon characteristics for relocation and the burst opening area for fuel dispersal.

This section is dedicated to the modelling during a LOCA of cladding behaviour on one hand and fuel behaviour on the other hand. Only a global overview of classic models implemented in various transient codes used for LOCA calculations is given here. Very good literature reviews on fuel and cladding behaviour during LOCAs are available and should be consulted for more details [7.2-1], [7.2-2].

7.2.1 Cladding behaviour

7.2.1.1 Cladding deformation

The pressure decrease and the temperature increase in the primary circuit during the LOCA transient can lead to large plastic deformation of the cladding due to the stress induced by the difference between internal and external pressures.

Stress-strain relations are then needed to model cladding deformation. Usually, various contributions to deformation are taken into consideration:

- elastic deformation
- thermal expansion
- creep deformation.

The mechanical properties of zirconium alloys are strongly linked to the crystallographic state (α , β , $\alpha+\beta$) of the material. Therefore a transient modelling of phase transformation is needed to compute the crystallographic state and phase fraction during the LOCA transient. The alpha phase fraction evolution depends on heating rates as illustrated in Figure 7.2-1.

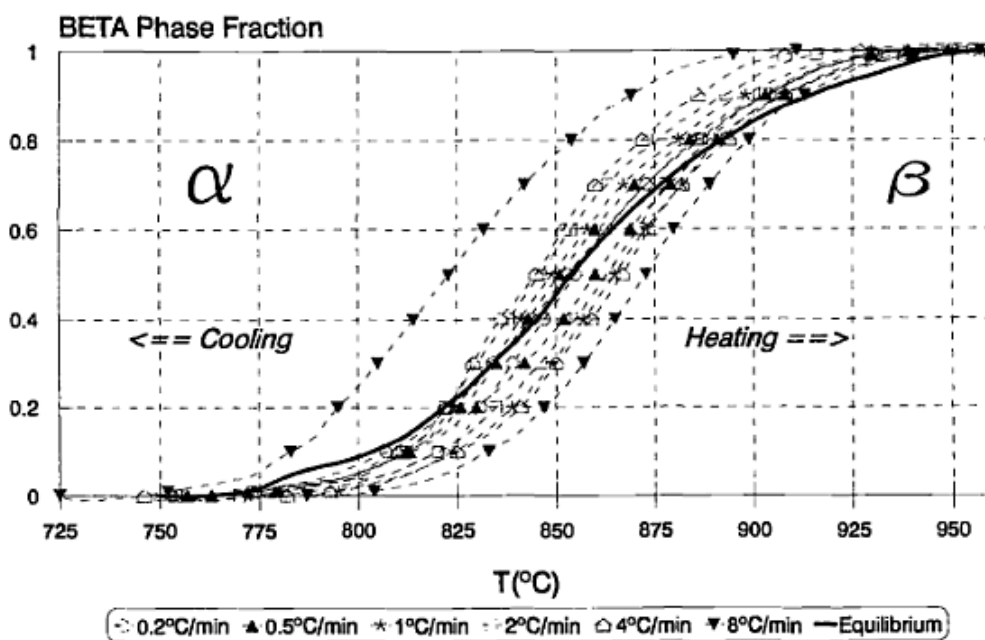


Figure 7.2-1: β -phase fraction at different heating rates derived from calorimetric measurements (M5 alloy) [7.2-3]

To model cladding deformation, stress and clad temperature must be known. Mechanical calculations are needed to calculate the stress in the cladding. Usually, the stress calculation relies on thin shell assumptions. Since the effective stress and strain are the ones linked by empirical stress-strain relations, the effective stress is deduced from the principal stress components.

The effective stress can be obtained with the von Mises (for isotropic material) or Hill (for anisotropic material) approaches [7.2-4], [7.2-5]. In cylindrical coordinates, the effective stress can be written as follow:

$$\sigma_e = \sqrt{\frac{1}{2}(\sigma_\theta - \sigma_z)^2 + \frac{1}{2}(\sigma_z - \sigma_r)^2 + \frac{1}{2}(\sigma_r - \sigma_\theta)^2} \quad (\text{von Mises})$$

$$\sigma_e = \sqrt{F(\sigma_\theta - \sigma_z)^2 + G(\sigma_z - \sigma_r)^2 + H(\sigma_r - \sigma_\theta)^2} \quad \text{with } F + G + H = 3/2 \quad (\text{Hill})$$

With σ_θ the hoop stress, σ_r the radial stress and σ_z the axial stress. F, G and H are the anisotropy coefficients.

In some models zirconium alloys are considered isotropic in all crystallographic phases since anisotropy coefficients are not well known at high temperature and after irradiation. The β -phase with a body-centered cubic structure is isotropic ($F = G = H = 0.5$) and consequently well described by the von Mises criterion.

The elastic contribution is computed knowing Young's modulus and Poisson's ratio, thermal deformation can be deduced from the thermal expansion coefficient.

Creep tests are used to determine the effective viscoplastic strain increment which is the main contributor to cladding ballooning at high temperature during a LOCA. The creep behaviour is composed of three main regimes as depicted on Figure 7.2-2.

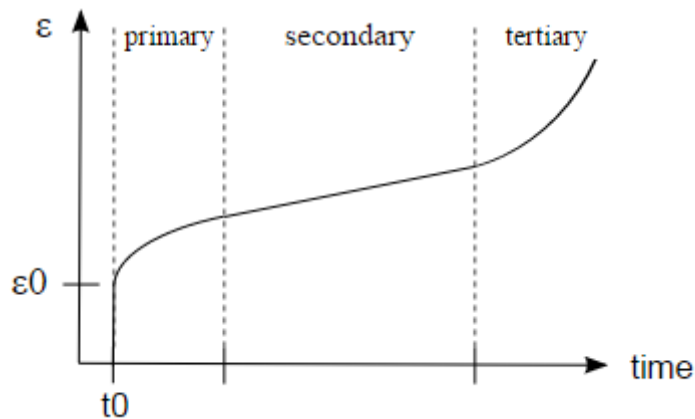


Figure 7.2-2: Strain versus time illustrating primary, secondary and tertiary creep

In most of the codes used for LOCA calculations only primary and secondary creep phases are taken into account. The tertiary phase is usually not taken into account since it is an unstable regime before the material failure. During the secondary phase, the strain rate is constant and is commonly described by an empirical Norton-like law relating effective strain rate to the applied effective stress:

$$\frac{d\epsilon}{dt} = A\sigma^n \exp\left(\frac{-Q}{RT}\right)$$

The A, n and Q coefficients are usually obtained from creep tests (associated to constant applied stress and isothermal conditions) or from ramp tests (pressure and/or temperature). These tests can be performed on various samples with different loading conditions (pure axial load, creep tests based on gas pressurised tubes ...).

Under mixed phases $\alpha+\beta$ conditions, creep properties are empirically deduced from creep tests or from properties of the pure phases (α and β) with mixing rules for high and low alpha fractions [7.2-2], [7.2-6], [7.2-7].

Moreover, various parameters like cladding material compositions, hydrogen content and oxide layer thickness should be taken into account. Indeed, these parameters may have a strong influence on clad creep during a LOCA transient [7.2-8], [7.2-9], [7.2-10].

Depending on the modelling approach, various more complex phenomena can be taken into account; a non-exhaustive list is given hereafter:

- 3D deformation
- rod-to-rod contact and balloon axial extension
- axial gas transport
- bending and Hot Side Straight Effect (HSSE)
- fuel cladding interaction if gap is closed
- transient FGR contribution to internal pressure.

The predictive capacity of calculation codes on cladding rupture is of primary interest for the FFRD modelling since it sets the balloon volume where fragmented fuel can move. Various criteria can be used to predict cladding rupture during a LOCA transient. The criterion can be defined based on hoop stress, hoop strain, temperature, a combination of stress and strain rate, or a damage concept.

The most common rupture criteria used for burst by ballooning are based on the comparison of hoop stress to a stress criterion that depends on temperature. This burst criterion is often associated with a criterion on maximum hoop strain that also depends on temperature. Other combinations are used such as limits on effective strain and strain rate.

An alternate approach consists in evaluating the increment of creep damage at each time step. This is particularly well suited for scenarios with temperature transients and temperature-dependent criteria like those usually used for burst modelling during a LOCA. The damage is cumulated over time with the general equation:

$$D = \int_0^t \frac{\dot{A}}{A_{burst}(T(t))} dt$$

Burst is reached theoretically when D exceeds unity. The physical parameter A can be strain, stress, temperature or a combination of several parameters.

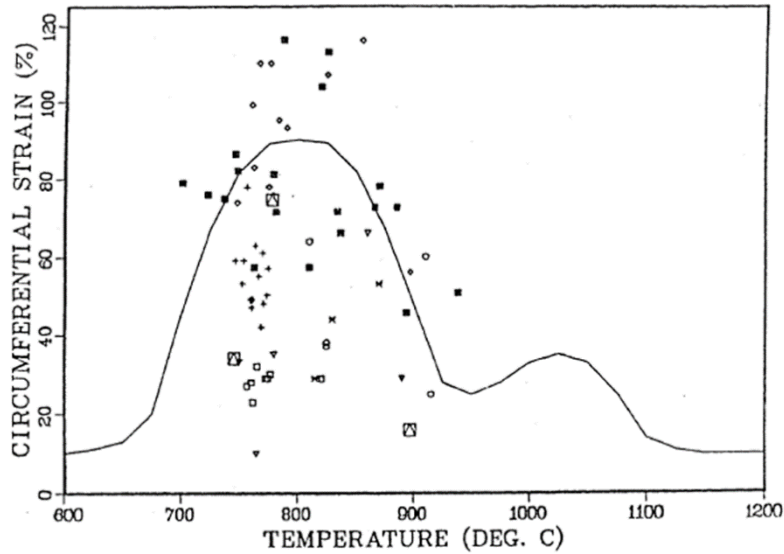


Figure 7.2-3: Maximum circumferential strain versus rupture temperature for Zircaloy cladding under steam environment internally heated below 10°C/s [7.2-11]

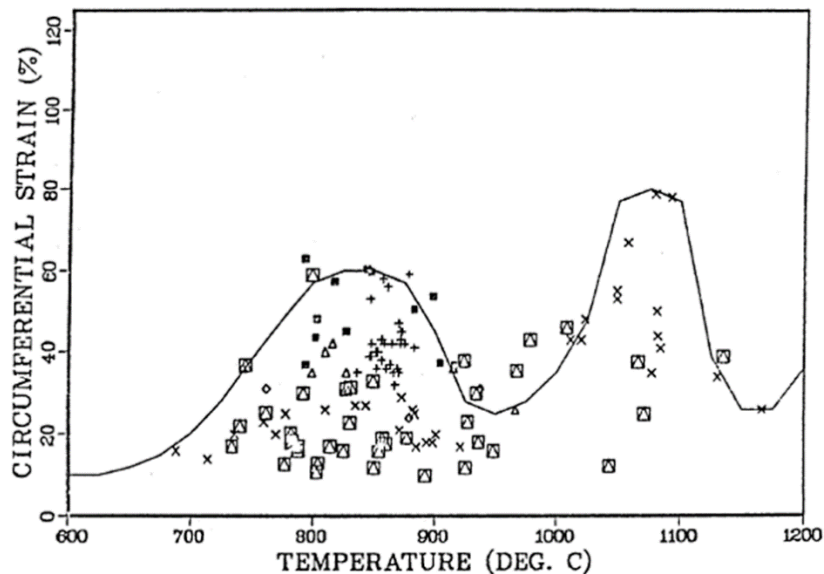


Figure 7.2-4: Maximum circumferential strain versus rupture temperature for Zircaloy cladding under steam environment internally heated greater than or equal to 25°C/s [7.2-11]

Many tests dealing with cladding deformation and rupture were described in detail in the NEA report [7.2-1]. Only a few selected ones are recalled here.

The so-called NUREG-0630 database was created in 1980 and contains rupture data in the form of burst temperature, engineering hoop stress at rupture, or rupture strain from various experimental tests with internally heated single rod or bundles. The data were classified depending on heating rates (see Figure 7.2-3 and Figure 7.2-4) [7.2-11].

An empirical correlation relating burst temperature and engineering stress was proposed in NUREG-0630:

$$T_R = 3960 - \frac{20.4 \sigma}{1 + H} - \frac{8,51 \cdot 10^4 \sigma}{(1 + H) + 27.90 \sigma}$$

Where T_R is the rupture temperature (°C), σ the hoop stress (kpsi) calculated on the undeformed cladding (engineering hoop stress) and H heating rate (0 to 28°C/s). This correlation is depicted on Figure 7.2-5.

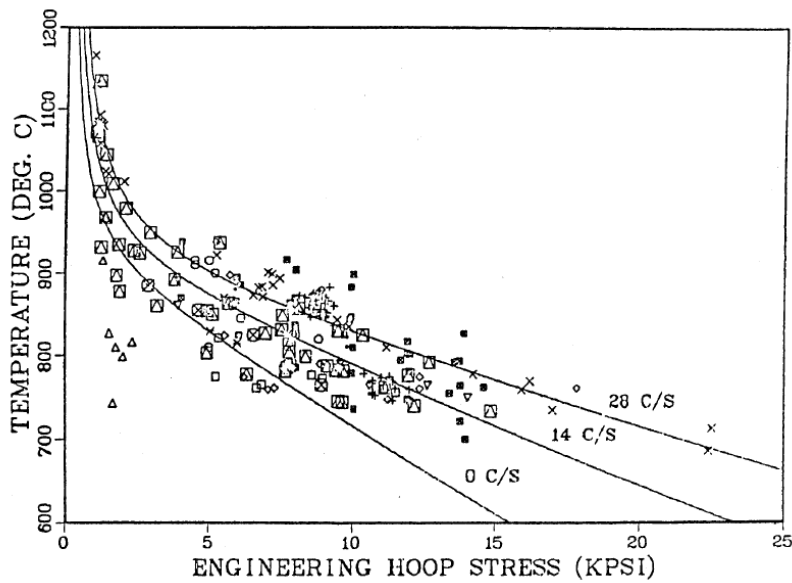


Figure 7.2-5: Correlation of rupture temperature as a function of engineering hoop stress and temperature ramp rate from internally heated Zircaloy cladding in aqueous atmospheres [7.2-11].

Other experimental programmes were conducted later to support the development of deformation models and rupture criteria. One of them is the French EDGAR programme performed by CEA since 1980 [7.2-1]. From these separate effect tests, an empirical rupture criterion on stress has been defined (see Figure 7.2-6), and is used in the CATHARE code fuel module.

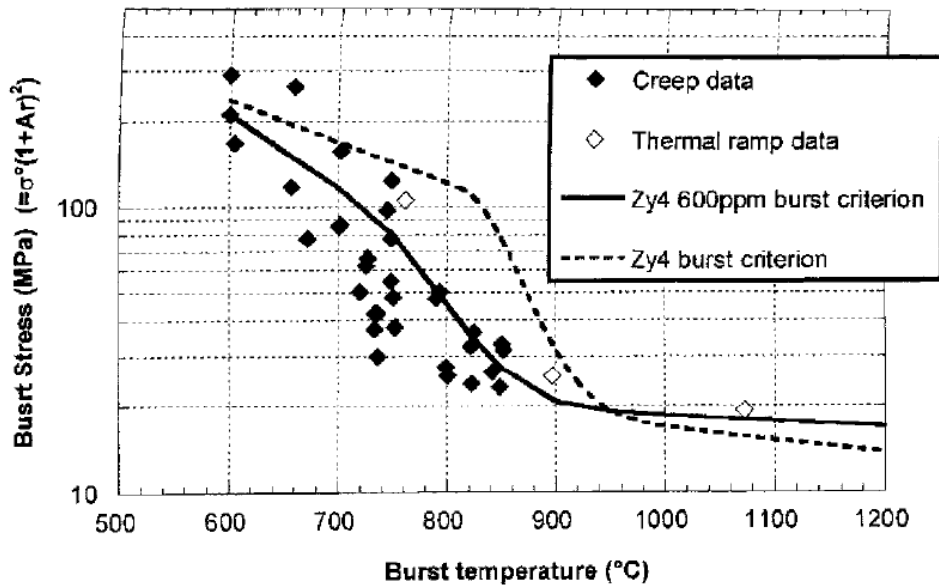


Figure 7.2-6: Comparison between the burst criterion for as-received and hydride at 600 ppm Zry-4 cladding tubes [7.2-8]

Similar burst tests were also performed by Kim et al. with Zry-4 PWR claddings [7.2-12]. The impact of heating rates was studied as illustrated on Figure 7.2-7.

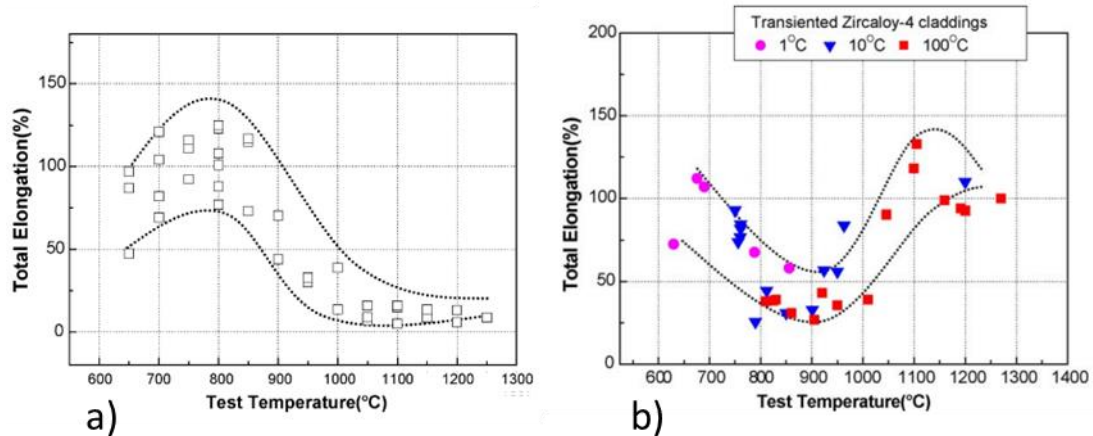


Figure 7.2-7: Total elongation at burst versus test temperature for iso-thermal tests (a) and transient tests (1°C/s, 10°C/s and 100°C/s) (b) from [7.2-12]

New programmes are being conducted nowadays to complete the rupture database by investigating the influence of hydrogen, oxide layer thickness, and neighbouring rods [7.2-13].

One has to keep in mind that experimental strain at burst is strongly dispersed and that models need to be adapted to the goal of the study. Indeed, for calculations on core coolability it is better suited that the rupture model should be the envelope of maximum burst strains in order to not underestimate flow blockage, rod-to-rod contact impact, and relocation impact. On the other hand, for radioactive release

estimations, the rupture models should not underestimate the number of burst rods and therefore the model should be the envelope of minimum burst strains.

7.2.1.2 Rupture opening

In traditional LOCA analyses, the extent of fuel rod ballooning and the prediction of cladding failure by ballooning and burst are important parameters because they have an impact of flow blockage and on ECR calculations, respectively.

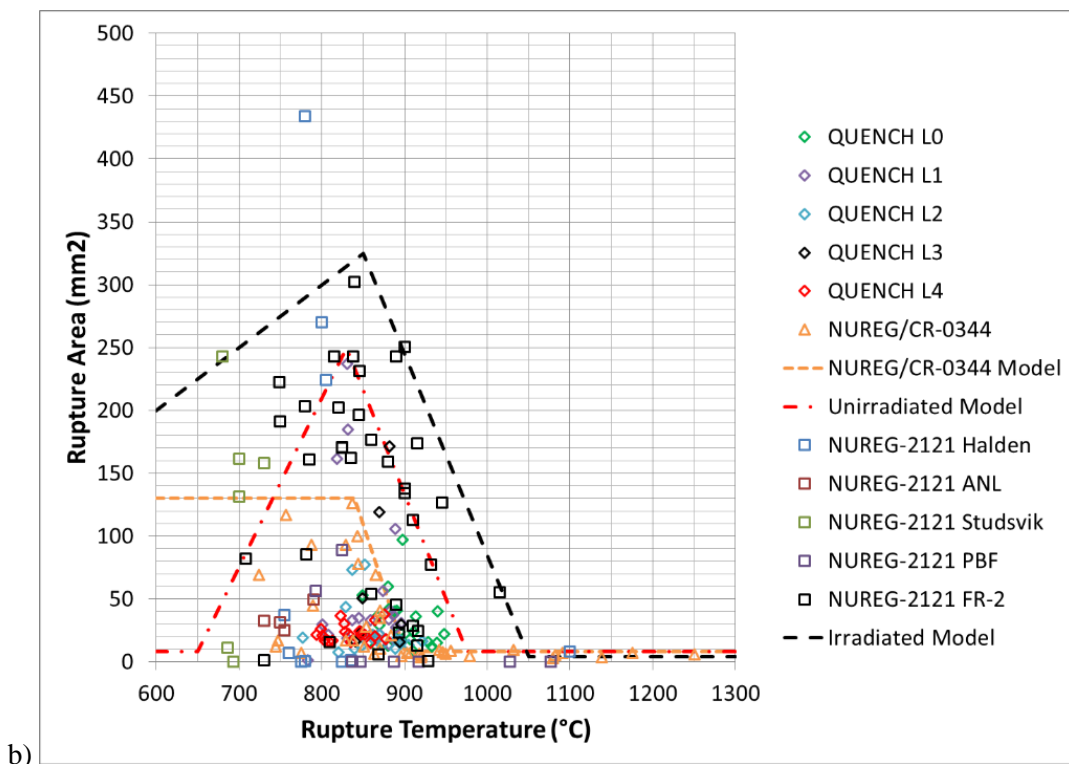
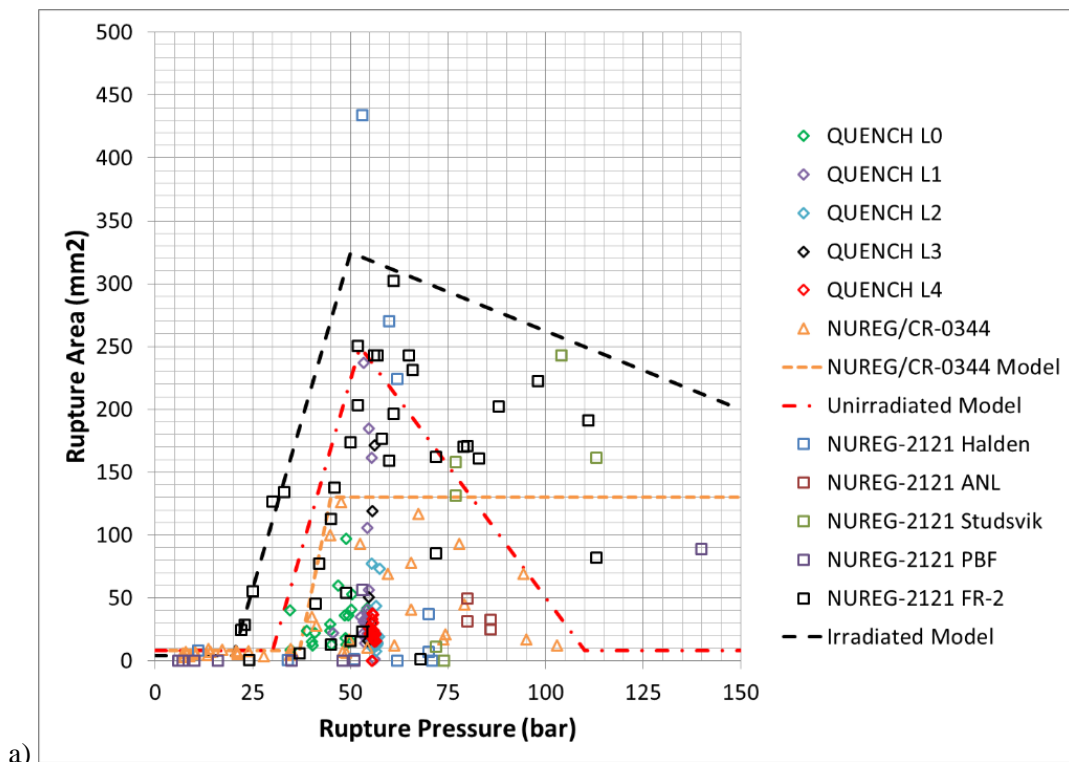


Figure 7.2-8: Rupture area as a function of a) rupture pressure and b) rupture temperature from several experimental programmes, for both un-irradiated and irradiated fuel, as well as proposed models.

In contrast, very little effort has been focused on modelling the shape and size of the rupture opening. However, with fuel dispersal in mind, the shape and size of the rupture opening become very important parameters, because only fuel fragments smaller than the rupture opening can physically fall out of the fuel rod. As a result, the comparison of the particle size distribution with the characteristics of the rupture opening could be used as a criterion for calculating the quantity of fuel that is dispersed in a given LOCA scenario.

Figure 7.2-8 shows the rupture area as a function of rupture pressure and rupture temperature, respectively. Five quench LOCA bundle tests (L0 through L4) have been performed by KIT on un-irradiated internally heated fuel rods, [7.2-14], [7.2-15], [7.2-16], [7.2-17]. In addition, the rupture opening area was characterised in the NUREG/CR-0344 burst tests on short segments of externally heated un-irradiated cladding [7.2-18].

NUREG-2121 also reported rupture opening area data from several test programmes on irradiated fuel rods: the NRC-ANL and NRC-Studsvik LOCA tests on externally heated rod segments, and the Halden, PBF, and FR-2 in-pile single rod tests [7.2-19].

Simple multi-linear bounding models for rupture opening area as a function of rupture pressure and temperature were proposed in NUREG/CR-0344 for the un-irradiated specimens that were tested. Similar models were developed for this report to encompass all the un-irradiated data and all the irradiated data, respectively, as shown in Figure 7.2-8. In both cases, the rupture opening is largest for rupture pressures around 50–55 bars, and rupture temperatures between 825°C and 850°C. The rupture opening area reported was generally larger for irradiated cladding (>300 mm²) than for un-irradiated cladding (<250 mm²).

7.2.2 Fuel behaviour

7.2.2.1 Fragmentation

As described in Chapter 3, it is important to distinguish steady-state fuel cracking from transient fuel fragmentation and pulverisation. Steady-state fuel cracking occurs primarily because of thermal stresses and begins as soon as the fuel rods are brought up to temperature during their life in the reactor. It is a relatively well understood and well characterised phenomenon that is fairly well modelled in virtually all fuel performance codes.

In contrast, transient fuel fragmentation can occur during some reactor transients such as a LOCA, and is believed to be dependent on a number of variables including the pellet burnup, the cladding strain, the fuel temperature, and whether fuel rod rupture occurs, among others.

Transient fuel fragmentation is not yet well understood, but modelling transient fuel fragmentation is necessary to be able to precisely determine the quantities of fuel dispersed in a given transient scenario.

As described in more detail in Chapter 4, several experimental programmes have characterised fuel that was dispersed from rods that were submitted to a LOCA transient, as shown in Figure 7.2-9 and Figure 7.2-10 a) for the PBF, FR-2, and NRC-Studsvik LOCA tests [7.2-19]. It can be seen from these figures that all tests at a burnup up to at least 60 MWd/kgU (NRC-Studsvik tests 196 and 198), the particle size distribution is rather coarse, with the majority of fragments being larger than 1 or 2 mm.

In contrast, the NRC-Studsvik LOCA tests performed at a burnup above 75–78 MWd/kgU (tests 191, 192, and 193) had at least 60% of fragments (by mass) with a size below 1 mm.

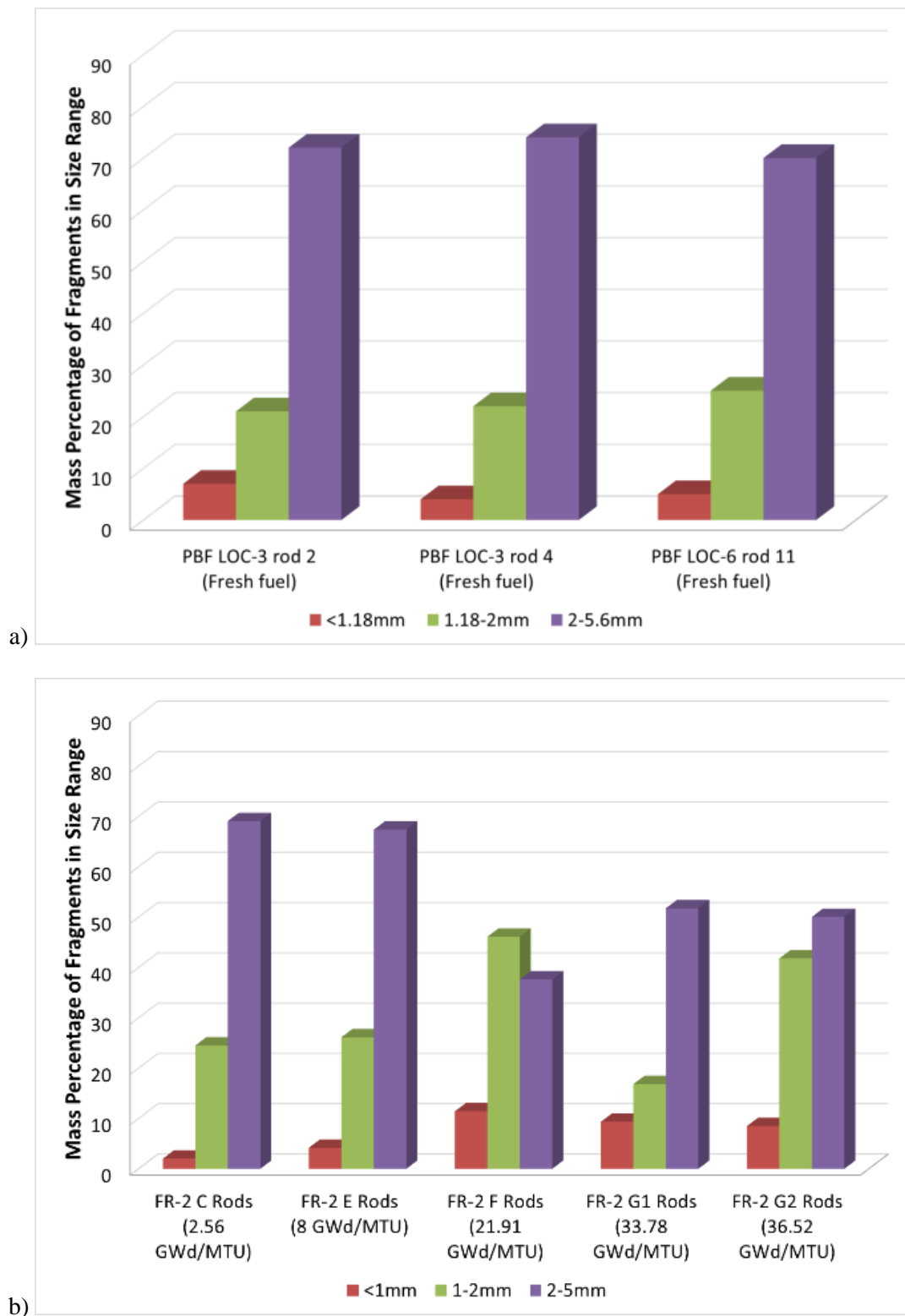


Figure 7.2-9: Fragment size distribution for (a) PBF and (b) FR-2 tests

It is generally accepted that burnup has a first-order influence on particle size distribution, such that the higher the burnup, the finer the transient fuel fragmentation. Figure 7.2-10 b) illustrates the simple

model developed by U.S.NRC for fragment size distribution, which assumed that the fragment size distribution is only a function of local pellet burnup [7.2-20].

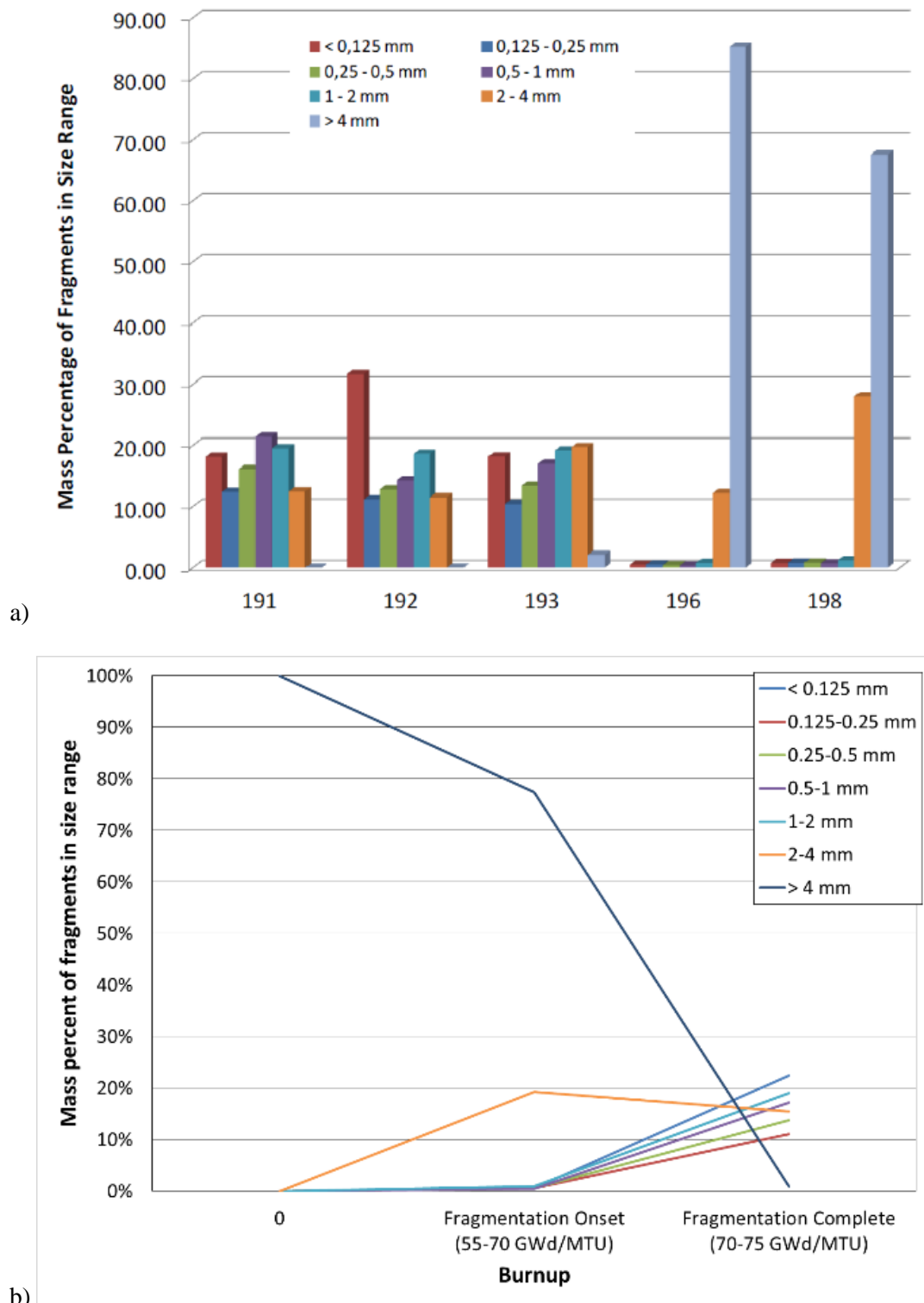


Figure 7.2-10: a) Fragment size distribution for the NRC-Studsvik LOCA tests and b) NRC model based on NRC-Studsvik LOCA test measurements

This model was developed based on the fragment size distributions measured in the NRC-Studsvik LOCA tests. It consists of a linear interpolation as a function of burnup between the average size distribution for the two tests at a burnup around 55 MWd/kgU (which had a coarse particle size distribution), and the average size distribution for the three tests at a burnup above 72 MWd/kgU (which had a fine particle size distribution). The model also assumed that a pellet with zero burnup only had fragments larger than 4 mm in size.

Aside from burnup, it appears the constraint exercised by the cladding on the fuel pellet has an important impact of fine fuel fragmentation [7.2-22]. In fact, a certain amount of cladding strain or an axial split in the cladding seem to be necessary conditions for fine fuel fragmentation, but cladding constraint has not yet been explicitly proposed as a variable in a transient fuel fragmentation model.

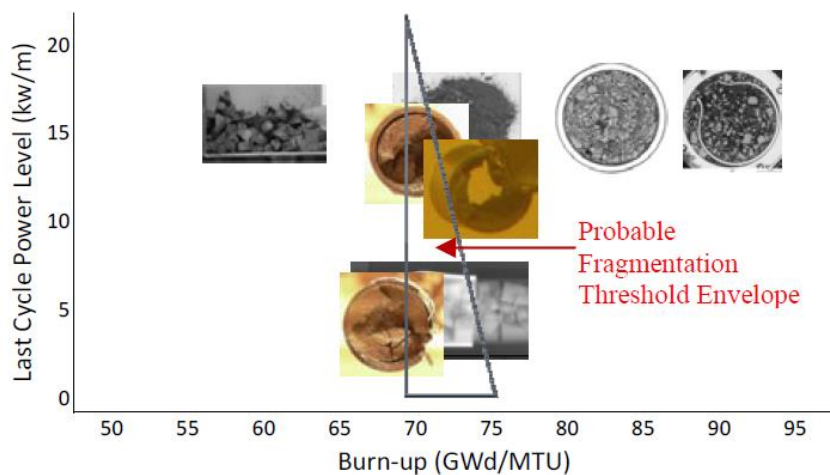


Figure 7.2-11: EPRI's proposed map of fuel fragmentation as a function of burnup and last cycle power [7.2-22]

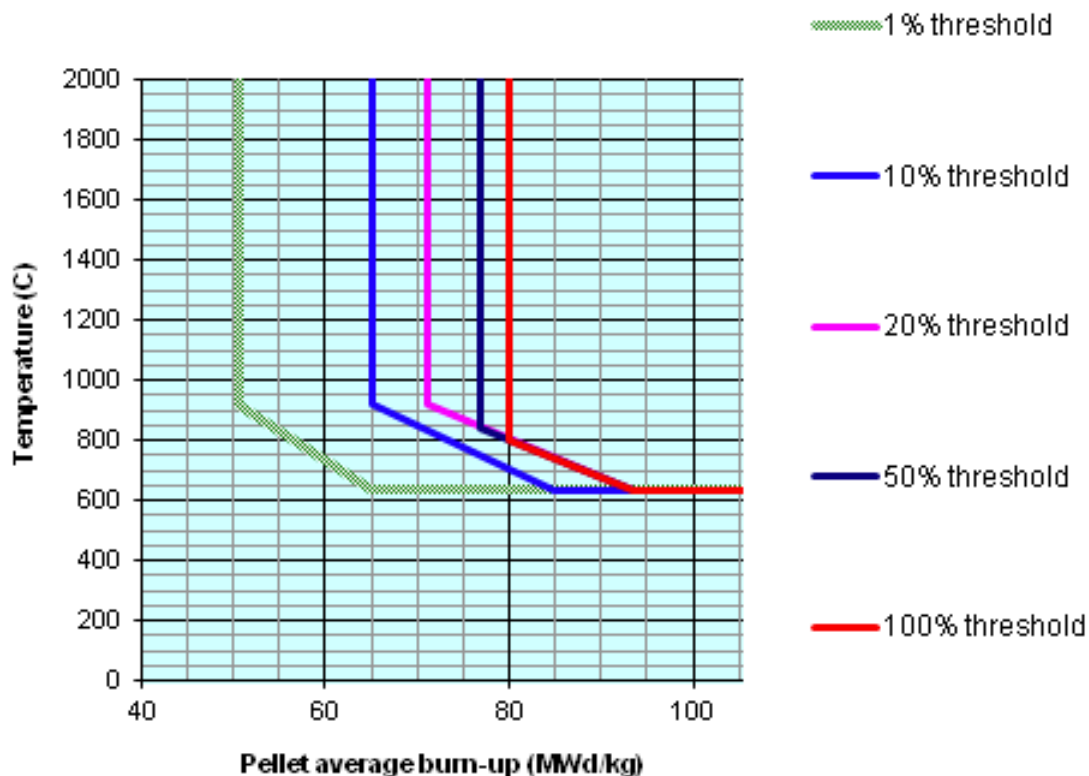


Figure 7.2-12: NFIR proposed threshold for different levels of pellet volume-% powder formation as a function of pellet average burnup and transient temperature [7.2-23].

More complex models that take into account other parameters such as last cycle power level and fuel temperature during the transient have recently been proposed by EPRI and NFIR, as illustrated in Figure 7.2-11 [7.2-22] and Figure 7.2-12 [7.2-23].

Yueh et al. proposed a fine transient fuel fragmentation threshold [7.2-22] based on both last-cycle power and burnup, while Turnbull et al. proposed a model based on fuel temperature during the transient and burnup [7.2-23].

To develop this fragmentation threshold, and to investigate the potential disintegration to powder of high-burnup fuel pellets during a rapid temperature transient, the Nuclear Fuels Industry Research (NFIR) Programme commissioned two independent scoping studies.

The first investigated the effect of hydrostatic restraint pressure on FGR during a series of fast temperature ramps. In the second study laser heating was used to investigate the temperature at which small samples of fuel fragmented. From the observations made in these studies, local burnup and temperature thresholds of 71 MWd/kg HM and 645°C were identified for fuel pulverisation during a loss-of-coolant accident (LOCA).

It is shown that fine fragment production in integral LOCA tests performed in other independent investigations at Studsvik and Halden was generally well predicted using these thresholds of burnup and temperature (Figure 7.2-12).

The NFIR investigations also reveal that the degree of pulverisation and resulting fragment size are dependent on the temperature ramp rate. Moreover, they confirm that pulverisation can be substantially reduced by the imposition of hydrostatic pressure.

The models proposed by EPRI and NFIR are well supported by both integral and separate effects experiments.

Generally speaking, at a given pellet burnup, the higher the last-cycle power and the higher the transient fuel temperature, the finer the transient fragmentation. Although this hypothesis has not yet been validated experimentally, the key to modelling fine fuel fragmentation may be related to transient fission gas behaviour and the behaviour of the HBU pellet rim. Further experiments and modelling are needed to better understand transient fuel fine fragmentation.

Other approaches similar to the NFIR model described by Yagnik et al. were proposed [7.2-24], [7.2-25]. Kulacsy and Molnar described a fine fragmentation and transient FGR model as a function of fuel temperature and burnup [7.2-25]:

- Below a local burnup of 66 MWd/kgU and a local temperature of 600°C, no micro-fragmentation occurs;
- Above a local burnup of 66 MWd/kgU and at a local temperature between 600°C and 1 050°C, a local FGR of 20% is assumed;
- Above a local burnup of 66 MWd/kgU and above a local temperature of 1 050°C, a local FGR of 90% is assumed.

In Kulacsy and Molnar's model, release is assumed to occur irrespective of the state of the cladding, i.e. regardless of ballooning and/or rupture.

7.2.2.2 Relocation

Axial fuel relocation during some LOCA transients has been evidenced in PBF (INL) or FR-2 (KfK) tests performed in the 1980s and more recently in the Halden IFA-650 and NRC-Studsvik tests.

Modelling fuel relocation is a big challenge since the impacts for example in terms of cladding temperature in the balloon have never been measured experimentally. Moreover, data on fuel after fragmentation are also needed to predict fuel relocation.

This section will only describe the key parameters needed to model relocation with some examples of methods and laws implemented in a few codes like FRAPTRAN-SCK [7.2-26], FALCON [7.2-27] or DRACCAR [7.2-28]. Indeed, axial relocation during LOCA has been rarely taken into account in LOCA calculations.

The first important parameter is the onset time of relocation. Fuel fragments can move only if free space is available at lower axial locations i.e. if cladding deformation is enough compared to fragments sizes. Therefore, a threshold on cladding strain to trigger axial fuel relocation could be used.

Another question is whether cladding burst is needed to trigger axial fuel relocation. The last Halden IFA test 650.14 seems to indicate that no burst is needed for fuel relocation. However, the cladding strain in this test is low, and the fuel relocation is limited [7.2-29].

When axial fuel relocation occurs, one has to model fuel movements from upper slices to the free volumes. First, the beginning of the balloon has to be set (minimum axial level where relocation can occur), in general this location depends on the gap between the fuel pellet and the cladding, as well as the fuel fragments sizes. Then, to know how much fuel will move, the filling ratio in the balloon and free volume must be known.

In current models, this filling ratio is imposed in the data deck by the user. Typical values are in the range of 40 to 75%, [7.2-26], [7.2-27], [7.2-30]. An example of an algorithm for fuel movement is illustrated on Figure 7.2-13 [7.2-26]. This algorithm is divided into two steps, the first one to determine the amount of fuel that can fall from above slices, and the second one to fill free spaces according to the

chosen filling ratio. This axial relocation impacts the LHGR and therefore cladding temperatures in the balloon. Some examples of scoping calculations on the impact of axial fuel relocation on cladding temperature will be described in the next section.

Thermal conductivity of relocated fuel must be calculated with specific models since it is considered as media made of solid fragments in a gas with a macroscopic porosity (1-filling ratio). Indeed, usual models used to calculate thermal conductivity of fuel depend on microscopic porosity (bubbles and cracks in the fuel) and are not convenient to take into account macroscopic porosity. Various correlations can be used, simple ones which are combinations of gas and fuel conductivities (by e.g. Missenard approach [7.2-31]) and more complex ones which take into account radiation between fuel fragments which depends on fragments size (by e.g. Imura-Yagi correlation [7.2-32])

A simpler empirical model to calculate the transient axial fuel relocation was also developed by INEL based on PBF and FR-2 data in the early 80s [7.2-33], and is shown in Figure 7.2-14. This experimental study reported that (1) no axial relocation of fuel occurs until the cladding hoop strain exceeds a value of 8%; (2) after the cladding hoop strain exceeds 8%, the fuel pellets crumble, and (3) as the cladding continues to strain, axial fuel relocation occurs so that the fuel void fraction in the balloon region remains equal to the void fraction at the time of fuel pellet crumbling. In fuel rods ballooning until rod-to-rod contact occurs, the model predicts that axial fuel relocation causes a 35% increase in the LHGR in the ballooned region of the fuel rod.

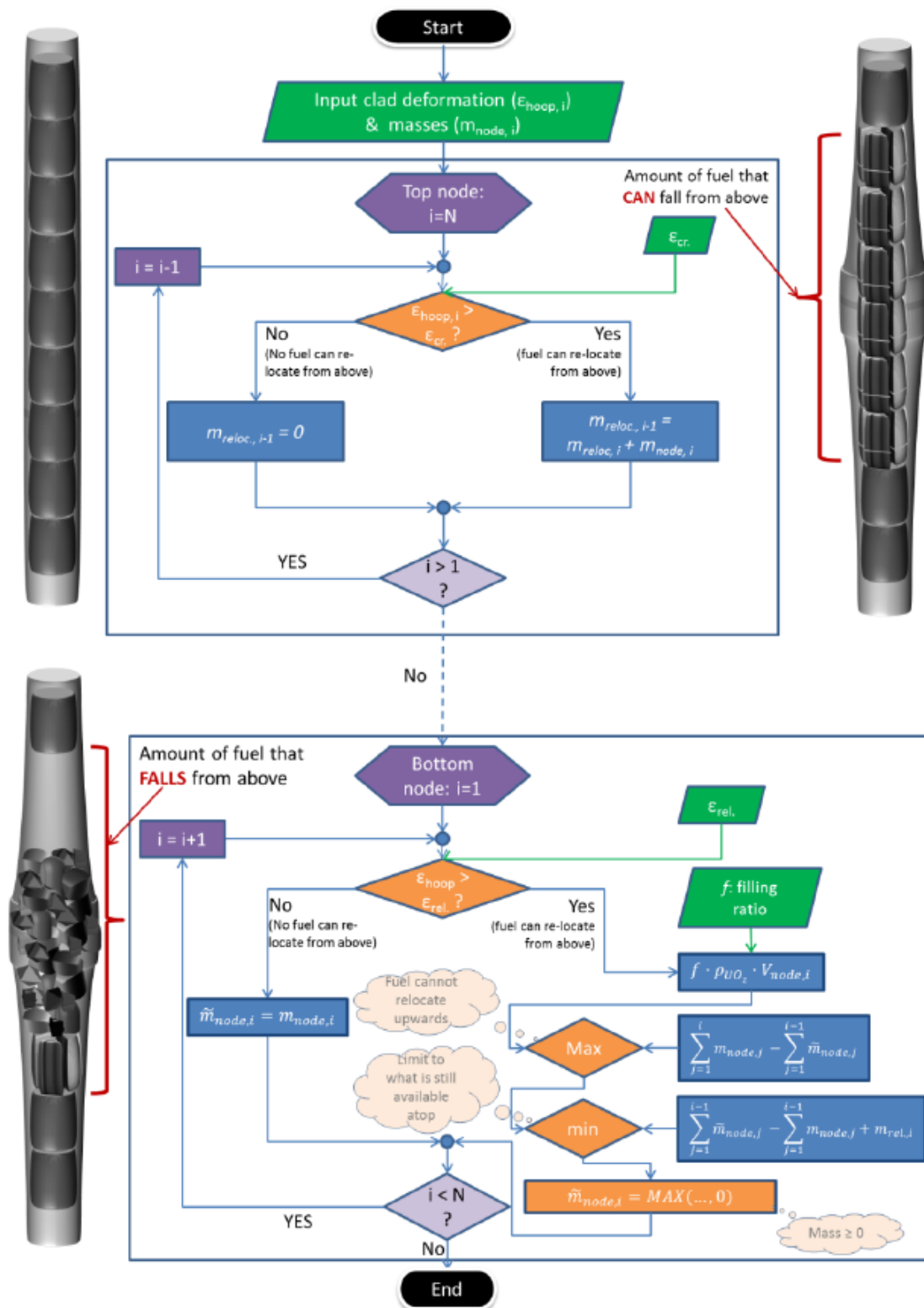


Figure 7.2-13: Schematic view of the algorithm for evaluating the amount of fuel that relocates. The first step evaluates the amount of fuel that is free to fall from upper locations, the second step then estimates the amount of fuel that actually relocates (cited from [7.2-26])

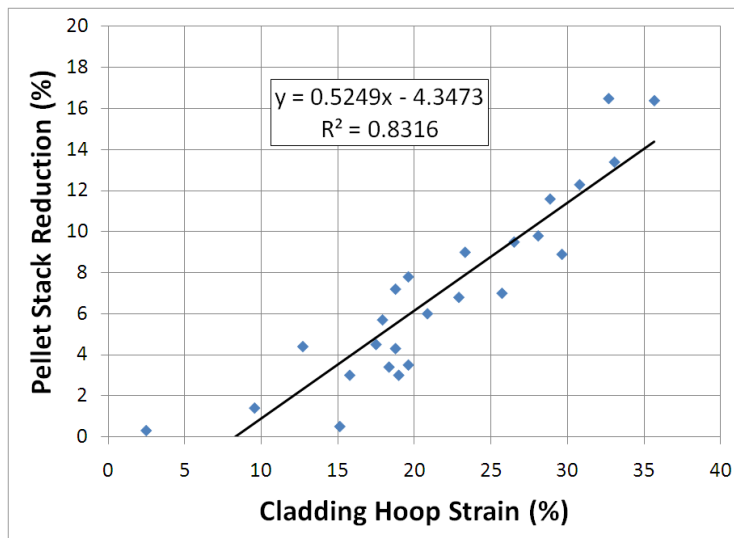


Figure 7.2-14: Pellet stack reduction as a function of cladding hoop strain for pre-irradiated fuel rods (based on the increase in volume in cladding balloon with no axial elongation)

7.2.2.3 Dispersal

Very few models for fuel dispersal have been documented in the open literature. In 2012, IBERDROLA presented an empirical model based on some of the data from NUREG-2121, whereby the quantity of dispersed fuel from a ruptured fuel rod is strictly a function of burnup, as shown in Figure 7.2-15, [7.2-34].

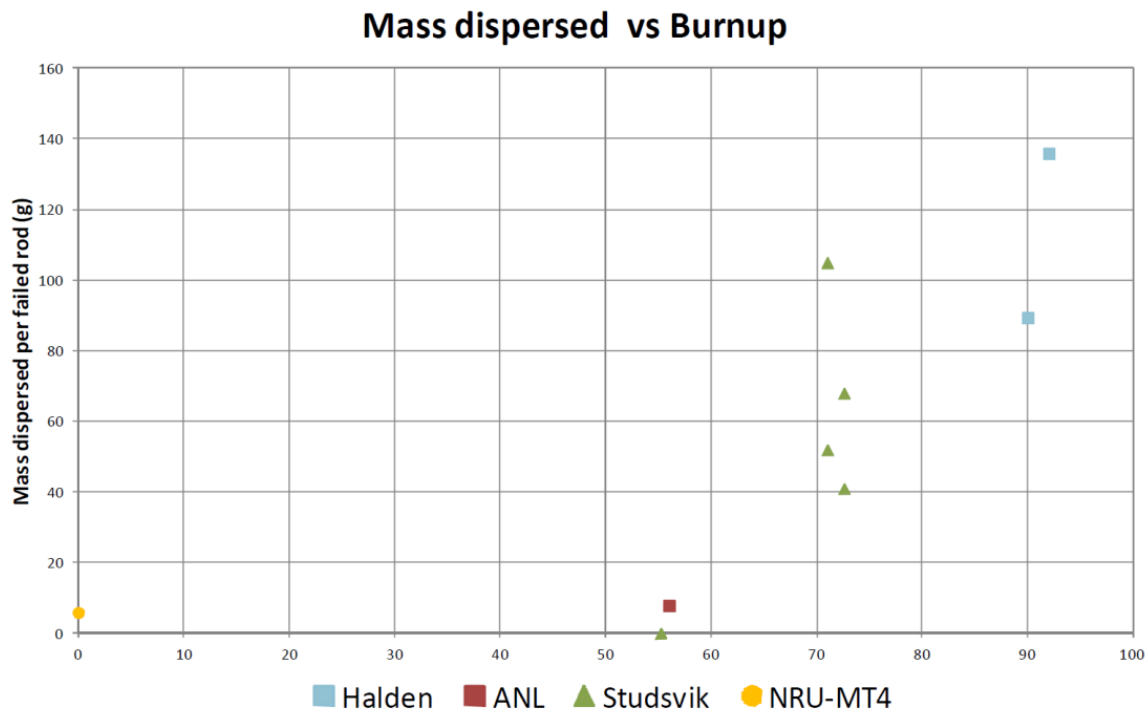


Figure 7.2-15: Fuel dispersal model presented by IBERDROLA at Top Fuel 2012 - mass of fuel dispersed per ruptured fuel rod as a function of burnup

A rather simple analysis based on an inventory of the fuel assemblies and hot rods in the core in terms of LHGR versus burnup was used to determine how many fuel rods ruptured in a large-break LOCA for a BWR-6. For each rupture fuel rod, the quantity of fuel dispersal was estimated based on the model shown in Figure 7.2-15, and the safety implications of the calculated fuel dispersal were discussed based on coolability and criticality analyses. The details of this study are summarised in Section 7.3 below.

More recently in 2013 and 2014, the U.S.NRC presented another simple model based on empirical data and chosen assumptions. This model relies on a very detailed LOCA calculation where each and every fuel assembly is individually modelled in the system thermal-hydraulic code TRACE. Each average assembly is also modelled in the steady-state and transient fuel performance codes FRAPCON and FRAPTRAN, and sequential coupling is implemented with TRACE [7.2-20], [7.2-35].

For each assembly, the thermal mechanical response is obtained by applying boundary conditions from TRACE in the FRAPTRAN code. For each rupture fuel rod, the number of axial nodes adjacent to the rupture and with sufficient cladding strain to result in fuel fragmentation and axial fuel mobility was computed: these were the ‘dispersible fuel’ nodes.

Then, the local nodal burnup was used to determine the particle size distribution for the ‘dispersible fuel’ nodes based on the U.S.NRC developed model shown in Figure 7.2-10b). Because of uncertainties in the rupture opening size and the lack of a good rupture opening area model, it was assumed that all the fuel fragments smaller than 1 mm would be dispersed.

Although more elaborate and more mechanistically based than the IBERDROLA model, the U.S.NRC model is still largely based on empirical data. Furthermore, the uncertainties associated with the U.S.NRC model are rather large, in part because of the chosen threshold values for fragmentation and relocation, but also because of the limited ability of transient fuel performance codes to accurately model the axial extent of ballooning in fuel rods.

7.3 Scoping Studies

Since taking into account FFRD in codes used for LOCA calculations is new and very few experimental data on FFRD impact on cladding behaviour are available, the results presented in this section can only be considered as scoping calculations.

7.3.1 Relocation impact

7.3.1.1 ICARE/CATHARE, DRACCAR (IRSN)

Since the 2000s IRSN has been performing some scoping calculations to assess the impact of axial fuel relocation on the PCT during LOCA transients. The first studies were made with the CATHARE-2 code with a modified fuel sub-module to simulate axial fuel relocation after burst [7.3-1].

The same approach was then slightly modified and included in the IRSN codes ICARE (axisymmetric) and DRACCAR (3D). The model associated to CATHARE-2 calculations allows fuel relocation in the burst mesh in agreement with the available volume and the filling ratio given in the data deck.

The thermal conductivity of relocated fuel, considered as a porous media is calculated with the Imura-Yagi correlation [7.2-32]. Results published in open literature only concerns calculations with the CATHARE-2 code, similar results were obtained with the new-developed code DRACCAR but will not be mentioned later on (unpublished results).

An example of axial fuel relocation impact on cladding temperature is given on Figure 7.3-1 [7.2-30]. This study was made with a filling ratio of 61.5% and an average particle size of 2.7 mm for the

conductivity of the relocated fuel calculation.⁶ The cladding burst occurred for an average circumferential cladding strain of 58% and the impact of fuel relocation is around 200°C.

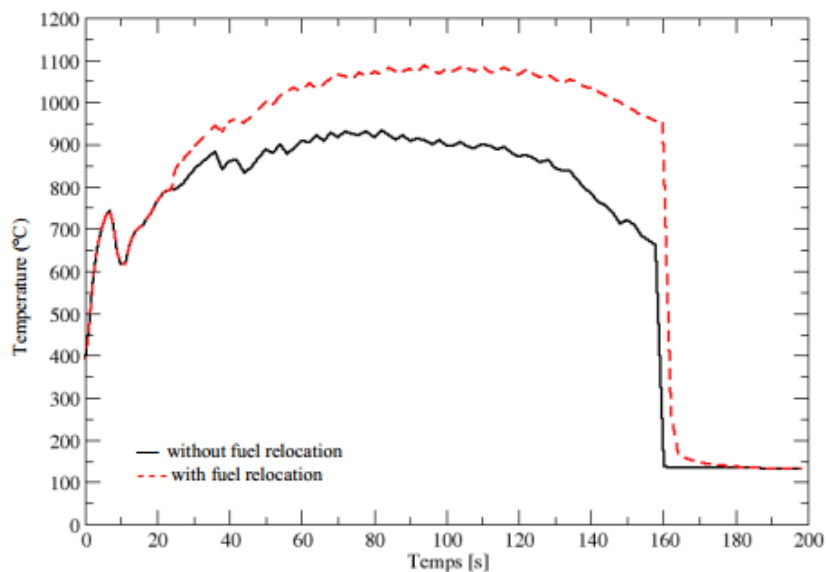


Figure 7.3-1: Impact of axial fuel relocation on cladding temperature at the rupture node of hot rod versus time (LB LOCA with irradiated UO₂ fuel) [7.2-30]

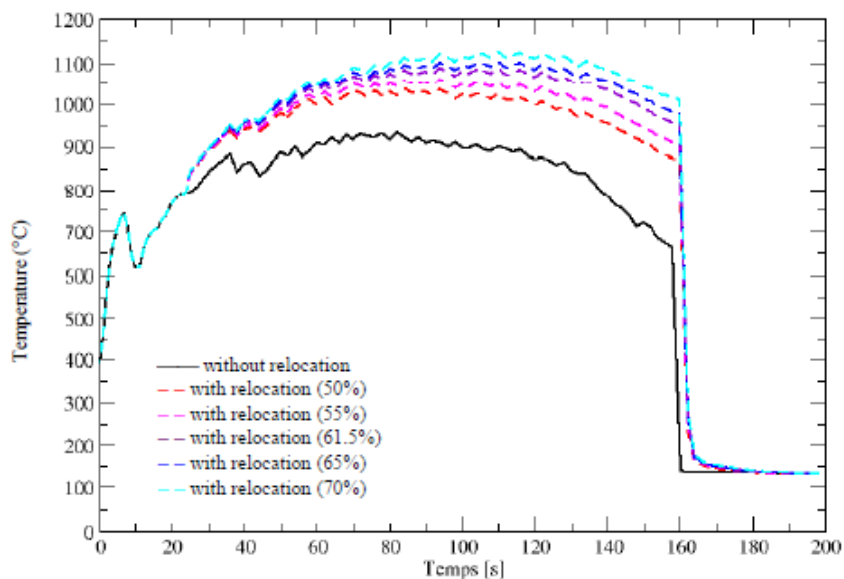


Figure 7.3-2: Impact of axial fuel relocation on cladding temperature at the rupture node of hot rod versus time with filling ratios from 50 to 70% (LB LOCA with irradiated UO₂ fuel) [7.2-30]

6. NB: By considering a porous media to represent the fuel fragments bed conductivity, the actual gap conductance between the fuel fragments and the inner side of the cladding is not properly modeled. Therefore, the calculated impact of fuel relocation on PCT might be slightly overestimated.

The impact of relocated fuel filling ratio is strong and depicted on Figure 7.3-2. The impact of a filling ratio of 70% (~200°C) is twice the one of a filling ratio of 50% (~100°C).

7.3.1.2 FRAPTRAN-1.4/SCK (SCK•CEN)

SCK•CEN performed a preliminary analysis of the clad ballooning and fuel relocation phenomena in Halden IFA-650.4 test, by means of the FRAPTRAN code [7.2-26]. The model makes use of FRAPTRAN as a standalone code and was validated on the IFA-650.2 test. The methodology is then applied to the IFA-650.4 test, where extensive fuel relocation (and ejection) was observed.

A parametric study is performed here, with a varying fuel filling ratio, in order to promote different power levels in the balloon. A thorough analysis is then performed of the evolution with time of the main rod parameters during the LOCA transient; they are compared to the measurements performed at Halden.

In particular, the evolution of the PCT and of the temperature at the upper thermocouple position during the transient for the IFA-650.4 case is presented in Figure 7.3-3, as a function of the assumed fuel filling ratio. The Halden thermocouple data are superimposed. Although the burst time is under-estimated, the approach provides a good agreement with the experimental observations.

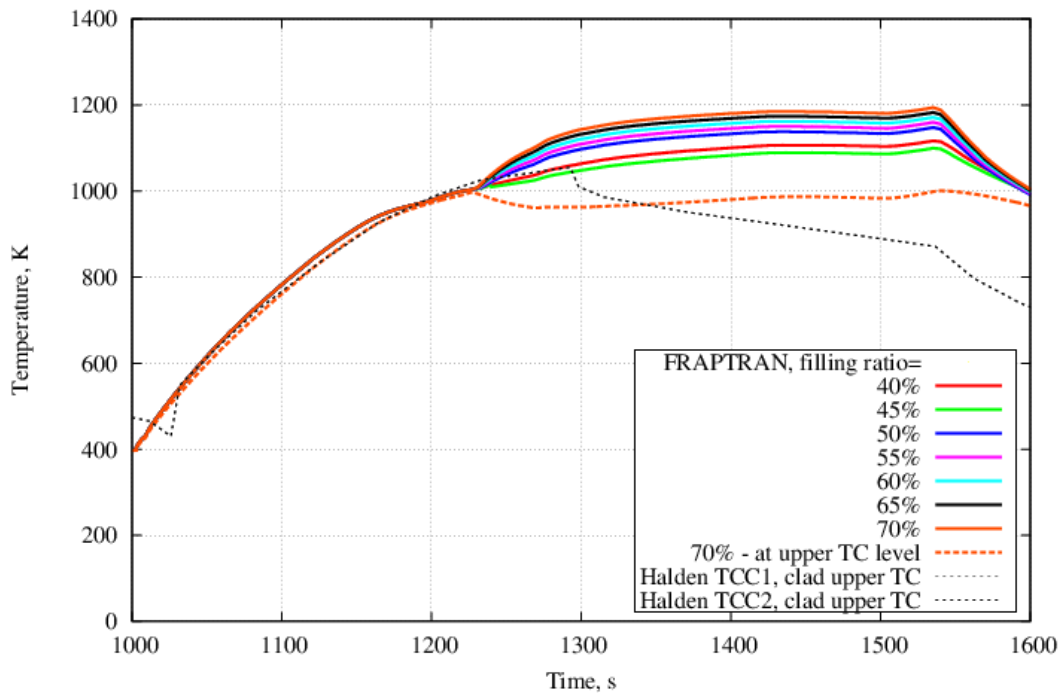


Figure 7.3-3: Evolution of PCT and of the temperature at node at upper thermocouple position during the transient for the IFA-650.4 case [7.2-26]

Figure 7.3-3 indicates that in the case of single rod tests, relocation often leads to higher temperatures than in the case of a non-deformed rod. If one looks at the heat balance at steady-state at the cladding wall, an increase in the heat exchange area is compensated by an increase of power.

Based on these results, it is recommended to consider the axial development of the balloon as a possibility that should not be disregarded in slow ramps at high burnup and/or in bundle configuration.

7.3.1.3 TRACE/FALCON (PSI)

Scoping analysis of FFRD related phenomena at PSI, so far, has been basically dealing with simulation of Halden LOCA tests. The core-wide analysis capability with coupled thermo-hydraulic (e.g. TRACE) and fuel-behavior (e.g. FALCON) codes is not available yet.

As far as Halden LOCA modelling at PSI is concerned, extensive calculations were started at the very early stage of experimental facility design and test planning. That analysis was largely based on loosely coupled TRACE and FALCON codes. The details were described e.g. in [7.2-44]. Furthermore, such a coupled TRACE-FALCON calculation was utilized by PSI within the Code Benchmark activity on Halden IFA-650 LOCA Tests [7.3-3].

Besides, a stand-alone TRACE model of the Halden LOCA Test Facility was applied to modelling selected Halden LOCA tests [7.3-4], which were found useful for TRACE code V&V.

The in-house code, FRELAX, was developed for interpretation of the Halden LOCA tests showing extensive fuel relocation and dispersal. This code is closely coupled to the FALCON fuel behaviour code.

First, the code incorporated a straightforward thermal-hydraulic analysis, addressing solely the specific conditions of the Halden LOCA experimental facility, and the phenomenon of axial fuel relocation and hot-spot effect during and after the ballooning [7.2-27]. This model is based on axial fuel mass conservation and radiation heat transfers.

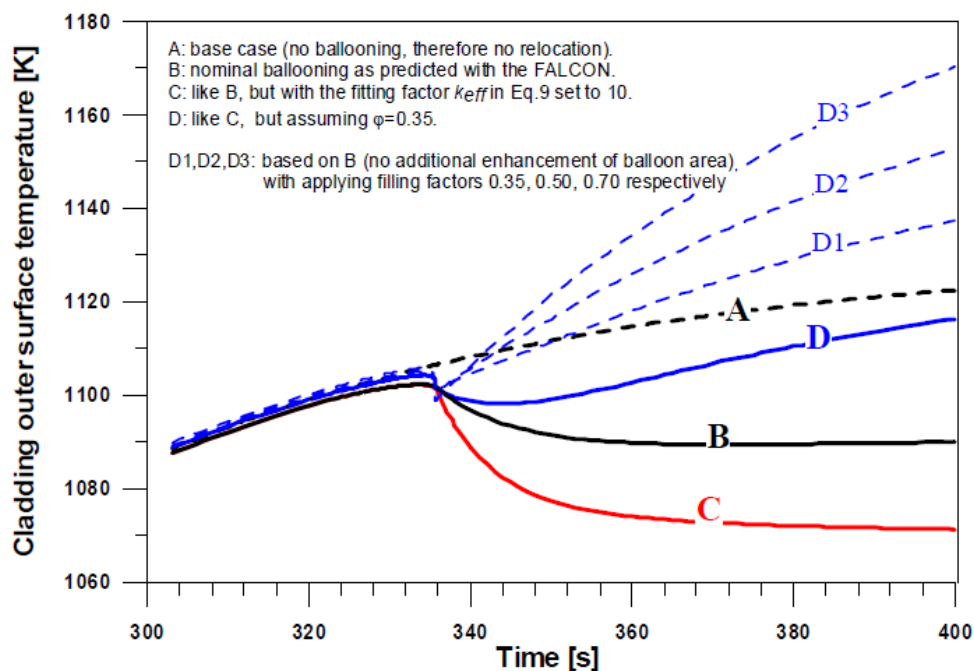


Figure 7.3-4: Case sensitivity study on effect of cladding balloon area and fuel relocation on PCT at the balloon position from [7.2-27].

The balloon is assumed to be able to accommodate the relocated fuel. Parametric calculations on key relocation factors as the relocation length, balloon filling ratio and local enhancement of the heat exchange surface area due to cladding ballooning were performed and are illustrated on Figure 7.3-4. Different sensitivities were tested:

- Scenario A: base case with no ballooning so no fuel axial relocation.

- Scenario B: FALCON predicted ballooning with no fuel relocation (impact of the increase of the heat exchange surface area only).
- Scenario C: as scenario B but with an increased balloon surface area.
- Scenario D: as scenario C with axial fuel relocation and a filling ratio of 0.35.
- Scenarios D1, D2 and D3: as scenario B with fuel axial relocation and filling ratios of 0.35, 0.5 and 0.7 respectively.

The combined effects of LHGR modification due to fuel axial relocation and the increase of heat transfer surface area due to cladding ballooning lead to PCT increases up to about 100°C.

Second, code extension was implemented to simulate the axial gas flow during the ballooning and after the cladding burst [7.3-5]. The coupled FALCON-FRELAX has been successfully applied for planning and interpretation of the test series using the BWR high-burnup fuels from KKL [7.3-6].

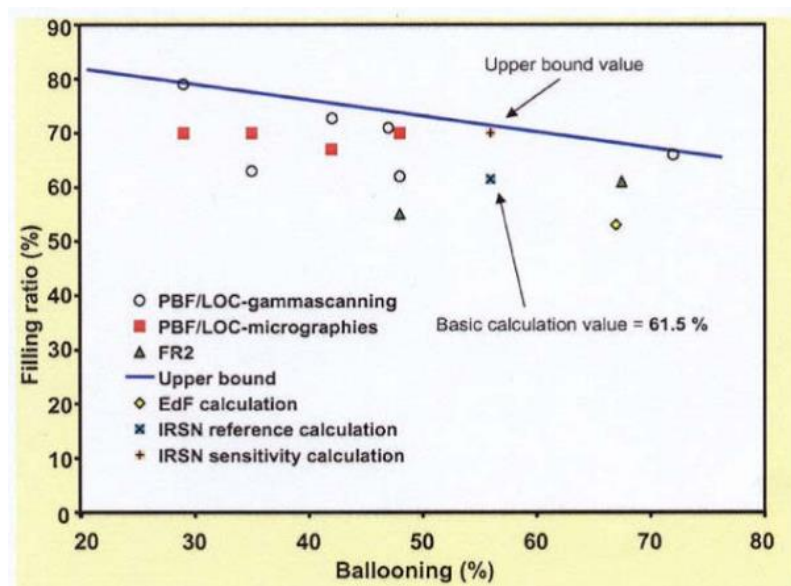
Core-wide simulation of the macroscopic consequences of FFRD is considered as a possible follow-up of the PhD project on Modelling FFRD during the LOCA, currently conducted at PSI.

7.3.1.4 FRAP-T6 APK (IBERDROLA)

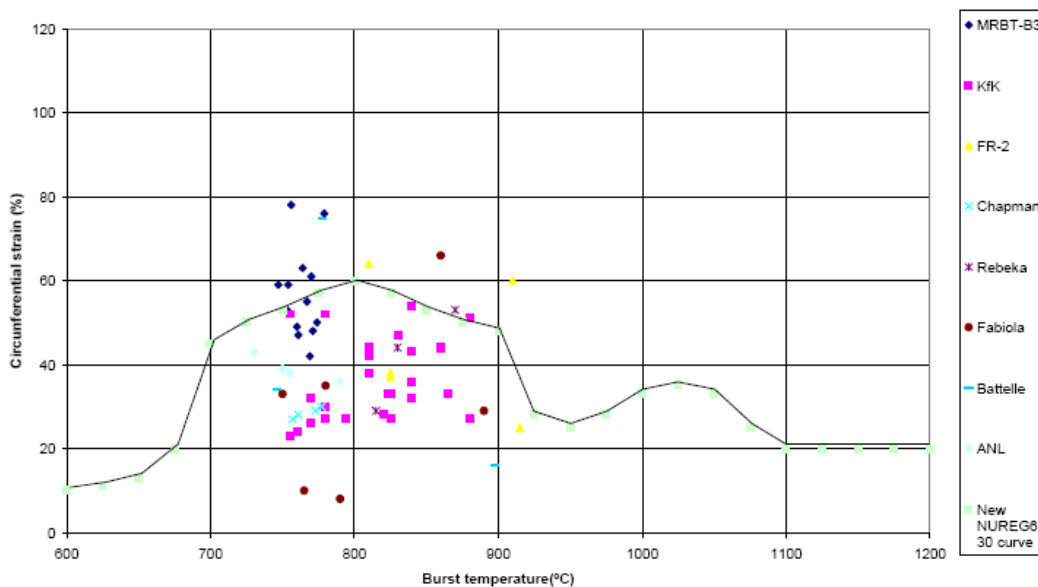
In 2009, IBERDROLA presented an analysis of fuel relocation based on modelling the IFA-650.4 and IFA-650.7 tests with their modified version of FRAP-T6/APK [7.3-7]. The modified code version of FRAP-T6/APK included:

- A filling ratio model based on balloon size (from Grandjean and Hache [7.3-8]) and shown in Figure 7.3-5a);
- Clad-to-fluid heat transfer area increase in ballooned region, whereby a new heat transfer coefficient was calculated considering the increased cladding surface in ballooned region, which resulted in a better cooling of the ballooned region;
- Local LHGR increase in the ballooned region;
- A best estimate hoop strain versus rupture temperature curve, which was implemented based on a selection of the NUREG-0630 experimental data [7.2-11], as shown in Figure 7.3-5b).

The authors studied the influence of cladding strain and balloon filling ratio for fuel relocation. Their base case simulations were performed without considering LHGR increase and heat transfer area increase models in the ballooned region, and by using the NUREG-0630 deformation curves.



a)



b)

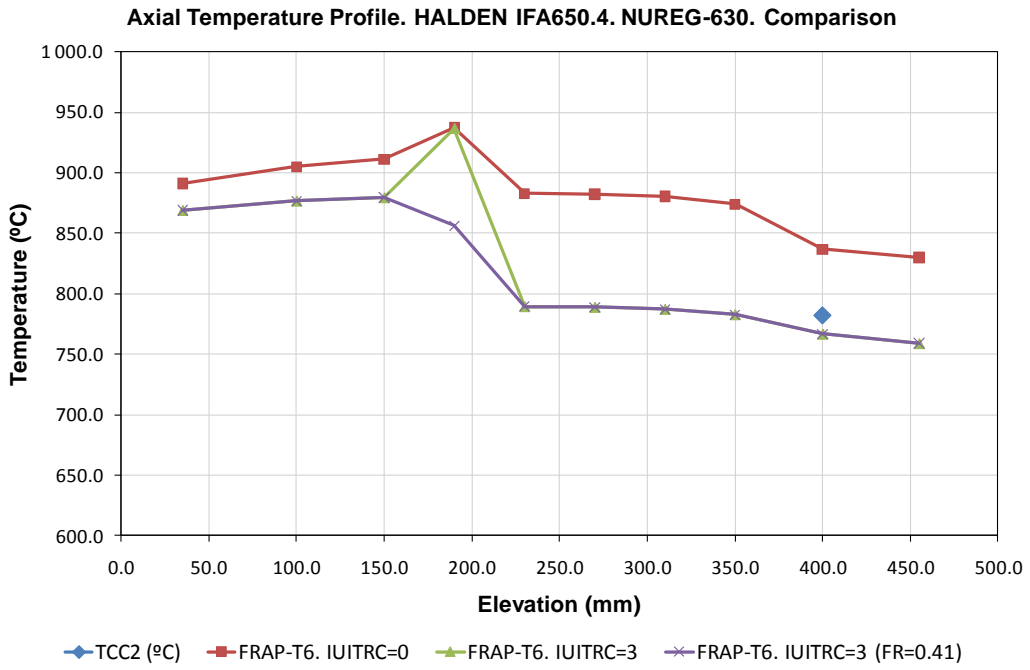
Figure 7.3-5: a) Balloon filling ratio by relocated fragments [7.3-8], b) Circumferential strain for low ramp tests excluding low azimuthal temperature gradient tests: Best Estimate Curve (BED) [7.3-7]

For IFA-650.4, Cathcart-Pawel oxidation was used in the base case. In subsequent cases, increase heat transfer and increased LHGR models were turned on. The filling ratio model in Figure 7.3-5a) was used in the second case, and the experimentally measured filling ratio of 41% was used in the third case. The results of these three calculations are shown in Figure 7.3-6b).

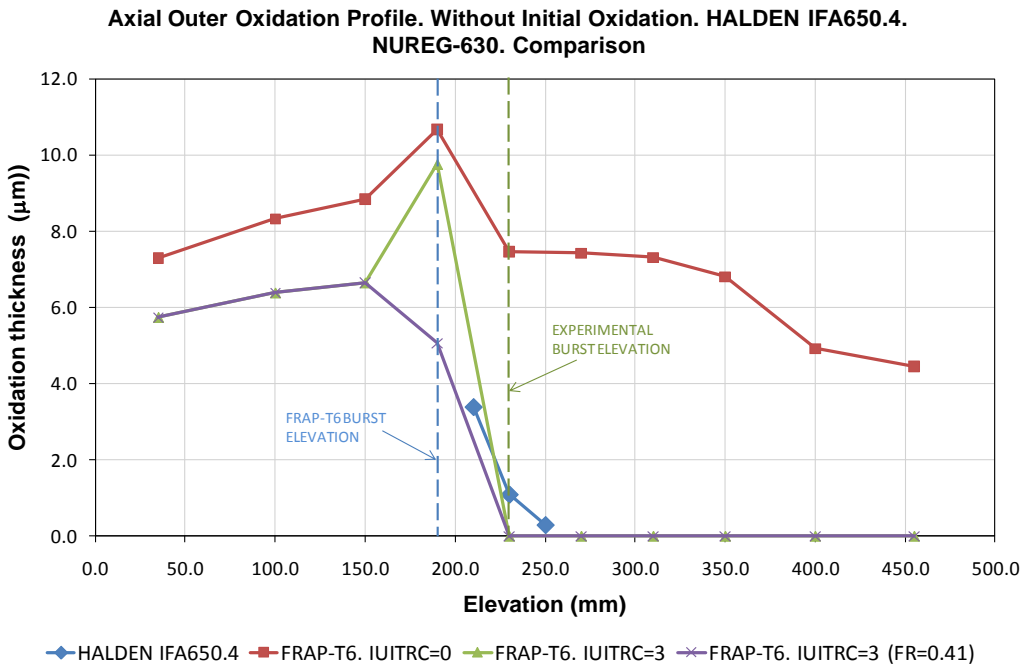
An important temperature decrease was observed at the burst elevation when the models for increased heat transfer area and LHGR at the balloon region were applied, particularly when the filling ratio experimental value of 41% was chosen instead of the bounding model. Applying the additional models and the experimental filling ratio resulted in much better agreement with Halden measurements.

For IFA-650.7, Baker-Just oxidation was used in the base case. In subsequent cases, increase heat transfer and increased LHGR models were turned on. Cathcart-Pawel oxidation was used in the second

case along with the bounding filling ratio model. The third case was the same as the second, except that the best-estimate deformation curve from Figure 7.3-5b) was used instead of the NUREG-0630 curve.



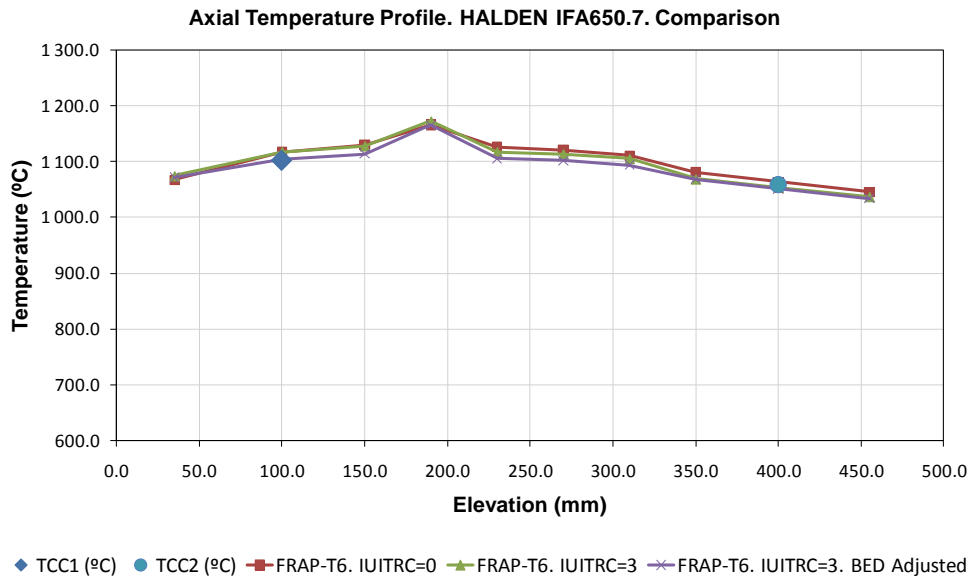
a)



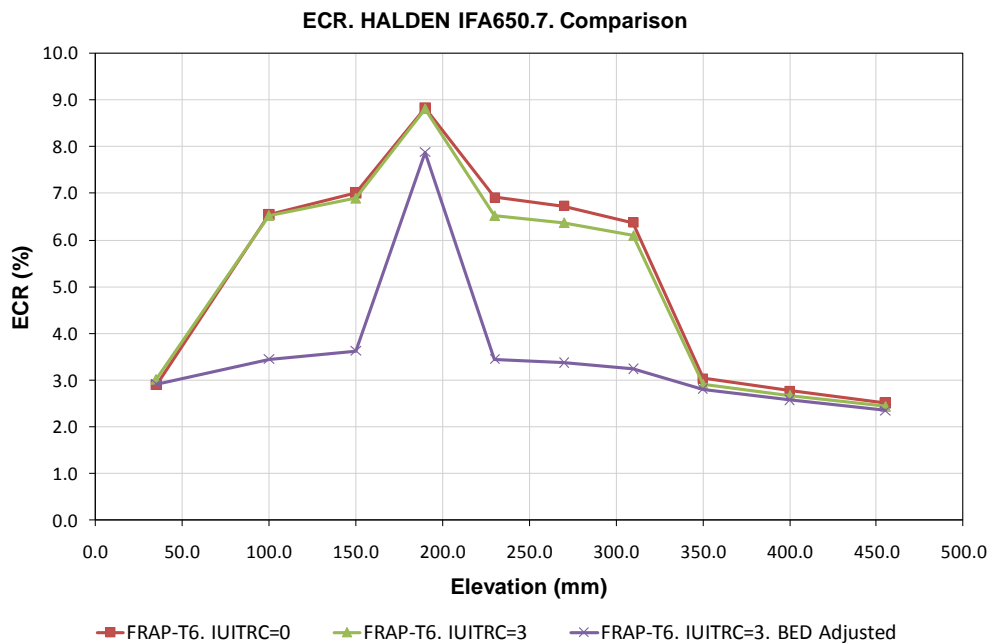
b)

Figure 7.3-6: a) Axial temperature profile and b) Outer oxidation axial profile comparisons for IFA-650.4, for the different modelling options chosen by IBERDROLA (blue diamond represent Halden data, the red line is the base case, the green line is the second case with the filling ratio model from Figure 7.3-5a), and the purple line is the third case with a filling ratio of 41% based on Halden measurements) [7.3-7]

The results of these three calculations are shown in Figure 7.3-7. The temperatures calculated in all three cases were very similar, but the ECR calculated for the third case using the best-estimate deformation model was significantly smaller than for the other two cases.



a)



b)

Figure 7.3-7: Axial temperature profile and b) ECR axial profile comparisons for IFA-650.7, for the different modelling options chosen by IBERDROLA [7.3-7]

IBERDROLA concluded that for IFA650.4, the LHGR increase due to fuel relocation was balanced by the effect of heat transfer area increase in the ballooned region, such that the fuel relocation impact on ECR and PCT was slightly beneficial or negligible.

The filling ratio model based on Reference [7.3-8] seemed to be over conservative since the better results for test IFA-650.4 were obtained with the experimental value of 41%, which was about 20% lower than the predicted upper bound value.

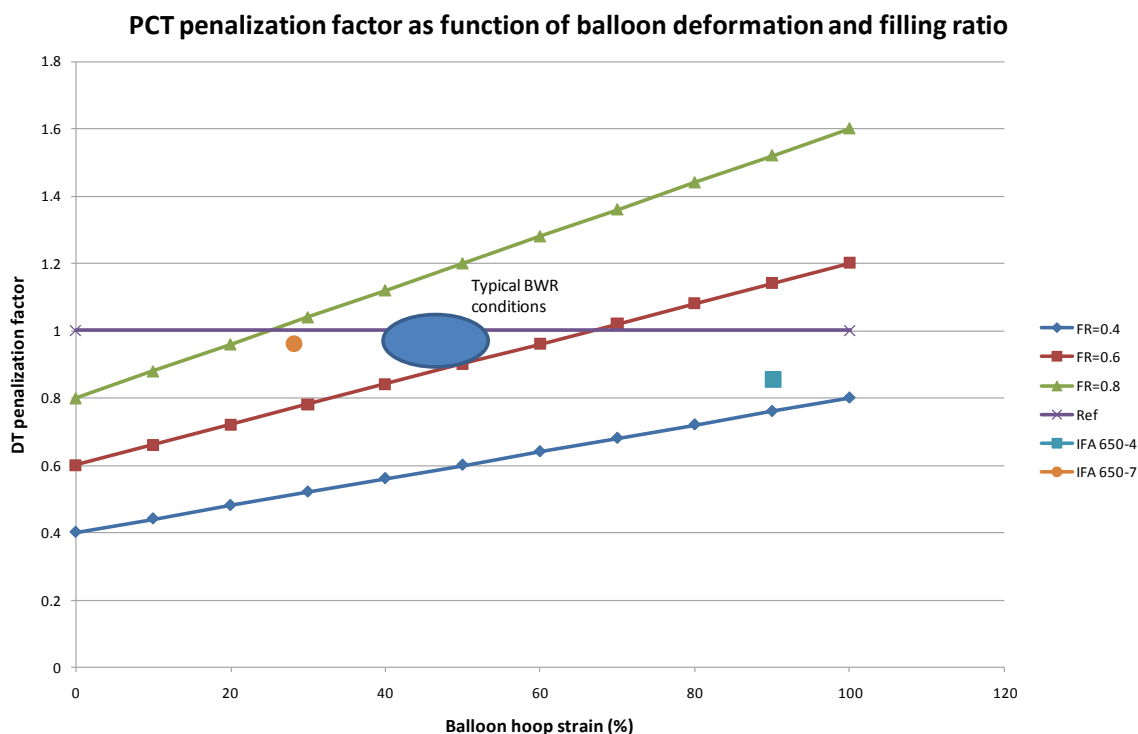


Figure 7.3-8: PCT Penalisation factor as function of balloon and filling ratio [7.3-7]

Figure 7.3-8 shows a comparison of IFA tests results in terms of PCT penalisation (PCT reached with fuel relocation and heat transfer area increase models over PCT reached without this models) as a function of balloon deformation and filling ratio, as calculated by IBERDROLA. The point corresponding to IFA-650.7 test is the FRAP-T6 calculated point. This figure shows that the PCT penalisation for typical BWR conditions was negligible.

7.3.1.5 FRAPTRAN-1.5 (Quantum Technologies/SSM)

Quantum Technologies AB has developed a computational model for axial relocation of fuel fragments during LOCA and its effects on the fuel rod heat load and failure processes, [7.3-11]. The model has been introduced in SSM's version of the FRAPTRAN-1.5 computer programme and validated against the IFA-650.4 test in Halden. This research was funded by the Swedish Radiation Safety Authority (SSM) as part of the IAEA Coordinated Research Project FUMAC–Fuel Modelling in Accident Conditions.

The model calculates the axial fuel relocation on the basis of the calculated cladding distension along the fuel rod and estimates for the filling ratio of crumbled fuel in ballooned parts of the rod. The latter estimates are based on the assumption that the crumbled fuel in the balloon consists of two different size classes of fragments: The first class includes mm-sized fragments, created by thermal stresses in the fuel during normal operation, and the second class comprises fine (<0.2 mm) fragments, created during LOCA by overheating HBU. The mass fraction of small fragments is calculated from the distributions of burnup and temperature in the fuel.

For each time step taken by FRAPTRAN, the relocation model provides output in terms of the change in fuel mass distribution along the fuel rod. This is used as input to the thermal calculations, so that the

radial heat transfer equation is modified in those parts of the fuel rod where fuel relocation occurs. Hence, the relocation model is implemented as an integral part of FRAPTRAN-1.5, and thermal feedback effects from the redistribution of fuel mass, stored heat and power are considered as the relocation progresses.

Simulations of the Halden IFA-650.4 LOCA test with the model suggest that thermal feedback effects from fuel relocation are strong enough to significantly affect the dynamics of cladding ballooning and rupture, even though the calculated duration of these processes is no more than 7–8 s.

Moreover, the axial relocation has a strong effect on the calculated PCT and oxidation after cladding rupture for the considered test; see Figure 7.3-9.

The work also suggests that “pulverisation” of HBU is important to axial fuel relocation during LOCA as it has the potential to increase the filling ratio of crumbled fuel. The pulverisation thereby eases axial movement of the fuel pellet column and also raises the local heat load in regions where fuel fragments accumulate.

The calculated results suggest that fuel with about 30 wt% small fragments created by pulverisation would have the highest filling ratio after crumbling; see Figure 7.3-10. From the empirical threshold for fuel pulverisation in [7.3-11], this weight fraction of small fragments is expected when overheating LWR fuel with a pellet average burnup of around 72 MWd/kgU.

These results underline the importance of axial fuel relocation in computational predictions of PCT and ECR as part of licensing analyses.

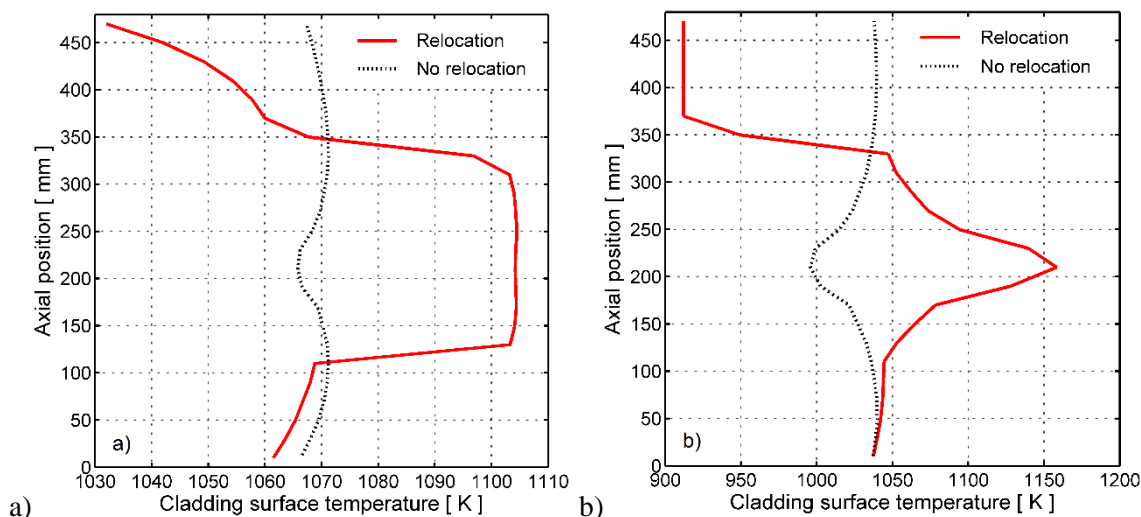


Figure 7.3-9: Calculated cladding outer surface temperature vs. axial position for the IFA 650.4 test at time of cladding rupture (a) and at time $t = 500$ s (b)

Calculations were made with and without consideration of fuel relocation. Fuel dispersal was not considered in the calculations.

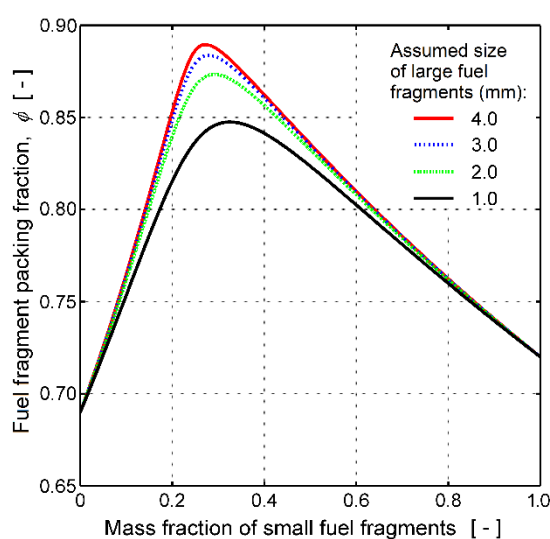


Figure 7.3-10: Estimated filling ratio of crumbled fuel versus relative amount of small fragments from pulverised HBU

7.3.2 Dispersal

7.3.2.1 Fuel dispersal analyses with TRACE-FRAPCON/FRAPTRAN (U.S.NRC)

In 2013 and 2014, the U.S.NRC presented results of detailed core-wide fuel rod rupture calculations performed by sequentially coupling the fuel performance codes FRAPCON and FRAPTRAN with the systems thermal-hydraulic code TRACE [7.2-20], [7.2-35]. For each reactor core modelled, each average fuel assembly was modelled in FRAPCON based on realistic power histories derived from available core burnup and radial power profiles over the course of a cycle. The power histories were generated to maximise the core-average discharge burnup while not exceeding U.S. burnup limits.

The FRAPCON output was used to initialise burnup dependent variables in both TRACE and FRAPTRAN. The TRACE transient results were then used as boundary conditions for FRAPTRAN to obtain the detailed transient thermal-mechanical response of the fuel rod.

Five different combinations of reactor type and transient were analysed:

- Westinghouse 4-loop PWR large-break LOCA
- Combustion Engineering PWR large-break and small-break LOCA, and
- General Electric BWR/4 large-break and small-break LOCA.

It was assumed that the emergency core cooling systems functioned as designed, which is the best-case scenario, and no additional conservatism was added, so as to obtain a ‘nominal’ plant response to the LOCA transients. Only the Westinghouse 4-loop PWR LBLOCA produced cladding temperatures high enough to lead to fuel rod failures as a result of cladding ballooning and rupture.

The transients were simulated at beginning, middle, and end of cycle (BOC, MOC, and EOC respectively), and for the Westinghouse 4-loop PWR LBLOCA, the EOC calculation resulted in more ruptures than the BOC and MOC calculations.

Predictions of fuel dispersal for the Westinghouse 4-loop PWR LBLOCA were obtained by comparing the local conditions near the rupture node for each average fuel rod representing an assembly in the core. It was assumed that the conditions for fuel dispersal were as follows:

- Fuel rod rupture must have occurred.
- All fuel particles with a particle size of 1mm and below were assumed to be fine fuel particles able to escape from the rod for the purpose of this study.
- The fuel particle size model used was the one described in Section 7.2.2.1 above, with linear transitions between coarse and fine fuel particle size distributions, as a function of local nodal burnup.
- The axial fuel mobility cladding strain threshold was assumed to be 5% permanent cladding strain.

The resulting dispersed fuel masses varied considerably depending on the burnup thresholds chosen for the particle size distribution and on the time of cycle: from 9.4 kgUO₂ to 207.3 kgUO₂. BOC and MOC resulted in much smaller quantities of dispersed fuel than EOC, mainly because at EOC, a number of rods in the core had exceeded the burnup for fine fragmentation to begin occurring, as shown in Figure 7.3-11. Even the largest predicted amount of fuel dispersal represents less than 1% of the mass of fuel in the core.

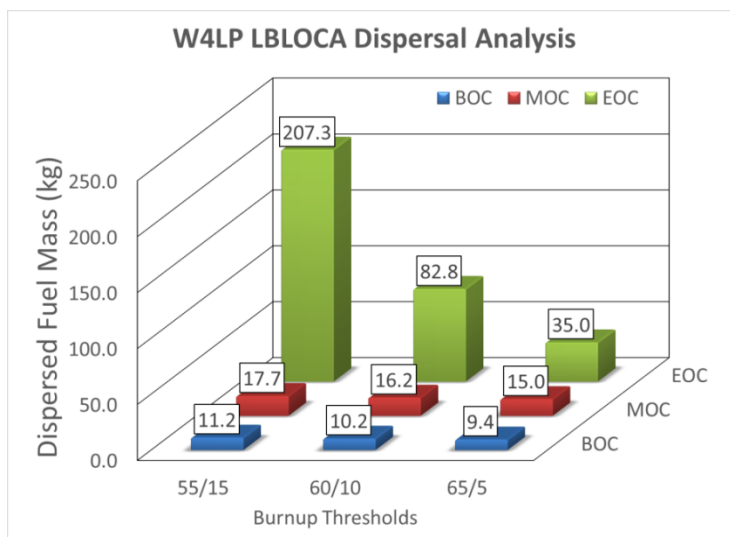


Figure 7.3-11: Dispersed fuel mass analyses for the Westinghouse-4-Loop (W4LP) Large-Break LOCA scenario as a function of time of cycle and chosen fine fragmentation burnup threshold [7.2-20].

In all cases, the strain threshold chosen for axial fuel mobility was 5% cladding hoop strain.

Annotation to Figure 7.3-11:

(1) in the burnup threshold labels, the first number indicates the burnup at which the fine fragmentation begins to occur, and the second number indicates the length of the linear transition from coarse to fine fragmentation, in MWd/kgU

(2) the dispersed fuel masses shown here are a factor of 3 smaller than those reported in [7.2-20], due to a correction that was made in the analysis after the TopFuel 2014 conference (the masses reported in [7.2-20] are a factor of 3 too large).

7.3.2.2 Fuel dispersal analyses with TRAC-BF1/APK and FRAP-T6/APK (IBERDROLA)

In order to proactively investigate the consequences of fuel dispersal during LOCA being proposed by U.S.NRC as a Generic Issue in 2012, IBERDROLA performed some core-wide fuel rod rupture calculations for a BWR/6 reactor [7.2-34].

In the IBERDROLA analysis, conservative LOCA thermal-hydraulic conditions (limiting thermal and burnup conditions) were used to analyse the fuel response at different burnups. In order to determine the LHGR threshold at which fuel failures are expected, the following procedure was used:

- First, the fuel rod initial conditions were determined for a conservative operating power history for every rod burnup point.
- Then, a fuel rod analysis was performed for a range of LHGR values (typically from zero to the maximum LHGR allowed (the Thermal Mechanical Operating Limit TMOL), or until failure was obtained).
- Finally, a determination of the minimum LHGR for fuel rod rupture was obtained at each burnup point, such that a curve of failure LHGR versus burnup was created.

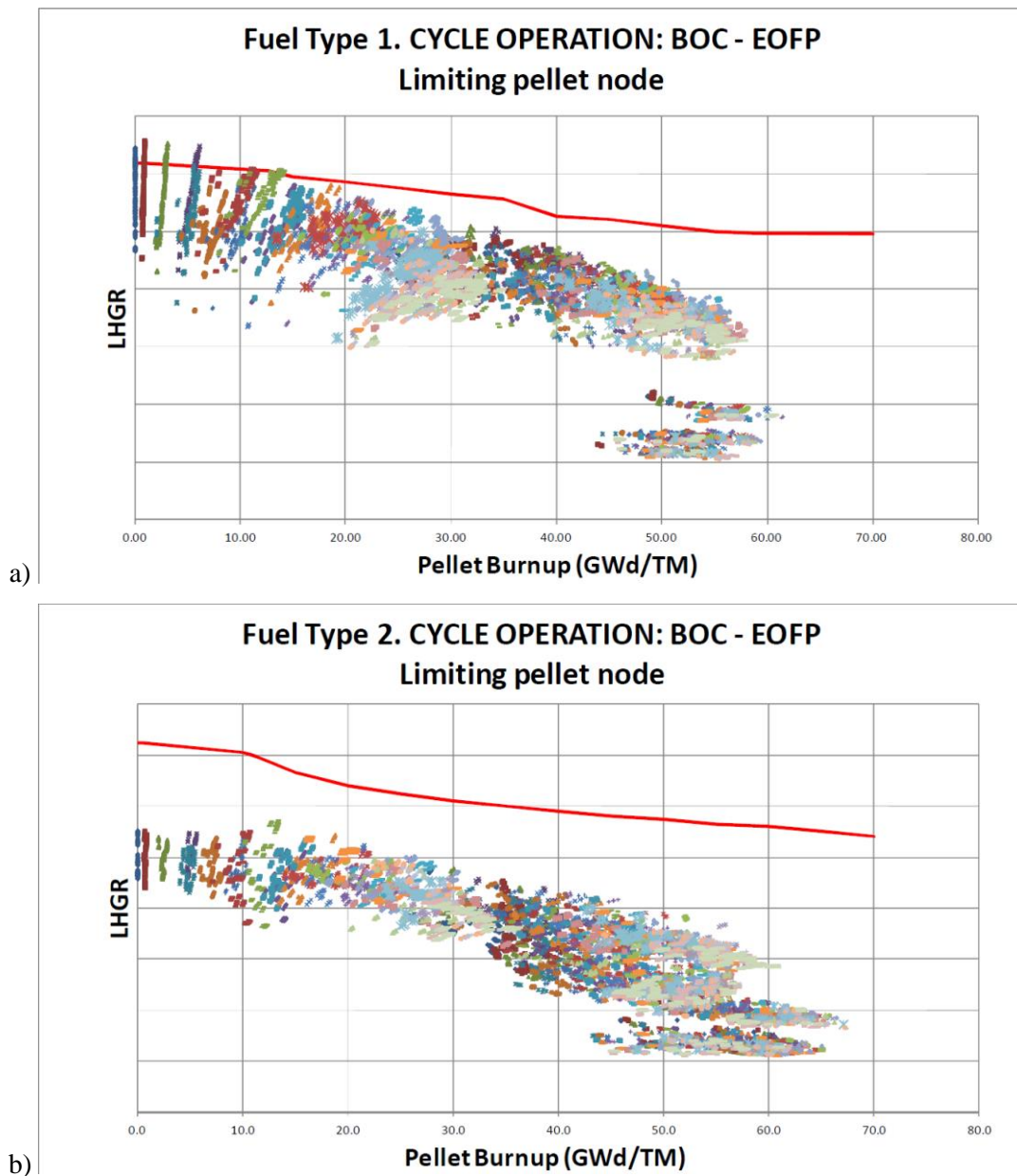


Figure 7.3-12: Limiting pellet node for fuel types a) 1 and b) 2 in the Spanish BWR/6 modelled by IBERDROLA, for each fuel rod, as a function of burnup, over the course of a whole cycle [7.2-34]

SIMULATE-3 was used with the IBERDROLA code FCOLIPBD (Full Core Limiting Pellet Burnup Distribution) to determine which fuel rods are expected to failure. For the particular BWR/6 modelled, which had two fuel types, only fuel type 1 was predicted to have fuel rod ruptures during the large-break LOCA, as shown in Figure 7.3-12, and the highest burnup where fuel rod failures were expected was 15 MWd/kgU.

The amount of fuel dispersal was calculated using the IBERDROLA model described in Section 7.2.2.3: for each failed fuel rod, the amount of dispersed fuel is assumed to be strictly a function of burnup, and is roughly about 1 pellet (~8 g) per rupture fuel rod up to 55 MWd/kgU. The maximum amount of fuel dispersal was predicted at a cycle step exposure of 2 MWd/kgU, and was equal to 1.78 kg.

The red line in Figure 7.3-12 indicates the fuel rod failure threshold. When LHGR of a fuel rod during normal operation exceeds the red line, this fuel rod will burst during LOCA transient.

IBERDROLA then used the Lipinski model to determine what mass of fuel could be tolerated from a coolability standpoint. It was determined that for an average particle size of 3 mm corresponding to the expected size of the fragments for low burnup fuel below 55 MWd/kgU, 5 700 kg of dispersed fuel (corresponding to a UO₂ particle bed height of 0.4 m) would be required to prevent coolability. This implied that over 700 000 rods would need to fail to exceed the coolability limit, implying all the rods in the core could rupture and disperse fuel without challenging coolability.

In addition, IBERDROLA performed bounding criticality studies using the KENO code and showed that for particle sizes of 3 mm, 840 kg of dispersed fuel was needed to achieve criticality in the UO₂ bed. As the burnup increases and the particle size decreases, the number of rods needed to challenge coolability and criticality both decreases, as shown in Figure 7.3-13.

However, in IBERDROLA’s calculations, it is only above burnups of 55 MWd/kgU cycle exposures that potential safety concerns could arise due to coolability or criticality. This would require very large numbers of HBU rods to failure, which is not predicted to occur in their model.

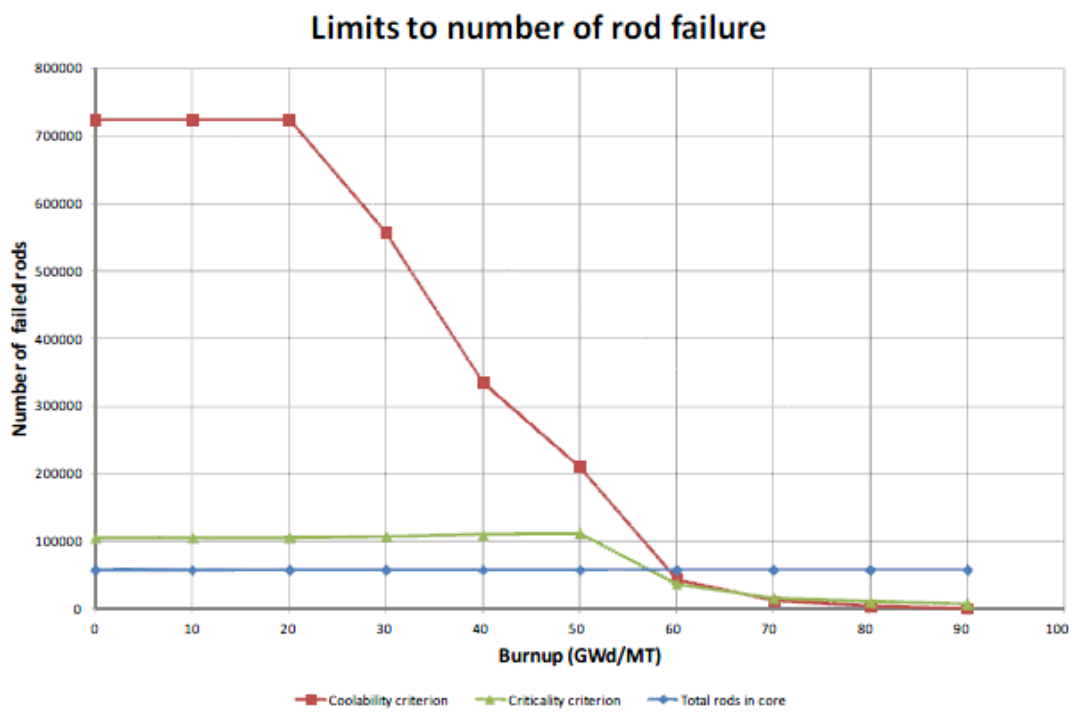


Figure 7.3-13: Number of failed rods required to challenge coolability and criticality limits, as a function of burnup [7.2-34]

7.3.2.3 LOCA analyses with the SAFER/CORCL methodology (General Electric)

This 2013 GE studied cases where LOCA analysis determines the thermal limits set for design and operation [7.3-9]. In this current analysis, a representative census of failures predicted by conservative LOCA calculations was contrasted against typical cycle bundle power distributions. The conservative calculations were carried out in a manner consistent with GE's approved licensing calculations using the SAFER/CORCL methodology [7.3-10].

The results of the GE study are summarised in Figure 7.3-14. The Analysis-Of-Record (AOR - i.e. the U.S.NRC - approved licensing analysis for a given reactor) results presented in the table correspond to the SAFER/CORCL evaluation results that constitute the basis for the licensed operation.

In the SAFER/CORCL fuel rod stress and failures models, the cladding hoop stress is calculated based on the pressure difference between the fuel rod internal gas pressure and the external coolant pressure during the transient. The model estimates the incidence of rupture based on applicable data including those data reported in NUREG-0630 [7.2-11].

From the AOR, the calculated Maximum Average Planar LHGR (MAPLHGR) values were gradually lowered in steps of 5%. For each combination of bundle exposure point and MAPRAT (MAPLHGR Ratio – the ratio of the planar power to the MAPLHGR limit), PCT results and the number of predicted failures in the hot bundle were tabulated.

According to the authors of the study, during the normal operation, the power levels of the actual bundles are lower than the assumed power level in the LOCA analysis, thus analysing the results for lower MAPLHGR values (~75%), provided valuable information regarding the extent of LOCA consequences on realistic core loading and operating patterns. In this analysis, as the exposure increased, the reduction in LHGR had more influence than the increase in fuel rod pressure and, therefore, fewer fuel rod failures were expected at very high exposures.

Nodal Burnup (MWd/kgU)	0	1.10	5.51	11.02	16.53	22.05	27.56	38.58	49.60	60.63	71.65	82.67
AOR PCT (°C)	1198	1197	1195	1197	1194	1188	1189	1170	1130	1092	1016	918
# of burst rods	92	92	92	92	92	92	92	92	64	92	56	56
95% PCT (°C)	1114	1094	1120	1110	1108	1115	1100	1079	1057	1033	984	876
# of burst rods	92	64	56	56	56	56	56	56	56	56	56	8
90% PCT (°C)	1059	1047	1036	1033	1042	1038	1038	1023	1005	984	938	840
# of burst rods	56	56	56	56	56	56	56	56	56	56	56	2
85% PCT (°C)	984	984	979	979	993	976	985	966	958	941	887	792
# of burst rods	56	56	56	56	56	56	56	56	56	56	36	-
80% PCT (°C)	938	932	934	933	944	939	935	932	913	888	851	755
# of burst rods	42	42	42	28	43	28	28	28	18	8	8	-
75% PCT (°C)	899	897	892	897	891	883	881	882	856	837	799	680
# of burst rods	10	10	-	-	-	-	-	-	-	-	-	-
70% PCT (°C)	872	851	849	850	844	840	838	811	798	778	739	666
# of burst rods	-	-	-	-	-	-	-	-	-	-	-	-
65% PCT (°C)	808	797	798	790	794	789	770	765	747	732	687	630
# of burst rods	-	-	-	-	-	-	-	-	-	-	-	-
60% PCT (°C)	759	751	746	729	725	723	725	719	683	686	657	602
# of burst rods	-	-	-	-	-	-	-	-	-	-	-	-

Notes:

- Red shading indicates the Analysis of Record (AOR) values and determines the thermal limit posed by the LOCA analysis.
- Blue shading represents the approximate LHGR values set by the thermal-mechanical operating limit (TMOL). Considering pin exposure and local peaking factors, the TMOL would not allow the bundle to operate at higher linear heat rates than the shaded cell for that nodal exposure.
- Yellow shading represents the typical burnup-LHGR combinations that can be found throughout a cycle.
- The thick line indicates the power levels at which no perforations are predicted using the conservative (Appendix K) SAFER-CORCL evaluation methodology.

Figure 7.3-14: PCT and number of burst rods in the hot assembly for different MAPLHGR Ratios [7.3-9]

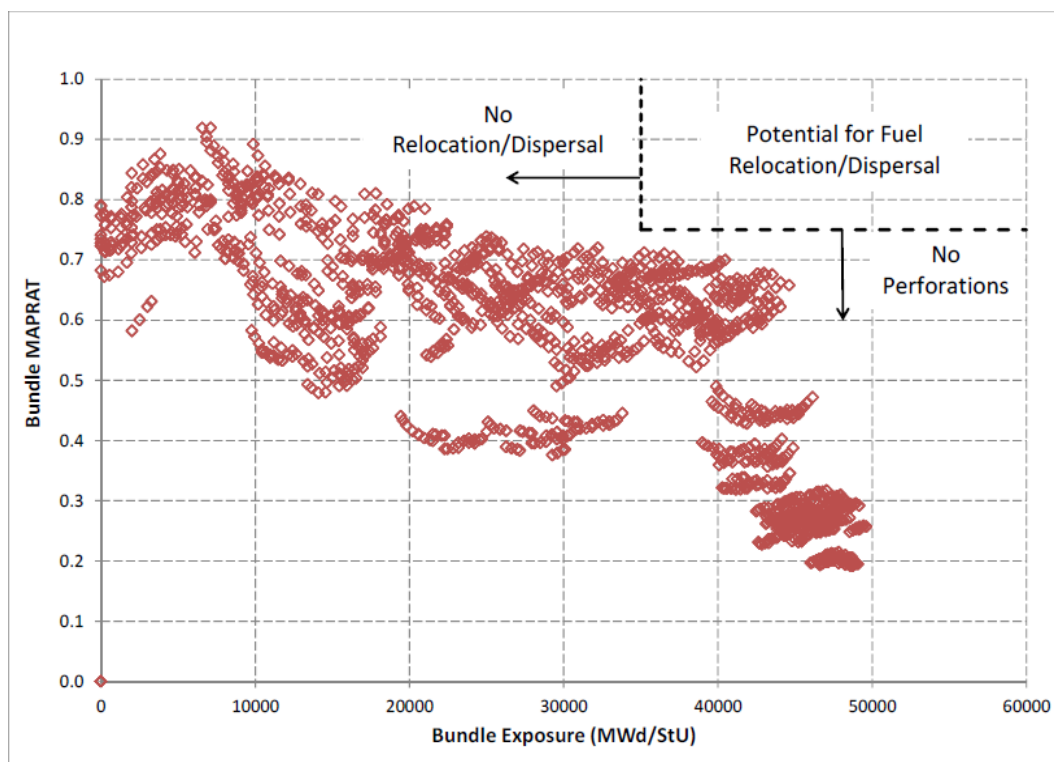


Figure 7.3-15: Bundle MAPRAT distributions for a typical cycle in a U.S.BWR [7.3-9]

This multi-dimensional comparison was presented by casting the results in scatter plots of bundle MAPRAT against bundle exposure. Figure 7.3-15 shows the distribution of bundle MAPRATs throughout the cycle. In this Figure 7.3-15 exposure points spanning from beginning of cycle (BOC) to end of cycle (EOC) for all the bundles in the core are pictured.

In Figure 7.3-15, the horizontal line indicates the boundary below which no ruptures were predicted to take place during LOCA. In the evaluation, the computations show that when MAPLHGR is lowered to 75% of the original analysis, there were no rods that burst at any bundle exposures, except very early in life.

The vertical line at 35 000 MWd/kgU bundle exposure approximately marked 45 MWd/kgU rod exposure. This approximation assumed a conservative pin exposure peaking factor at this burnup. 45 MWd/kgU was considered as a burnup value that does not show fuel relocation and/or dispersal due to fragmentation. At this burnup, the average particle size of the fragmented fuel was deemed too coarse to result in dispersal.

The GE study concluded that the conditions at which the HBU specimens were tested for fragmentation and dispersal purposes are beyond the conditions those rods can most likely experience during LOCA in a commercial BWR. This was attributed to the fact that thermal mechanical limits imposed on fuel and core loading and exposure plans prevent HBU from operating at elevated LHGR.

In addition, the study stated that any extension of the exposure limit accompanied by applicable thermal-mechanical limits did not represent any additional risk or safety concern for potential dispersal of fragmented fuel. Finally, the results indicated that the rods with fuel dispersal potential did not burst, and that the rod ruptures having exposures closer to the onset of significant fragmentation with medium to small particle size were quite limited.

7.4 Consideration of fuel cladding failures and FFRD in LOCA safety analyses in different countries

FFRD impacts safety analysis LOCA calculations on various points, in particular:

- fuel fragmentation and relocation impacts PCT, ECR and core coolability
- fuel dispersal impacts radioactive release.

This section is a brief summary of safety analysis practices in various OECD nuclear power countries concerning consideration of cladding failures during LOCA transients. The objective is to see if FFRD is of safety concern in the current safety analyses. Indeed, if safety calculations predict low ballooning and few cladding failures, then FFRD impact on safety criteria may be negligible.

This topic was treated extensively in 1999 by some European countries like Belgium, France, Germany, Netherlands, Spain, Switzerland and United-Kingdom [7.3-10]. A less detailed but updated description of current practices is given in the Appendix of this report, and is extended to most OECD countries.

7.5 Conclusions

A realistic evaluation of the impact of FFRD on the design basis LOCA safety analyses requires first appropriate modelling of the involved key physical phenomena. Unfortunately, the existing models are mostly empirical and conservative.

Some scoping studies have been performed recently, showing various degrees of impacts of the relocation and dispersal. The results depend strongly on the assumptions and the models that need to be validated.

Consideration of FFRD in the current licensing basis LOCA safety analyses are not required in most of the OECD countries, except for France where the relocation will be considered in coolability analyses in the new regulation. In a few countries, a limit on the failed rods rate is imposed for radiological assessment, which may also limit the impact of FFRD.

8. CONSEQUENCES OF RELOCATION AND DISPERSAL

8.1 Coolability

In a hypothetical loss of coolant accident (LOCA) fuel rod cladding may reach temperatures above 800°C depending on the effectiveness of the emergency core cooling system. This temperature excursion may hold for a period of about a few minutes depending also on the efficiency of the emergency core cooling system. Under these conditions the fuel rod cladding strains and even may burst.

Halden-tests of series IFA-650 and related Studsvik experiments have shown that fuel separates during the temperature excursion into fine fragments if such fuel is attributed to high burnup. The burnup level for such transition has been discussed in previous chapters which allow concluding the threshold certainly is above 55 MWd/kg. These fuel fragments relocate within the fuel rod cladding as far as the cladding has been locally strained above 7%. In case of a strained cladding with burst opening, these HBU fragments even disperse through the burst opening into the neighbouring coolant channel in variable quantities.

Subsequent chapters discuss the coolability of relocated fuel in a non-burst fuel rod cladding first and discusses the coolability of fuel fragments which have been dispersed into a coolant channel secondly.

8.1.1 Coolability of fragmented fuel relocated into a ballooned fuel rod region

If fuel fragments relocate within a closed but strained fuel rod cladding, this relocation is then associated with a redistribution of LHGR along the fuel rod cladding. Since this relocation is at the same time accompanied with a filling ratio of about 80 to 90%, such accumulation of fuel fragments in a ballooned fuel rod region increases the local LHGR, but due to porosity increase the power density increase is relatively small. According to a conservative estimation, it could reach a LHGR of less than doubled value compared to the initial value $LHGR_0$.

$$LHGR = LHGR_0(1 + \varepsilon)^2(FR)$$

$$\varepsilon: \text{strain } e. g. \quad 0.6 \quad - \quad 60\%$$

$$FR: \text{filling ratio } e. g. \quad 0.8 \quad - \quad 80\%$$

$$LHGR = LHGR_0 (1.6)^2 0.8 \cong LHGR_0 2$$

Fuel rods in a core with a burnup level above the fine fragmentation threshold are usually at a power level far below the maximum power level. If they are even below one-half of the maximum power level, the increase of LHGR due to fuel relocation would not go above the prevailing highest LHGR in the core. In this case the regulatory concept for LOCA transients by analysing the PCT for a single hot rod in a core (the hot rod is associated with low burnup level) remains valid.

In addition, a strained cladding constricts the surrounding coolant channel and thus causes an acceleration of the coolant. That is, the steam/droplet-entrainment within the restricted coolant channel is more effective primarily due to droplet breakup mechanisms [8.1-1] and thereby improving the heat transfer on the strained cladding surface. Extensive investigation in the 80 s of the KfK show [8.1-2], [8.1-3] that these cooling improvement reaches even up to an extreme cooling channel blockage of 90%. A blockage of 90% corresponds to a strained cladding of about $\epsilon=0.6$ (60%).

In sum, it can be expected for the non-ruptured but strained cladding that,

- straining cladding allows fuel relocation
- local power density might increase due to this relocation, but this increase is limited by a filling ratio of less than 80% in the ballooned cladding region
- heat transfer in constricted cooling channel improves much because of extra cooling mechanism like droplet breakup and increase of cladding surface
- level of power density in the presence of high burnup is much lower than in the rest of the reactor core.

However, the above do not account for contacts between deformed rods that induce two negative effects:

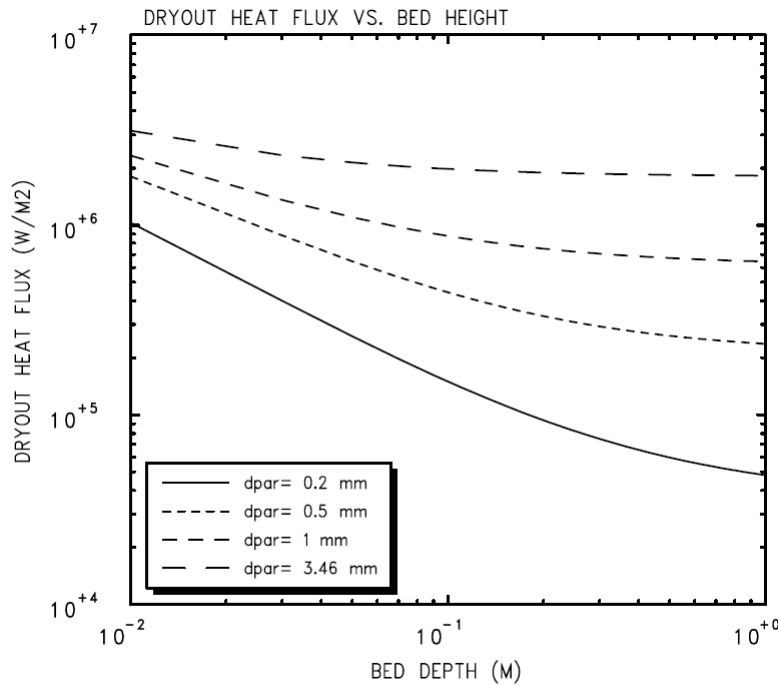
- a reduction of the surface for heat exchange between the clad and the fluid
- a diversion of the flow out of the considered channel because of the blockage formed.

Finally, the balance between positive and negative effects is not obvious and will depend on the models, assumptions and provisions used in the safety analysis.

8.1.2 Coolability of dispersed fuel aggregated on spacer grids

When considering the fuel relocation associated with burst opening of the cladding with subsequent fuel dispersal, the required evaluation is more complex. Here, the fuel enters the cooling channel, although it remains unclear exactly where a deposition of the fuel takes place in the cooling channel. In the worst case, the fuel will be dispersed from burst opening and then deposited on the next lower spacer grid.

In Reference [8.1-8] GRS presented an evaluation of the coolability of a debris bed. According to this presentation the evaluation of fuel particle cooling aggregated on a spacer grid requires that a) the porosity of the particle bed and b) the characteristic particle diameter and c) the bulk bed depth are known. Figure 8.1-1 shows the relationship between particle diameters, packed bed depth and dry-out heat flux for a constant porosity of 40%.



porosity=0.4, P= 1.2 bar, T= 50 C

Figure 8.1-1: Relationship between dry-out heat flux and particle diameters, particle bed depth with porosity of 40% (Lipinski-Model) [8.1-4]

The significant influence of porosity on the other hand can be seen from Figure 8.1-2. In both figures, the results of the 0-dimensional Lipinski model are respectively shown, which provides realistic boundary for the coolability of pebble beds.

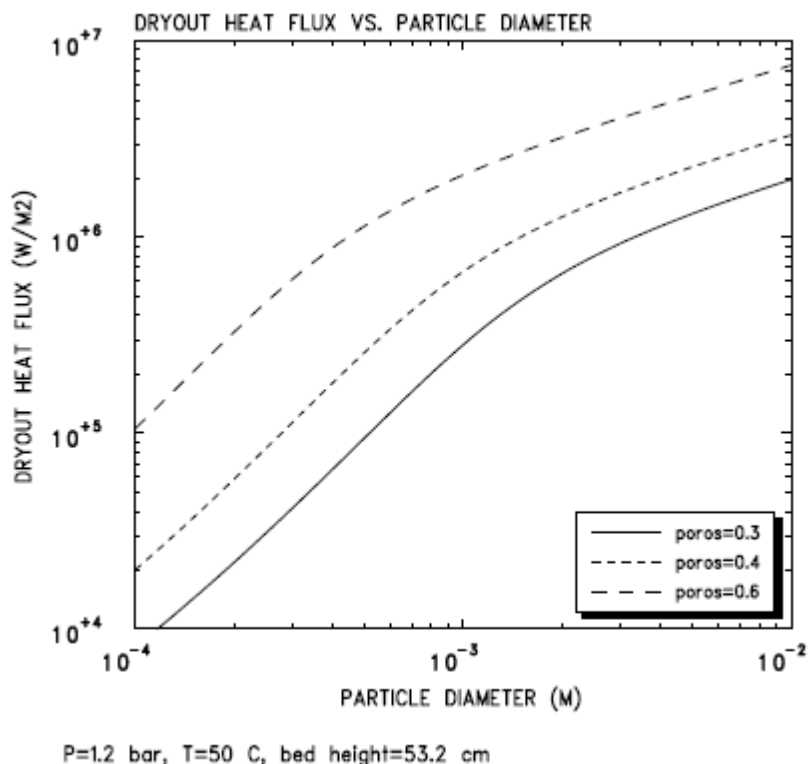


Figure 8.1-2: Dry-out heat flux depending on particle diameters and porosity for constant particle bed depth of 53.2 cm (Lipinski model) [8.1-4]

In a particle bed height of 10 cm and a characteristic particle diameter of 0.2 mm (this would roughly correspond to the expected values for HBU rods having fuel dispersed from the burst opening and aggregated on a spacer grid), the heat flux reaches a maximum of $\dot{q}''_{dryout} = 0.2 \text{ MW/m}^2$. Higher heat fluxes would lead to both dry-out and loss of coolability. Such dry-out within the particle bed would occur regardless the entire particle bed is submerged in coolant or not, because the low heat conduction within particle beds hinders the progress of quench fronts within the particle bed.

Nota bene: In this consideration, the heat flux is not related to a fuel rod surface but on the surface of the debris bed.

The surface of a fuel debris bed height of $H_{debris\ bed} = 10 \text{ cm}$, with a LHGR during normal operation of $\dot{q}'_0 = 100 \text{ W/cm}$, an original diameter of the fuel pellet of $D_{Pellet} = 0.0085 \text{ m}$, a decay heat of 5% (Decay=0.05), a porosity of the debris bed of 30% ($p = 0.3$) and heat removal in two directions (upwards and downwards - $\frac{1}{2}$ in each direction) would require a heat flux of about 0.3 MW/m^2 in order to keep the heat production in balance with heat release.

$$\dot{q}'' = \frac{1}{2} \frac{\dot{q}'_0 H_{debris\ bed}}{\frac{\pi D_{Pellet}^2}{4}} \text{Decay} (1 - p) \approx 0.3 \text{ MW/m}^2$$

Thus, the required heat removal from such fuel debris bed (0.3 MW/m^2) would exceed the dry-out heat flux of 0.2 MW/m^2 significantly. Under these conditions it must be assumed that the debris bed heats up and further core damage mechanisms take place, despite the presence of emergency cooling water surrounding the debris bed.

8.1.2.1 Expected parameters of the fuel debris bed

Previous consideration relies on characteristic parameters of the debris bed which need further discussion about their degree of realism. The most significant characteristic parameters are the fuel particle bed height, the mean fuel particle diameter and the fuel particle bed porosity. Most of them can be taken e.g. from Studsvik integral LOCA tests (191, 192, 193, 196, 198) [8.1-5].

8.1.2.2 Debris bed height

According to the experimental results from Studsvik integral LOCA tests, the fuel particle bed height can be estimated when, as observed in Studsvik tests, a fuel column of up to 15 cm could be mobilised and fall out from the fuel rod burst opening. This quantity would enter into the cooling channel and may be aggregated on the fuel rod spacer grid below.

The cross-sectional area of the fuel column is approximately one half of the cross-sectional area of the surrounding cooling channel (0.5). Thus, a fuel column height of 15 cm could fill a cooling channel with fuel debris of about 10 cm in height. At porosities of the debris bed of more than 30% ($p > 0.3$), debris bed heights of more than 10 cm could be reached. Therefore, the debris bed height is related to both the fuel column depleted from the burst fuel rod and the porosity of the aggregated fuel particle bed:

$$H_{debris\ bed} = H_{fuel\ column\ depleted} \cdot \frac{0.5}{1 - p}$$

$$10\ cm \cong 15\ cm \cdot \frac{0.5}{1 - 0.3}$$

8.1.2.3 Porosities

With regard to the fuel which relocates within a fuel rod, various ATHLET-CD analyses for Halden-LOCA test IFA-650.4 have been performed [8.1-6]. These analyses provide a rough estimate about the porosity of relocated fuel.

When running the ATHLET-CD simulation of test IFA 650.4 with a porosity of 50% in the ballooned fuel rod region, the cladding temperature prediction of ballooned region significantly underestimates the measured cladding temperature. It could be shown that a successful prediction is achievable if the porosity is assumed to be at 0% which would indicate the ballooned fuel rod region is entirely filled with fuel.

Because the accuracy of cladding temperature predictions involves large uncertainties beside the uncertainty about porosity, the final conclusion from these test predictions is, the porosity of relocated fuel within a fuel rod is far below 50% and probably close to zero.

The evaluation of INEL in-pile test data (PBF tests and FR-2 tests at a burnup level of about 30 MWd / kg), [2.2-2], provides a linear relationship between the reduction of a pellet stack and the respective cladding hoop strain (see Figure 8.1-3).

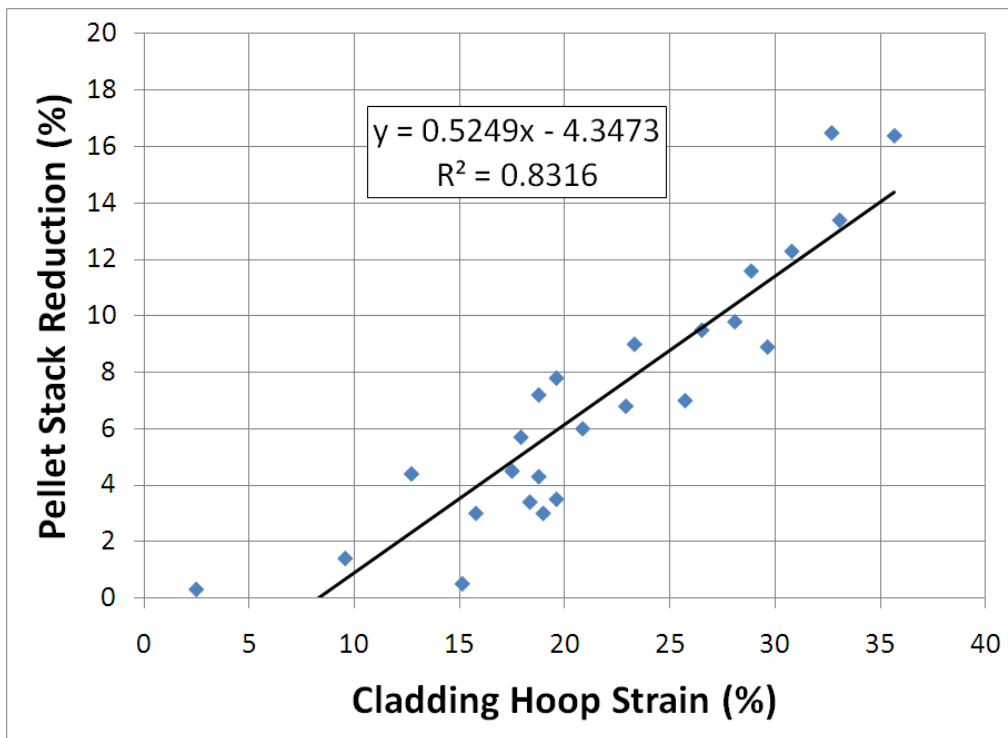


Figure 8.1-3: Relationship between pellet stack reduction and cladding hoop strain from inpile-tests, [2.2-2]

The cladding hoop strain provides extra space in the fuel rod thus relocating fuel enters into this space while the fuel column simultaneously reduces its height and therefore opening a space on top of the fuel column. Thus, a volume balance under the assumption of a homogeneously distributed porosity allows quantifying the average porosity of the relocated fuel.

Each data point in Figure 8.1-3 can be recalculated for porosity. For the sake of simplicity, it is assumed the maximum cladding hoop strain occurs at mid-elevation of the test rod and the strain linearly decreases from mid-elevation towards test rod ends. Figure 8.1-4 illustrates the geometrical situation.

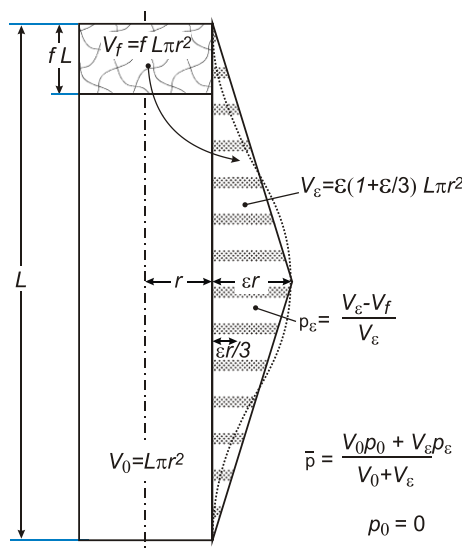


Figure 8.1-4: Average porosity \bar{p} in fuel debris under strained cladding condition

According to Figure 8.1-4 average porosity can be recalculated from pellet stack reduction f and cladding hoop strain ε with:

$$p = \frac{\varepsilon \left(1 + \frac{\varepsilon}{3}\right) - f}{1 + \varepsilon \left(1 + \frac{\varepsilon}{3}\right)}$$

The relationship above is also valid if the axially distributed strain follows more a Gaussian distribution than a linear distribution which is more realistic, see dashed line in Figure 8.1-4. The data from Figure 8.1-3 give porosities as shown in Figure 8.1-5.

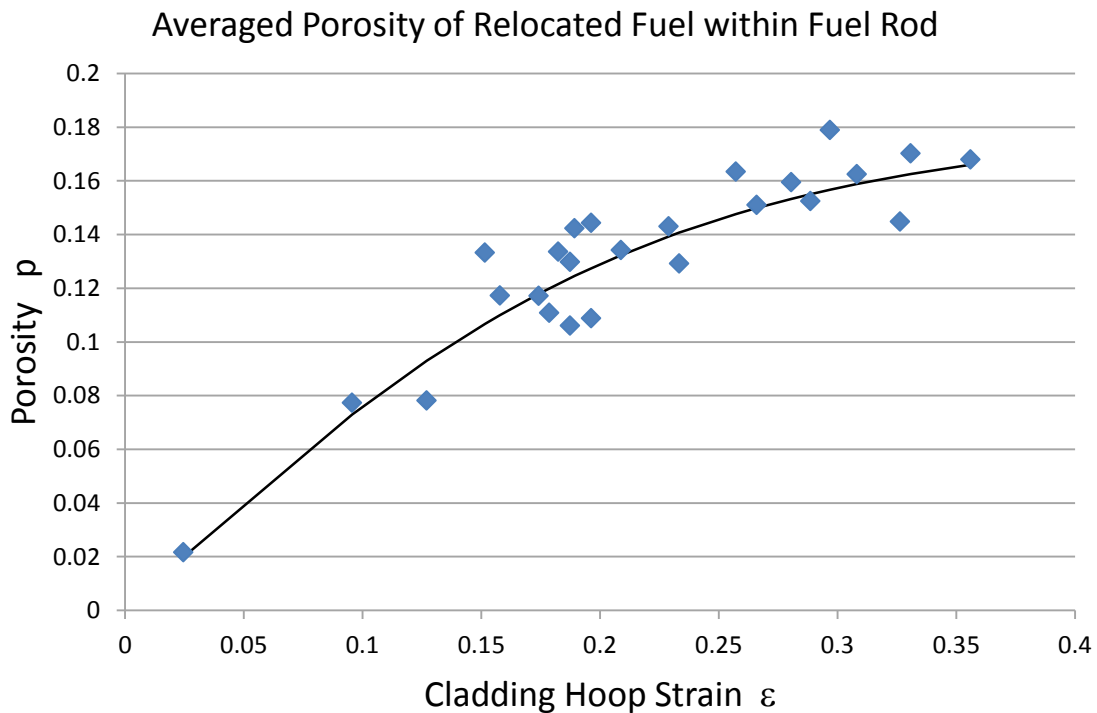


Figure 8.1-5: Porosity of relocated fuel within strained and none-burst fuel rod cladding

Figure 8.1-5 illustrates that porosity of fuel relocated within a strained fuel rod cladding reaches a maximum of about 20% for large cladding strains. In general, the porosity can be correlated with cladding strain by:

$$p = 0.18 \tanh[4.5 \varepsilon]$$

This low porosity might come from the supportive effect of the cladding on the fuel particles. Thus fuel particles may slide on each other providing only small inter-particle volumes.

In contrast to that, porosity of fuel dispersed into the coolant channel will reach much higher porosities. Reason for the higher porosity is the irregular movement of fuel particles when expelled from burst opening in a turbulent flow of fission gas. Fuel particles aggregate on spacer grid in a more chaotic manner. Free space between fuel particles might give porosities in the range of 20% to 40%.

8.1.2.4 Particle size

Figure 8.1-6 shows at a burnup level of 55 MWd/kg at least to a small extent (here about 5% of the total quantity of the expelled fuel particles) fragment sizes in a range between micrometre and millimetre.

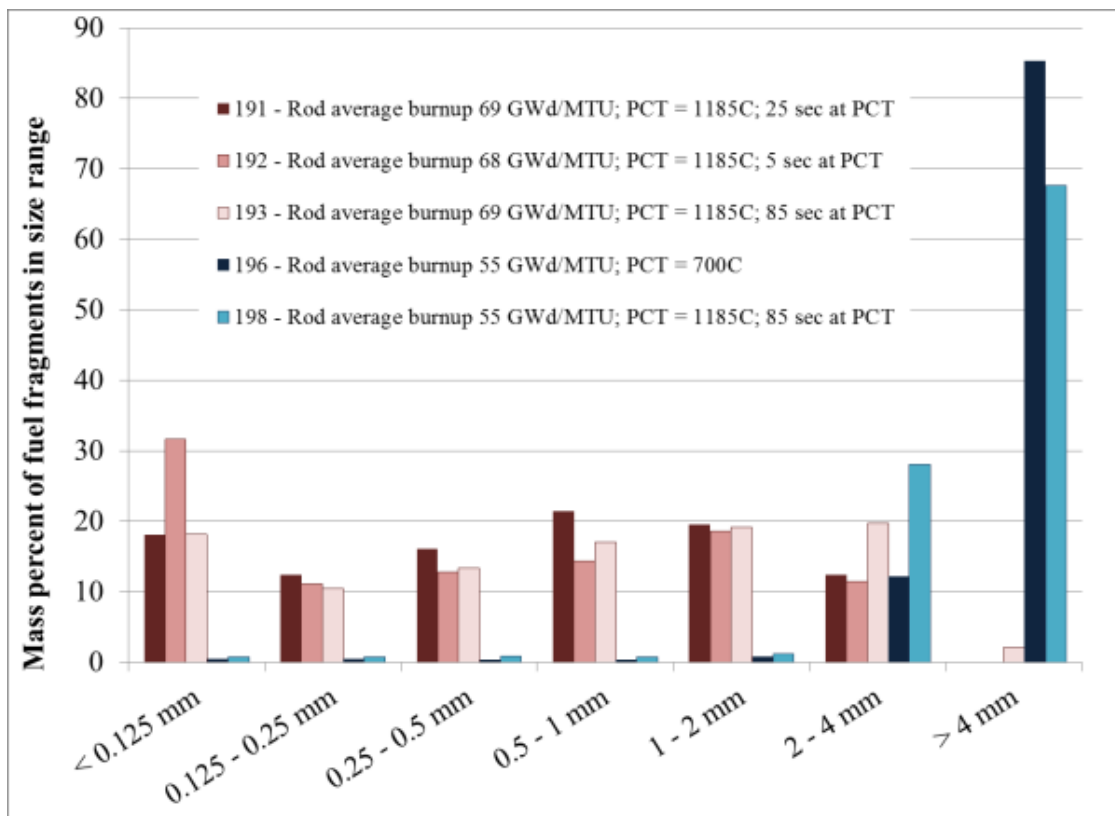


Figure 8.1-6: Fragment sizes as measured in Studsvik Integral-LOCA-Tests (191, 192, 193, 196, 198) [8.1-5]

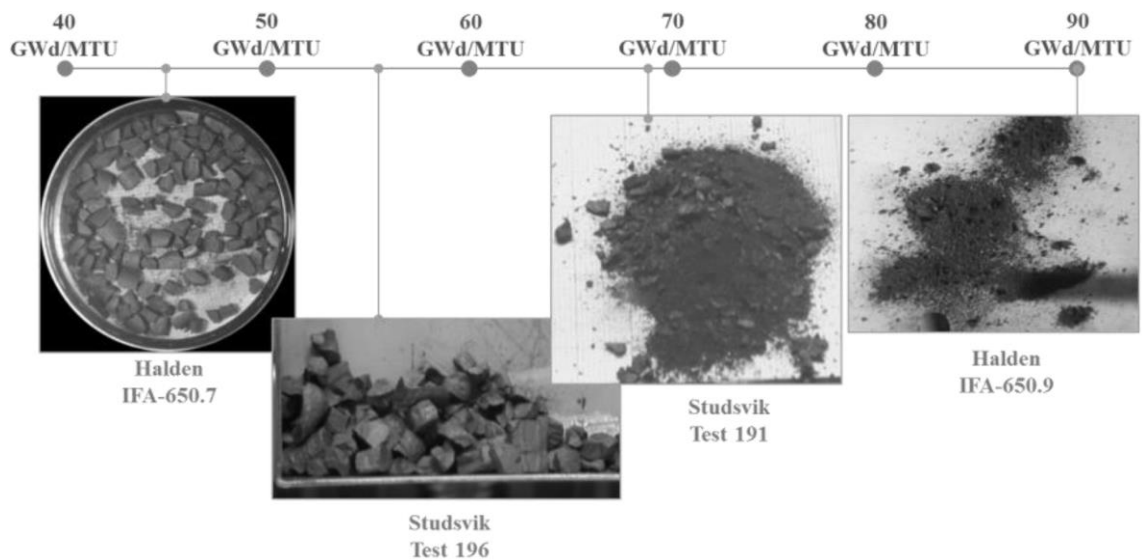


Figure 8.1-7: Appearance of fuel particles in Halden IFA 650 LOCA tests and Studsvik tests when manually shaken out from test rod [8.1-5]

According to both Studsvik tests [8.1-5] and Halden IFA 650 LOCA tests [8.1-5], the transition in the particle size spectrum with prevailing coarse-grained particles towards a particle size spectrum with

prevailing fine-grained particles takes place between burnup of 55 MWd/kg and 69 MWd/kg (see Figure 8.1-6 and Figure 8.1-7).

Fluidising of fine-grained particles limits the particle size spectrum of a debris bed which aggregates on a spacer grid. The permanent flow of coolant during long term cooling (about 0.01 m/s) entrains fine-grained particles. Thus, the minimum (and unfavourable) particle size with regard to the particle bed cooling need to be determined from additional fluid mechanical considerations.

8.1.2.5 Fluidising of fine-grained particles from a fuel particle bed

If fragment sizes fall below e.g. 0.2 mm, then such small particles could be carried away by the flow of coolant as a kind of mud. This fluidising provides a lower cut-off value for the particle size distribution. Because the smallest particle size determines the maximum dry-out heat flux, it is important to have a reliable model about fluidising. Otherwise the particle spectrum as found in Studsvik and Halden tests would not be amenable to cooling at all. For that also see Figure 8.1-2.

Fluidisation is dependent on the coolant velocity, in the case of the LOCA transient this velocity could be estimated to about $u_{mf} = 0.01 \text{ m/s}$. This velocity corresponds to the vertical coolant velocity in the core provided by recirculation pumps.

According Boger and Yeow [8.1-7] the maximum fluidized particle size $d_{partikel}$ at coolant velocity of $u_{mf} = 0.01 \text{ m/s}$, viscosity $\eta = 2 \cdot 10^{-4} \frac{\text{kg}}{\text{m s}}$, density difference between fuel particle and coolant $\rho_s - \rho_f = 8000 \frac{\text{kg}}{\text{m}^3} - 1000 \frac{\text{kg}}{\text{m}^3}$ and gravitational acceleration $g = 9.81 \frac{\text{m}}{\text{s}^2}$ is:

$$d_{partikel} = \sqrt{\frac{u_{mf} \cdot 150 \cdot \eta \cdot (1-p)}{(\rho_s - \rho_f) \cdot g \cdot p^3}} = 65 \mu\text{m} \sqrt{\frac{1-p}{p^3}}$$

In case of a porosity of the particle bed of 40% ($p = 0.4$), the particle spectrum is limited to a minimum particle size of about 0.2 mm. Lower porosities would give larger particle sizes which could be fluidised. And hence, according to Figure 8.1-1, the porosity of 40% and the minimum particle size of 0.2 mm would give in combination with a particle bed height of about 10 cm a maximum dry-out heat flux of about $\dot{q}''_{dryout} = 0.2 \text{ MW/m}^2$. Coolability of such a particle bed would be questioned.

8.1.2.6 Long term cooling under zinc-borate precipitation

Regarding the long term core cooling further aspects require additional consideration. Recirculation of coolant from the containment sump might transport zinc-borate into the core region. This zinc-borate stems from zinc-coated surfaces of gratings mounted within the containment building.

Zinc-borate preferably precipitates at structures in the core which may have temperatures in the range from 60°C to 80°C. Such temperatures could be reached in fuel particle beds aggregated on spacer grids as discussed above. The precipitation of zinc-borate closes the pores of the fuel particle bed and due to that again coolability of such bed is questioned.

Zinc-borate precipitation might be relevant when the duration of sump coolant recirculation exceeds 1 or 2 days after occurrence of LOCA. At this time, the decay heat production falls below 1%. Thus cooling of the particle bed with closed pores could be reached via heat conduction. In this situation, one-dimensional heat conduction allows quantifying the debris bed height which is still amenable to cooling.

The definition of coolability here differs from the previous one. Compliance with a new coolability criterion could be to demonstrate that the mid-layer position of the debris bed will not exceed temperatures of the fuel melting temperature.

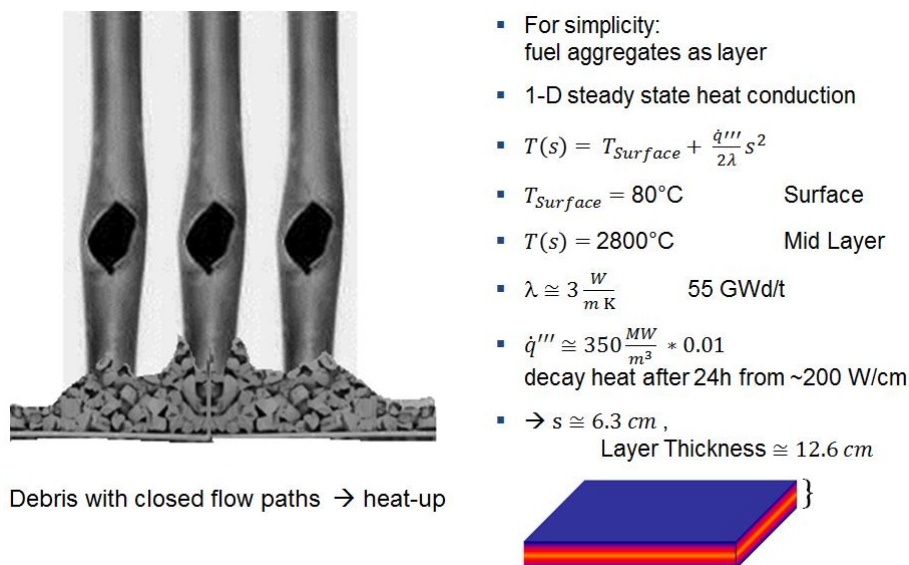


Figure 8.1-8: Debris bed cooling via heat conduction

Figure 8.1-8 shows the result for a debris bed which reaches fuel melting temperature at mid-layer position. According to this simple analysis, the debris bed height should stay below 12.6 cm. The height of 12.6 cm is related to a burnup level of 55 MWd/kg, a LHGR during normal operation of 200 W/cm and a relative decay heat of 1% which corresponds to about 24 hours after occurrence of LOCA. Reduction of thermal conductivity of fuel due to porosity has been neglected because it cancels out with the effect of porosity on power density.

If the coolability criterion “mid-layer temperature at melting temperature of fuel (2 800°C)” is replaced by “mid-layer temperature at melting temperature of cladding (1 800°C)”, the debris bed height would reduce by 2 cm to 10.8 cm only.

Since the topic of zinc borate precipitation is still an unresolved safety issue, this aspect should be kept in mind when discussing coolability of fuel which is dispersed into the coolant channel of a reactor core.

8.1.2.7 Concluding remarks on coolability

Cooling of the fuel which disperses into the coolant channel and aggregates on a spacer grid below the burst opening leads to a complex safety demonstration. This cooling decisively depends on the LHGR of the fuel during normal operation. Furthermore, the coolability significantly depends on characteristic parameters like fuel particle sizes, porosities of the fuel particle bed and heights of the fuel particle bed. This particle bed cooling cannot profit from circulating coolant flows in adjacent coolant channels surrounding the particle bed because of the low heat conduction prevailing in particle beds. The particle bed cooling follows separate cooling processes which would require specific consideration in safety demonstrations.

As described above the related safety demonstration requires considerable analytical effort. This effort might also involve additional experimental investigation.

Furthermore, the aspect of "zinc-borate precipitation", when applicable, makes the safety demonstration for dispersed fuel more complex. This aspect should be kept in mind when judging on long term coolability.

8.2 Re-criticality

Experimental observations of FFRD under LOCA conditions showed that irradiated fuel could fragment into small pieces and may disperse into the core from the ruptured fuel rod during a LOCA transient [8.2-1]. If sufficient fissile material is contained in the dispersed fuel, the possibility exists for the dispersed fuel to become critical under re-flooding conditions. Therefore, the possibility of critical for the dispersed fuel was studied analytically based on the experimental observations of fuel fragmentation and dispersal under LOCA conditions [8.2-2].

8.2.1 Criticality aspects and characteristics of dispersed fuel

For the dispersed fuel to achieve critical, the following conditions are required:

- sufficient fissile material
- sufficient moderator
- not much of neutron absorbers (poisons) and
- sufficient physical size to reduce the effect of neutron leakage.

Basically, a criticality of dispersed fuel in water is not possible unless the fissile material is sufficiently contained in the fuel. The concentration of fissile material decreases with burnup, therefore the possibility of criticality is strongly affected by fuel burnup. The depletion of fissile material due to burnup is described in the section below.

On the other hand, the fuel burnup effects to cause a fine particle distribution of fuel fragments under LOCA conditions. A local pellet average burnup threshold exists at which point the fuel fragment size distribution begins to transition from coarse to fine particle distribution [8.2-1]. This burnup threshold is discussed in Chapter 6.

Furthermore, it is considered that the fine fragments will be able to escape from the rod, but that coarse fragments cannot escape [8.2-1]. This implies that only a fuel pellet with high burnup will be fragmented to fine particles and will be dispersed into the core from the ruptured fuel rods during a LOCA transient. Therefore, the fuel burnup is a key parameter to evaluate potential for criticality of dispersed fuel under LOCA conditions.

8.2.2 Potential for re-criticality

The possibility of criticality for dispersed fuel has been studied preliminary for a typical PWR fuel. In this study, several assumptions were made based on the experimental observations of fuel fragmentation and dispersal under LOCA conditions for convenience, as follows:

- Fine particle size dispersed from the ruptured fuel rod into the core is below 1 mm [8.2-1].
- For the criticality calculation, it was assumed that fine fuel particles are dispersed and merged in water homogeneously, and it was treated as homogeneous fuel-water mixture.
- According to the report [8.2-3], the effect on increase of reactivity from homogeneous to heterogeneous configuration is less than 1.5% for fuel particle of 1 mm.
- Critical mass and critical volume were calculated for a sphere model as optimum geometry.

8.2.2.1 Burnup calculation of 17x17 PWR fuel assembly

The changes in fuel compositions and k-infinity of fuel assembly with burnup were calculated according to the detailed specifications of 17x17 PWR fuel assembly using CASMO-5 code [8.2-4]. Figure 8.2-1 shows

the cross-section of 17x17 PWR fuel assembly with an average enrichment of 4.8 wt% U-235 containing 24 Gd fuel rods (10 wt% Gd₂O₃) with an enrichment of 3.2% U-235 [8.2-5].

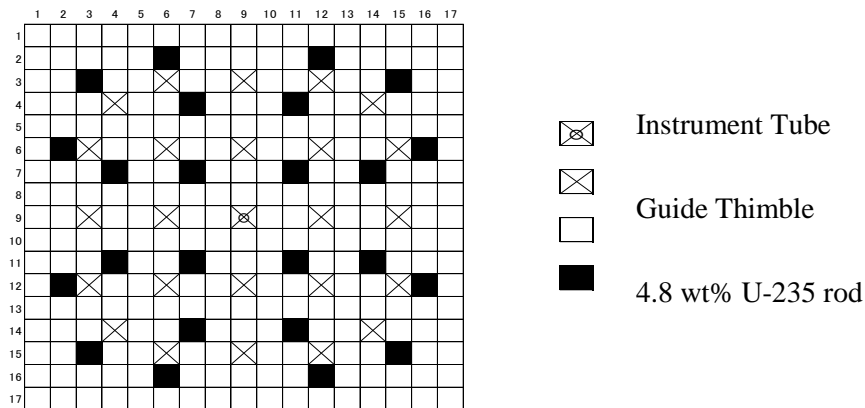


Figure 8.2-1: Typical 17x17 PWR fuel assembly with an average enrichment of 4.8% U-235 containing 24 Gd fuel rods [8.2-5]

The burnup calculation of 17x17 PWR fuel assembly for an infinite array was conducted with the following Hot Full Power (HFP) core conditions:

- average fuel temperature: 973.15 K
- average moderator temperature: 575.65 K
- boron concentration: 600 ppm
- rated power density: 100.0 kW/L.

Figure 8.2-2 shows the k-infinity of fuel assembly, together with the depletion of U-235 and the build-up of the fissile Pu as a function of fuel burnup. As shown in this figure, the k-infinity decreases after burn out of Gd, and it decreased less than unity with burnup above 35 GWd/t.

The enrichment of U-235 decreased to nearly 1 wt%, but the fissile Pu concentration increased to nearly 0.9 wt% at burnup of 50 GWd/t, as shown Figure 8.2-2. The fissile Pu concentration will saturate at a value determined by the balance between the U-238 transmutation rate and the fissile Pu depletion rate. As shown in Figure 8.2-2, potential for criticality is quite low for HBU.

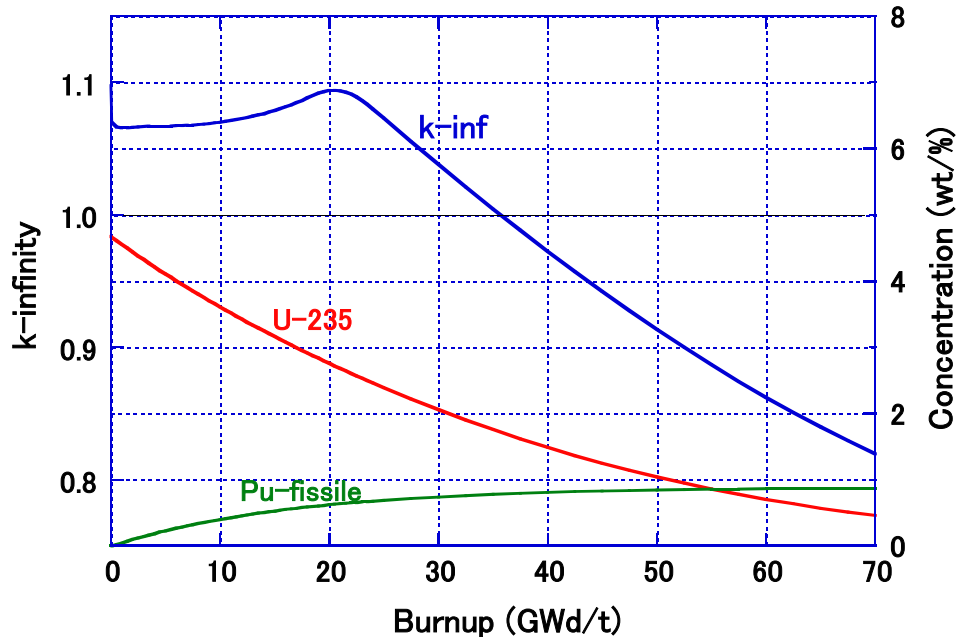


Figure 8.2-2: k-infinity trend of 4.8 wt% enriched PWR assembly due to depletion of U-235 and build-up of fissile Pu under HFP core conditions, Boron concentration at 600 ppm

8.2.2.2 Infinite multiplication factor (k_{∞}) for fuel-water mixture

A series of calculations of infinite multiplication factor (k_{∞}) were performed for infinite medium of homogeneous fuel-water mixture using the Monte Carlo code MVP [8.2-6] to study the burnup conditions required for the dispersed fuel to achieve critical.

The following burnup levels have been considered in this study: 30, 40, 50, and 60 GWd/t. The fuel compositions consist of twelve actinides and fifteen fission products as shown in Table 8.2-1, and these values at each burnup were calculated according to the detailed specifications of 17x17 PWR fuel assembly using CASMO-5 code [8.2-4]. Criticality calculations were conducted with a temperature of 293 K, and conservatively no-borated water was assumed.

For each burnup, the infinite multiplication factor (k_{∞}) for homogeneous fuel-water mixture was calculated with varying fuel concentration.

^{234}U	^{235}U	^{236}U	^{238}U	^{237}Np	^{238}Pu
^{239}Pu	^{240}Pu	^{241}Pu	^{242}Pu	^{241}Am	^{243}Am
^{95}Mo	^{99}Tc	^{101}Ru	^{103}Rh	^{109}Ag	^{133}Cs
^{143}Nd	^{145}Nd	^{147}Sm	^{149}Sm	^{150}Sm	^{151}Sm
^{152}Sm	^{153}Eu	^{155}Gd	-	-	-

Table 8.2-1: Actinide and fission product nuclides taken in fuel compositions for criticality calculations

Figure 8.2-3 shows the infinite multiplication factor (k_{∞}) as a function of fuel concentration for each burnup. As shown in this figure, a criticality is no longer possible irrespective of the mass for the fuel with burnup above 50 GWd/t considering the effect of heterogeneous configuration on k_{∞} .

On the other hand, only a fuel pellet with burnup above 55 GWd/t will be fragmented to fine particles and will be dispersed into the core from the ruptured fuel rods during a LOCA transient. From these results, it was found that the dispersed fuel during a LOCA transient may have no potential to reach criticality condition.

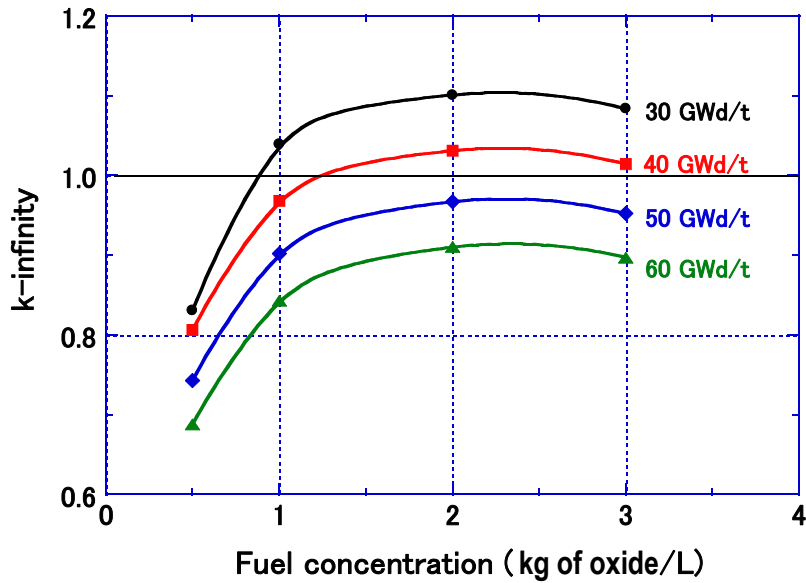


Figure 8.2-3: Infinite multiplication factor (k_{∞}) for homogeneous fuel-water mixture as a function of fuel concentration, Boron concentration at 0 ppm

8.2.2.3 Critical masses and critical volumes

The critical mass and critical volume for fuel-water mixture within sphere geometry were calculated using the Monte Carlo code MVP [8.2-6]. Figure 8.2-4 shows a sphere geometry model of homogeneous fuel-water mixture reflected by 30 cm thick (effectively infinite) water. The calculations were conducted for burnup level less than 40 GWd/t within which a criticality is possible, as shown in Figure 8.2-5. Criticality calculations were conducted with a temperature of 293 K.

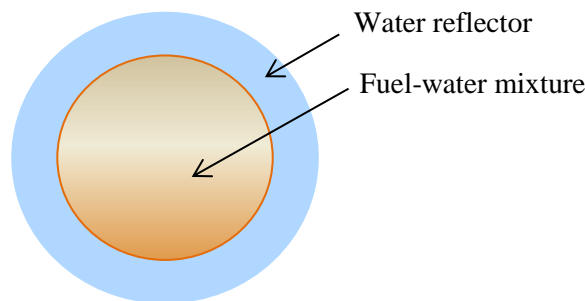


Figure 8.2-4: Sphere geometry model of fuel-water mixture reflected by an effectively infinite thickness of water.

The critical values were calculated for burnup levels of 30 and 40 GWd/t with varying fuel concentration.

Figure 8.2-5 and Figure 8.2-6 show the critical masses and critical volumes as a function of fuel concentration for each burnup. The minimum critical masses and critical volumes for each burnup are shown in Table 8.2-2

Burnup (GWd/t)	Minimum Critical Value		
	Mass of Fuel (kg of oxide)	Volume of Sphere (L)	Radius of Sphere (cm)
30	824	465	48
40	6,624	3,312	92

Table 8.2-2: Minimum critical masses and critical volumes for fuel-water mixture within sphere geometry

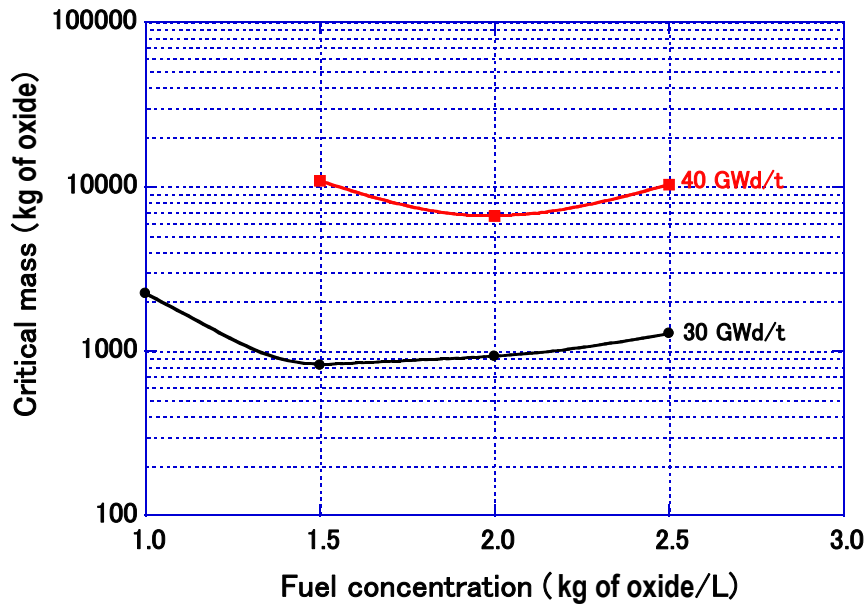


Figure 8.2-5: Critical masses of fuel within spheres of homogeneous fuel-water mixture as a function of fuel concentration

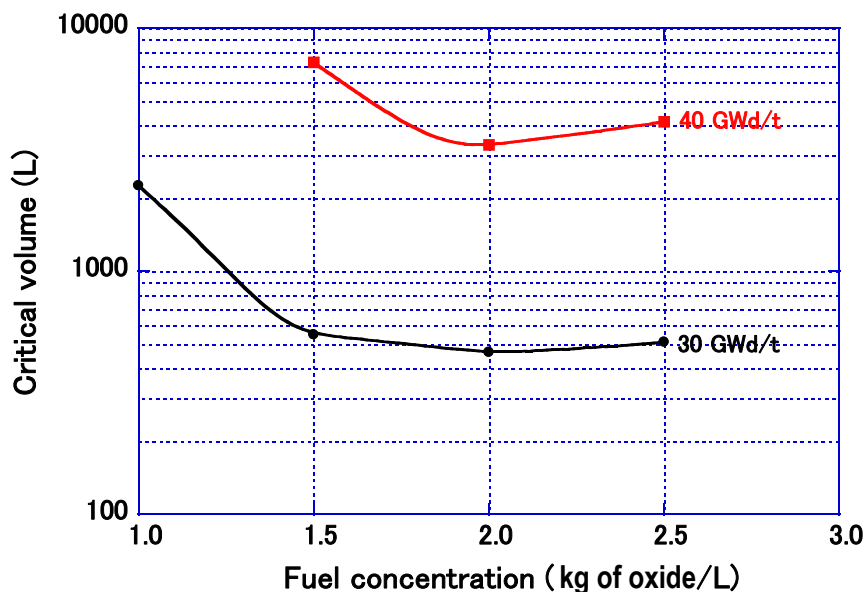


Figure 8.2-6: Critical volumes of spheres of homogeneous fuel-water mixture as a function of fuel concentration

From the results, it is indicated that roughly more than 6.6 ton of fuel are necessary to achieve a critical level for burnup of 40 GWd/t, and roughly more than 800 kg of fuel are necessary for burnup of 30 GWd/t. A total amount of fuel contained in a typical 4-loop PWR is approximately 86 ton, then 800 kg is roughly 1% of total fuel of 4-loop PWR.

8.2.3 Summary

The possibility of re-criticality for the dispersed fuel was studied analytically based on the experimental observations of fuel fragmentation and dispersal under LOCA conditions. The calculations performed for this study show that the potential for re-criticality significantly depends on the burnup of dispersed fuel.

From the results of preliminary calculations based on the assumption that fine fuel particles below 1 mm are dispersed and merged in water homogeneously, it is shown that the fuel particles with burnup above 50 GWd/t have little potential to reach criticality condition irrespective of the mass of fuel.

However, the results of this study are obtained under the assumptions based on the experimental observations up to date. Therefore, it is foreseen that more valid observations related on burnup threshold and particle size for fuel fragmentation and dispersal will be obtained in the future, and this study will be refined based on the renewed conditions.

8.3 Radiological consequences

A LOCA is a design basis accident. Reactors are designed to withstand design basis events without resulting in a core melt. During a LOCA event rods could heat up and burst due to increase of fuel rod cladding differential pressure before ECCS floods the core. Such kind of phenomena has been taken into account when radiological consequences of LOCA transients are to be evaluated. In particular the gaseous release from bursting fuel rods is considered in this context.

Fuel fragmentation and subsequent dispersal of fine fragmented fuel which might even reach the reactor containment is a phenomenon which is out of scope in the present licensing. To which extent the

dispersal of fine fragmented fuel additionally to the gaseous fission product releases could affect the dose rates in the environment of a plant is an open question. At present there are very few investigations on this matter available and the information in the following section is from a (phenomenological) study based on conservative assumptions, see Reference [8.3-1].

LOCA events in both BWR and PWR were considered. It was shown that Recirculation Line Break in BWR is the most limiting event in terms of fuel fragments dispersal and relocation to the containment and the impact on the source term was estimated for this limiting case.

8.3.1 Amount of released fuel

Fuel fragments dispersal refers to the ejection of fuel fragments or particles through a rupture or burst opening in the fuel rod cladding. To estimate the radiological consequences from fuel fragments dispersal during LOCA, the expected maximum amount of fuel that is released outside the cladding per cladding opening has to be determined.

The maximum amount of fuel dispersed from one cladding rupture comprises all the fuel material between two adjacent spacers. This is due to the fact that the spacers counteract the cladding diametrical strain such that the strain is expected to be smaller than 5% in the vicinity of the spacers. This in turn prevents axial movement of fuel pellets and fragments over the spacer grids. The following assumptions are made regarding the amount of dispersed fuel:

- For BWR fuel: The maximum amount of released fuel fragments for one cladding rupture is around 270 g based on a typical BWR assembly with a fuel pellet outside diameter of 0.848 cm and an average distance between two adjacent spacers of 44 cm.
- For PWR fuel: The maximum amount of released fuel fragments for one cladding rupture is around 290 g based on a typical PWR assembly with a fuel pellet outside diameter of 0.8192 cm and an average distance between two adjacent spacers of 50 cm.

A burnup threshold of 65 MWd/kgU for fuel fragments dispersal under LOCA conditions is conservatively applied. The size distribution of the fuel fragments is assumed to be similar to that in Figure 2.2-4 for fuel with burnup larger than 65 MWd/kgU.

The mobility of fuel fragments refers to the transportation or settling of fuel fragments within the reactor coolant pressure boundary, the containment and/or in the auxiliary systems. After a cladding rupture that leads to fuel fragments dispersal, the fuel fragments will either settle in the internal structures of the reactor pressure vessel or be transported out of it, depending on the flow conditions, particle size and shape etc.

To determine whether the fuel fragments will escape from the reactor pressure vessel or settle in the bottom of it, a detailed Computational Fluid Dynamics code must be used. Nevertheless, a rough estimate can be given whether the particles will sink and settle in the bottom or on internal structures of the reactor pressure vessel or lift with the flow for vertical flow conditions, by considering the gravitational and buoyance forces and the drag on the particles from the surrounding fluid.

8.3.2 Release from reactor pressure vessel

The motion of the released fuel fragments depends on the thermal-hydraulic state during the transient progression, which is affected by the break flow and the injected ECCS flow. Depending on fluid phase, velocity, direction, as well as the size and shape of the fragments, the fragments will either follow the flow or sink under influence of the gravitation force, and thus be accumulated at various locations in the lower part of the reactor pressure vessel. Consequently, a detailed thermal-hydraulic code should be employed to determine whether the fuel fragments settle or deposit at various locations in the reactor pressure vessel or

may escape from it. A simplified assessment is done in Reference [8.3-1] to determine the mobility of the fuel fragments. This assessment basically relies on the following two assumptions:

- Fuel fragments dispersal occurs during the reflood/core spray part of the event where the coolant conditions are assumed to be quasi-stationary.
- The core flow is density driven and can be estimated from the ECCS flow.

Based on these assumptions, the average core flow is estimated and the fragment terminal velocity (the velocity when the weight of the object is exactly balanced by the upward buoyancy force and drag force) is calculated. This terminal velocity is used to determine the mobility of the fuel fragments.

For the following four limiting LOCA cases, in terms of fuel fragments dispersal, the amounts of material that might escape reactors are calculated based on estimated flow velocities and mobile fragment sizes:

- Low Pressure Coolant Injection Line Break in a BWR with external recirculation pumps. The average core flow velocity is based on capacity of the HPCI and estimated to 0.01 m/s. This gives a particle size that can be dragged out of the reactor pressure vessel by the liquid flow to maximum 0.08 mm. In total it is estimated that 60 g per cladding burst may be transported by the liquid, thus escaping through the double ended guillotine pipe break to the containment wetwell.
- Recirculation Line Break in a BWR with external recirculation pumps. Due to the location of the break, it is not possible to reflood the core unless the containment is flooded up to a certain level. Consequently, a reasonable assumption regarding the mobility of the fuel fragments is to assume that all fuel particles are flushed out of the reactor pressure vessel through the pipe break to the containment wetwell, 270 g per cladding burst.
- SBLOCA in Cold Leg in a PWR. The average core flow velocity is based on capacity of the LPSI and estimated to 0.01 m/s. This gives that a particle size less than 0.03 mm will be mobile. In total it is estimated that 25 g per cladding burst may follow the flow up into the hot legs, preferable to the broken loop because of pressure drop considerations, and eventually might escape through the break to the containment sump. In comparison with LBLOCA, the SBLOCA accidents are characterised by a slower drop in pressure and in water level.
- LBLOCA in Cold Leg in a PWR. The average core flow velocity is based on capacity of the LPSI and estimated to 0.05 m/s. This gives that a particle size less than 0.2 mm will be mobile. In total it is estimated that 130 g per cladding burst may follow the flow up into the hot legs, preferable to the broken loop because of pressure drop considerations, and eventually might escape through the break to the containment sump.

8.3.3 *Activity release assessment*

Fuel fragments dispersal refers to the ejection of fuel fragments through a rupture or burst opening in the cladding but one cannot exclude that additional gaseous radionuclides, contained inside the fuel pellet prior to the LOCA event, are released as well. A significant portion of the gaseous radionuclides contained in the fuel pellet are expected to be released during fuel fragmentation at high temperatures occurring during LOCAs.

The following definitions are made to distinguish between the different types of release of radionuclides outside the cladding boundary:

- Gaseous radionuclides. Gap inventory refers to the gaseous and in some cases easily dissolved radionuclides in the fuel pin which will be released when a cladding rupture occurs. In the safety assessments performed according to US. NRC Regulatory Guide 1.183 this is traditionally assumed to be the amount of gaseous species found in the gap between pellet and cladding during

normal operation, but as will be discussed below, fuel fragmentation could result in an increased gap inventory. Here, this increase will be seen as an additional amount of gaseous activity being released from the fuel pin. The solid fission products and actinides released due to fuel fragmentation will be treated separately.

- Fuel fragments. Fuel fragments refer to the fragments or particles that are ejected through a rupture or burst opening in the cladding.

The release of gaseous radionuclides from fuel fragments dispersal and from the gap inventory is discussed in Section 8.3.3.1 whereas the release of fuel fragments is discussed in Section 8.3.3.2. The evaluation is done for BWR recirculation line break as it is judged, see Chapter 8.3.2, that this event among the assessed events, for both BWR and PWR, yields the largest mass fraction of fuel fragments that may escape from the reactor pressure vessel.

8.3.3.1 Release of gaseous radionuclide

Traditionally the gap inventory from a broken fuel pin is assumed to consist of the gaseous fission products which are released to the fuel gap during operation. This gap inventory is closely connected to the FGR, since the release mechanism of fission gases from the pellet is the same as for the radionuclides in the gap inventory.

During a LOCA event cladding rupture is expected to be caused by overpressure in the fuel pin. Therefore, it is reasonable to assume that the FGR in the bursting pins to be among the highest in the core. For the same reason it is reasonable to assume that the gap inventory in these pins to be among the highest in the core.

For calculation of source terms the US. NRC Regulatory Guide 1 183 [8.3-2] has been used. In this guide, two gap inventories are defined. One core average value used in the conservative LOCA methodology is described in the guide, and one non-LOCA gap inventory is suggested for events where a single or few fuel assemblies are damaged.

The former, core average values, are not representative for the bursting pins, since the bursting pin will have a higher gap inventory than the core average. However, the non-LOCA gap inventory, given in the guide, represents a gap inventory applicable to assemblies with a gap inventory above the core average. Those values are given in Table 8.3-1.

Gap inventory	
Group	Fraction of total inventory
I-131	0.08
Kr-85	0.10
Other noble gases	0.05
Other halogens	0.05
Alkali metals	0.12

Table 8.3-1: Gap inventories for a HBU assembly according to Reference [8.3-2]

The exact numerical value of this gap inventory in a Swedish context can be discussed, but given the results presented in Reference [8.3-3] and Reference [8.3-4] for FGR it can be concluded that the values in Table 8.3-1 are good approximations for gap inventories in fuel pins with a risk to burst during a LOCA. The limitation with this assumption is that it only takes into account the gap inventory formed during normal operation when activity of dose significant radionuclides reaches equilibrium or maximum values.

During a LOCA the gap inventory can increase due to two different phenomena. Firstly, an increase in temperature can result in more gaseous radionuclides being released. Secondly, the fragmentation of pellets during the burst itself could result in an increased release of gaseous radionuclides. The first of these two phenomena are outside the scope of this report and will not be discussed further. The second one of these two is discussed more in detail below and an example quantifying this increase in gap inventory due to fuel fragmentation is given.

In a HBU pellet, a significant amount of gaseous radionuclides is found in pores located at the grain boundaries. If these high burnup pins burst during a LOCA and the pellet is fragmented, the probability for the gaseous radionuclides to be released is very high. Therefore, the most reasonable assumption is to assume all gaseous radionuclides in the pellets which are being fragmented to be released, and thereby contribute with an increase to the gap inventory.

As an example, taken the assumption that the maximum released fragment amount corresponds to the fuel quantity between two adjacent spacers, the increase in gap inventory can be roughly estimated. For BWR fuel pins it corresponds to 44 cm or about 12% of the entire fuel column which equals to 365 cm.

Assuming that all pellets between two adjacent spacers to be fragmented during a burst, it results in an increase of the gap inventory with about 12% for noble gases and halogens. For alkali metals, mainly Cs, the increase in gap inventory could be expected to be slightly lower since some of the alkali metals will form oxides together with molybdenum, which are solid at the expected fuel temperature and hard to dissolve.

Since the gap inventory created prior to a LOCA event as well as fuel fragments and gaseous radionuclides released during the fragmentation, will be dispersed via the cladding rupture as long as the internal rod overpressure is maintained, it is reasonable to assume that all these inventories can be transported into the reactor core coolant.

8.3.3.2 *Release from fuel dispersal*

The change in the source strength due to fuel fragments dispersed during a LOCA is discussed in this section by taking two different scenarios into consideration:

- Reference case. This case is a conservative estimate employing the calculation guidelines laid out in Reference [8.3-2] regarding fission product inventory, release fractions, timing of release phases and radionuclide composition, see Section 8.3.3.2.1.
- Additional contribution from fuel dispersal. This case addresses the additional contribution to source terms from fuel fragments dispersal. It is based on the assumption that 10% of the fuel pins in the core has a pin local burnup above the fuel fragmentation threshold of 65 MWd/kgU. Furthermore, it is assumed that the accident causes one cladding rupture per fuel pin for all these fuel pins. See Section 8.3.3.2.2.

These two cases are compared in terms of gamma source strengths to determine the relative additional contribution from fuel fragments dispersal. The calculation is carried out for BWR recirculation line break as this case is judged to yield the largest mass fraction of fuel that can escape from the reactor pressure vessel from one cladding rupture.

The nuclide composition in the core (core inventory) is based on a BWR equilibrium core inventory for 1-year cycle with 10x10 fuel and high EOC core burnup. The nuclide composition for fuel pins above the fuel fragmentation threshold is based on a conservative nuclide composition applicable to HBU. Gamma source strengths are calculated for 12 time points from 0.5 hr up to 2 years after the initiation of the event.

The difference between the reference case and the case with additional contribution from fuel fragments is the fact that the transuranium elements are released in the case of fuel fragments dispersion. In

the reference case the low solubility of these elements results in low releases, but for the case when the pellet is fragmented and released as particles the transuranium elements will also be dispersed. These nuclides will not contribute significantly to the gamma source strength but are to large extent alpha emitters. For the fuel particles which reach the condensation pool, there is a possibility that they will be spread out in the containment due to the containment spray.

8.3.3.2.1 Reference case

The release of radionuclides to the containment is based on the assumptions shown in Table 8.3-2 and Table 8.3-3. These assumptions originate from the NRC Regulatory guide 1 183 Reference [8.3-2] and are used for environmental qualification of components with regard to radiation at the Swedish utilities. With these assumptions the release of fission products is assumed to occur during two different phases:

- Gap release phase. This is the first stage of the event where a significant amount of cladding ruptures is assumed to occur. The majority of the core inventory of fission gases in the gap between the fuel pellet and the cladding is released during this phase.
- Early in-vessel phase. During this stage of the event, it is assumed that the fuel is overheated and some part of the fuel is melted. Fission gases from the fuel and some fuel material due to melting are released during this phase.

The released core inventory to the containment and nuclide data from EAF-2007 [8.3-5] is used to calculate the equivalent gamma source strength. The calculated gamma source terms constitute the reference values in Figure 8.3-1 to Figure 8.3-3. These values are to be compared with the corresponding gamma source strengths, from the release of fuel fragments, in Section 8.3.3.2.2. To capture the basic chemistry of this system, the gamma source strengths are grouped into noble gases, halogens and other fission products.

Group	Gap release phase	Early in-vessel phase	Group Nuclides
Noble gases	0.05	0.95	Kr, Xe
Halogens	0.05	0.25	I, Br
Alkali metals	0.05	0.2	Cs, Rb
Tellurium metals	0	0.05	Te, Sb, Se, (Ba, Sr)
Ba, Sr	0	0.02	Ba, Sr
Noble metals	0	0.025	Ru, Rh, Pd, Mo, Tc, Co
Cerium group	0	0.0005	Ce, Pu, Np
Lanthanides	0	0.0002	La, Zr, Nd, Eu, Nb, Pm, Pr, Sm, Y, Cm, Am

Table 8.3-2: Release fractions during gap and early in-vessel release phases [8.3-2].

Phase	Onset	Duration
Gap release	2 min	0.5 hr
Early in-vessel	0.5 hr	1.5 hr

Table 8.3-3: Timing of release phases [8.3 2]

8.3.3.2.2 Additional contribution from fuel dispersal

The additional contribution, from fuel fragments dispersal to the gamma source strengths, is in the study [8.3-1] based on the assumption that 10% of the fuel pins in the core has a pin local burnup above the assumed fuel fragmentation threshold of 65 MWd/kgU. The cladding for all these fuel pins is conservatively assumed to rupture at the initiation of the event with one cladding rupture per fuel pin. Moreover, for simplicity, it is assumed that all fuel pins are full length rods of 365 cm. All this together, yields a release of 1.2% of the total core inventory.

Note that the nuclide composition, assumed for these rods, is for higher burnup fuel in contrast to the core inventory employed for the reference case in Section 8.3.3.2.1. Additionally, it is noted that the increase of the gap inventory due to the fuel fragmentation is not included in this section. It is treated separately in Section 8.3.3.1.

The released fuel inventory to the containment and nuclide data from EAF-2007 [8.3-5] is used to calculate the equivalent gamma source strengths. Analogously with the reference case, the gamma source strengths are grouped into noble gases, halogens and other fission products.

Figure 8.3-1 to Figure 8.3-3 show the relative gamma source strengths. The data points given in the figures are normalised to the reference case for time 0.5 h. For instance, for noble gases at time 2 days, the value given is normalised to the reference case given at time 0.5 h. This comparison gives a good illustration of the relative impact from fuel fragments dispersal to the reference case. Note that the y-axis is in logarithmic scale and all figures are utilising an equidistant scale for time.

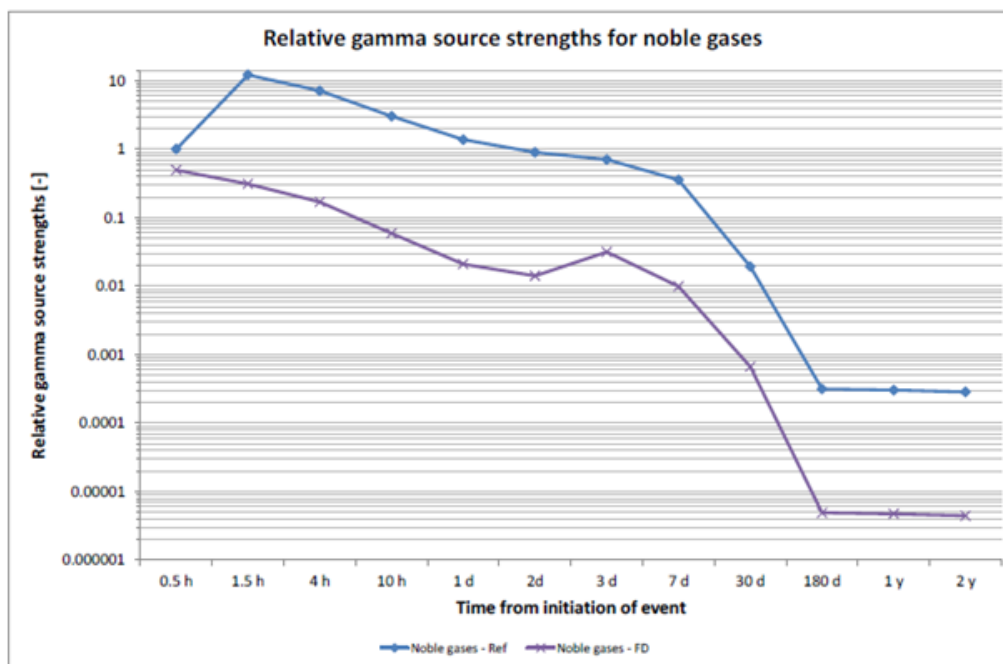


Figure 8.3-1: Relative gamma source strengths for noble gases where all data points are normalised to the reference case given at time 0.5 h

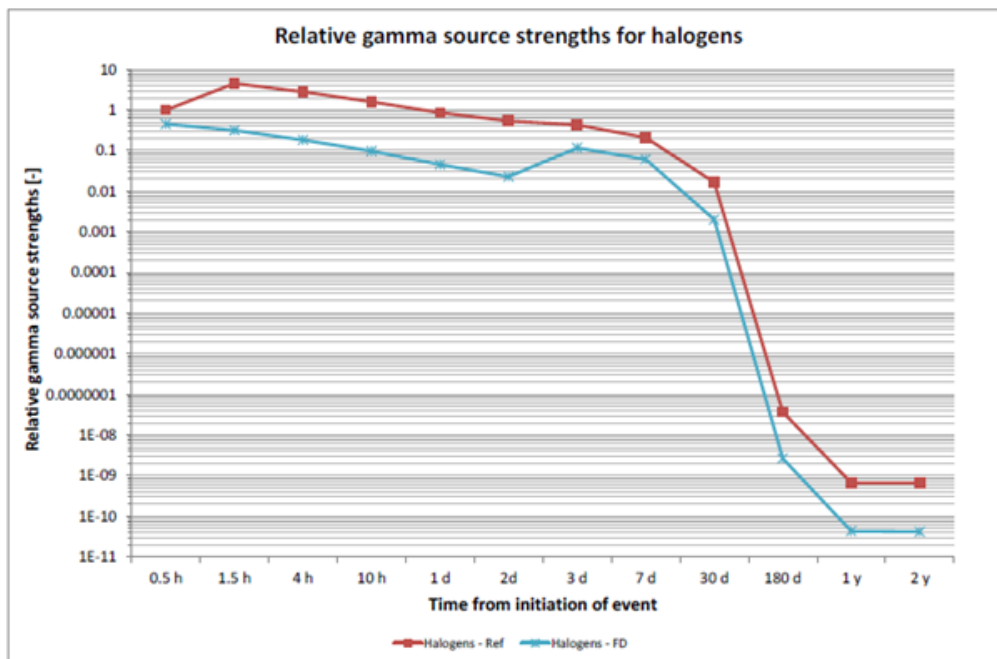


Figure 8.3-2: Relative gamma source strengths for halogens where all data points are normalised to the reference case given at time 0.5 h.

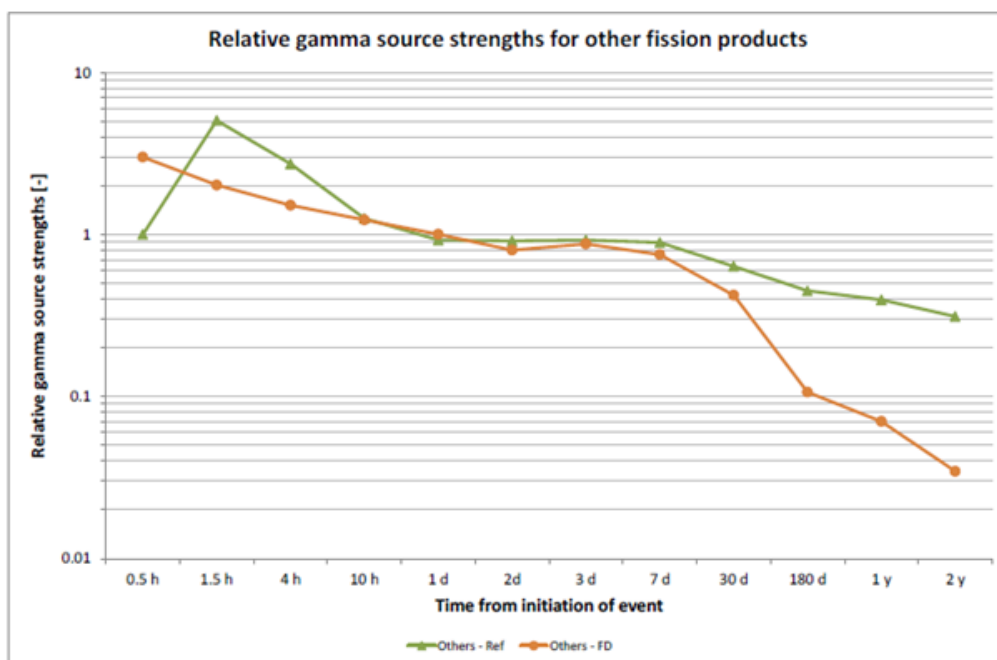


Figure 8.3-3: Relative gamma source strengths for other fission products where all data points are normalised to the reference case given at time 0.5 h.

The relative gamma source strengths for noble gases are shown in Figure 8.3-1. As can be seen in the figure, the contribution from fuel fragments dispersal is of minor order. This is due to the assumption employed for the reference case where 100% release of noble gases is assumed to occur during early in-

vessel phase. Thus, the release of noble gases due to fuel fragments dispersal is already, implicitly, accounted for.

Figure 8.3-2 shows the relative gamma source strengths for halogens. The impact from fuel fragments dispersal for halogens is also of minor order as the reference case is assuming a release of 30% of the halogens up to the early in-vessel phase. The contribution from fuel fragments dispersal is roughly 1.2%. Also, as can be seen in the figure, a significant portion of the halogens have decayed to stable nuclides within 30-180 days as the halogens of importance from a radioactive perspective (Iodine and Bromine) have half-lives in orders of hours or days.

The relative gamma source strengths for other fission products are given in Figure 8.3-3. The figure shows that the fuel dispersal case has larger gamma source strength at time 0.5 h. This is due to the assumption employed for the fuel dispersal case where the release of fuel particles is assumed to occur at the initiation of the event. Thus, this data point should be excluded in the evaluation.

For the other data points in hour scale, the gamma source strengths for the reference case are larger than the gamma source strengths for the fuel dispersal case. This is due to the fact that the gamma source strengths, for the reference case, are dominated by alkali metal nuclides. The half-lives for these nuclides span the range from minutes to years, and due to their high solubility the reference case utilises a release fraction of 25% for these nuclides.

8.3.4 Conclusion

Fuel fragments dispersal has the potential to affect the radiation environment in the plant partly due to the increased gap inventory and partly due to more dissolvable fission products being released in the source terms from fuel fragments. Such increase in radiation environment can possibly impact both the radiation protection assessment and the environmental qualification of components.

Employing conservative assumptions regarding release and mobility of HBU fragments, it was shown that the gamma source strengths for noble gases and halogens for the fuel dispersal case are well lower than the reference case. For other fission products, the gamma source strengths are of the same order in the short time frame. However, for time beyond 7 days, the gamma source strength is higher for the reference case due to the conservative nuclide composition employed for the released fuel.

Fuel fragmentation also has an impact on the gap inventory as it is plausible that all gaseous radionuclides trapped in the pellets which are being fragmented to be released, and thereby contribute with an increase to the gap inventory.

The additional contributions from fuel fragments dispersal are the transuranium elements released in the case of fuel fragmentation and dispersion. These nuclides will not contribute significantly to the gamma source strength but are to large extent alpha emitters. For the fuel particles which reach the condensation pool, there is a possibility that they will be spread out in the containment due to the containment spray.

9. APPENDICES

9.1 Appendix: Development of high burnup structure during normal operation

In a Light Water Reactor (LWR) or a Heavy Water Reactor (HWR), resonance absorption of epithermal neutrons by ^{238}U occurs at pellet periphery due to the vicinity of the moderator. This results in an extra plutonium build-up, increasing with pellet burnup, on the pellet periphery.

The local burnup, hence the local fission product concentration, on the pellet periphery is therefore higher than in the centre of the pellet, the difference increasing with irradiation. Consequently, in a UO_2 pellet, a particular microstructure called HBS forms at the pellet periphery.

There are still some discussions about the formation mechanisms and it is not the purpose of this section to further discuss this point. Nevertheless, extensive HBU observations allow describing the main HBS characteristics. These have been well detailed in the literature [9.1-1], [9.1-2], [9.1-3], [3.1-16], [9.1-4], [9.1-5], [9.1-6], [9.1-7] with several synthesis of published work in [9.1-12], [9.1-20]. Only key points are recalled in this section.

With the increasing burnup and the moderate temperature on the rim area of the UO_2 fuels, fission products, point defects and dislocations accumulate in the grains. The average lattice parameter of the oxide also increases. The first clear change towards the formation of the HBS is the formation of planar defects [9.1-8], [9.1-9], [3.1-16]. Sub-micronic bubbles are then detected. Depending on the observations, these small bubbles can start along or around the grain boundaries or be found randomly spread over the grains. They are surrounded by sub-micronic round shape grains.

The formation of the HBS structure in commercial rods is reported to start at about 60 – 75 MWd/kgU (local burnup) [9.1-10], [9.1-11], [9.1-6] but some small variations around these values can be found in the literature, for different reasons:

- The High Burnup Rim Project⁷ proposed for UO_2 disks the threshold (presented in Figure 9.1-2) as a function of irradiation temperature and of local burnup (i.e. burnup in the periphery of the fuel pellet) [9.1-2]. The onset of restructuration has been found to occur between 51 and 55 MWd/kgU local burnup (very local HBS initiation, [9.1-12]). According to the experimental results derived from fuel wafers irradiation, fully restructured structure is observed at 73 MWd/kgU and the threshold for full restructuration is determined between 55 and 83 MWd/kgU. Nevertheless, the irradiation conditions and in particular the instantaneous fission density is 2 to 6 times higher in these fuel wafers than in a commercial PWR fuel rod [9.1-12]. This may promote HBS formation.
- Some authors use pellet average burnup rather than local burnup, which gives lower threshold values but may be consistent with the above mentioned 60–70 MWd/kgU local burnup [9.1-13], [9.1-3]. In this case, a formation threshold close to 30–40 MWd/kgU pellet average burnup with a significant extension of the HBS area above 65 MWd/kgU pellet average burnup can be derived from different measurements, which are consistent with the Lassmann equation [9.1-10].

In summary, there is a common agreement to define a conservative burnup threshold for HBS formation in commercial fuels around 60 MWd/kgU local burnup (30–40 MWd/kgU fuel pellet average

7. HBRP: irradiating 5mm diameter and 1mm thick UO_2 disks (25.8% ^{235}U enrichment) between Mo plates up to 96 MWd/kgU in the Halden reactor, with different irradiation temperatures

burnup), provided the local temperature stays below the HBS formation limit ($1\ 100^{\circ}\text{C}\pm 100^{\circ}\text{C}$ as proposed by HBRP programme [9.1-2] and consistent with other literature data).

The number of HBS bubbles increases gradually and, being continuously fed with fission gases, their size increases. Eventually, all the initial microstructure is replaced by a new microstructure made of small rounded grains surrounding inter-granular bubbles and polyhedral grains located in between [9.1-14]. These bubbles are not interconnected [9.1-4], [9.1-5]. At this stage, nowhere the Xe can be measured at its generation level at the scale of an EPMA quantitative analysis ($\sim 1\ \mu\text{m}^3$).

Fission gases are mainly located within the bubbles and Xe concentration outside the bubbles stabilises at a level between 0.1 and 0.2 wt% [9.1-22], [3.1-16]. Nonetheless, no major FGR can be directly associated with this HBS formation. The bubbles pressure in the HBS area has been estimated between 65 and 80 MPa at 377°C for UO_2 at 62 and 78 MWd/kgU pellet average burnup [3.1-16] (with an appropriate equation of state).

The lattice parameter of UO_2 is lower than it was immediately before the HBS restructuring [9.1-11]. HBS also exhibits metallic fission product precipitates and SIMS measurements show that the pores of the HBS contain part of the volatile fission products Te, Cs, I and Rb (and likely Br) [9.1-15].

This fully restructured HBS continues to evolve with burnup: porosity and bubble sizes increase with burnup while bubble density decreases. This mechanism results from bubble coalescence and maybe from ripening, [3.1-16], [9.1-5], [9.1-7].

Porosity reaches values between 10 and 15%. At the extreme periphery there can be an intertwining of HBS and internal zirconia (Figure 3.1-8).

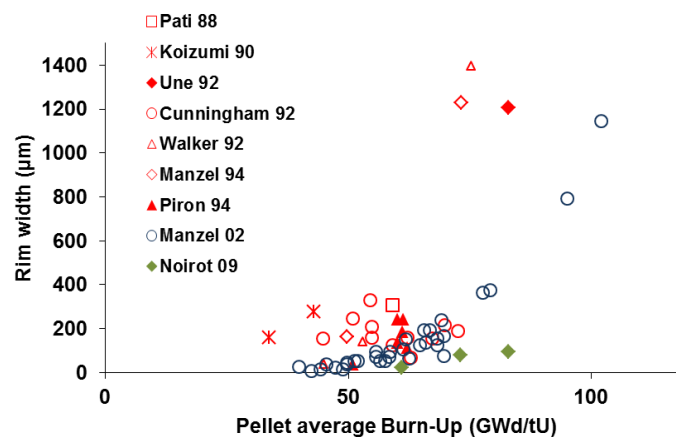


Figure 9.1-1: Penetration depth of the HBS in PWR fuel, from [9.1-16], [9.1-3] and [3.1-9]

The width of the HBS zone increases inwards with increasing burnup (see Figure 9.1-1) and may depend on the irradiation conditions (local temperature or fuel characteristics for instance). HBS extension between 70 and 300 μm have been observed on fuel irradiated up to 60 MWd/kgU (fuel pellet average burnup).

However, studies of the inwards extension with burnup of the HBS area (Figure 9.1-2) show higher and higher local burnups can be reached without a total HBS formation [9.1-17]. This can be linked to a combined effect of:

- a progressive decrease of the local fission density rates at the inner boundary of the HBS area, implying longer period of times for HBS formation

- a progressive decrease of the local Pu content in the inner boundary of the HBS area. As a matter of fact, if Pu content has an influence on the HBS formation, there is less and less Pu near the inner boundary of the HBS area despite the progressive build-up of Pu in the pellet periphery
- a progressive increase of the local temperatures at the HBS boundary as it progresses towards the pellet centre.

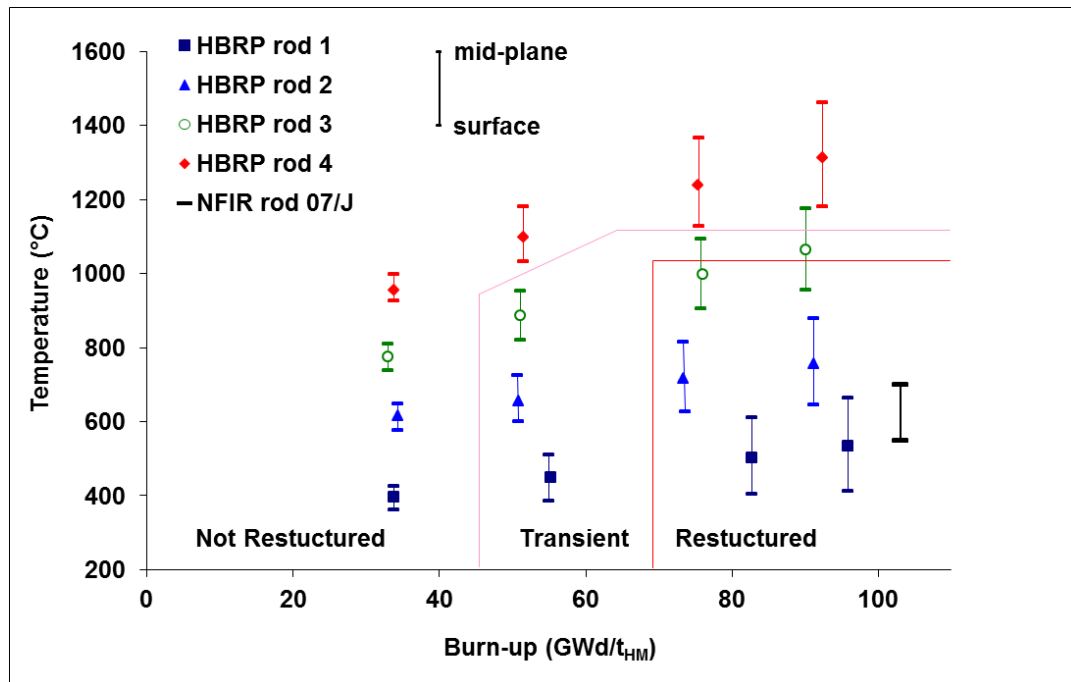


Figure 9.1-2: Restructuration threshold observed on the UO₂ disks irradiated in the HBRP, burnup and irradiation temperature of the 16 stacks of HBRP [9.1-2].

The error bars in Figure 9.1-2 represent the temperature difference between the surface and the centre of the discs, obtained by a finite element calculation.

Due to its heterogeneous and porous structure, thermal-mechanical properties of HBS are hard to determine, nevertheless the following properties can be underlined:

- HBS exhibits good deformation capabilities, illustrated by the interaction with the inner zirconia layer [3.1-16].
- Due to its high Pu content, its high fission product concentration or its high porosity HBS should exhibit a reduced local thermal conductivity as compared to non-HBS areas.
- As a matter of fact, this expected trend is counteracted by the gas and defects depletion and by the precipitation of metallic fission products.
- Thus, diffusivity measurements on fully restructured UO₂ discs in the HBRP programme showed that thermal conductivity degradation is not enhanced after restructuration [9.1-2], it might even have been improved [9.1-18].

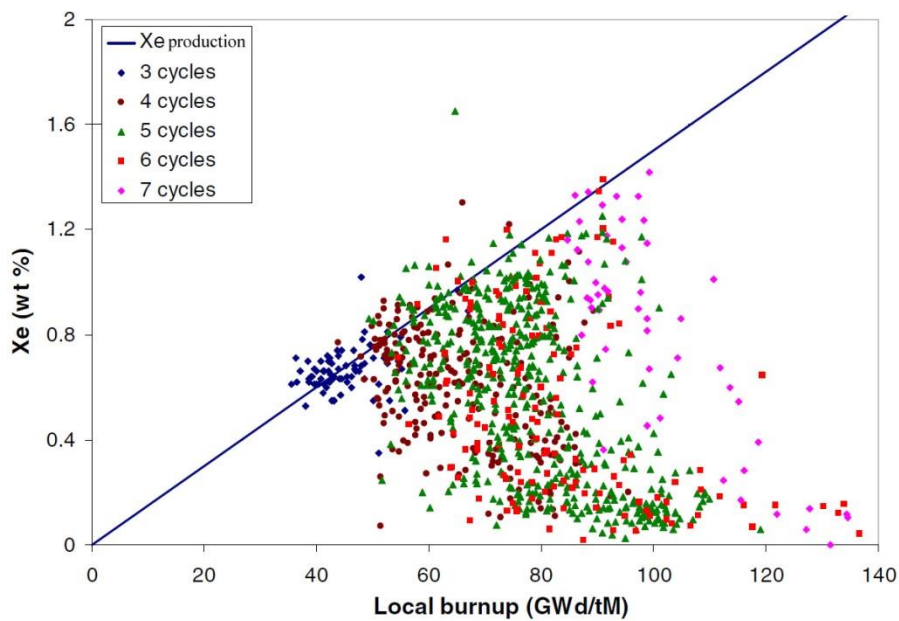


Figure 9.1-3: EPMA local Xe-detection versus local burnup in UO₂ fuel (4.5% ²³⁵U) [9.1-17]

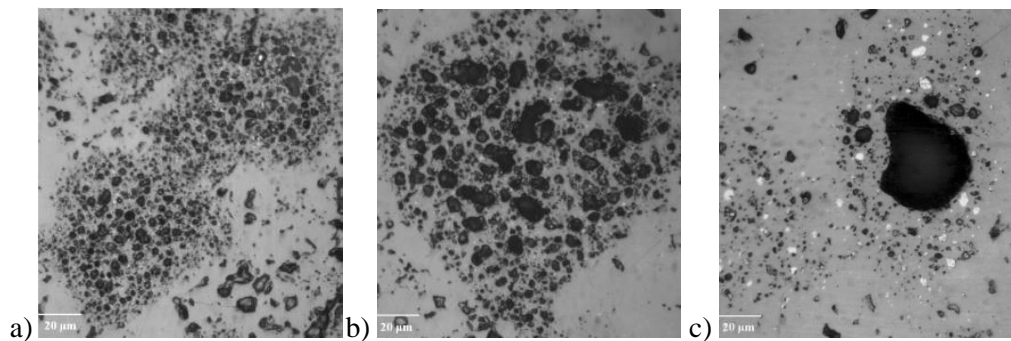


Figure 9.1-4: Optical micrograph of Pu rich agglomerates on a MOX MIMAS AUC after 55 GWd/t [3.1-13], a) periphery, b) mid radius, c) centre

For MOX fuel, the main differences with what has been observed for UO₂ are:

- The HBS structure is mainly localised in the (U,Pu)O₂ rich phases, as shown in Figure 9.1-4.
- The bubbles size increases with burnup and with temperature: in a 3 cycles MOX fuel pellet it has been observed that the bubbles size increases from the pellet periphery (1 to several µm) to mid-radius (about 5 to 10 µm) and to the centre (cavities >20 µm are observed in this area in the large Pu rich areas).
- The bubble density varies the opposite way [3.1-13].
- Since the average burnup reached in the UO₂ matrix of the MOX fuel pellet is lower than the pellet average burnup, a continuous HBS structure at pellet periphery doesn't appear until much later than in a standard UO₂ fuel [3.1-14].
- Due to fission product recoil after fission, the fission product build-up is not as high in small agglomerates (<~20 µm) than in larger ones, a great part of the fission products being implanted around the agglomerates.

- The boundary between HBS and non-HBS areas are usually well defined [3.1-16], but this may depend on the Pu concentration distribution.
- For the same pellet average burnup, the local burnup in the Pu-rich agglomerates can reach higher values than in a UO₂ fuel pellet peripheral zone: for instance local burnup as high as 180 MWd/kgU have been measured in Pu-rich agglomerates of a MOX pellet irradiated up to 57 MWd/kgU [3.1-16]. In some cases, local values up to 300 MWd/kgU have been observed. These high local burnups create larger bubbles within the Pu-rich agglomerates than within the UO₂ HBS rim (bubbles diameters > 10 μm have been observed in a 270 MWd/kgU local burnup Pu-rich agglomerate [3.1-16]).
- Due to higher irradiation temperatures and higher burnups, local porosities higher than 30% have been found in the Pu rich agglomerates.
- For a given Pu content in the master blend (i.e. for a given Pu content in the agglomerates), the lower the initial pellet average Pu content, the lower the fractional volume of Pu rich agglomerates and therefore the higher the burnup in the agglomerates for the same pellet average burnup [3.1-13].
- HBS formation starts for slightly lower local burnups in MOX fuels as compared to standard UO₂ but shows the same evolution with burnup [9.1-17], see Figure 9.1-5.
- The grain size in the restructured HBS zones varies from 0.6 μm at periphery to 2 μm at pellet mid-radius [3.1-13]. In the centre (at temperatures above 1 000°C), the grains sizes do not evolve, [3.1-13], [3.1-14].

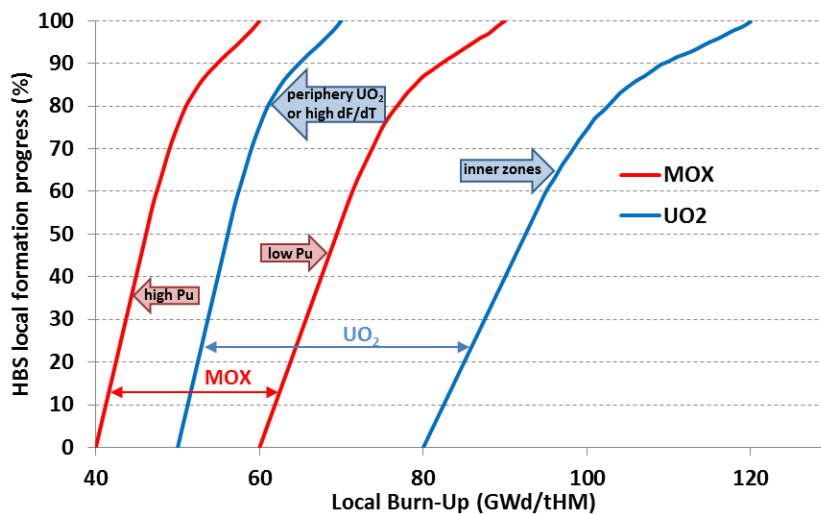


Figure 9.1-5: Local HBS restructuration rate versus local burnup for UO₂ and MOX) [9.1-17]

In summary, the parameters which promote HBS formation (and, for a given burnup, its extension) are:

- a high local burnup
- a high local Pu content
- a low ²³⁵U initial enrichment (leading to higher local Pu contents for a given burnup)

- a low irradiation temperature⁸
- a high instantaneous fission density [9.1-12]
- An initial large density of micrometric pores enhances grain subdivision at low temperature [9.1-12].

Some other parameters may have an impact on HBS formation and extension but the quantification of this impact or the nature of the mechanisms involved are still under discussion:

- Local stress field in the pellet periphery may play a role on HBS formation but no quantified threshold has been proposed in literature data.
- Grain size effect is not fully shared in the literature: Large grain size delays the HBS formation and reduces HBS width, [9.1-13], [9.1-19], but the effect is rather small below 25 μm grain size. Noirot et al. suggest that there is no direct impact of grain size on the HBS development [3.1-16] and that the observed effect could be linked to other parameters in relation with the specific fabrication processes.
- Additives effects on HBS formation is still questioned and likely depends on their nature [9.1-12]. The addition of alumino-silicates has been analysed in [9.1-20]: The authors showed that HBS formation is reduced in large grain fuels, with or without alumino-silicate additions. On the other hand, Baron [9.1-12], on specific fuel, has noticed that the use of chromium additives may accelerate the formation of HBS structure which may not be observed on commercial Cr_2O_3 -doped fuel. HBS formation seems to occur at lower local burnup in fuel rods containing Gadolinium, but this is compensated by the fact that Gadolinium fuel rods reach lower burnups than those of the surrounding standard UO_2 fuel rods. Also the amount of fission products generated in Gadolinium fuel is lower [9.1-21].

9.2 Appendix: Consideration of fuel cladding failures and FFRD in LOCA safety analyses in different countries

9.2.1 Belgium

In Belgium, the current final safety analysis report (FSAR) LOCA for all seven nuclear power plants use one of the following types of methodologies:

- Appendix K conservative methodology: Strictly follows the Appendix K requirements or follows only the mandatory Appendix K requirements. This method was developed and used since 1974 following 10CFR50.46 final acceptance criteria and Appendix K [9.2-47], and contains much arbitrary conservatism due to the lack of knowledge.
- SECY bounding methodology: Uses best estimate codes (with quantified code uncertainty or possible modifications according to Appendix K requirements) and conservative assumptions on the initial/boundary conditions. This method was developed and used since 1983 following SECY-83-472, and contains certain conservatism due to improved knowledge.
- CSAU best estimate plus uncertainty (BEPU) methodology: Uses best estimate codes and statistic combination of uncertainties in the initial/boundary conditions and the models. This method was developed and used since 1988 following 10CFR50.46 revision and RG-1.157, as

8. As shown in Figure 9.1-2 the maximum temperature under which HBS can appear and extent is around $1100^\circ\text{C} \pm 100^\circ\text{C}$ for the current burnups. This threshold is consistent with the former values derived from commercial rods PIEs (no restructuration above 1200°C). It is interesting to note that irradiation temperature usually does not modify the HBS morphology once HBS has been formed [9.1-2].

well as the recommended CSAU (code scaling, applicability, and uncertainty) methodology [9.2-48]. It contains little arbitrary conservatism due to the comprehensive understanding of ECCS performance through extensive research programme since 1970s.

The latest LOCA safety analyses were performed with best estimate plus uncertainty (BEPU) methodology, such as Westinghouse's ASTRUM (Automated Statistical Treatment of Uncertainty Method) [9.2-49].

The current applicable LOCA safety criteria in Belgium are the U.S.NRC's 10CFR50.46 final acceptance criteria established in 1974. The clad ballooning and burst models used by the fuel suppliers are mostly based on the NUREG-0630 model [7.2-11]. They are conservatively predicted to determine the flow blockage and oxidation content, however, no quantification of the fraction of the burst rods is needed, as all fuel rods are assumed failed in the radiological consequence calculations. The fuel fragmentation and consequent relocation is considered in the steady-state fuel rod calculation, but the relocation and dispersal during the LOCA heat-up transients are not considered. Some improvements have to be made to the codes and models for realistic simulation of relocation and dispersal [7.2-26].

Tractebel has performed some statistical uncertainty analysis on the FRAPTRAN simulation of the Halden LOCA tests IFA-650.5, in order to assess the capability of the FRAPTRAN code for predicting fuel behaviours under LOCA [9.2-50]. Those results showed the importance of the uncertainty analysis of the input parameters and the key models. The perspectives for further model improvements and benchmarks are also discussed.

9.2.2 Czech Republic

Currently the conservative approach is used when the LOCA relevant acceptance criteria (ECR, peak fuel and cladding temperatures and H production) are evaluated in Czech Republic, although the best estimate analysis were also performed and reported in the safety analysis for the recent Temelín NPP power uprate.

In the assessment of the radiological consequences it is conservatively assumed that 100% of the rods will fail and the quantification of fuel rod failures is not required. However, further fuel rod performance analyses are performed in order to show that the number of failures would be much smaller as a part of the ALARA case. These analyses are performed either by fuel vendors or by domestic organisations, depending on the decision of licensee.

Both calculations use the boundary conditions provided by the system analysis conservative from the ECR and PCT point of view. No direct coupling between fuel performance code and the system code has been used so far. Current vendor (TVEL) uses Rapta 5.2 code.

In order to assess the number of failed rods the system code (usually Relap5) calculation is performed for several channels with different power. Resulting cladding outside temperature is prescribed as a boundary condition to fuel performance code and the calculation is performed for each power for several burnup states. The number of the rods in the groups where the cladding failure is predicted is estimated by the census in typical equilibrium cycle.

UJV Řež uses FRAPTRAN or TRANSURANUS codes, the heat transfer coefficient and coolant conditions obtained from the system code are prescribed as a boundary condition. Fuel rod analysis is performed for several burnup states, at each burnup state the threshold linear heat rate at which the cladding failure is predicted is found. Obtained curve is used to estimate the number of potential failures in typical cycles and may be used to re-evaluate the number of failures if a different loading pattern is used.

Neither methodology (system code or fuel performance code analysis) used in the licensing process considers the effects of FFRD so far. On the other hand, Czech NPPs apply an operating limit restricting the LHGR of higher burnup fuel. It has been shown that with the current limit there is no possibility of ballooning of HBU rods, which seems to be a necessary condition for significant fuel relocation.

Nonetheless, R&D is ongoing to address this issue by both model development based on international programmes (HRP, SCIP III...) and by experiments performed at ÚJP Praha with the samples of the E110 cladding alloy variants used at the Czech NPPs (high temperature oxidation, burst tests...).

9.2.3 Finland

The Finnish nuclear safety authority (STUK) introduced various criteria to be fulfilled by fuel in accidental conditions. In particular, the maximum number of failed rods during a LOCA (class 2 accidents) must be lower than 10% to limit the release of radioactive substances and radiation doses [9.2-51].

To estimate the number of failed rods after a LOCA the analysis method must be either the conservative analysis method supplemented with sensitivity studies or the best estimate method supplemented with uncertainty analysis. Since the safety criteria has been established for conservative analysis methods, if a best-estimate method is used the result is acceptable if there is a 95% probability with 95% confidence that the examined parameter will not exceed the acceptance limit set for the conservative analysis method.

VTT has been developing since 2006 a new systematic tool to evaluate the number of ruptures, [9.2-52], [9.2-53]. The approach is a non-parametric statistical method, with the use of Wilk's formula to determine the minimum number of simulations needed to reach the probability content and confidence level required by the safety authority.

The simulation is made with the coupled codes FRAPTRAN (fuel performance) GENFLO (thermal-hydraulics) and power histories and thermal- hydraulic boundary conditions are obtained from the system code APROS.

Recent calculations related to a LBLOCA in an EPR-type nuclear power plant are described in Reference [9.2-52]. 59 global scenarios were considered with 1 000 rods simulated. In the worst case only 1.2% of the rods failed which meets the safety criteria of 10% (see Figure 9.2-1).

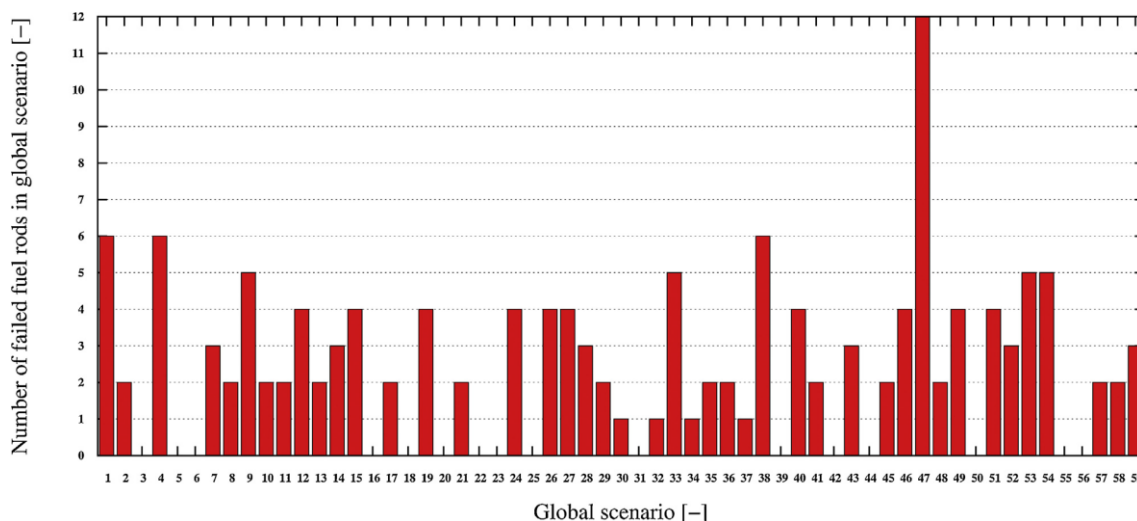


Figure 9.2-1: Numbers of the failed fuel rods among the 1 000 rods simulated in each of the 59 global scenarios from [9.2-52]

9.2.4 France

Two types of safety analyses concerning LOCAs are performed in France depending on the objective:

- demonstrate core coolability by verifying safety criteria such as a PCT and ECR

- evaluate radiological consequences by justifying fuel cladding failure rate criteria.

Regarding the first point, in the new French LOCA demonstration which will be first applied for the fourth 10-yearly safety review of EDF's 900 MWe nuclear reactors [9.2-54], the rulemaking review finalised in 2014 concluded that break sizes limited by pipe whip restraints define the reference transients, instead of the "doubled-ended guillotine break" [9.2-55].

Up to now, with regard to physical phenomena, FFRD was not taken into account. Also, during this rulemaking, the nuclear safety authority (ASN) asked the utility EDF to model the impact of fuel relocation in calculations performed by the CATHARE code to verify core coolability [9.2-56].

Fuel dispersal during LOCAs is not of safety concern in France with current core loadings and burnup limits, since rods with the highest burn ups would not reach high enough temperatures to lead to fine fuel fragmentation and fuel dispersal. However, additional experiments must be carried out to obtain data on MOX fragmentation behaviour during LOCAs [9.2-55].

Regarding the calculations of radiological consequences, during LOCAs the fuel cladding failure rate must not exceed 33% for plants operated by the utility EDF except for the EPR in construction in France for which the limit is 10%. For EPR, EDF brought elements to justify the value of 10% which is being assessed [9.2-57].

In practice, taking into account the composition and the burn up of fuel rods, EDF must calculate the maximum number of failed rods using the CATHARE code. Currently, the evaluation of fuel cladding failure rate is based on Intermediate Break (IB) LOCA for EPR and in Large Break (LB) LOCA for other EDF's PWR plants.

As an example, for EPR, the approach focusses on maximising the main transient parameters regarding rod failure occurrence (i.e. internal rod pressure and clad temperature) and on penalising the fuel cladding failure models in the CATHARE code. Thus, rupture criteria in this code are adapted from EDGAR models (stress criterion) [7.2-1] or NUREG-0630 curves (strain criterion) [7.2-11]. No rod rupture is predicted for EPR.

9.2.5 *Germany*

Beyond the well-known embrittlement criteria (limits for PCT and for equivalent cladding reacted) German regulation [9.2-58] also requires a failure rate analysis for a postulated LOCA whereby penalising assumptions (e.g. regarding single failure and repair case) related to safety level 3 (accidents) are demanded.

In a LOCA failure rate analysis the number of fuel rods in the core failing due to creep and burst is calculated and divided by the total number of rods in the core. In case of a small-break (0.1A break) the pertaining limit for the failure rate is 1% while for a large-break (2A break) it is 10%.

The safety goal originally related to the limitation of the large-break LOCA failure rate is to show compliance with the assumptions made in radiological analysis. However, in the context of the experimental results of recent LOCA tests a further aspect regained attention: By explicitly limiting the fraction of failed rods an implicit limit is imposed on the number of strained rods, thus, contributing to the safety goal of retaining core coolability.

As the large-break LOCA analysis reveals cycle-specific characteristics which are mainly related to the core loading patterns it is performed individually for each new cycle. The methodology currently applied for German PWRs is outlined below.

The methodology for a 0.1A break follows that for the large break, however, yields much lower cladding temperatures during the transient. Therefore, fuel rod burst can be practically precluded and the

small-break LOCA failure rate analysis can be performed in a generic manner with covering cycle-independent boundary conditions.

To determine the fuel rod failure rate during a postulated large-break (2A) LOCA the following accepted procedure in the German licensing and surveillances of PWR is used: a LOCA failure rate analysis is performed for each new fuel management plan (loading pattern), i.e. specific and realistic power histories for all fuel rods in the core are available. At certain time-points during the cycle (e.g. BOC and EOC) the nominal power distribution in the core is axially distorted to a top-peaked one (see Figure 9.2-2) which penalises the resulting failure rate. Thus, initial power distributions for the postulated LOCA transient are accounted for which may deviate from the nominal one but are still in accordance with the limits of the core surveillance system (I&C).

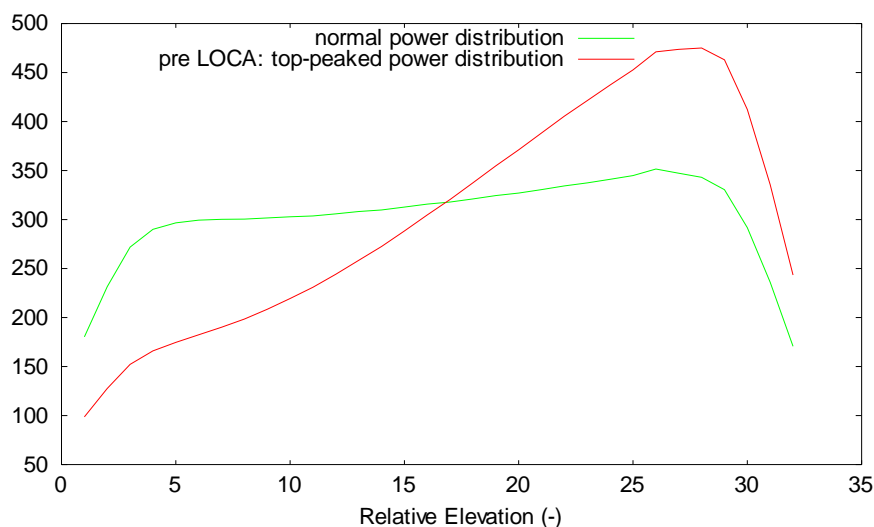


Figure 9.2-2: Example of assumed pre-LOCA axial power distortion in the core

The failure rate analysis consists of three parts:

- Generic determination of thermal-hydraulic boundary conditions for the failure rate analysis: Thermal hydraulic boundary conditions during the transient are determined by applying a system code such as S-RELAP5 or ATHLET to the LOCA scenario. In these calculations the core is partitioned in specific heat structures and thermal-hydraulic channels, e.g. a hot bundle hosting the hot rod, surrounding channels, break-through channels, etc. The result is a set of thermal-hydraulic boundary conditions for the hot rod comprising relevant time-dependent parameters (e.g. coolant pressure, stream-out rate, core flow rate and heat transfer coefficients) which is considered conservative regarding the hot rod's cladding temperature. Due to their sensitivity the resulting thermal-hydraulic boundary conditions for the hot are appropriately parametrised according to maximum LHGR of hot rod, power of hot bundle and burnup.
- Determination of fuel rods' conditions at LOCA initiation by a stationary fuel rod code: the individual power history of each fuel rod, its related rod specific input data set (geometrical, as fabricated and model parameter) and its pertaining power distribution provide the input to calculate the fuel rod condition at LOCA initiation by a stationary fuel rod code (e.g. CARO-E3, Transuranus).

Calculation of the fuel rod behavior during the hypothetical LOCA accident by a transient fuel rod code (heat-up code): for each fuel rod a bounding thermal hydraulic condition is selected, which covers the relevant parameters hot rod, power of hot bundle and burnup at LOCA initiation. The heat-up code (e.g. BETHY, TespaRod, Transuranus) resumes the rod condition at LOCA initiation from the stationary

code and determines the fuel rod behaviour during the transient under the cooling conditions imposed by the thermal hydraulic file. Thus, all relevant effects as occurrence of cladding creep (ballooning) and burst are calculated for each fuel rod under consideration of rod-specific data (e.g. fabrication data, material data, model parameter).

According to the appropriate choice of conservative boundary conditions for the single steps the methodology yields a conservative failure rate for the core is calculated for the large-break LOCA failure rate analysis. A typical graphical representation of the results is shown in Figure 9.2-3 where all rods in the core are depicted in a scheme maximum power of hot rod versus burnup and different symbols are used for failed and non-failed rods.

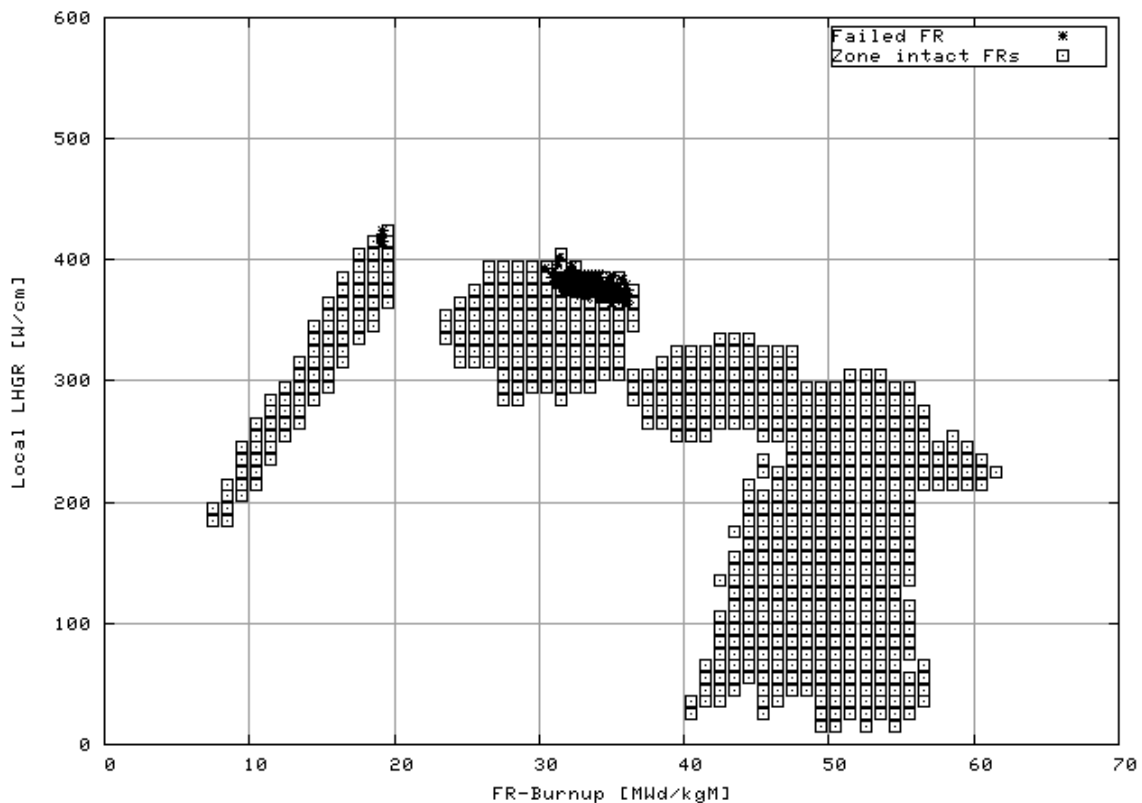


Figure 9.2-3: Exemplary results of a failure rate analysis.

9.2.6 Hungary

According to the Hungarian Nuclear Safety Regulation, the acceptance criteria for the safety analyses of Condition III and IV events [9.2-59] are such that the calculated dose of the reference population does not exceed 1 mSv and 5 mSv per event, respectively. The maximum extent and character of fuel failures have to be determined in order to comply with long-term cooling and handling requirements. No limit is set for the cladding rupture ratio.

As regards dose computations, up to the latest safety analyses 100% and 1% of the fuel rods were conservatively assumed to fail during a large-break and a small- or medium-break LOCA, respectively. However, a new methodology is under development to determine the cladding rupture during LOCA.

9.2.7 *Japan*

The following lines show how the cladding rupture is taken into account in safety analysis in Japan. Cladding temperature is predicted by the conservative deterministic analysis (the Westinghouse model [9.2-60] for PWRs and the GE model [9.2-61] for BWRs) with boundary conditions as calculation inputs. Cladding rupture condition is predicted by best fit rupture models based on experimental data.

Cladding high temperature burst test results are obtained to create best fit model curves (T , ϵ vs. ΔP). Since the effect of cladding burst is not one way effect on PCT but bidirectional effect, such as follows, best estimate curve is employed for the analysis.

- PCT decreases with increased gap between fuel and cladding.
- PCT increases as a result of formation of inner oxide layer.
- PCT increases as a result of poorer heat removal by coolant, caused by flow blockage by cladding burst.
- Circumferential and surface increases of the ballooned and ruptured cladding are calculated with the model, and the results are used in evaluations of PCT and ECR.

However, the “number” of ruptured cladding is not used in the safety analysis since the radioactive dose is evaluated assuming that all the fuel rods in the reactor fail and radioactive gases in the gap are released from the failed fuel rods. Therefore, there is no limit for the number of ruptured cladding in Japan. The influence of FFRD on the reactor safety is not currently taken into account. Therefore, there is no limit for the number of ruptured cladding in Japan.

9.2.8 *Republic of Korea*

Current LB LOCA analysis methodologies utilised for licensing application and also for audit calculation in Korea are based on the ‘best-estimate’ approach [9.2-62], [9.2-63]. In these methodologies, in conjunction with the thermal-hydraulic system code such as RELAP5, MARS-KS [9.2-64], SPACE [9.2-65], about twenty uncertainty parameters were considered.

In the codes the well-known fuel rod rupture model, which is described in NUREG-0630, was adopted, and cladding rupture related uncertainty parameters were also chosen as an independent uncertainty parameter. The cladding rupture criteria, described in NUREG-0630, were modelled as rupture temperature and rupture strain.

Typically cladding rupture phenomena combined with FFRD were not considered as a significant factor in LOCA safety analysis in Korea because the LOCA analysis was performed at the BOL fuel condition from a PCT point of view. In BOL condition fuel pellet is relatively intact and possibility of cladding rupture will be low due to the lower RIP.

Thereby, the criteria such as cladding rupture ratio in a core-wide perspective were not developed, specifically. But recently as the limiting fuel burnup for LOCA analysis moved from BOL to MOL due to the factorisation of thermal conductivity degradation of UO_2 fuel [9.2-66], the possibility of cladding ballooning and rupture, which potentially can result in flow blockage in hot assemblies, could be increased due to the increased RIP and fuel stored energy as well. But still the possibility of occurrences of FFRD in MOL fuel condition, and also within current licensing fuel burnup in Korea, 60 MWd/kgU (maximum rod average), seems to be insignificant.

In this context, for the maintenance of coolability, effects of flow blockage are being assessed by means of experimental and computer code analysis works. Some experimental works for the evaluation of rod heat transfer and cladding temperature change during LOCA period are under performing by simulating the ballooned bundle geometry [9.2-67].

The assessments of rod ballooning and burst in a core-wide perspective are planned with combining the system code and detailed fuel analysis code. Based on these results with other available research information, the necessity of new safety criteria will be discussed, if necessary.

9.2.9 Slovakia

The Slovak regulatory body (UJD SR) new decree issued in 2011 gives acceptance criteria on nuclear fuel damage for maximum Design Basis Accident without giving quantitative limits [9.2-68]. The criteria on cladding damage extent are deduced from acceptance criteria on radiological consequences. Radiological consequences must be carried out with a conservative evaluation of the calculated doses with defined assumptions [9.2-69].

VUJE performed calculations to quantify fuel rod cladding failure during a LOCA with RELAP5 and TRANSURANUS codes externally coupled [9.2-70]. The methodology was developed for VVER-440 reactors with a conservative approach consistent with licensing safety analyses.

The core was divided into twenty groups of fuel rods to reduce the number of thermo-mechanical analyses. The results of thermal-hydraulic calculations by RELAP5 were used as input data for the thermal-mechanic calculations by TRANSURANUS. The final step consisted in calculating the probability of fuel rod cladding failure by a statistical calculation based on Monte Carlo methods. The cladding outer temperatures were randomly varied with a uniform distribution. This methodology was applied to a LBLOCA on a cold leg in a VVER440/213 reactor.

9.2.10 Spain

In Spain, there are 7 Nuclear Power Plants from American design, and another one from German design. As Spanish regulation on radiological consequences of design basis accidents has not been developed, the plants follow mostly the regulation of the country origin of the technology.

So, for both Westinghouse and General Electric NPPs, different possibilities of 10CFR50.46 are used in different plants (from Appendix K to BEPU). Anyway, for all of them, no quantification of damaged rods is needed as far as the radiological consequences assume that all the rods leak.

On the other side, for German design plant, LOCA analysis assumes some conservatism (especially in initial power), but a realistic code is used to perform the analyses. Furthermore, German regulation accepts a maximum of 10% of damaged rods, so a calculation must be produced. This is achieved by a comparison between an upward scaled power for each rod in the core (to a level equivalent to some protection system setpoint), and a damage limit specific of the type of the cladding. This comparison is realised both at beginning and end of cycle. The actual results show a low number of damaged rods.

Related to Fuel Fragmentation, Relocation and Dispersion, nothing is required nowadays in Spain. Some scoping studies have been realised by some Spanish organisations, [7.2-34], [7.2-42].

9.2.11 Sweden

In Sweden the deterministic analysis of LOCA, with the aim to determine operating limits, is separated from the radiological consequence analysis. For example in reactivity initiated accidents (RIA) the connection is clearer. The overall objective with the LOCA-analysis is to show that the ECCS is capable to maintain a coolable core geometry. This is the general requirement for accidents in event class H4 Design basis accident (DBA), and no specific amount of fuel damage is determined neither by the authority nor by the licensees. Maintenance of coolable geometry is one of the acceptance criteria from NRC 10CFR50 Appendix K and is in practice shown by fulfilment of the requirement on PCT and maximum local oxidation.

The reactor designs in Sweden are of three different types; W 3-loop PWR, ABB BWR with internal main circulation pumps (MCP) and ABB BWR with external main circulation pumps and spray cooling. For the BWRs with internal MCPs, it can be demonstrated that LOCA scenarios which drain the reactor vessel can be prevented and no fuel damage occurs. For the BWRs with external pumps and for the PWRs this cannot be prevented and reactor specific analyses have to be performed in order to demonstrate fulfilment of acceptance criteria.

The LOCA-analyses submitted to the Swedish Radiation Safety Authority (SSM) represent two generations of evaluation models: analyses for BWR units and SB-LOCA for PWR units follow conservative Appendix K methods whereas LB-LOCA for PWR units are performed using a Best Estimate approach (CQD for Ringhals 2, ASTRUM for Ringhals 3 and RLB-LOCA for Ringhals 4).

Fuel cladding failure is included in all currently applied evaluation models of LB-LOCA however failure rates are not explicitly calculated since the acceptance criteria on PCT and maximum local oxidation reflects the situation for the highest worth rod. It is supposed that meeting the acceptance criteria for the highest worth rod implies verification for the rest of the core as well.

FFRD is today (2015) not considered in the submitted LOCA safety calculations, nor are detailed calculations of changes of fuel geometry. The radiological consequences are based on the amount of noble gases, iodine and other volatile fission products and do not include fragmented fuel.

Radiological consequence analyses are performed using two approaches; one conservative and one realistic. This is a requirement from SSM from 2009. The conservative approach is based on the U.S.NRC Reg guide 1 183 which provides assumptions for the source term and TEDE dose acceptance criteria to be met.

The conservative approach has been used by the utilities in SAR since the construction of the Swedish NPP, and was therefore kept and formalised in the SSM requirement from 2009. The realistic approach was added as a requirement for the assessment of radiological consequences, and one rationale for this was to provide assessments to the emergency preparedness at both SSM and the utilities. In the realistic approach there is no source term assumptions provided, and the licensee has to demonstrate realistic and “best-estimate” assumptions for these radiological consequence assessments.

During the application review by SSM for power uprates FFRD and changes in fuel geometry was one of the focus areas, as power increase was based on raising the load on all fuel rods and at the same time lowering the load on the highest worth rod, resulting in a situation with high load on many fuel rods.

Besides power uprates, FFRD is a focus area also with regards to high burnups and long time at high temperature. In 2014 the Swedish industry stated that current actual burnups are not in the range of significant fuel fragmentation.

9.2.12 Switzerland

The generic approach to safety licensing analysis of fuel behaviour during the LOCA was described in Reference [9.2-46], which still remains in force at present. From perspective of the regulator ENSI, safety analysis is acceptable if e.g. the criteria of Appendix K to 10CFR50.46 [9.2-47] are fulfilled.

As far as the cladding failure-related limitations are concerned, the new ENSI directive G20 [9.2-71] about the design and operation of the reactor core reads, specifically, that “The release of fuel into the coolant must be limited”. It is to be noted that, in Switzerland, there is no explicit limit for cladding failure ratio, like in Germany. The Swiss Radiation Protection Ordinance gives the limit indirectly by stating that the dose resulting from such an accident must not exceed 100 mSv for non-occupationally exposed persons. The worst single failure in the safety systems has to be assumed in the safety analysis (directive ENSI-A01 [9.2-72]).

In order to demonstrate compliance with the criteria, the operators must submit to ENSI detailed safety calculations performed by best-estimate codes with conservative initial and boundary conditions [9.2-71]. Detailed clad thermal-mechanical behaviour, such as cladding ballooning, however, may not be modelled within the licensing analysis, given a proper consideration is taken that the consequences of cladding swelling and rupture are not underestimated by the licensee. Conservatism of the appropriate system code analysis must thus be shown.

The Swiss Nuclear Energy Ordinance states that the licensee must check the applicability of new research results to his plant. Based on the Halden und Studsvik LOCA tests, ENSI asked the licensees for adequate statements. New analyses by the vendors based on actual core designs showed that the highest PCT appeared at low burnup and that there is a steep decrease of rod power between 45 and 55 MWd/kgU. Thus, above the critical burnup there would be weak deformation, nearly no relocation, and no burst. The answers were accepted by ENSI and no need for immediate action was identified if the NPPs keep their reactor core loading patterns.

9.2.13 United Kingdom

In U.K., the magnitude of the release from the fuel is based on modelling the FGR from a limiting fuel rod, experiencing the LOCA transient. The bounding LOCA source term evaluation is based on the assumption that 100% of the fuel rods fail.

The fuel rod model does not account for additional release as a result of high-burnup transient pellet fragmentation. This is because the LOCA calculation demonstrates that high-burnup fuel will not achieve sufficient cladding strain for the cladding to fail. Detailed calculations indicate that the actual value of failed rods would be substantially less.

The evaluation of PCT in large LOCA is performed using the WCOBRA/TRAC system code; employing a best-estimate plus uncertainty method. One of the quantified uncertainties is the effect of PCT of ballooning of the fuel cladding in hot fuel assemblies. This introduces cross flows, which are represented in the BART code [9.2-73]. BART represents the flow on the basis of single vapour phase and a multi-group droplet field (grouped to represent the dynamics of the droplet size distribution).

BART provides a penalty value to add to the PCT predicted by WCOBRA/TRAC. In some cases, BART has been replaced by the MATARE code this has a less detailed droplet model, but better represents the geometry [9.2-74].

The criteria are that the cladding should remain ductile and this is currently achieved by limiting the local total accrued metal loss; in operation and faults to 17% ECR and the PCT to 1 204°C.

Concerning fuel relocation, the UK regulator does not recognise the concept of an approved method of analysis and requires analysis methods to be justified for each application. However, the issue of fuel relocation was addressed as part of the licensing of Sizewell B.

Irradiated fuel with irradiation levels up to 35 MWd/kgU were tested by ballooning the cladding in a test rig designed to simulate the conditions of the reflood phase of a LBLOCA at Sizewell B. The relocation of the fuel pellets was observed by a X-ray source in combination with a video camera [9.2-75]. The fuel pellet stack was observed to remain largely intact until a diametric strain of approximately 50% was reached or the cladding burst. The subsequent pellet-fragment relocation resulted in filling ratios below 60% of the available volume in the balloon. These filling ratios were used in a detailed model of the heat transfer, using a ballooned geometry derived from a number of dynamic ballooning experiments on nuclear fuel; ballooning during the reflood phase of the transient.

The study indicated that the cladding temperature immediately above the balloon was reduced, while the temperature at the blockage was increased. The net effect on PCT was essentially neutral and therefore this sensitivity study justified omitting explicit consideration of the effect of axial relocation on PCT.

Subsequently, it has been noted that higher filling ratios linked to 'micro fragmentation' effects may be possible at very high burnups but this arises at burnups beyond the level permitted by the Safety Case.

9.2.14 United States of America

The NRC's regulatory framework for LOCA analysis is set forth in Title 10 of the US Code of Federal Regulations (10 CFR) part 50, Section 46 (50.46), "Acceptance Criteria for Emergency Core Cooling Systems for Light-Water Nuclear Power Reactors." LOCA analysis must be performed using an acceptable emergency core cooling system (ECCS) evaluation model (EM), and the regulation provides for two types of acceptable evaluation models.

The first, as set forth in 10 CFR 50.46(a)(1)(i), requires that the EM realistically describe the behaviour of the reactor system under the conditions of a postulated LOCA. Such models, which are interchangeably called realistic or best-estimate plus uncertainty (BEPU), rely on analytic methods that are based largely on knowledge obtained through experiments.

These methods require an expression of the confidence or certainty associated with the predicted results. The regulation specifies neither how these EMs must be developed, nor what features they must contain. An approach acceptable to the NRC is delineated in NUREG/CR-5249, "Quantifying Reactor Safety Margins: Application of Code Scaling, Applicability, and Uncertainty Evaluation Methodology to analysis of a Large-Break Loss of Coolant Accident Analysis."

The second, as provided by 10 CFR 50.46(a)(1)(ii), may be based on the required and acceptable features set forth in Appendix K to 10 CFR 50. These models are generally understood to be significantly more conservative than the realistic EMs. Appendix K EMs must incorporate analytic methods that are specified in 10 CFR 50 Appendix K, such as the use of the ANS 1 979 decay heat standard with a 1.2 multiplier. Appendix K models may also use an approach delineated in SECY 83-472. Such evaluation models retain the required and acceptable features established in Appendix K, but also implement more realistic analytic elements, including an uncertainty analysis.

Typically, with very few, if any, exceptions, fuel vendors provide ECCS evaluations.

There are roughly 10 NRC-approved, Appendix K-based ECCS EMs in use today; three for BWRs and the remainder for PWRs. The NRC has also approved three realistic ECCS EMs. In addition, the NRC staff is currently reviewing two new realistic ECCS EMs, and a revision to a currently approved, realistic EM.

Typically, BWRs are analysed using Appendix K-conformant methods; however, at the time of the publication of this report, at least one realistic ECCS EM, applicable to BWRs, was under NRC staff review.

The PWR fleet has a more diverse set of evaluation models in use. Plants designed by Combustion Engineering (CE) and Westinghouse may use one of several different ECCS EMs; each type of plant has at least one Appendix K and one realistic evaluation model that is approved and applicable to it. The NSSSs designed by Babcock and Wilcox (B&W) are analysed using the AREVA-furnished BWNT-LOCA EM. The NRC has not approved any other analytic methods for application to B&W plants.

Realistic methods rely on various techniques to determine results and quantify uncertainty. Two examples include simulating a large number of trials using a response surface technique, and using non-parametric statistical analysis.

The response surface serves as a CPU-time-saving surrogate for actual analysis, such that Monte-Carlo methods can be used to simulate thousands of trials. From these trials, upper tolerance limits can be identified for the figures of merit. This process is accomplished by determining and applying adders to nominal results to express an upper tolerance limit.

Other methods, by contrast, may rely on non-parametric statistics. These models use actual computational simulation of a fixed, but usually lower, number of run sets. The run sets use randomly varied plant and model uncertainty parameters. Results are chosen from among the worst cases from the run set to serve as an indicator of the upper tolerance limit. The number of run sets for a non-parametric statistical analysis may be determined using an order statistics approach such as Wilks's theorem.

Since the required and acceptable features contained in 10 CFR 50 Appendix K are rather prescriptive, there tends to be a lot of commonality among the Appendix K methods. Separate codes tend to be used for different analyses. For example, the blowdown phase of the LOCA may be analysed using one code, while to refill and reflood stages may be analysed with a separate code. In addition, a system analysis may be performed with one code, while a hot bundle heat-up analysis is performed using a separate code, which relies on boundary conditions supplied by the system code.

Due to the requirements for conservatism in the decay heat modelling, Appendix K analyses tend to be dominated more by core decay heat than initial stored energy, and in an Appendix K analysis, the PCT tends to occur after the blowdown as a result.

Most vendors supplying ECCS EMs to the domestic fleet are transitioning to realistic methods, and licensees are similarly transitioning; the number of licensees relying on Appendix K EMs has decreased significantly since the first realistic methods were approved.

In both Appendix K and realistic EMs, fuel rod rupture should be considered in the analysis, but there are not set limits on the number of fuel rods allowed to fail. In fact, radiological consequence calculations are required to assume that all the fuel rods in the core have failed and that all the noble gasses and half of the iodine in the gap are released, per Regulatory Guide 1.19 [9.2-76].

Most EMs use the rupture model described in NUREG-0630, consisting of an engineering stress to failure as a function of temperature. Similarly, the cladding plastic hoop strain at the rupture node (also referred to as the balloon strain) is typically tabulated based on data and correlations from NUREG-0630.

The regulations specify that ECR should account for double-sided high-temperature steam oxidation for fuel rods that are predicted to rupture. Furthermore, the wall thickness of the cladding that is used in the ECR calculation must be adjusted to take into account the balloon strain for ruptured fuel rods before significant oxidation.

Fuel rods that do not rupture are usually not assumed to have ballooned for the purposes of cladding oxidation calculations, and thus no ECR correction is made for those rods to account for balloon strain. This is deemed acceptable because fuel rods that do not rupture are not considered limiting fuel rods, and they do not correspond to the peak ECR rods, even if applying a factor of two on ECR.

Some EMs take into account the effect of fuel axial relocation due to fuel rod ballooning, though this is not the case for all EMs, and arguments have been made to support the hypothesis that fuel relocation in the ballooned region is not detrimental, because the filling ratio of the fuel is low and the ballooned region has enhanced heat transfer due to the 'fin' effect, as well as a larger heat exchange surface.

Fuel dispersal is never taken into account in the ECCS EMs approved in the U.S., and there is currently no requirement for the EMs to take this phenomenon into account.

9.2.15 Summary table

This section was dedicated to fuel failures estimations in safety analyses and to FFRD impact consideration. Table 9.1-1 summarises the various approaches described above.

Country	Failed rod rate for radiological assessment	FFRD modelling in safety analyses
Belgium	100%	NO
Czech Republic	100%	NO
Finland	10%	NO
France	EPR 10% (proposed) Other PWRs 33%	Currently not taken into account. Relocation will be (from 2017) considered in coolability analyses (ECR and PCT calculations) except for the EPR.
Germany	SB LOCA 1% LB LOCA 10%	NO
Hungary	SB and MB LOCA 1% (changing) LB LOCA 100% (changing)	NO
Japan	100%	NO
Republic of Korea	No explicit limit	NO
Slovakia	No explicit limit	NO
Spain	100% for American design NPPs 10% for the German design NPP	NO
Sweden	No explicit limit	NO
Switzerland	No explicit limit	NO
U.K.	100%	NO
U.S.A.	100%	NO

Table 9.1-1: Fuel failure rate considered in radiological assessment and FFRD consideration in safety analyses

REFERENCES

- [2.1-1] W. Wiesenack, L. Kekkonen, B Oberländer. "Axial gas transport and loss of pressure after ballooning rupture of high burnup fuel rods subjected to LOCA conditions", Physor 2008, Interlaken, Switzerland, 2008
- [2.1-2] Reimann, M., "Analytische Untersuchungen von Gasströmungen in Ringspalten beim Aufblähvorgang von Zirkaloy-Hüllrohren; Kernforschungszentrum Karlsruhe", Projekt Nukleare Sicherheit, KFK 2280, 1976.
- [2.1-3] Dagbjartsson, S. et al., "Axial gas flow in irradiated PWR fuel rods"; TREE-NUREG-1158,
- [2.1-4] G. Khvostov, M.A. Zimmermann, W. Wiesenack, G. Ledergerber, "Some insights into the role of axial gas flow in fuel rod behaviour during the LOCA based on HRP experiments and results of calculation by FALCON coupled with the FRELAX model", EHPG Meeting, Storefjell, 2010
- [2.2-1] M. Flanagan, (2012), "Mechanical behavior of ballooned and ruptured cladding", NUREG-2119
- [2.2-2] P. A. C. Raynaud, (2012), "Fuel Fragmentation, Relocation, and Dispersal during the Loss-of-Coolant Accident", NUREG-2121
- [2.2-3] M. Flanagan, P. Askeljung and A. Puranen, "Post-Test Examination Results from Integral, High-Burnup, Fuelled LOCA Tests at Studsvik Nuclear Laboratory", NUREG-2160, August 2013
- [2.2-4] P. Askeljung, J. Flygare, J. Martinsson, "NRC LOCA testing program at Studsvik, results on high burnup fuel", 2011 Water Reactor Fuel Performance Meeting, Chengdu, China, Sept. 11-14, 2011
- [2.2-5] M. Helin and J. Flygare, (2011), "NRC LOCA tests at Studsvik. Design and construction of test train device and tests with unirradiated cladding material", Studsvik Report N-11/130. Link <http://pbadupws.nrc.gov/docs/ML1221/ML12215A431.pdf>
- [2.2-6] M. Flanagan, B. C. Oberländer, A. Puranen, (2013), "Fuel Fragmentation, Relocation and Dispersal under LOCA Conditions: Experimental Observations", TopFuel 2013, Charlotte, North Carolina, September 15-19, 2013
- [2.2-7] P. Askeljung, J. Flygare, D. Minghetti, (2012), "NRC LOCA Testing Program at Studsvik, Recent Results on High Burnup Fuel", TopFuel 2012, Manchester, UK, September, 2012
- [2.2-8] A. Puranen, M. Granfors, P. Askeljung, D. Jädernäs, M. Flanagan, (2013), "Burnup Effects of Fine Fuel Fragmentation in Simulated LOCA Testing", TopFuel 2013, Charlotte, North Carolina, September 15-19, 2013
- [2.2-9] Ken. H. Yueh, N. Snis, D. Mitchell, and C. Munoz-Reja, (2014), "Fuel Fragmentation Data Review and Separate Effects Testing", Proceedings of WRFPM 2014, Sendai, Japan, Sep. 14-17, 2014
- [2.3-1] M. Bruet, J.C. Janvier, FLASH Experiments in SILOE Reactor; Fuel Rod Behaviour During LOCA Tests, OECD-NEA-CSNI/IAEA Specialists' Meeting on Water Reactor Fuel Safety and Fission Product Release in Off-Normal and Accident Conditions, Risø, 1983.

- [2.3-2] M. Bruet, C. Lemaignan, J. Harbottle, F. Montagnon, G. Lhiaubet, High burnup fuel behavior during a LOCA type accident: The FLASH 5 experiment. IAEA technical committee meeting: Behaviour of core materials and fission product release in accident conditions in LWRs Aix-en-Provence, 1992; Vol. TECDOC-706.
- [2.3-3] Y. Pontillon, M.P. Ferroud-Plattet, D. Parrat, S. Ravel, G. Ducros, C. Struzik, I. Aubrun, G. Eminet, J. Lamontagne, J. Noirot, A. Harrer, Experimental and theoretical investigation of fission gas release from UO₂ up to 70 GWd/t under simulated LOCA type conditions: the GASPARD program International Meeting on LWR Fuel Performance, Orlando, 2004; pp 490-499, Paper 1025.
- [2.3-4] Y. Pontillon, D. Parrat, M.P. Ferroud-Plattet, S. Ravel, G. Ducros, C. Struzik, A. Harrer, Fission gas release from high burnup UO₂ fuels under simulated out-of-pile LOCA conditions. Proceedings of the technical committee meeting: Advanced fuel pellet materials and designs for water cooled reactors, Brussels, 2003; Vol. IAEA-TECDOC-1416, pp 187-204.
- [2.3-5] M. Marcet, Y. Pontillon, L. Desgranges, J. Noirot, J. Lamontagne, I. Aubrun, B. Pasquet, C. Valot, H. Cognon, P. Blanpain, Contribution of High Burnup Structure to fission gas release under transient conditions. Proceedings of Top Fuel 2009, Paris, France, Paper 2055.
- [2.3-6] J. Noirot, C. Gonner, L. Desgranges, Y. Pontillon, J. Lamontagne LWR fuel gas characterization at CEA Cadarache LECA-STAR Hot Laboratory; 2009; IAEA-TECDOC-CD-1635
- [2.3-7] J. Noirot, Y. Pontillon, S. Yagnik, J.A. Turnbull, T. Tverberg, Fission gas release behaviour of a 103 MWd/kgHM fuel disc during a 1200°C annealing test, Journal of Nuclear Materials 446: 163-171, 2014
- [2.3-8] J. Noirot, Y. Pontillon, S. Yagnik, J.A. Turnbull, Post-Irradiation Examinations and High-Temperature Tests on Undoped Large-Grain UO₂ Discs, Journal of Nuclear Materials, 2015
- [2.3-9] M. Marcet, Y. Pontillon, L. Desgranges, D. Simeone, I. Aubrun, I. Felines, L. Brunaud, In situ Characterization of UO₂ Microstructure Changes During an Annealing Test in an Environmental Scanning Electron Microscope. MRS 2009 Proceedings, 1215, 2009.
- [2.3-10] M. Marcet. Etude de la fragmentation mécanique de la structure à haut taux de combustion des combustibles irradiés (rim) en traitement thermique. PhD Thesis, Université d'Aix-Marseille II, CEA, 2010
- [2.3-11] J. Noirot, I. Aubrun, L. Desgranges, K. Hanifi, J. Lamontagne, B. Pasquet, C. Valot, P. Blanpain, H. Cognon, High Burnup Changes in UO₂ fuels irradiated up to 83 GWd/t in M5 Claddings, Nuclear Engineering and Technology 41: 155-162, 2009
- [2.3-12] J. Noirot, Th. Blay, X. Pujol, J. Lamontagne, L. Fayette, Radial origin of fragments formed during a fast 1200 °C heating test of a 83 MWd/kgU UO₂ fuel, LOCA Workshop, Aix-en-Provence, France 2015.
- [2.4-1] Narukawa, T., et al., “Ballooning and rupture behavior of Zircaloy-4 cladding under transient-heating conditions”, WRFPM 2014, Sendai, Japan, 2014.
- [2.4-2] Nagase, F., et al., “Behavior of High Burnup Fuel Cladding under LOCA Conditions“, Journal of Nuclear Science and Technology, Vol. 46, No. 7, p.763–769, 2009.
- [2.4-3] V.I. Kuznetsov et al., “Researches of VVER high burnup fuel behavior under LOCA conditions”, Halden Reactor Project LOCA Workshop, Aix en Provence, France, May 20-21st 2015.

- [3.1-1] A. Puranen, "A Review of Recent FFRD Investigations at Studsvik", presentation at the Halden Reactor Project LOCA Workshop, Aix en Provence, France, May 20-21st 2015.
- [3.1-2] B. C. Oberlander, H. K. Jenssen and M. Espeland, "PIE results from the high burnup (83MWd/kg) PWR segment after LOCA testing in IFA 650-5," Loen, Norway, 2008.
- [3.1-3] G. Ledergerber, "HWR-1033: Characterization of KKL BWR Fuel for Test Series in IFA-610, IFA-629 and IFA-650," IFE, Halden, Norway, 2013.
- [3.1-4] B. C. Oberlander and H. K. Jenssen, "HWR-925: PIE results from the low burnup (~44 MWd/kgU) BWR segment after LOCA testing in IFA-650-7," IFE, Halden, Norway, 2011.
- [3.1-5] M. Billone, Y. Yan, T. Burtseva and R. Daum, "Cladding Embrittlement During Postulated Loss-of-Coolant Accidents, NUREG/CR-6967," USNRC, Washington, DC, USA, 2008.
- [3.1-6] M. Flanagan et al., "Fuel fragmentation, relocation and dispersal under LOCA conditions: experimental observations", TopFuel 2013, Charlotte, North Carolina, September 15-19, 2013.
- [3.1-7] A. Puranen, M. Granfors, P. Askeljung, D. Jädernäs, M. Flanagan, "Burnup Effects of Fine Fuel Fragmentation in Simulated LOCA Testing", TopFuel 2013, Charlotte, North Carolina, September 15-19, 2013.
- [3.1-8] P. Guedeney, M. Trotabas, M. Boschiero, C. Forat: Standard PWR fuel rod characterization at high burnup. International topical meeting on LWR fuel performance, Avignon, France, (1991).
- [3.1-9] J. Noirot, I. Aubrun, L. Desgranges, K. Hanifi, J. Lamontagne, B. Pasquet, C. Valot, P. Blanpain, H. Cognon, Nuclear Engineering and Technology 41: 155-162, (2009)
- [3.1-10] J Noirot et al.: Fission Gas Inventory in PWR High Burnup Fuel: Experimental Characterization and Modeling, Proceedings of the Light Water Reactor Fuel Performance Meeting (Top Fuel) 2004, Orlando, Florida, September 19-22.
- [3.1-11] J. Noirot, C. Gonnier, L. Desgranges, Y. Pontillon, J. Lamontagne LWR fuel gas characterization at CEA Cadarache LECA-STAR Hot Laboratory; IAEA-TECDOC-CD-1635,(2009).
- [3.1-12] H. Stehle, Performance of oxide nuclear fuel in water-cooled power reactors Journal of Nuclear Materials 153: 3-15, (1988)
- [3.1-13] Guérin, Y., et al.: Microstructure evolution and in-reactor behaviour of MOX fuel, Light Water Reactor Fuel Performance (Proc. ANS Int. Top. Mtg Park City, 2000), American Nuclear Society, La Grange Park, IL (2000) p. 706–719.
- [3.1-14] M. Lippens, et al.: Highlights on R&D work related to the achievement of high burnup with MOX fuel in commercial reactors. International Symposium on MOX Fuel Cycle Technologies for Medium and Long Term Deployment. Vienna Austria, May 1999.
- [3.1-15] L. Desgranges: Internal corrosion layer in PWR fuel, Proceedings of seminar « Thermal Performance of High Burnup PWR Fuel », OCDE IAEA (1998) p. 187-196.
- [3.1-16] J. Noirot, L. Desgranges, J. Lamontagne: Detailed characterisations of high burnup structures in oxide fuels, Journal of Nuclear Materials, 372 (2008), p. 318-339.
- [3.1-17] B. Petitprez, et al., "No clad lift-off criterion and associated methodology developed by EDF and FRAMATOME-ANP on the basis of IFA-610 experiments", paper F5-13, proceedings of the EHPG, Lillehammer, October 2005.

- [3.1-18] K. Tanaka et al.: Fuel – cladding chemical interaction in MOX fuel rods irradiated to high burnup in an advanced thermal reactor, *Journal of Nuclear Materials* 357 (2006), p. 58–68
- [3.1-19] J. Lamontagne, C. Eysseric, L. Desgranges, C. Valot, J. Noirot, T. Blay, I. Roure, B. Pasquet, Study of structural material resulting from the nuclear fuel cycle using SEM-WDX, EPMA and SIMS techniques, *Microchimica Acta* 161: 355-362, 2008.
- [3.1-20] W. Wiesenack, “Summary of HRP IFA-650 LOCA experiments with respect to FFRD”, Halden Reactor Project LOCA Workshop, Aix en Provence, France, May 20-21st 2015.
- [3.1-21] J. Noirot et al., “Size and radial origin of fragments formed while heating a 83 MWd/kgU PWR fuel up to 1200 °C”, Halden Reactor Project LOCA Workshop, Aix en Provence, France, May 20-21st 2015.
- [3.1-22] J.A. Turnbull, “An Investigation into Fuel Pulverization with Specific Reference to High Burnup LOCA”, Halden Reactor Project LOCA Workshop, Aix en Provence, France, May 20-21st 2015.
- [3.1-23] C. Struzik et al., “LOCA test IFA 650 analysis through the fuel state at the end of base irradiation and its thermo-mechanical behaviour during the experiment”, Presentation at the EHPG 2014, Roros, Norway, Paper F3.4.
- [3.1-24] Y. Pontillon et al., “Experimental and theoretical investigation of fission gas release from UO₂ up to 70 GWd/t under simulated LOCA type conditions: the GASPARD program”, International Meeting on LWR Fuel Performance, Orlando, 2004, pp 490-499, Paper 1025.
- [3.1-25] JP. Hiernaut et al., “Fission product release and microstructure changes during laboratory annealing of a very high burnup fuel specimen », *Journal of Nuclear Materials*, 377, 2008, p. 313-324.
- [3.1-26] F. Sontheimer, H. Landskron: Puzzling features of EPMA radial fission gas release profiles: the key to realistic modelling of fission gas release up to ultra-high burnup of 100MWd/kgM with CARO-E; Nuclear fuel behaviour modelling at high burnup and its experimental support, Proceedings of a Technical Committee meeting held in Windermere, United Kingdom, IAEA-TECDOC-1233 (2000).
- [3.1-27] C. Gibert: Influence de l'irradiation et de la présence de lithium sur la nature cristallographique de la zircone dans le cadre de l'étude de la corrosion du Zircaloy 4 en milieu réacteur à eau pressurisée. Ecole Centrale Paris, CEA-R-5848 1998.
- [3.1-28] K. Nogita et al., Formation of Pellet-Cladding Bonding Layer in High Burnup BWR Fuels, *Journal of Nuclear Science and Technology*, Vol. 34, No. 7 (1997), p. 679-686.
- [3.2-1] K. Yueh et al, “Fuel Fragmentation Data Review and Separate Effects Testing”, Proceedings of WRFPM 2014 Sendai, Japan, Sep. 14-17, 2014 Paper No. 100117
- [3.3-1] J. A. Turnbull et al., “An Assessment of the Fuel Pulverization Threshold during LOCA Type Temperature Transients,” *Nuclear Science and Engineering*, vol. 179, Apr 2015, 477-485.
- [3.3-2] J. Bertsch et al., “(High) burnup microstructural changes”, Halden Reactor Project LOCA Workshop, Aix en Provence, France, May 20-21st 2015.
- [3.3-3] K. Nogita, K. Une “ High resolution TEM observation and density estimation of Xe bubbles in high burnup UO₂ fuels”, *Nuclear Instruments and Methods in Physics Research B* 141, 1998,481-486.
- [3.3-4] L.E. Thomas in: S.E. Donnelly, J.H. Evans (Eds.), *Fundamental Aspects of Inert Gases in Solids*, Plenum Press, New York, 1991, p. 431.

- [3.3-5] C. Esnoul et al., “Use of a micromechanical approach to investigate transient fuel fragmentation mechanisms”, Halden Reactor Project LOCA Workshop, Aix en Provence, France, May 20-21st 2015.
- [3.3-6] A. Bianco et al.,” Experimental Investigation on the Causes for Pellet Fragmentation under LOCA Conditions”, Journal of Nuclear Materials (2015) to be published.
- [4.1-1] M. Reocreux, E. F. Scott de Martinville; “A Study of Fuel Behavior in PWR Design Basis Accident: An Analysis of Results from the Phebus and EDGAR Experiments”; Nuclear Engineering and Design 124 (1990), 363-378
- [4.1-2] E. Kolstad et al.; ”High burnup fuel behaviour under LOCA conditions as observed in Halden experiments”; IAEA technical meeting on fuel behaviour and modelling under severe transient and LOCA conditions; Mito, Japan, 18-21 October 2011
- [4.1-3] F. J. Erbacher, S. Leistikow; “A Review of Zircaloy Fuel Cladding Behavior in a Loss-of-Coolant Accident”; KfK 3973, September 1985
- [4.1-4] CSNI Report on Benchmark calculations on Halden IFA-650 LOCA test results, November 2010, NEA/CSNI/R(2010)6
- [4.1-5] T. Erbacher, H. J. Neitzel, K. Wiehr; "Studies on Zircaloy Fuel Clad Ballooning in a Loss-of-Coolant Accident - Results of Burst Tests with Indirectly Heated Fuel Rod Simulators". Proceedings of the Fourth International Conference on Zirconium in the Nuclear Industry, Stratford-upon-Avon, England, June 1978, ASTM-STP 681, pp. 429-446
- [4.1-6] M. E. Flanagan, P. Askeljung, A. Puranen; “Post-Test Examination Results from Integral, High-Burnup, Fueled LOCA Tests at Studsvik Nuclear Laboratory”; NUREG-2160, August 2013
- [4.1-7] G. Khvostov, W. Wiesenack, M.A. Zimmermann, G. Ledergerber; “Some insights into the role of axial gas flow in fuel rod behaviour during the LOCA based on Halden tests and calculations with the FALCON-PSI code”; Nuclear Engineering and Design 241 (2011) 1500–1507
- [4.1-9] C. Struzik, V. Blanc, A. Cabrera, V. Garat. “LOCA tests IFA 650 analysis through the fuel state at the end of base irradiation and its thermo-mechanical behaviour during the experiment”. EHPG meeting, 8-12 september 2014
- [4.1-10] M. Le Saux, V. Vandenberghe, P. Crébier, J.C. Brachet, D. Gilbon, J.P. Mardon, P. Jacques, A. Cabrera. “Influence of steam pressure on the high temperature oxidation and post-cooling mechanical properties of Zircaloy-4 and M5™ cladding (LOCA conditions)”. 17th International Symposium on Zirconium in the Nuclear Industry, February 03-07, 2013, Hyderabad, India
- [4.1-11] Carl Adamsson, “Modelling pressure and temperature in reference test” SCIP III meeting oral presentation. January 2015.
- [4.1-12] Tony Glantz “Deformation and Reflooding of a rod Assembly during a Loss of Coolant Accident”. EHPG meeting. 10 au 15 mars 2013.
- [4.3-1] NEA (2010), CSNI Report on “Safety Significance of the Halden IFA-650 LOCA Test Results”, NEA/CSNI/R(2010)5.
- [5.1-1] Patrick A.C. Raynaud, “Fuel Fragmentation, Relocation, and Dispersal during the Loss-of-Coolant Accident”, NUREG-2121, 2012

- [5.1-3] Michelle E. Flanagan, Peter Askeljung, Anders Puranen, “Post-Test Examination Results from Integral, High-Burnup, Fueled LOCA Tests at Studsvik Nuclear Laboratory”, NUREG-2160, 2013
- [5.1-4] § 50.46 Acceptance criteria for emergency core cooling systems for light-water nuclear power reactors, NRC Regulations 10 CFR, <http://www.nrc.gov/reading-rm/doc-collections/cfr/part050/part050-0046.html>
- [5.1-6] G. Khvostov, W. Wiesenack, B.C.Oberländer, E. Kolstad, G. Ledergerber, M.A. Zimmermann, O. Brémond, “Pre-calculation using the FALCON fuel behaviour code of the fuel rod design parameters and the test-conditions for a two-run Halden LOCA test with KKL BWR high-burnup fuel”, EHPGM’11, Norway, October 2011
- [5.1-7] Yueh, K., et al., Fuel Fragmentation Data Review and Separate Effects Testing, in TopFuel. 2014: Sendai, Japan.
- [5.1-8] G. Khvostov, “Modeling Fuel Rod Behaviour During LOCA”, Presentation on Workshop on HRP LOCA testing, Lyon, France, 28-29 May 2012
- [5.2-1] Khvostov, G., A. Romano, and M.A. Zimmerman, Modeling the effects of axial fuel relocation in the IFA-650.4 LOCA test, in Enlarged Halden Programme Group Meeting 200711–16 March 2007: Storefjell Hotel, Gol, Norway
- [5.3-1] B.C.Oberländer, H.K.Jenssen, PIE the rod from LOCA test IFA-650.14 on high burnup BWR fuel, HWR-1096, 2014
- [5.3-3] M. Flanagan, M. Ozawa, “Recommendation for LOCA bundle experiments including simulation of fuel dispersal using surrogate fuel pellet fragments” HRP LOCA Workshop, Aix en provence, France, May 20-21, 2015.
- [5.4-1] Chung H.M. and Kassner T.F. “Deformation Characteristics of Zircaloy Cladding in Vacuum and Steam under Transient-Heating Conditions: Summary Report”. NUREG/CR-0344, July 1978
- [5.4-2] G. Khvostov, E. Kolstad, G. Ledergerber, “Analysis of Halden LOCA test with the BWR high burnup fuel”, 2013 LWR Fuel Performance Meeting / Top Fuel, Charlotte, NC, USA, September 2013, paper 8297
- [5.5-1] Nagase, F., “Behavior of LWR fuel during Loss-of-Coolant Accidents”, Comprehensive Nuclear Materials, Volume 2: Material Properties/Oxide Fuels for Light Water Reactors and Fast Neutron Reactors, 2012, Pages 595–608
- [5.5-2] B.C.Oberländer, M.Espeland, H.K.Jenssen, N.O. Solum, “PIE results from the low burnup (~44 MWd/kgU) BWR segment after LOCA testing in IFA 650-7”, OECD HRP Report, HWR-925, 2010
- [5.6-1] W. Wiesenack, “Summary of the Halden reactor Project LOCA Test Series IFA-650”, HPR-380, 05-14-2013
- [5.6-2] Nuclear Fuel Safety Criteria – Technical Review, NEA No. 7072, ISBN 978-92-64-99178-1, 2012
- [5.6-3] C. Delafoy, P. Dewes, AREVA NP Cr2O3-doped fuel development and qualification, Annual Meeting on Nuclear Technology, May 2007, Karlsruhe
- [5.6-4] J. Arborelius et al., Advanced doped UO₂ pellets in LWR Applications, Journal of Nuclear Science and Technology, Vol. 43, No. 9, 2006

- [5.6-5] A. R. Massih, Effects of Additives on Uranium Dioxide Fuel Behaviour, SSM report 2014:21 ISSN: 2000-0456, Januarys 2014
- [5.6-6] J. H. Davies et al., Modified fuel for high burnup, Proceedings of the TopFuel Conference, SFEN/ENS, 1999
- [5.6-7] B. Cazalis, V. Georgenthum, MOX Fuel Behaviour under Reactivity Initiated Accidents, Transactions Topfuel Manchester, 2012
- [5.6-8] International Atomic Energy Agency, Status and advances in MOX fuel technology, Technical Report Series No. 145, Vienna, 2003
- [5.6-9] F. Lemoine, Estimation of the grain boundary gas inventory in MIMAS7AUC MOX fuel and consistency with REP-Na test results, Journal of Nuclear Science and technology, Vol. 43 (2006) No. 9
- [5.8-1]] T. Narukawa, M. Amaya, "The effect of oxidation and crystal phase condition on the ballooning and rupture behavior of Zircaloy-4 cladding tube-under transient-heating conditions", J. Nucl. Sci. Technol., vol. 53, pp.112-122, 2016.
- [6.1-1] B. C. Oberlander, H. K. Jenssen and M. Espeland, "PIE results from the high burnup (83MWd/kg) PWR segment after LOCA testing in IFA 650-5," Loen, Norway, 2008.
- [6.1-2] G. Ledergerber, "HWR-1033: Characterization of KKL BWR Fuel for Test Series in IFA-610, IFA-629 and IFA-650," IFE, Halden, Norway, 2013.
- [6.1-3] B. C. Oberlander and H. K. Jenssen, "HWR-925: PIE results from the low burnup (~44 MWd/kgU) BWR segment after LOCA testing in IFA-650-7," IFE, Halden, Norway, 2011.
- [6.1-4] M. Billone, Y. Yan, T. Burtseva and R. Daum, "Cladding Embrittlement During Postulated Loss-of-Coolant Accidents, NUREG/CR-6967," USNRC, Washington, DC, USA, 2008.
- [6.1-5] M. E. Flanagan, P. Askeljung and A. Puranen, "NUREG-2160: Post-Test Examination Results from Integral, High-Burnup, Fueled LOCA Tests at Studsvik Nuclear Laboratory," U.S. NRC, Washington, DC, USA, 2013.
- [6.1-6] M. E. Flanagan, B. C. Oberlander and A. Puranen, "Fuel Fragmentation, Relocatoin and Dispersal Under LOCA Conditions: Experimental Observations," in Top Fuel 2013, Orlando, FL, USA, 2013.
- [6.1-7] B. C. Oberlander and H. K. Jenssen, "LOCA IFA650.9: PIE of the 90 MWd/kg PWR rod subjected to a high temperature transient," in Enlarged Halden Program Group Meeting, Storefjell, Norway, 2010.
- [6.2-1] E. H. Karb, M. Prussmann, L. Sepold, P. Hofmann and G. Schanz, "KfK-3346: LWR Fuel Rod Behavior in the FR-2 In-Pile Tests Simulating the Heatup Phase of a LOCA," Kernforschungszentrum Karlsruhe, Karlsruhe, 1983.
- [6.2-2] E. H. Karb, L. Sepold, P. Hofmann, C. Petersen, G. Schanz and H. Zimmermann, "KfK-3028: KfK In-Pile Tests on LWR Fuel Rod Behavior During the Heatup Phase of a LOCA," Keinforschungszentrum Karlsruhe, Karlsruhe, 1980.
- [6.2-3] M. Bruet and J. C. Janvier, "FLASH Experiments in SILOE Reactor. Fuel Rod Behaviour during LOCA Tests," in OECD-CSNI/IAEA Specialists' Meeting on Water Reactor Fuel Safety and Fission Product Release in Off-normal and Accident Conditions, Riso, Denmark, 1983.
- [6.2-4] M. Bruet and et al., "High Burnup Fuel Behavior During a LOCA type Accident : the FLASH 5 Experiment," in IAEA Technical Committee Meeting on Behavior of Core

- Material and Fission Products Release in Accident Conditions in LWR's, CADARACHE, FRANCE, 1992.
- [6.2-5] T. F. Cook, "NUREG/CR-0590: An Evaluation of Fuel Rod Behavior during Test LOC-11," U.S. Nuclear Regulatory Commission, Washington, DC, 1979.
- [6.2-6] J. M. Broughton and et al., "NUREG/CR-2073: PBF LOCA Test Series, Test LOC-3 and LOC-5 Fuel Behavior Report," U.S. Nuclear Regulatory Commission, Washington, DC, 1981.
- [6.2-7] J. M. Broughton and et al., "NUREG/CR-3184: PBF LOCA Test LOC-6 Fuel Behavior Report," U.S. Nuclear Regulatory Commission, Washington, DC, 1983.
- [6.2-8] B. C. Oberlander and H. K. Jenssen, "Extended Summary, HWR-1019: PIE of a high burnup PWR rod subjected to the LOCA test IFA-650.10," in Enlarged Halden Program Group Meeting, Sandefjord, Norway, 2011.
- [6.2-9] B. C. Oberlander, "Extended Summary, HWR-1020: PIE of a VVER rod subjected to LOCA test IFA-650.11," in Enlarged Halden Program Group Meeting, Sandefjord, Norway, 2011.
- [6.2-10] B. C. Oberlander, H. K. Jenssen and N. O. Solum, "LOCA IFA650.12 : PIE of a BWR rod subjected to LOCA testing in the HBWR," in Halden Program Group Meeting, Halden, Norway, 2012.
- [6.2-11] G. E. Russcher, R. K. Marshall, G. M. Hesson, J. Wildung N, W. N. Rausch, L. L. King, C. L. Wilson, L. J. Parchen, B. J. Webb, W. D. Bennett and C. L. Mohr, "NUREG/CR-2152: LOCA Simulation in the NRU Reactor, Materials Test - 1," U.S. Nuclear Regulatory Commission, Washington, DC, 1981.
- [6.2-12] J. O. Barner, G. M. Hesson, L. L. King, R. K. Marchall, L. J. Parchen, J. P. Pilger, W. N. Rausch, G. E. Russcher, B. J. Webb, N. J. Wildung, C. L. Wilson, M. D. Wismer and C. L. Mohr, "NUREG/CR-2509: Materials Test-2 LOCA Simulation in the NRU Reactor," U.S. Nuclear Regulatory Commission, Washington, DC, 1982.
- [6.2-13] C. L. Mohr, G. M. Hesson, L. L. King, R. K. Marshall, L. J. Parchen, J. P. Pilger, G. E. Russcher, B. J. Webb, N. J. Wildung, C. L. Wilson and M. C. Wismer, "NUREG/CR-2528: LOCA Simulation in the National Research Universal National Research Universal, Data Report for the Third Materials Experiment (MT-3)," U.S. Nuclear Regulatory Commission, Washington, DC, 1983.
- [6.2-14] C. L. Wilson, C. L. Mohr, G. M. Hesson, N. J. Wildung, G. E. Russcher, B. J. Webb and M. D. Freshley, "NUREG/CR-3272: LOCA Simulation in NRU Program, Data Report for the Fourth Materials Experiment (MT-4)," U.S. Nuclear Regulatory Commission, Washington, DC, 1983.
- [6.2-15] M. D. Freshley and G. M. Hesson, "PNL-SA-11536: Summary Results of the LOCA Simulation Program Conducted in NRU," Pacific Northwest Laboratory, Battelle Memorial Institute, Richland, WA, 1983.
- [6.2-16] P. A. Raynaud, "NUREG-2121: Fuel Fragmentation, Relocation, and Dispersal During the Loss-of-Coolant Accident," U.S. Nuclear Regulatory Commission, Washington, DC, 2012.
- [6.2-17] K.J. Geelhood, W.G. Luscher, C.E. Beyer, "FRAPCON-3.4: A Computer Code for the Calculation of Steady-State Thermal-Mechanical Behavior of Oxide Fuel Rods for High Burnup" NUREG/CR 7022, Vol. 1, PNNL-19418, Vol. 1, March 2011.
- [6.3-1] W. Wiesenack, "HPR-380: Summary of the Halden REactor Project LOCA Test Series IFA-650," Halden Reactor Project, Halden, Norway, 2013.

- [7.2-1] Nuclear Fuel Behaviour in Loss-of-Coolant Accident (LOCA) Conditions, State of the art report, ISBN 978-92-64-99091-3, NEA No. 6846, OECD 2009
- [7.2-2] Mangard, T. and A.R. Massih, Modelling of nuclear fuel cladding under loss-of-coolant accident conditions, 2013, SSM.
- [7.2-3] Forgeron, T., Experiment and Modeling of Advanced fuel rod Cladding Behavior Under LOCA Conditions: Alpha-beta Phase Transformation Kinetics and EDGAR Methodology. ASTM Special Technical Publication, 2000(1354): p. 256-278.
- [7.2-4] Hill, R., Plasticity 1950: Oxford University Press.
- [7.2-5] Murphy, G., Advanced Mechanics of Materials 1946: New York: McGraw-Hill Book Company, Inc.
- [7.2-6] Van Uffelen, P., et al., Extending the application range of a fuel performance code from normal operating to design basis accident conditions. Journal of Nuclear Materials, 2008. 383(1-2): p. 137-143.
- [7.2-7] Massih, A.R., Review of experimental data for modelling LWR fuel cladding behaviour under loss of coolant accident conditions, 2007, SKI.
- [7.2-8] Brachet, J.C., et al. Influence of Hydrogen content on the α/β phase Transformation and on the Thermal-mechanical Behavior of Zr-4, M4 and M5 Alloys During the First Phase of LOCA transient. in Zirconium in the Nuclear Industry: 13th International Symposium, ASTM-STP 1423. 2001. Annecy, France: ASTM International, West Conshohocken, PA.
- [7.2-9] Portier, L., et al. Influence of Long Service Exposures on the Thermal-mechanical Behavior of Zr-4 and M5 Alloys in LOCA conditions. in Zirconium in the Nuclear Industry: 14th International Symposium, ASTM STP 1467. 2004. Stockholm, Sweden: ASTM International, West Conshohocken, PA.
- [7.2-10] Kim, J.H., et al., Effects of Oxide and Hydrogen on the Behavior of Zircaloy-4 Cladding During the Loss of the Coolant Accident (LOCA). Nuclear Engineering and Design, 2006. 236(22): p. 2386-2393.
- [7.2-11] Powers, D.A. and R.O. Meyer, Cladding Swelling and Rupture Models for LOCA Analysis, in NUREG-0630, 1980, U.S. NRC.
- [7.2-12] Kim, J.H., et al., Deformation of Zircaloy-4 Cladding During a LOCA Transient up to 1200°C. Nuclear Engineering and Design, 2004. 234: p. 157-164.
- [7.2-13] Repetto, G., et al. Core coolability in loss of coolant accident: the PERFROI project. in WRFPM 2014. 2014. Sendai.
- [7.2-14] Stuckert, J., et al. Results of the commissioning bundle test quench -L0 performed under LOCA conditions. in 16th International quench Workshop. 2010. Karlsruhe.
- [7.2-15] Stuckert, J., et al. First results of the bundle test quench -L2 with M5® claddings. in 19th International quench Workshop. 2013. Karlsruhe.
- [7.2-16] Stuckert, J., et al. First results of the bundle test quench -L4 with hydrogenated M5® claddings. in 20th International quench Workshop. 2014. Karlsruhe.
- [7.2-17] Stuckert, J., et al. First results of the high temperature bundle test quench-L3HT with optimized ZIRLO™ claddings. in 20th International quench Workshop. 2014. Karlsruhe.
- [7.2-18] Chung, H.M. and T.F. Kassner, Deformation Characteristics of Zircaloy Cladding in Vacuum and Steam Under Transient Heating Conditions: Summary Report, in NUREG-0344, 1978, U.S. NRC.

- [7.2-19] Raynaud, P.A., Fuel Fragmentation, Relocation, and Dispersal During the Loss-of-Coolant Accident, in NUREG-2121,2012, U.S. NRC.
- [7.2-20] Raynaud, P.A. and I. Porter. Predictions of Fuel Dispersal During a LOCA. in WRFPM 2014. Sendai.
- [7.2-21] Flanagan, M.E., Post-Test Examination Results from Integral, High-Burnup, Fueled LOCA Tests at Studsvik Nuclear Laboratory, in NUREG-2160,2013, U.S. NRC.
- [7.2-22] Yueh, K.H., et al. Fuel Fragmentation Data Review and Separate Effects Testing. in WRFPM. 2014. Sendai.
- [7.2-23] Yagnik, S., et al. An Investigation into Fuel Pulverization with Specific Reference to High Burnup LOCA. in WRFPM. 2014. Sendai.
- [7.2-24] Gyóri, C., Post-test analyses of VVERspecific Halden LOCA tests, in VVER workshop, HPG 20112011: Sandefjord.
- [7.2-25] Kulacsy, K. and A. Molnar. Estimation of Core Average FGR due to Fragmentation during DB LB LOCA for a VVER-440 reactor. in EHPG. 2014. Roros.
- [7.2-26] Govers, K. and M. Verwerft. Simulation of ballooning & relocation in the Halden LOCA tests with FRAPTRAN. in EHPG meeting 2014. Røros.
- [7.2-27] Khvostov, G., A. Romano, and M.A. Zimmermann, Modeling the effects of axial fuel relocation in the IFA-650.4 LOCA test, in Enlarged Halden Programme Group Meeting 200711–16 March 2007: Storefjell Hotel, Gol, Norway.
- [7.2-28] Bascou, S., et al., Development and validation of the multi-physics DRACCAR code. Annals of Nuclear Energy, 2014. in press.
- [7.2-29] Oberländer, B.C. and H.K. Jenssen. PIE ON THE ROD FROM THE LOCA TEST IFA-650.14 ON HIGH BURNUP BWR FUEL. in EHPG meeting 2014. Røros.
- [7.2-30] Guillard, V., et al. USE OF CATHARE2 REACTOR CALCULATIONS TO ANTICIPATE RESEARCH NEEDS. in NURETH-11. 2005. Avignon.
- [7.2-31] Missenard, A., Conductivité thermique des solides, liquides, gaz et de leurs mélanges1965.
- [7.2-32] Repetto, G. and S. Ederli, Application of the Porous Medium Heat transfer model of ICARE/CATHARE code against debris bed and “bundle” “ experiments, in Eurotherm 2007: reactive heat transfer in porous media; Ecole des Mines d'Albi (France)2007.
- [7.2-33] Siefken, L. J.: "Axial fuel relocation in ballooning fuel rods", 7th International Conference on Structural Mechanics in Reactor Technology (SMiRT-7), Chicago, IL, USA, August 22-26, 1983.
- [7.2-34] Concejal, A., P.J. Garcia Sedano, and A. Crespo. Impact of the Potential High Burnup Fuel Dispersal During a Large Break LOCA in a BWR-6 NPP. in Top Fuel. 2012. Manchester.
- [7.2-35] Raynaud, P.A. Core-Wide Estimates of Fuel Dispersal During a LOCA. in Top Fuel. 2013. Charlotte.
- [7.3-1] Grandjean, C., G. Hache, and C. Rongier. High Burnup UO₂ Fuel LOCA Calculations to Evaluate the Possible Impact of Fuel Relocation After Burst. in OECD/NEA Proceedings of the Topical Meeting on LOCA Fuel Safety Criteria. 2001. Aix en Provence.
- [7.3-2] Aounallah, Y., et al., Simulation of the Halden IFA-650.3/4 high burnup LOCA tests with TRACE and FALCON: a preliminary study on axial relocation, in Proc. International Meeting on LWR Fuel Performance (TopFuel 2006)22-26 October 2006: Salamanca.

- [7.3-3] Benchmark Calculation on Halden IFA-650 LOCA Test Results, NEA/CSNI/R(2010)6, 15.11.2010.
- [7.3-4] Aounallah, Y., Simulation of HALDEN IFA-650 loss-of-coolant accidents tests with TRACE, 2012.
- [7.3-5] Khvostov, G., et al., Some insights into the role of axial gas flow in fuel rod behaviour during the LOCA based on Halden tests and calculations with the FALCON-PSI code. Nuclear Engineering and Design, 2011. 241(5): p. 8.
- [7.3-6] Khvostov, G., et al. Analysis of Halden LOCA test with the BWR high burnup fuel. in LWR Fuel Performance Meeting / Top Fuel. 2013. Charlotte.
- [7.3-7] Tofino, Y., A. Concejal, and P.J. Garcia Sedano. Evaluation of ECR and PCT in balloon region under LOCA conditions of the Halden IFA 650 tests (single rod tests). in TopFuel. 2009. Paris.
- [7.3-8] Grandjean, C. and G. Hache. LOCA Issues Related to Ballooning, Relocation, Flow Blockage and Coolability in SEGFSM Topical Meeting on LOCA Issues. 25-26 May 2004 ANL.
- [7.3-9] Muftuoglu, K., et al. Analytical Assessment of High-Exposure Fuel Dispersal Potential During Boiling Water Reactor Loss-of-Coolant Accident. in NURETH-15. May 12-17, 2013. Pisa.
- [7.3-10] F. D. Shum, e.a., SAFER Model for Evaluation of Loss-of-Coolant Accidents for Jet Pump and Non-Jet Pump Plants, in NEDE-30996P-A,1987.
- [7.3-11] Lars Olof Jernkvist, Ali Massih; "Models for axial relocation of fragmented and pulverized fuel pellets in distending fuel rods and its effects on fuel rod heat load"; SSM Report 2015:37, <http://www.stralsakerhetsmyndigheten.se/Global/Publikationer/Rapport/Sakerhet-vid-karnkraftverken/2015/SSM-rapport-2015-37-eng.pdf>
- [8.1-1] Nithianandan,, C.K.; Gerken, L.M.; Dunn, B.M.; Carlson, K.E. and Baxter, R.L.: THERMAL-HYDRAULIC EFFECTS OF CLADDING RUPTURE, FUEL FRAGMENTATION AND RELOCATION DURING A LARGE BREAK LOCA. 15th International Topical Meeting on Nuclear Reactor Thermal-Hydraulics, NURETH-15, paper 577, Pisa, Italy, May 12-17, 2013
- [8.1-2] Ihle, P.: Heat Transfer in Rod Bundles with Severe Clad Deformations. KfK 3607 B, April, 1984
- [8.1-3] Ihle, P.; Rust, K.: FEBA-Flooding Experiments with Blocked Arrays Evaluation Report. KfK 3657, März, 1984
- [8.1-4] SKI Report 02:17: A Review of Dryout Heat Fluxes and Coolability of Particle Beds. APRI 4, Stage 2 Report, ISSN 1104-1374, ISRN SKI-R-02/17-SE, April 2002
- [8.1-5] Flanagan, M.; Oberländer, B. C.; Puranen, A.: FUEL FRAGMENTATION, RELOCATION AND DISPERSAL UNDER LOCA CONDITIONS: EXPERIMENTAL OBSERVATIONS. TopFuel 2013, Charlotte, North Carolina, September 15-19, 2013
- [8.1-6] Sonnenburg, H.G.: Weiterentwicklung der Methoden zur Analyse des Brennstabverhaltens bei Reaktivitäts- und Kühlmittelverlust-Störfällen. Abschlussbericht, Reaktorsicherheitsforschung-Vorhabens RS 1149, GRS-A-3368, 2007
- [8.1-7] Boger, D. V. and Yeow, Y. L.: Ullmann's Encyclopedia of Industrial Chemistry (B. Evers, S., Hawkins und G. Schulz, Hrsg.), 5th. Aufl., Bd. B1, Chapter 5, VCH, Weinheim 1990

- [8.1-8] Sonnenburg, H.G.: Coolability of Relocated and Dispersed. Presentation from GRS for the LOCA Workshop on Fuel fragmentation, relocation and dispersal (FFRD), experimental basis, mechanisms and modelling approaches, Session 3: Implications of FFRD, 21.05.2015
- [8.2-1] Raynaud, P., et al., Prediction of fuel dispersal during a LOCA, Proceedings of WRFPM 2014, Paper No. 100026, Sendai, Japan, (2014).
- [8.2-2] Nakajima, T., et al., Potential for re-criticality of dispersed fuel during a LOCA transient, HRP/NEA WGFS LOCA Workshop on FFRD, Aix-en-Provence, France, (2015).
- [8.2-3] Okuno, H., et al., Computation on fuel particle size capable of being regarded as homogeneous in nuclear criticality safety analysis, J. Nucl. Sci. Technol., 31[9], 986-995 (1994).
- [8.2-4] Rhodes, J., et al., CASMO-5 development and applications, PHYSOR-2006, Vancouver, Canada, (2006).
- [8.2-5] <http://www.ensc.jp/pc/user/HOUDOU/%E5%A7%94%E5%93%A1%E4%BC%9A%E9%83%A8%E4%BC%9A150904/3-1%E6%8A%80.pdf>
- [8.2-6] Nagaya, Y., et al., MVP/GMVP II: General Purpose Monte Carlo Codes for Neutron and Photon Transport Calculations based on Continuous Energy and Multigroup Methods, JAERI-1348, (2005).
- [8.3-1] A. Wikström, L. Mileshina, "Radiological consequences from the release of fuel fragments during Loss of Coolant Accident", Studsvik Nuclear AB, Studsvik ALARA Engineering, N-15-059R Rev. 1, 2016-01-29
- [8.3-2] Alternative radiological source terms for evaluating design basis accidents at nuclear power reactors, U.S. NRC, RG 1.183 (July 2000)
- [8.3-3] K. Oldberg, "Distribution of fission gas release in 10x10 fuel", SKB report TR-09-25 (September 2009)
- [8.4-4] E. Nordström, "Fission gas release data for Ringhals PWRs", SKB report TR-09-26 (September 2009)
- [8.3-5] R. A. Forrest, "The European activation file: EAF-2007 decay library", UKAEA FUS 537 (2007).
- [9.1-1] M.E. Cunningham, M.D. Freshley and D.D. Lanning: Development and characteristics of the rim region in high burnup UO₂ fuel pellets, Journal of Nuclear Materials, 188 (1992), p.19-27.
- [9.1-2] M. Kinoshita et al.: HIGH BURNUP RIM PROJECT: (III) Properties of Rim-Structured Fuel, Proceedings of the 2004 International Meeting on LWR Fuel Performance, Orlando, Florida, September 19-22, 2004.
- [9.1-3] R. Manzel, C.T. Walker: EPMA and SEM of fuel samples from PWR rods with an average burnup of around 100 MWd/kgHM, Journal of Nuclear Materials, 301 (2002), p. 170–182.
- [9.1-4] J. Spino, K. Vennix, M. Coquerelle: Detailed characterisation of the rim microstructure in PWR fuels in the burnup range 40-67 GWd/tM, Journal of Nuclear Materials, 231 (1996) p.179-190.
- [9.1-5] J. Spino, et al.: Stereological evolution of the rim structure in PWR-fuels at prolonged irradiation: Dependencies with burnup and temperature, Journal of Nuclear Materials 354 (2006), p.66-84.

- [9.1-6] C.T. Walker et al.: Concerning the microstructure changes that occur at the surface of UO₂ pellets on irradiation to high burnup, *Journal of Nuclear Materials* 188 (1992), p.73-79.
- [9.1-7] A. Romano, M.I. Horvath, R. Restani, Evolution of porosity in the high-burnup fuel structure *Journal of Nuclear Materials* 361: 62-68, (2007)
- [9.1-8] S.R. Pati, A.M. Garde, L.J. Clink, in: *Proceedings ANS International Topical Meeting on Fuel Performance*, Williamsburg, Virginia, 1988, p. 204.
- [9.1-9] L.E. Thomas, C.E. Beyer and L.A. Charlot: Microstructural analysis of LWR spent fuels at high burnup, *Journal of Nuclear Materials* 188 (1992), p. 80-89.
- [9.1-10] K. Lassmann, et al.: Modelling the High Burnup UO₂ Structure in LWR Fuel, *Journal of Nuclear Materials*, 226 (1995), p. 1-8.
- [9.1-11] J. Spino, D. Papaioannou: Lattice parameter changes associated with the rim structure formation in high burnup UO₂ fuels by micro X-ray diffraction, *Journal of Nuclear Materials* 281 (2000) p.146-162.
- [9.1-12] D. Baron et al.: Discussion about HBS Transformation in High Burnup-up Fuels, *Nuclear Engineering and Technology*, 41, N°2 (March 2009), p.199-214.
- [9.1-13] Y.H. Koo et al.: Conservative Width of High Burnup Structure in Light Water Reactor UO₂ fuel as a Function of Pellet Average Burnup, *Nuclear Technology*, 164 (2008), p. 337-347.
- [9.1-14] N. Lozano, L. Desgranges, D. Aymes, J.C. Niepce, High magnification SEM observations for two types of granularity in a high burnup PWR fuel rim, *Journal of Nuclear Materials* 257: 78-87, (1998)
- [9.1-15] C.T. Walker et al.: SIMS analysis of an UO₂ fuel irradiated at low temperature to 65 MWd/kgHM, *Journal of Nuclear Materials*, 393 (2009), p. 212–223
- [9.1-16] K. Une, K. Nogita, S. Kashibe, T. Toyonaga, M. Amaya In Effect of irradiation-induced microstructural evolution on high burnup fuel behavior, *International Topical Meeting on LWR Fuel Performance*, Portland (Oregon, USA), pp 478-489.
- [9.1-17] F. Lemoine, P. Blanpain, D. Baron, Key parameters for the High Burnup Structure formation thresholds in oxide fuels. In *LWR Fuel Performance/TopFuel/WRFPM*, Orlando (FL), (2010).
- [9.1-18] C. Ronchi et al. : Effect of burnup on the thermal conductivity of uranium dioxide up to 100.000 MWd/tU, *Journal of Nuclear Materials*, 327 (2004), p. 58-76.
- [9.1-19] K. Nogita et al. : Effect of grain size on recrystallization in high burnup fuel pellets, *Journal of Nuclear Materials*, 248 (1997), p. 196-203.
- [9.1-20] K. Une et al. : Rim structure formation and high burnup fuel behavior of large-grained UO₂ fuels, *Journal of Nuclear Materials* 278 (2000), p.54-63.
- [9.1-21] R. Delorme et al. : Study of fission gas behavior and fuel restructuring in irradiated (U,Gd)O₂ fuel, *Proceedings of the Light Water Reactor Fuel Performance*, Manchester, UK, 2-6 September 2012.
- [9.1-22] C.T. Walker, Assessment of the radial extent and completion of recrystallisation in high burnup UO₂ nuclear fuel by EPMA, *Journal of Nuclear Materials* 275: 56-62, 1999.
- [9.2-46] Fuel Cladding Failure Criteria, 1999, European Commission Nuclear Safety and Environment.
- [9.2-47] 10 CFR Part 50. Domestic Licensing of Production and Utilization Facilities. 50.46 Acceptance criteria for emergency core cooling systems for light water nuclear power reactors.

- [9.2-48] Boyack, B.E., et al., Quantifying Reactor Safety Margins, in NUREG/CR-5249,1989.
- [9.2-49] Nissley, M.E., et al., Realistic Large-Break LOCA Evaluation Methodology Using the Automated Statistical Treatment of Uncertainty Method (ASTRUM), in Technical Report WCAP-16009-NP, 2005, Westinghouse Electric Company.
- [9.2-50] Zhang, J.e.a. Simulation of fuel behaviors under LOCA and RIA using FRAPTRAN code and uncertainty analysis with DAKOTA. in IAEA Technical Meeting on Modeling of Water-Cooled Fuel Including Design Basis and Severe Accidents. 2013. China.
- [9.2-51] Regulatory Guides on Nuclear Safety, 2013, STUK-Radiation and Nuclear Safety Authority.
- [9.2-52] Arkoma, A., et al., Statistical analysis of fuel failures in large break loss-of-coolant accident (LBLOCA) in EPR type nuclear power plant. Nuclear Engineering and Design, 2015. 285: p. 1-14.
- [9.2-53] Arffman, A. and J. Rintala. Statistical Analysis of Fuel Failures in Accident Conditions. in Water Reactor Fuel Performance Meeting. 2011. Chengdu.
- [9.2-54] Graff, G. and S. Boutin. A new LOCA safety demonstration in France. in submitted to TopFuel. 2015. Zurich.
- [9.2-55] Courrier ASN à EDF: Nouveau référentiel d'étude de l'accident par perte de réfrigérant primaire (APRP), 2014.
- [9.2-56] Lettre ASN : Orientations pour l'évolution du référentiel d'étude de l'Accident de Perte de Réfrigérant Primaire (APRP), 2011.
- [9.2-57] TECHNICAL GUIDELINES FOR THE DESIGN AND CONSTRUCTION OF THE NEXT GENERATION OF NUCLEAR POWER PLANTS WITH PRESSURIZED WATER REACTORS, in Adopted during the GPR/German experts plenary meetings October 19th and 26th 2000.
- [9.2-58] Sicherheitsanforderungen an Kernkraftwerke, November 11, 2012.
- [9.2-59] Nuclear Fuel Safety Criteria Technical Review, in Second Edition, ISBN 978-92-64-99178-1 ,2012, OECD NEA.
- [9.2-60] Bordelon, F.M., et al., LOCTA IV Program: Loss-of-Coolant Transient Analysis, in WCAP-8301 (Proprietary), WCAP-8305 (Nonproprietary),1974.
- [9.2-61] General Electric Company Analytical Model for Loss-of-Coolant Analysis in accordance with 10CFR50 Appendix K, in NEDO-20566 (Nonproprietary), 1976.
- [9.2-62] Topical Report for the Application of KREM to Korea Standard Nuclear Power Plants, in TR-KHNP-0010, Proprietary, Seoul, Korea, 2007 KHNP.
- [9.2-63] Kim, I.G., et al., APR-1400 ECCS Performance Evaluation by Using KINS Realistic Evaluation Methodology, in KINS/RR-307,2005, KINS, Daejeon, Korea
- [9.2-64] MARS CODE MANUAL Vol. I: Code Structure, System Models, and Solution Methods, 2009, KAERI/TR-2812/2004, Daejeon, Korea.
- [9.2-65] SPACE 2.14 Manual Vol.1 : Theory Manual, in S06NX08-K-1-TR-36, Proprietary, Seoul, Korea,2013, KHNP.
- [9.2-66] Lee, J. and S. Woo, Effects of fuel rod uncertainty on the LBLOCA safety analysis with limiting fuel burnup change. Nuclear Engineering and Design, 2014. 273: p. 367-375.
- [9.2-67] THSR2013: Thermal Hydraulics Safety Research Division Annual Report 2013, in KAERI/GP-391/2014, Daejeon, Korea ,2014.

- [9.2-68] UJD SR Decree No. 430/2011 Coll., which lays down details of requirements for nuclear safety, 16th of November 2011.
- [9.2-69] Bujan, A. and Z. Kusovská, Methodology and criteria for safety analyses of the radiological accidents and radiological threat of population, 2012, VUJE.
- [9.2-70] Hatala, B., Evaluation of fuel rod cladding failure during a loss-of-coolant accident Int. J. Nuclear Energy Science and Technology, 2007. 3(3).
- [9.2-71] ENSI-G20: Reaktorkern, Brennelemente und Steuerelemente: Auslegung und Betrieb.
- [9.2-72] ENSI-A01: Anforderungen an die deterministische Störfallanalyse für Kernanlagen.
- [9.2-73] El-Shanawany, M., C.G. Kinniburgh, and K.T. Routledge, Comparison of Calculations Using the Best Estimate Reflood Heat Transfer Code BART-A1 with Data from the FEBA and REBEKA Facilities, in Fifth International Meeting on Thermal Nuclear Reactor Safety Sept. 9-13, 1984: Karlsruhe.
- [9.2-74] Jones, J.R. and M. Trowe, Multi-pin Studies of the Effect of Changes in PWR Fuel Design on Clad Ballooning and Flow Blockage in a Large-break Loss-of Coolant Accident, in LWR Fuel Performance Meeting/Top Fuel 2007: San Francisco.
- [9.2-75] Manley, A.J., P. Hindmarch, and A. Garlick. Application of X-radiography techniques to LOCA simulation tests on irradiated PWR fuel in Post-Irradiation Examination Techniques For Water Reactor Fuel Proceedings of a Technical Committee Meeting Organized By The international Atomic Energy Agency. ;Report IWGFPT--37, Workington (UK); 11-14 Sep 1990
- [9.2-76] Regulatory Guide 1.195, Methods and Assumptions for Evaluating Radiological Consequences of Design Basis Accidents at Light-Water Nuclear Power Reactors, in U.S. NRC, Office of Nuclear Regulatory Research, 2013.